



**HAL**  
open science

# Biomass gasification in bubbling fluidized bed : high temperature interaction between inorganic compounds and granular materials

Judit Kaknics

► **To cite this version:**

Judit Kaknics. Biomass gasification in bubbling fluidized bed : high temperature interaction between inorganic compounds and granular materials. Other. Université d'Orléans, 2014. English. NNT : 2014ORLE2042 . tel-01145266

**HAL Id: tel-01145266**

**<https://theses.hal.science/tel-01145266>**

Submitted on 23 Apr 2015

**HAL** is a multi-disciplinary open access archive for the deposit and dissemination of scientific research documents, whether they are published or not. The documents may come from teaching and research institutions in France or abroad, or from public or private research centers.

L'archive ouverte pluridisciplinaire **HAL**, est destinée au dépôt et à la diffusion de documents scientifiques de niveau recherche, publiés ou non, émanant des établissements d'enseignement et de recherche français ou étrangers, des laboratoires publics ou privés.

**ÉCOLE DOCTORALE**  
**ENERGIE, MATERIAUX, SCIENCES DE LA TERRE ET DE L'UNIVERS**

LABORATOIRE CEMHTI

(Condition Extrêmes et Matériaux : Haute Température et Irradiation)

**THÈSE** présentée par :  
**Judit KAKNICS**

soutenue le **03 Octobre 2014**

pour obtenir le grade de : **Docteur de l'université d'Orléans**  
Discipline/ Spécialité : Sciences des Matériaux

**Gazéification de la biomasse en lit fluidisé bouillonnant:  
interactions à haute température entre les composés  
inorganiques et les matériaux granulaires**

**THÈSE dirigée par :**

**Jacques POIRIER** Professeur, CEMHTI, Université d'Orléans

**RAPPORTEURS :**

**Karine FROMENT** Ingénieur, LITEN-LTB, CEA Grenoble

**Yann ROGAUME** Professeur, LERMAB, Université de Lorraine

---

**JURY**

**Karine FROMENT** Ingénieur, LITEN-LTB, CEA Grenoble

**Yann ROGAUME** Professeur, LERMAB, Université de Lorraine

**André AYRAL** Professeur, IEM, Université Montpellier 2

**Olivier AUTHIER** Ingénieur, EDF R&D

**Sylvain SALVADOR** Professeur, Mines Albi

**Jean André ALARY** Docteur, IMERYS – CARRD GmbH

**Jacques POIRIER** Professeur, CEMHTI, Université d'Orléans



# ACKNOWLEDGEMENTS

This work was done within the Refractory Materials Group at laboratory CEMHTI, CNRS Orléans.

First of all, I want to express my gratitude to my professor, Jacques Poirier for supervising my work during the last three years. I appreciate that he could always find the time to answer my questions and to guide me in spite of being extraordinary busy. I am grateful for his encouragement, good humour and taking care of me. I could not wish for better supervisor than him.

I would like to express my gratitude to all the committee members for accepting to be a member of the evaluating committee, for reviewing my manuscript, for their relevant suggestions and for letting my defence be an enjoyable moment.

I want to thank for the Direction and for all the members of CEMHTI for their support in the last three years. It was a great opportunity to be part of this laboratory, I will always think of this experience with gratitude.

I want to thank to the Group of Refractory Materials for technical and personal support.

Special thank for Rudy Michel, with whom we accomplished the miscanthus mission.

I owe my heartiest gratitude for Marie-Laure Bouchetou for her encouragement and the successful *tarte au citron* recipe; it was a pleasure to share the office with her.

Special thanks to Didier Zanghi and to Séverine Brassamin for their help and kindness.

Emmanuel Véron is thanked for his help with the XRD analyses.

Sandra Ory is thanked for the TGA and DSC measurements.

I would like to thank to François Vivet and Florent Poupard for their help with informatics.

I express my warm thanks to Raphaëlle Dhennin and Marie-France Rouillier for their enormous help in the labyrinth of administration issues.

I am sincerely grateful to the group LTB-LITEN at CEA Grenoble for sharing their truthful views on my work and for welcoming me in November 2013. Although I spent only two weeks in the laboratory, I felt part of their group from the very first day. I

would like to thank to Karine Froment for her encouragement and precious remarks. Special thanks to Françoise Defoort for her aspiring guidance. I am grateful for her frank and always relevant remarks and for taking care of me also outside of working hours.

I express my warm thanks to Annie Richard at Centre Microscope Optique for the hundreds of SEM analyses and beautiful SEM images. Thanks to her kindness and welcoming personality, it was always a pleasure to go to the "SEM-sessions".

I would like to thank for all the members of the GAMECO research project for their valuable feedbacks and for the good ambiance at the progress meeting.

Dr. Bernard Gratuze at laboratory IRAMAT, CNRS Orleans is thanked for the ICP-MS analysis.

Linseis, Thermal Analysis is thanked for the optical dilatometry measurements.

I would like to acknowledge for the financial support provided by the Region Centre, by CNRS and by the ANR research project, GAMECO.

I am also grateful for having a chance to meet so many wonderful people and professionals at the different conferences -especially at the Impact of Fuel Quality conferences in 2012 and 2014- who inspired and motivated me in my work.

I express my deepest gratitude to my family and friends for their love, support and encouragement. Speaking with them always felt like recharging the batteries! We are all spread around the world but it is great to know that we can always count on each other.

And finally, I cannot be enough grateful to Yann for his support and for taking the weight off my shoulders throughout the endless hours of writing.

*« Le vent se lève !... Il faut tenter de vivre ! »*

*I dedicate this work to my parents.*

# TABLE OF CONTENTS

<b>Introduction</b> .....	<b>i</b>
<b>Chapter I: Context and objectives</b> .....	<b>1</b>
I.1 Issues of energy demand.....	2
I.2 Biomass classification and characterisation.....	6
I.2.1 The interest of lignocellulosic biomass .....	6
I.2.2 Biomass characteristics.....	7
I.2.3 Giant Miscanthus as attractive biomass feedstock.....	9
I.3 Biomass into energy.....	12
I.3.1 Renewable energy conversion routes .....	12
I.3.2 Fundamentals of gasification .....	13
I.3.3 Stoichiometric oxygen requirement, equivalent ratio (ER).....	15
I.4 Reactor types .....	16
I.4.1 Fixed bed gasifier .....	16
I.4.2 Fluidized bed gasifier .....	17
I.4.3 Entrained flow gasifier .....	18
I.4.4 Challenges in biomass gasification in fluidized bed.....	19
I.5 Objectives of the thesis .....	20
I.6 References of Chapter I.....	21
<b>Chapter II: Characterisation of miscanthus</b> .....	<b>25</b>
II.1 Introduction.....	26
II.2 State of the art.....	28
II.2.1 The structure of miscanthus stem .....	28
II.2.2 The role of inorganics.....	29
II.2.3 The transformation of inorganics at high temperature .....	31
II.2.4 Prediction of biomass ash behaviour .....	34
II.3 Study of the inorganics in miscanthus stem .....	37
II.3.1 Composition of Miscanthus X Giganteus.....	37
II.3.2 Preparation of samples for SEM-EDX analysis .....	38
II.3.3 Transformation of inorganics at low temperature .....	40
II.3.4 Discussion of inorganic transformation at low temperature.....	48

II.4 Study of the ash behaviour at high temperature.....	49
II.4.1 Preparation of start-up batch for high temperature analysis.....	49
II.4.2 Experimental setup in reducing atmosphere.....	50
II.4.3 Characterisation of ash samples.....	53
II.4.4 Thermal analysis of miscanthus.....	57
II.4.5 Ash fusibility test.....	58
II.4.6 Inorganic composition based on the chemical fractionation analysis .....	59
II.4.7 Transformation of crystalline phases .....	62
II.4.8 Effect of harvest time on the chemical composition of miscanthus ashes.....	67
II.4.9 Effect of atmosphere on the chemical composition of miscanthus ashes.....	69
II.4.10 Composition of liquid phases in miscanthus ashes at high temperature .....	71
II.5 Conclusion.....	72
II.6 References of Chapter II.....	74
<b>Chapter III: Thermodynamic calculation .....</b>	<b>77</b>
III.1 Introduction .....	78
III.2 State of the art .....	79
III.3 Modelling the inorganic transformation in miscanthus .....	82
III.3.1 Input data for thermodynamic calculations.....	82
III.3.2 Choice of databases and solution phases .....	84
III.3.3 Transformation of miscanthus ashes.....	85
III.3.4 Comparison of FToxid and GToxid databases .....	90
III.4. Validation of the thermodynamic model with laboratory experiments.....	96
III.4.1 Comparison: liquid to liquid plus solid (L/(L+S)) with ash fusibility test .....	98
III.4.2 Comparison of equilibrium solid phases with X-ray diffraction .....	99
III.4 Conclusion.....	104
III.5 References of Chapter III.....	105
<b>CHAPTER IV: Interaction between molten miscanthus ashes and bed particles.....</b>	<b>107</b>
IV.1 Introduction .....	108
IV.2 State of the art .....	110
IV.2.1 Agglomeration mechanism .....	110
IV.2.3 Counteracting agglomeration .....	113

IV.3 Materials and methods.....	116
IV.4.Phase transformation of olivine at high temperature.....	118
IV.5 Wettability of bed materials by molten ashes.....	122
IV.6 Bed materials and miscanthus ash Interaction tests.....	128
IV.6.1 Effect of bed material .....	129
IV.6.2 Effect of miscanthus harvest time .....	130
IV.6.3 Effect of elevated temperature and contact time .....	133
IV.6.4 Effect of reducing atmosphere.....	135
IV.7 Conclusion.....	139
IV.8 References of Chapter IV .....	141

## **Chapter V:Ash-bed material interaction under dynamic conditions 143**

V.1 Introduction.....	144
V.2 A short overview of fluidization theory .....	146
V.3 Dynamic interaction tests in laboratory fluidized bed.....	149
V.3.1 Bed materials and fuel.....	149
V.3.2 Description of laboratory high temperature device .....	149
V.3.3 Determining the minimum fluidization velocity ( $U_{mf}$ ) .....	150
V.3.4 Fluidization tests in the laboratory high temperature device .....	152
V.3.5 Effect of bed material on the agglomeration ratio.....	154
V.3.6 Effect of process parameters on the agglomeration ratio .....	155
V.3.7 Effect of additives on the agglomeration ratio.....	158
V.3.8 Morphology of agglomerates .....	161
V.3.9 Discussion of laboratory high temperature experimentation .....	167
V.4 Gasification trials in fluidized bed pilot .....	168
V.4.1 Experimental setup .....	168
V.4.2 Fluidization tests in the gasification pilot.....	170
V.4.3 Agglomeration ratio in the gasification pilot.....	171
V.4.4 Evolution of agglomeration ratio during gasification .....	172
V.4.5 Morphology of agglomerates .....	174
V.5 Conclusion .....	180
V.6 References of Chapter V .....	181

## **Conclusion and perspectives..... 183**

## **Appendices ..... 191**

List of appendices.....	192
Appendix-A 1 : Staining method.....	194
Appendix-A 2: Observation of stem degradation with optical microscope.....	195
Appendix-A 3: LM1 ashes after 10 min heat treatment at 1000 °C in Air.....	196
Appendix-A 4: XR diffractog of LM2 ashes .....	197
Appendix-A 5: Calculating the input data of miscanthus ashes for FactSage .....	198
Appendix-A 6: FToxid, FTsalt and FTpulp database- solution phases with components for the miscanthus ash system.....	199
Appendix-A 7: Selecting the solution phases for thermodynamic calculations.....	202
Appendix-A 8: Comparison of liquid and solid phases at 850 °C .....	209
Appendix-A 9: Influence of main ash forming elements .....	210
Appendix-A 10: FToxid and GToxid databases.....	220
Appendix-A 11: Comparing liquid phase composition at 1000 °C.....	222
Appendix-A 12: Wetting of bed materials by molten LM1 and LM2 ashes.....	223
Appendix-A 13: Magnesium Ferrite in calcined olivine .....	224
Appendix-A 14: Determining the minimum fluidization rate at 750 °C .....	225
Appendix-A 15: Dolomite plus ashes heat treated at 900 °C .....	228
Appendix-A 16: SEM-EDX analysis of agglomerates from laboratory fluidized bed (CEMHTI).....	229
Appendix-A 17: Minerals from laboratory fluidized bed (CEMHTI) .....	230
Appendix-A 18: SEM-EDX analysis of agglomerate from the gasification pilot.....	231

# INTRODUCTION

Due to the future decline of fossil fuel reserves and growing awareness of greenhouse gas emission, alternative energy resources receive great attention from governments and international organizations. Biomass is a seducing alternative as it is widely available and it can be directly converted into fuel, electricity or value added chemicals using the existing power generation infrastructure [1]. The term biomass refers to all organic matter renewable on a human timescale, such as wood, manure or agricultural by-products.

Concerned about the economic issues of land use, lignocellulosic biomass (agricultural and forest residues, energy crops) are good candidate for energy production as they do not compete with the food supply chain. Generally, lignocellulosic biomass is converted into energy via thermal processes such as combustion, gasification or pyrolysis.

In combustion, biomass is directly converted into carbon dioxide and the released heat is used for electricity production via steam cycle turbine. Gasification produces a combustible gas mixture, also called syngas, with CO and H<sub>2</sub> as main components, which can be used in gas engines and gas turbines having higher electrical efficiency than steam turbines (30-40% compared to 15-25%)[2]. Moreover, syngas can be also converted into value added chemical feedstocks such as methanol and methane or into fuel via Fischer-Tropsch synthesis[3].

To increase the efficiency of thermal processes, combined heat and power (also known as cogeneration) plants have been developed. Cogeneration technology recovers the waste heat of the electricity production resulting in an extra 30% of thermal efficiency, which means in total 70% process efficiency.

Combined heat and power technologies based on gasification are more attractive solution for smaller units (1 to 12MWe) than combustion plants as their productivity is not influenced by the size of the system [4].

Concerning the reactor, fluidized beds are suitable for biomass gasification as they provide good mixing, longer residence time and isothermal conditions. Although the gasification of biomass is an attractive method, until now most of the installation are only in pilot scale in France due to the technical problems to resolve[5]. The main challenges of fluidized bed gasification are the complexity of gas treatment, the decomposition of heavy organics (tar), the improvement of hydrodynamics and the agglomeration issues [5].

This thesis, financed by Region Centre, is connected to the ANR program GAMECO (Gazéification AMEliorée pour des applications COgénération), which aims to improve the technology of small size air-blown bubbling fluidised bed gasification.

The GAMECO research project gathers several industrials and research laboratories, namely *EDF R&D* as project coordinator, *EQTEQ Iberia* as technology supplier and developer, *Novabiom* as biomass producer and supplier, the *Laboratoire Réactions et Génie des Procédés (LRGP UPR 3349)* for the study of tar kinetics, the *Laboratoire d'Etudes et de Recherches sur le Matériau Bois (LERMAB EA4370)* for pilot scale tests, the *Laboratoire d'Energétique et de Mécanique Théorique et Appliquée (LEMTA, UMR7563)* for hydrodynamic issues and at last but not least the laboratory *Condition Extreme et Matériaux (CEMHTI, CNRS UPR 3079)* for high temperature inorganics-bed materials interactions.

In the frame of this thesis we also worked in collaboration with the *Laboratoire des Technologies de la Biomasse (LTB, CEA/Grenoble)* on the thermodynamic aspects of phase transformations in biomass ashes and experiments in reductive atmosphere.

This work focuses on the biomass ash behaviour at high temperature. The biomass ash undergoes phase transformations (volatilisation and melting) and forms silicates with lower melting point than the usual operating temperature of a fluidized bed. The presence of liquid phase alters the fluidization behaviour by modifying the inter-particle forces [6].

The two main reverse forces in a bubbling fluidized bed are the adhesive force between sticky, ash-coated particles and the breaking forces created by the movement of gas bubbles [7]. When the inter-particle forces are greater than the breaking force of gas bubbles, the particles will agglomerate resulting in segregation and uneven temperature profile in the bed. Agglomeration can lead to the defluidization of the bed and profit loss [8].

Agglomeration is influenced by different factors such as the reactor geometry, the process conditions, the ash chemistry and the choice of bed materials. This work studies the agglomeration phenomenon from physicochemical aspects: it investigates the phase transformations of the ashes and the ash-bed material interaction.

The experiments were carried out with *Giant Miscanthus*. *Miscanthus* is a herbaceous plant originated in Eastern-Asia. It has received great attention as energy feedstock in the last 20 years both in Europe and the United States. Despite the many annealing characteristics of *miscanthus* for energy conversion, its high alkaline content, as it is the case for all grassy biomass, causes agglomeration in fluidized bed.

This work had three main objectives:

1. to describe the transformation of inorganics at high temperature
2. to reveal their role in the agglomeration phenomenon
3. to provide recommendations for *miscanthus* gasification in fluidized bed

The thesis is divided into 5 chapters.

The first chapter gives an overview of renewable energy context, the situation of biomass in the global energy sector and in France. It summarises the possible biomass conversion techniques focusing on the thermochemical processes, in more particular the fluidized bed gasification.

The second chapter presents the transformation of miscanthus ashes at high temperature. It describes the structure of the miscanthus stem and the role of the inorganics. The transformation of the inorganics is studied in details; the effects of different parameters such as the harvest time and atmosphere are also investigated.

The third chapter presents the thermodynamic calculations. Thermodynamic calculations are often used as predictive tools for ash behaviour, but they have certain limits as equilibrium state cannot be reached in industrial processes. Moreover, the existing databases are not always accurate to study biomass ashes. Our aim is to validate these calculations with experimental results for the case of miscanthus thermal conversion.

The fourth chapter reveals the interaction between the biomass ashes and different bed materials under static conditions at high temperature. It studies the importance of interfacial forces and the different interactions at the ash-bed particle interface with a parametric experimentation.

The fifth chapter reports the results of the dynamic interaction tests performed at two scales; a bench scale high temperature device and a laboratory pilot reactor.

The bench scale device served to describe the agglomeration tendencies using directly miscanthus ashes with different bed materials in oxidizing atmosphere. Different parameters were tested; the temperature, the ash/fuel ratio, the fluidization velocity and the addition of anti-agglomerates to the olivine bed.

The pilot reactor was set up at the laboratory of LRGP, Nancy. It allows studying the agglomeration in reductive atmosphere close to industrial gasification with miscanthus pellet feed and olivine bed.

In both cases, the bed agglomeration was evaluated by sieving the bed material before and after the tests. The agglomerates were analyzed by SEM-EDX and they were compared to the samples from the static interaction tests.

This work is closed with the summary of the main findings and future perspectives.

## References of Introduction

- [1] Heaton EA, Dohleman FG, Miguez AF, Juvik JA, Lozovaya V, Widholm J, et al. Miscanthus : A Promising Biomass Crop Biology. *Adv Bot Res* 2010;56:75–137.
- [2] BioenergyNet.com. [Http://www.bioenergynet.com/page/about](http://www.bioenergynet.com/page/about) 2014.
- [3] Basu P. Introduction (Chapter 1). *Biomass Gasif. Pyrolysis*, 2010.
- [4] Khalfi AE. BIOMAP-EDC 6- Comparaison de la combustion et gazéification pour la cogénération à partir de biomasse. 2009.
- [5] Quelles perspectives pour la gazéification en France ?  
<http://www.enerzine.com/12/8915+quelles-Perspectives-Pour-La-Gazeification-En-France+.html> 2009.
- [6] Lin W. Agglomeration in bio-fuel fired fluidized bed combustors. *Chem Eng J* 2003;96:171–85.
- [7] Steenari B-M, Lundberg A, Pettersson H, Wilewska-Bien M, Andersson D. Investigation of Ash Sintering during Combustion of Agricultural Residues and the Effect of Additives. *Energy & Fuels* 2009;23:5655–62.
- [8] Bartels M, Lin W, Nijenhuis J, Kapteijn F, van Ommen JR. Agglomeration in fluidized beds at high temperatures: Mechanisms, detection and prevention. *Prog Energy Combust Sci* 2008;34:633–66.

---

# CHAPTER I: CONTEXT AND OBJECTIVES

---

## ABSTRACT

This chapter is dedicated to the state of the art of biomass gasification in fluidized bed applications. It discusses briefly the context and issues of global energy demand, fossil fuel and alternative energy resources. It gives an overview of biomass classification, its main characteristics, different conversion routes and reactor designs.

## I.1 ISSUES OF ENERGY DEMAND

At the beginning of the 21<sup>st</sup> century, we are all aware of the environmental and economic concerns of continuously increasing energy consumption. There are three main aspects to take into consideration. Firstly, as shown in Figure I-1, the demand for oil and natural gas is continuously rising, while the fossil fuel resources have been exploited and their quantity is limited. Moreover, the prices of crude oil and natural gas increase every year and they are influenced by the different geopolitical crises (Figure I-2). Thirdly, the increasing energy consumption results in elevated level of CO<sub>2</sub> in the atmosphere (Figure I-3). All these issues signify the need for the diversification of energy resources and better usage of locally available alternative sources.

In this context, biomass is a seducing alternative as it is locally available in different forms and it can be directly converted into fuel, electricity or chemical products using the existing power generation infrastructure [I-1].

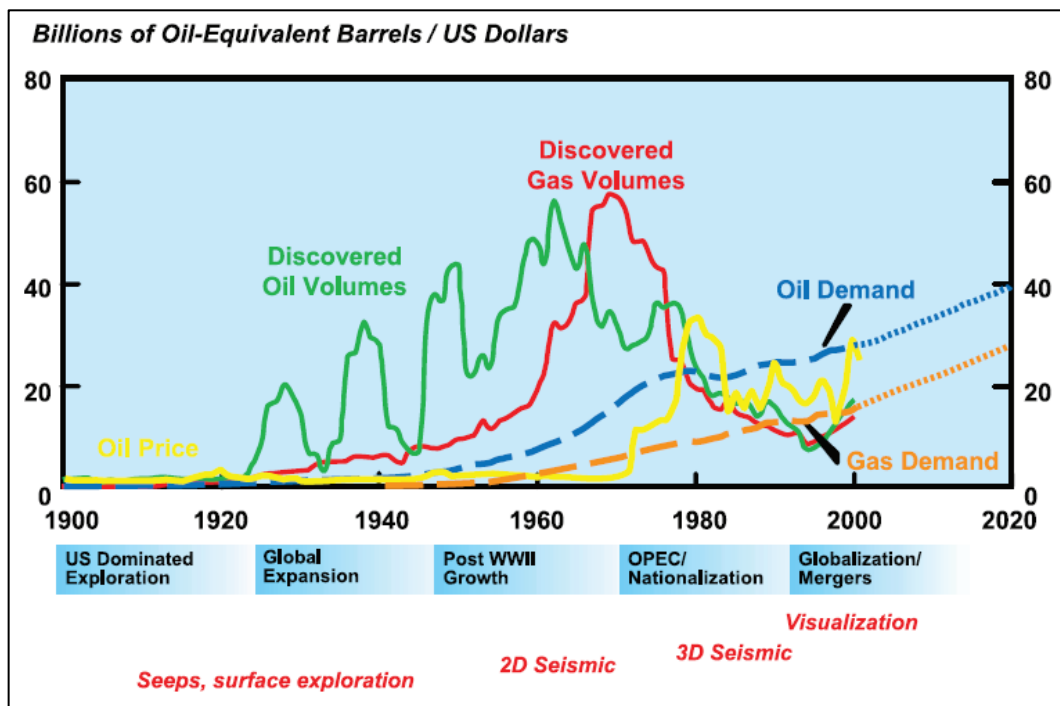


Figure I-1: Fossil fuel demand versus available resources [I-2]

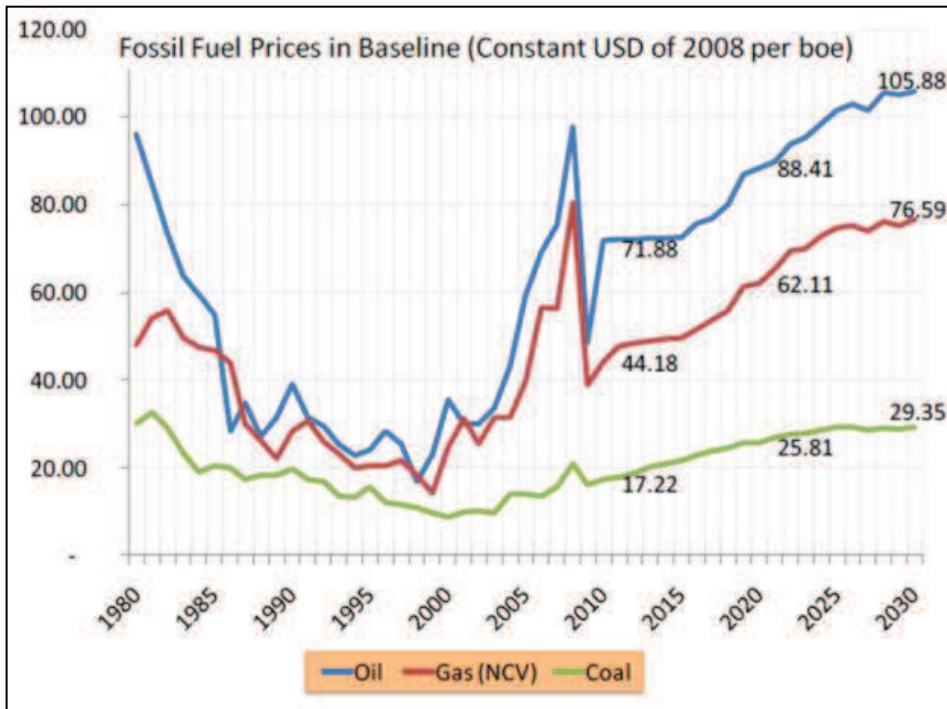


Figure I-2: Evolution of world fossil fuel prices between 1980 and 2030 [I-3]

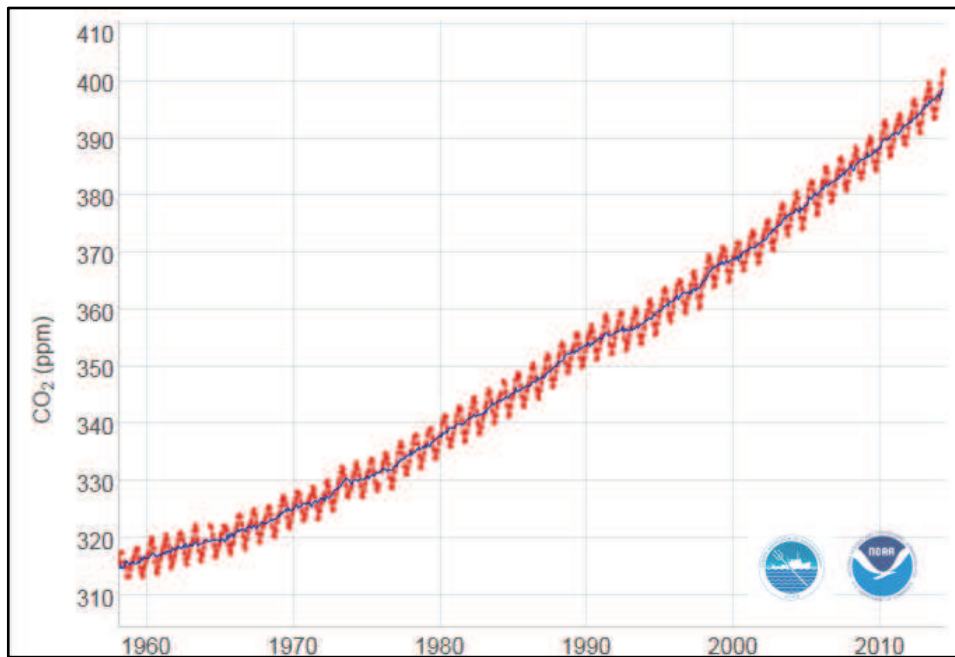


Figure I-3: Evolution of CO<sub>2</sub> concentration in the atmosphere between 1960 and 2010, measured at Manua Loa, Hawaii [I-4]

*THE SITUATION OF BIOMASS IN FRANCE*

As illustrated in Figure I-4, in 2011 biomass contributed with 10% to the global energy division and it covered 80% of renewable energy sources [I-5]. In France, 46% of the renewable energy derives from biomass, in more particularly from wood. However, between 2005 and 2011, 85% of the invested cost on renewables was dedicated to the wind and solar energy development [I-5].

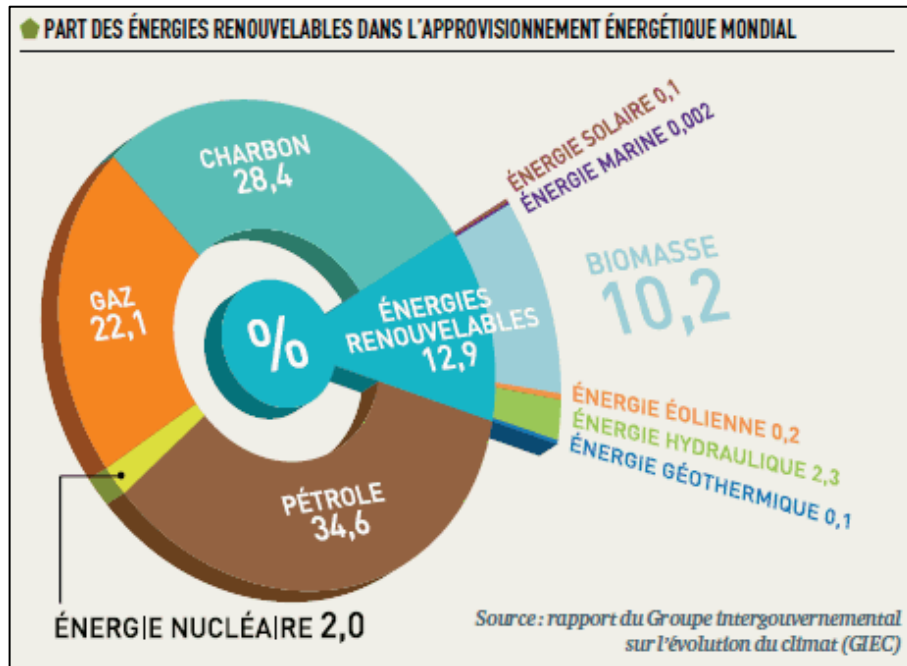


Figure I-4: Contribution of the different energy sources to the global demand in 2011 [I-5]

For the moment, biomass is mostly exploited in the form of biogas (CH<sub>4</sub>) and biofuel (ethanol). France is the fourth producer in biogas in Europe (after Germany, Great Britain and Italy), and it is the second producer in biofuels after Germany [I-5]. The energy production from lignocellulosic biomass is mostly related to wood combustion but the forest sector has been significantly touched by the economic crisis since 2008 [I-5].

Figure I-5 shows the situation of biomass fuelled combined heat and power (CHP) plants in France. In 2011, only a dozen of combined heat and power (CHP) plants was operating and another dozen was under development [I-5].

Although the main renewable resource in France is the hydraulic energy, the perspectives of the European Union on energy diversification might change the present trends. In Figure I-6, the objectives settled for 2020 show that half of the increase of renewable energy sector will be dedicated to the biomass application [I-5], which give rise to biomass gasification development in France.

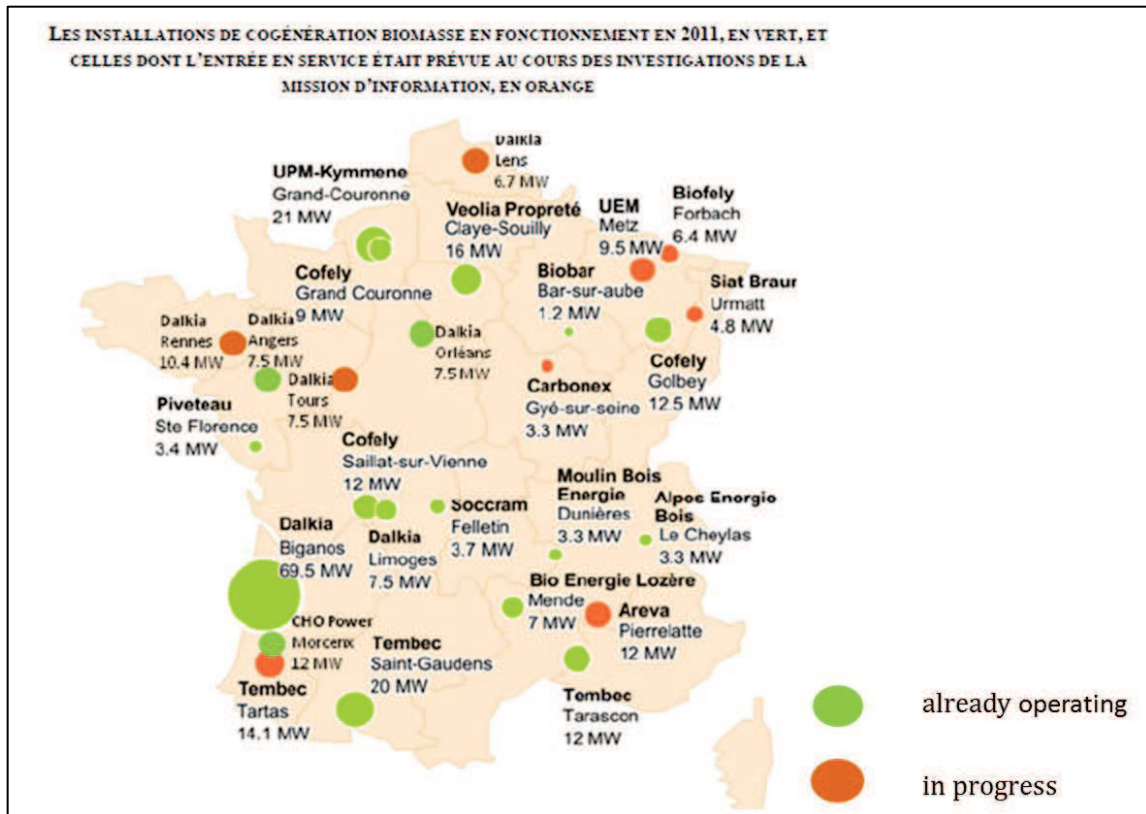


Figure I-5: Biomass combined heat and power (CHP) plants in France in 2011; Green circle- already working, orange circle- in progress [I-5]

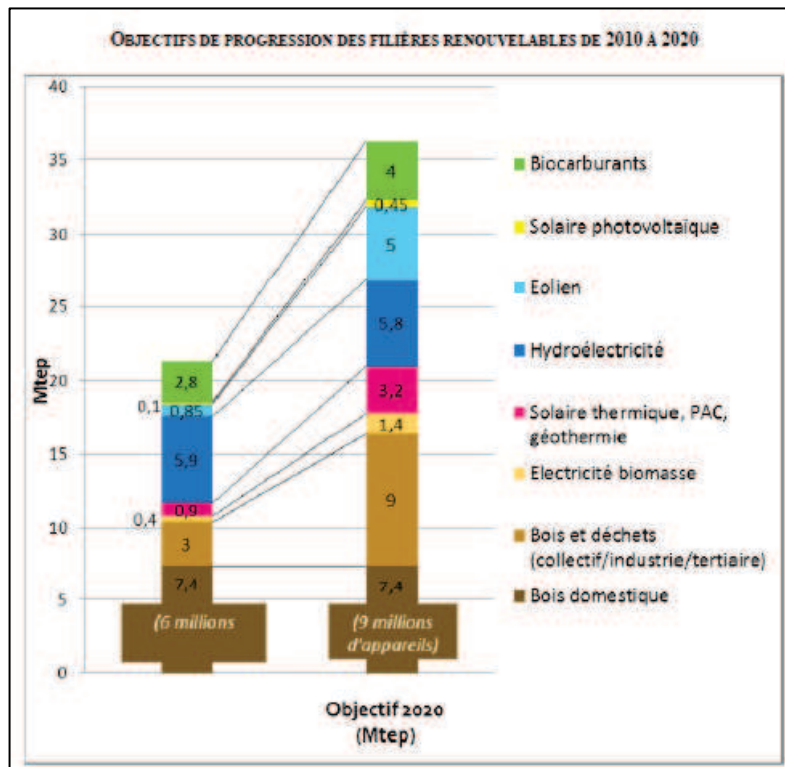


Figure I-6: Objectives to increase renewable energy resources in France from 2010 to 2020 [I-5]

## I.2 BIOMASS CLASSIFICATION AND CHARACTERISATION

The term biomass includes all non-fossilized and biodegradable organic matter deriving from plants, animals and micro-organisms [I-6, I-7]. It equally includes agricultural and forestry residues and the organic fractions of industrial and municipal wastes [I-6, I-7].

According to their sources, biomass can be classified as follows [I-6, I-8]:

- Agricultural residues (grains, bagasse, corn stalks, straw, seed hulls, nutshells, manure)
- Forestry by-products (wood chips, logs, bark, sawdust)
- Municipal waste (sewage sludge, food waste, refused-derived fuel, paper)
- Dedicated energy coppice and crops (poplars, willows, switchgrass, corn, canola and other vegetable oil)
- Biological (animal waste, aquatic species, biological waste)

### I.2.1 THE INTEREST OF LIGNOCELLULOSIC BIOMASS

The decline of fossil fuel reserves and growing awareness of environmental pollution led to producing biodiesel and bioethanol from vegetable oil, sugarcane and corn. However, there are some concerns regarding to the so called *first generation biofuels*, as they compete with food resources and can increase the food prices [I-9]. As a solution, new biomass resources have been exploited. The expression "*second generation biomass*" refers to lignocellulosic, not food-competitive materials.

The main groups of lignocellulosic biomass are: trees, short rotation forestry, short rotation coppice and energy crops [I-10]. The first group includes the forestry residues such as sawdust, thinning and clear-fell. Short rotation forestry refers to fast growing species resulting in relatively early yield (5 to 10 years) [I-10]. It includes alder, birch, poplar and different willow species [I-10]. Short rotation coppice are intensively growing species like willow salix or poplar, which can be harvested in 3 year cycles [I-11]. Energy crops are perennial herbaceous biomasses dedicated to energy production, like switchgrass or miscanthus.

Biomass feedstocks can also be differentiated according to their photosynthetic pathway. Terrestrial plants can fix CO<sub>2</sub> in three different ways. C<sub>3</sub> and C<sub>4</sub> pathways are the most common ones; the third pathway (CAM) is limited to very few plants [I-12].

The difference between C<sub>3</sub> and C<sub>4</sub> photosynthesis is the number of carbon molecules in the initial photosynthesis product [I-12]. While the C<sub>3</sub> pathway produces phosphoglycerate (C<sub>3</sub>H<sub>7</sub>O<sub>7</sub>P), the C<sub>4</sub> pathway forms oxaloacetate (C<sub>4</sub>H<sub>4</sub>O<sub>5</sub>) [I-12]. As C<sub>4</sub> plants build in greater amounts of carbon compared to C<sub>3</sub> plants, they are more appealing as biomass feedstock. Typical C<sub>3</sub> plants are trees and shrubs such as poplar, willow, but also wheat and cereal crops belong to this group [I-7, I-12]. The C<sub>4</sub> pathway is more typical for grasses and sedges such as miscanthus, sweet sorghum or maize [I-7, I-12].

## I.2.2 BIOMASS CHARACTERISTICS

The main characteristics of biomass as energy source are [I-7]:

➤ *the moisture content*

The moisture content decides the conversion route as the drying of biomass requires a big amount of unrecoverable energy, approximately 2260 kJ/kg moisture [I-13]. Therefore, high moisture content plants are more suitable for biological conversion pathways, while thermochemical processes require low moisture content (<15%) [I-14].

➤ *the calorific heating value (MJ/kg or MJ/L or MJ/Nm<sup>3</sup>)*

- *higher heating value (HHV)*; the heat released by cooling down the gas products to 25°C, including the latent heat of the steam condensation [I-6]
- *lower heating value (LHV) or net calorific value*; it does not take into account the latent heat of steam condensation (product gases are usually cooled to 120 to 180°C) [I-6]. While the LHV of bituminous coal is around 34 MJ/kg, biomass contains only 15-20 MJ/kg energy (19 MJ/kg for woody biomass and 17 MJ/kg for wheat straw) [I-7].

The heating value of different fuels can be well correlated to the atomic ratio of H/C and O/C [I-7, I-15]. As illustrated in the Van Krevelen diagram in Figure I-7, the heating value of the feedstock decreases with increasing H/C and O/C ratio.

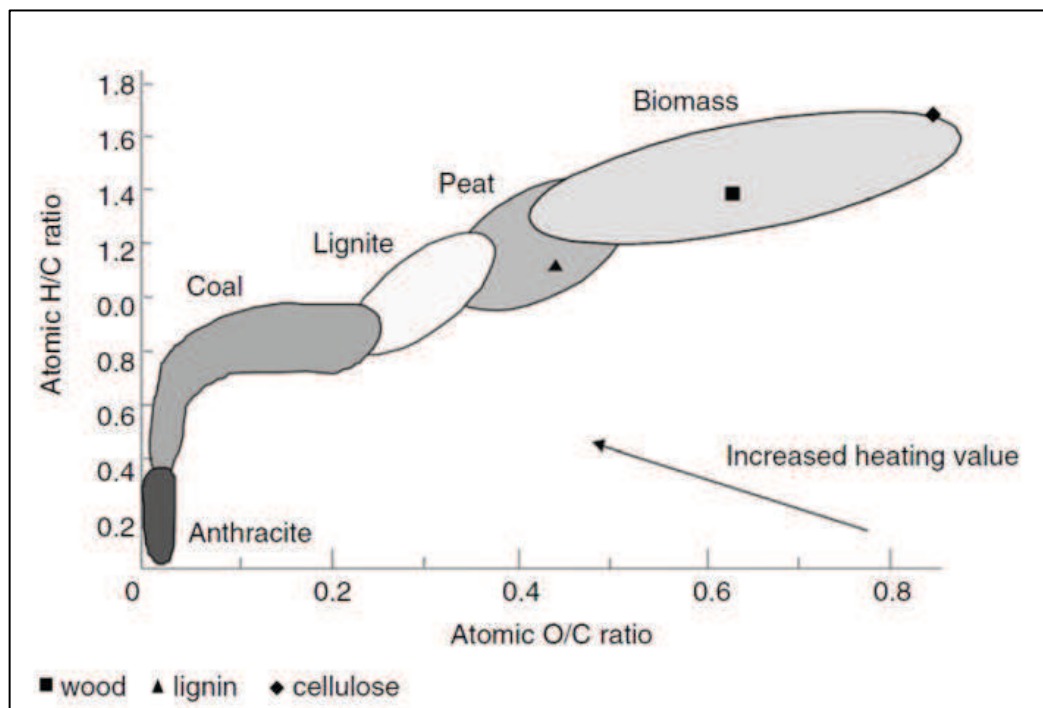


Figure I-7: Van Krevelen classification of fuels by atomic ratio [I-16]

➤ *the cellulose/lignin ratio*

The three main components of biomass are cellulose, hemicellulose and lignin [I-16]. Their proportion defines the way of suitable biomass conversion method [I-16]. While high cellulose content plants are more suitable for bioethanol production due to the easier enzymatic digestion [I-17], high lignin content plants are more favourable for thermochemical processes [I-18, I-19].

➤ *the proportions of fixed carbon (FC) and volatile matter (VM)*

The volatile matter means the condensable and non-condensable fraction of the fuel heated to a standard temperature (ASTM test protocol D-1102 and E-1755-01) [I-15].

The fixed carbon (FC) content is calculated by substituting the moisture, the volatile matter (VM) and the ash content of the fuel. The fixed carbon is an important evaluation of the fuel as it is related to the gasification rate and yield and it determines the size of the gasifier [I-15].

➤ *Ash content, alkali metal content*

It is important to take into consideration the composition and the amount of ash in biomass. Biomass feedstocks with elevated ash content, especially with high alkali concentration in the ashes can cause slagging<sup>1</sup>, fouling<sup>2</sup> and corrosion in different parts of a boiler [I-20] and they are likely to agglomerate with bed material [I-21].

➤ *Bulk density( $t/m^3$ ) or bulk volume ( $m^3/t$ )*

Bulk density and bulk volume describe the place needed for a certain amount of biomass. The bulk volume depends on the way of packing the biomass [I-15].

➤ *Yield (dry matter  $t/ha$ )*

The biomass yield means the availability of biomass per unit of land. The energy yield (GJ/ha) can be expressed by combining the yield with the higher heating value (HHV).

Table I-1 compares the main characteristics of different lignocellulosic biomasses, lignite and coal. The data are the average of different samples taken from the ECN Phyllis database [I-22]. All the biomasses contain around 10-15 wt % moisture, 80wt% volatile matter and 20wt % fix carbon. Their average heating value is around 20MJ/kg. In contrast to biomasses, fossil fuels contain less moisture and more ash, their volatile matter is less (35-50 wt %) and the fixed carbon and heating values are higher.

---

<sup>1</sup> Ash deposition in the hottest part of the boiler, slags are chemically active and difficult to clean [I-47]

<sup>2</sup> Ash deposition at lower temperatures (heat exchangers surfaces) [I-47]

Table I-1: comparing the main characteristics of different biomasses and fossil fuels

Biomass	Moisture	Volatile matter (VM)	Fixed carbon (FC)	Ash	Higher heating value (HHV)
	(ar %)* <sup>1</sup>	(daf %)* <sup>2</sup>	(daf %)* <sup>2</sup>	(dry %)* <sup>3</sup>	(MJ/kg) daf* <sup>2</sup>
Wood (fir/pine/spruce)	15	83	17	1	20
Willow	14	83	17	1	20
Wheat straw	10	81	19	7	20
Miscanthus Giganteus	14	83	17	2	20
Switchgrass	12	84	16	6	19
Lignite	13	50	50	9	26
Bituminous coal	4	32	68	10	33

\*<sup>1</sup>ar=as received (wt %), \*<sup>2</sup>daf=dry and ash free (wt %), \*<sup>3</sup>dry=dry basis (wt %)

### I.2.3 GIANT MISCANTHUS AS ATTRACTIVE BIOMASS FEEDSTOCK

Miscanthus is a commercially planted herbaceous energy crop (Figure I-8). It has about ten different genotypes, such as *Miscanthus floridulus*, *Miscanthus giganteus*, *Miscanthus sacchariflorus*, *Miscanthus sinensis*, *Miscanthus tinctorius* or *Miscanthus transmorrisonensis* [I-23]. Its most available type is a sterile clone, Giant Miscanthus or Miscanthus X Giganteus (MXG), which is the hybridisation of *Miscanthus Sinensis* and *Miscanthus Sacchariflorus* [I-19]. It can be propagated by rhizomes or in vitro cultures [I-24]. The botanical classification of Giant Miscanthus is given in Table I-2.



Figure I-8: Miscanthus X Giganteus (Chartres, France)

Table I-2: Botanical classification of *Miscanthus X Giganteus* [I-25]

Classification	
Kingdom	<i>Plantae</i> – Plants
Subkingdom	<i>Tracheobionta</i> – Vascular plants
Superdivision	<i>Spermatophyta</i> – Seed plants
Division	<i>Magnoliophyta</i> – Flowering plants
Class	<i>Liliopsida</i> – Monocotyledons
Subclass	<i>Commelinidae</i>
Order	<i>Cyperales</i>
Family	<i>Poaceae</i> – Grass family
Genus	<i>Miscanthus</i> Andersson – silvergrass
Species	<i>Miscanthus x giganteus</i> J.M. Greef & Deuter ex Hodkinson & Renvoize [ <i>I-sacchariflorus</i> x <i>sinensis</i> ] – Giant Miscanthus

Figure I-9 shows the key activities of the investigation of miscanthus as potential biomass in Europe and United States over the last century. Miscanthus is originated in Eastern-Asia and was introduced in Europe in the 1930s. Its renaissance has started as a potential biomass source in Northern European countries at the end of the 1980s [I-24]. Several studies examined the accessibility of miscanthus as biomass feedstock [I-1, I-9, I-18, I-24, I-26, I-27].

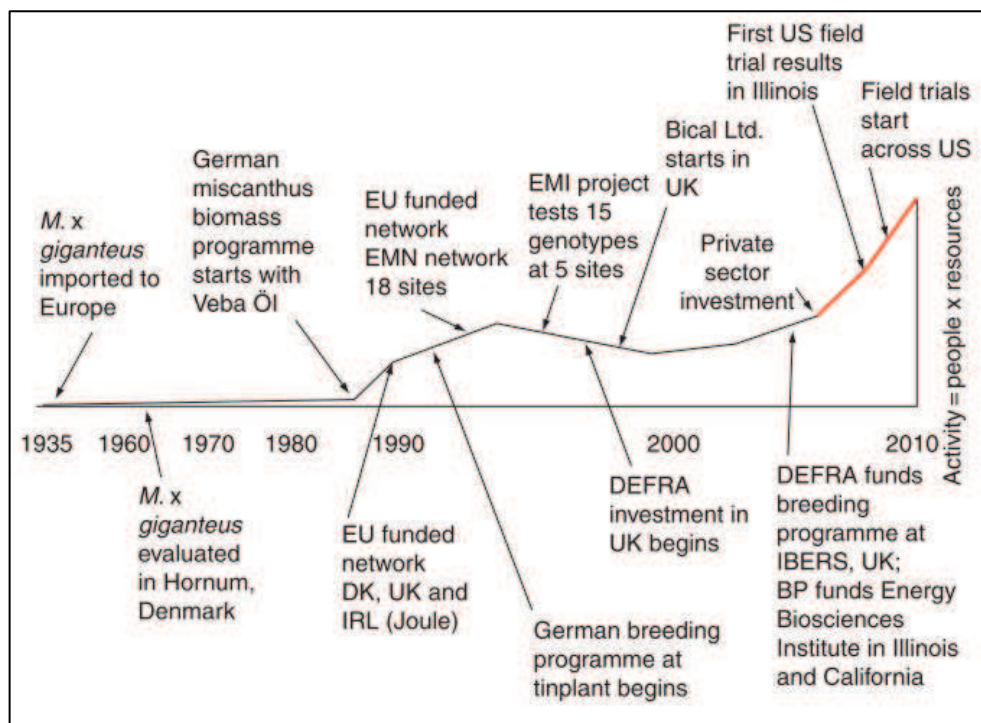


Figure I-9: Illustration of the key activities in miscanthus investigation [I-1]

Over the last 20 years, Giant Miscanthus proved to be a sustainable choice both from economic and ecological point of view due to the following properties:

- C<sub>4</sub> photosynthetic pathway
- High yield [I-24]; twice the amount compared to switchgrass production [I-1, I-26]
- Adaptability to different climates [I-24]; it can survive cold winters -20°C [I-26] and to different soils (pH 5.5 to 8)
- High CO<sub>2</sub> assimilation at lower temperatures (15°C) [I-18]
- Low fertilizer and pesticide requirement after the first 2 years
- Low nitrate leaching and water pollution [I-18]
- Hiding place for animals during the winter [I-18, I-24]

Though, there are still some difficulties to overcome:

- High establishment costs [I-24]
- Poor over-wintering at the first winter [I-24]
- Lack of water supply in South European region [I-24]
- Invasiveness in case of other genotypes such as *Miscanthus sinensis* [I-18]

### **Harvesting**

*Miscanthus* is usually harvested from February to April [I-24]. The standard machinery used in the agriculture has to be adapted to its height (2 to 4 metres) and stiffness [I-24]. Although an autumn harvest would give 30 to 60% higher yield, the quality of *miscanthus* improves with delayed harvest [I-24]. The ash content decreases over the winter due to the leaf loss and the mineral wash out. Its moisture content declines as well due to the drying effect of the wind [I-24].

### **Energy yield**

While some studies reported an energy efficiency ratio of 1:14 or 1:20 (the energy invested into the biomass cultivation, harvest, storage etc. versus the recovered energy) [I-24], others estimated a ratio as high as 1:37, which makes *miscanthus* highly competitive in comparison with other energy crops (switchgrass, willow, reed canary grass) [I-19]. The calorific heating value of *miscanthus* (MXG) is 16400 kJ/kg, approximately half that of fossil fuel [I-28]. Among other things, the composition of *miscanthus* depends on its harvesting time; it contains less ash, alkali metals and moisture if harvested late winter/early spring compared to harvest at autumn [I-19]. *Miscanthus* has a high concentration of lignin (>10%) therefore it is more adequate for combustion and gasification than for biofuel production [I-18]. As its lignin content is lower in the autumn, it could be adequate for biofuel production [I-18].

### **Ash content**

*Miscanthus* contains less minerals than wheat straw but it has higher ash content than willow or poplar [I-24]. Its ash content was reported between 2 to 4 wt % in case of spring harvest with about 25-40 wt % of SiO<sub>2</sub>, 20-25 wt % of K<sub>2</sub>O, 5 wt % of P<sub>2</sub>O<sub>5</sub>, 5 wt % of CaO and 5 wt % of MgO [I-24]. The composition of the ash can vary with weather conditions and soil type.

## I.3 BIOMASS INTO ENERGY

### I.3.1 RENEWABLE ENERGY CONVERSION ROUTES

Biomass can be transformed into heat, electricity, transport fuel or chemical feedstock [I-7]. The form of the required energy defines the conversion route, and the conversion route defines the adequate type of biomass [I-7]. Figure I-10 summarises the different biomass conversion techniques. The two main way of biomass conversion are the biochemical and thermochemical routes. Fermentation is used for ethanol production, while anaerobic digestion results in biogas (the mixture of  $\text{CH}_4$  and  $\text{CO}_2$ ). The thermochemical conversion includes pyrolysis, gasification, liquefaction and combustion.

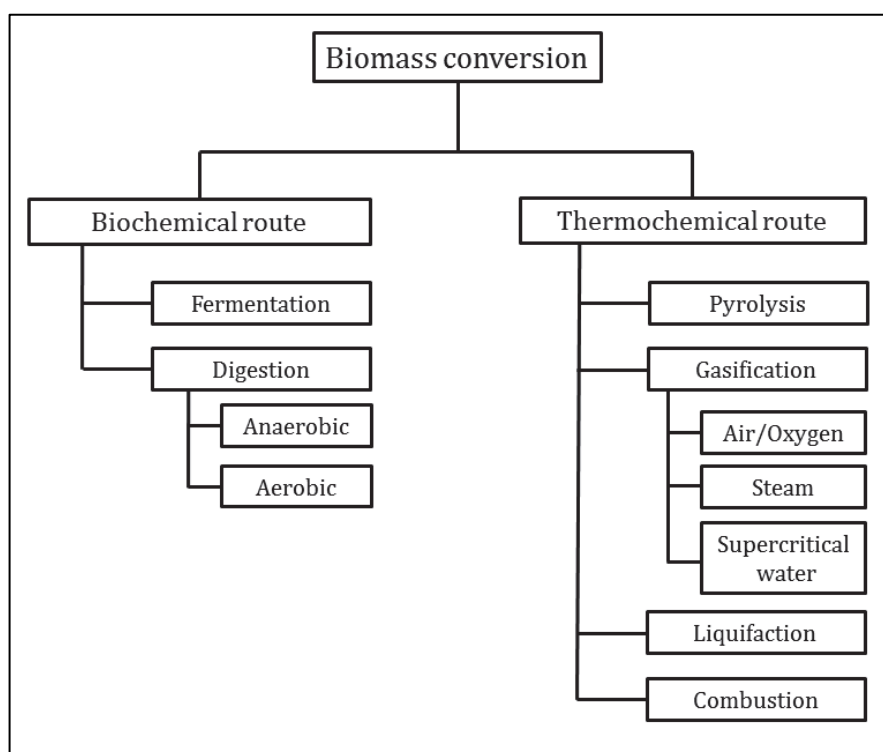


Figure I-10: Biomass conversion routes [I-6]

The main differences between the thermochemical conversion routes are the process temperature, pressure and the presence or partial/total absence of oxygen [I-29]. In case of *combustion*, biomass is burnt at around 800-1000 °C in oxygen excess for heat production. *Gasification* means the partial oxidation of biomass by air, oxygen or steam at elevated temperature (750-1400 °C) to produce a combustible gas mixture ( $\text{H}_2$ ,  $\text{CO}$ ,  $\text{CH}_4$ ) [I-13]. *Pyrolysis* means the thermal decomposition of biomass in the absence or limited supply of oxygen, typically in nitrogen atmosphere. The proportion of solid, liquid and gaseous products varies as a function of process parameters, such as heating rate, pyrolysis temperature (500-1000 °C) and vapour residence time [I-30–32].

Torrefaction is the mild form of pyrolysis, biomass is treated at 200-320 °C in the absence of oxygen when water and superfluous volatiles are removed and bio-coal is produced. During *liquefaction*, low temperature and high H<sub>2</sub> pressure are used to produce liquid hydrocarbons [I-29].

### I.3.2 FUNDAMENTALS OF GASIFICATION

Gasification is the partial oxidation of biomass, which transforms the organic matter into combustible gases [I-13]. The synthesis gas (CO and H<sub>2</sub>) allows a wide range of application: heat and electricity production, value added chemicals or biofuel via Fischer-Tropsch synthesis [I-28, I-33]. The process temperature varies from 750 to 1400 °C depending on the gasifier design technology [I-14].

Fundamentally, gasification means the endothermic reactions of carbon with carbon-dioxide or steam [I-13]. As illustrated in Figure I-11, in industrial applications gasification consists of different conversion zones [I-13,I-14]:

- *heating and drying* the biomass
- *thermal decomposition* (pyrolysis): in the range of 150-400°C resulting in char, hydrocarbons, H<sub>2</sub>O, CO<sub>2</sub> and H<sub>2</sub>
- *partial combustion* of gases into CO, CO<sub>2</sub> and H<sub>2</sub>O to promote the endothermic reactions and also to provide heat for drying and pyrolysis
- *reduction(gasification)* of char into CO, CH<sub>4</sub> and H<sub>2</sub>

The different reactions during gasification are listed in Figure I-12 .

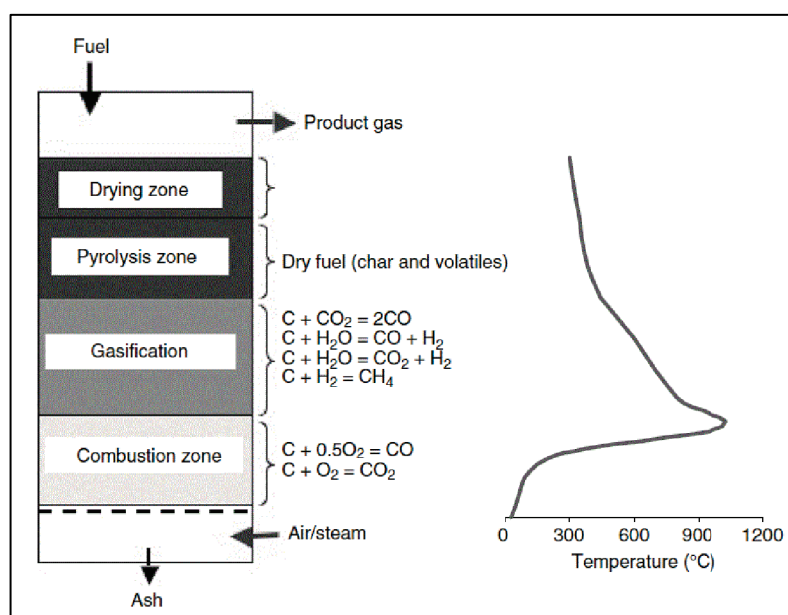


Figure I-11: The different conversion zones(drying, pyrolysis, gasification, combustion) and their temperature profile in a fixed bed gasifier [I-13]

Reaction Type	Reaction
<b>Carbon Reactions</b>	
R1 (Boudouard)	$C + CO_2 \leftrightarrow 2CO + 172 \text{ kJ/mol}$
R2 (water-gas or steam)	$C + H_2O \leftrightarrow CO + H_2 + 131 \text{ kJ/mol}$
R3 (hydrogasification)	$C + 2H_2 \leftrightarrow CH_4 - 74.8 \text{ kJ/mol}$
R4	$C + 0.5 O_2 \rightarrow CO - 111 \text{ kJ/mol}$
<b>Oxidation Reactions</b>	
R5	$C + O_2 \rightarrow CO_2 - 394 \text{ kJ/mol}$
R6	$CO + 0.5O_2 \rightarrow CO_2 - 284 \text{ kJ/mol}$
R7	$CH_4 + 2O_2 \leftrightarrow CO_2 + 2H_2O - 803 \text{ kJ/mol}$
R8	$H_2 + 0.5 O_2 \rightarrow H_2O - 242 \text{ kJ/mol}$
<b>Shift Reaction</b>	
R9	$CO + H_2O \leftrightarrow CO_2 + H_2 - 41.2 \text{ kJ/mol}$
<b>Methanation Reactions</b>	
R10	$2CO + 2H_2 \rightarrow CH_4 + CO_2 - 247 \text{ kJ/mol}$
R11	$CO + 3H_2 \leftrightarrow CH_4 + H_2O - 206 \text{ kJ/mol}$
R14	$CO_2 + 4H_2 \rightarrow CH_4 + 2H_2O - 165 \text{ kJ/mol}$
<b>Steam-Reforming Reactions</b>	
R12	$CH_4 + H_2O \leftrightarrow CO + 3H_2 + 206 \text{ kJ/mol}$
R13	$CH_4 + 0.5 O_2 \rightarrow CO + 2H_2 - 36 \text{ kJ/mol}$

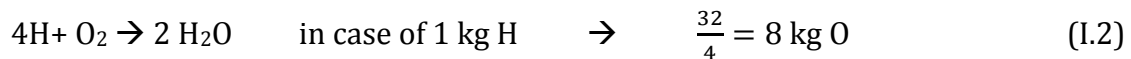
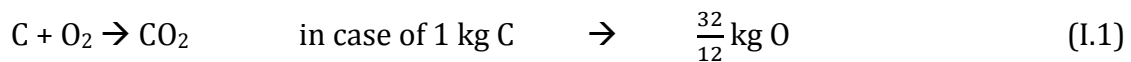
Figure I-12: Typical gasification reactions and associated enthalpies at 25 °C [I-13]

### I.3.3 STOICHIOMETRIC OXYGEN REQUIREMENT, EQUIVALENT RATIO (ER)

The gasifying agent can be oxygen, steam or air. While air and oxygen results in higher ratio of CO or CO<sub>2</sub> in the product gases, steam generates more H<sub>2</sub> [I-6]. The heating value of the product gas is also related to the gasifying medium [I-34]. Using air results in a net calorific value of 4-6 MJ/Nm<sup>3</sup>. Oxygen produces gas with a net calorific value of 10-15 MJ/Nm<sup>3</sup>, and steam creates a gas mixture with a net calorific value of 13-20 MJ/ Nm<sup>3</sup> [I-34]. In comparison, natural gas has a net calorific value of 36 MJ/ Nm<sup>3</sup> [I-34].

The application of some indices facilitates the comparison of different conditions during thermal processes [I-13].

The **stoichiometric oxygen requirement (kg)** means the amount of oxygen required to the complete combustion of the fuel, namely to transform the entire C content of the biomass into CO<sub>2</sub>, the entire H into H<sub>2</sub>O and the entire S into SO<sub>2</sub> [I-35].



It is calculated as:

$$\text{Stoichiometric oxygen requirement} = \frac{32}{12} C + 8 H + S - O \quad (I.4)$$

where C, H, S and O means the weight percent of carbon, hydrogen, sulphur and oxygen in the biomass.

During gasification, the oxygen supply is limited compared to combustion. The **equivalent ratio (ER)** expresses the ratio between the oxygen supply and the stoichiometric oxygen requirement. Usually, ER is 0.25 for industrial gasification [I-13].

$$ER = \frac{O_2 \text{ supply}}{\text{stoichiometric oxygen requirement}} \quad (I.5)$$

In case of steam gasification another index, the steam to biomass ratio (SB [kg]) can be used. It means the amount of steam used per kilogram biomass. According to the literature it is usually in the range of 0.25-0.35 [I-36].

## I.4 REACTOR TYPES

Gasifiers can be classified into three main types via their gas-solid contacting mode: (1) fixed bed, (2) fluidized bed and (3) entrained flow gasifiers [I-28, I-34, I-35].

Each type is suitable for different capacity. Fixed bed gasifiers are used for 10 kW<sub>th</sub> to 10MW<sub>th</sub> units (0.2-200 kg/h for downdraft and 0.5-15 t/h for updraft gasifier). Fluidized beds are suitable for medium scale applications between 5 MW<sub>th</sub> and 100 MW<sub>th</sub> (0.5-15 t/h for bubbling fluidized bed and 2-50 t/h for circulating fluidized bed). Entrained flow gasifiers are favourable for large scale applications (>50 MW<sub>th</sub>) [I-35, I-37, I-38].

### I.4.1 FIXED BED GASIFIER

In a fixed bed (also called as moving bed) gasifier, the biomass is fed at the top of the reactor and it slowly moves downwards [I-35]. The fixed bed installations are cheaper than fluidized bed gasifiers but the mixing and heat transfer in the reactor is at low rate which results in uneven temperature distribution [I-35]. Fixed bed reactors can be classified according to the release of the product gases in three main types; updraft, downdraft and cross-flow gasifier [I-34, I-35, I-37].

In updraft gasifiers (Figure I-13/A), the gasifying medium is introduced at the bottom of the reactor. The counter current design of biomass feed and gas flow allows a very effective heat utilisation: the gaseous products give their heat to the fuel and leave at the top of the reactor at relatively cold temperature [I-35]. The updraft design also has the ability to function with varying particle size, high-ash or high-moisture contents and low-volatility fuels [I-35,I-39]. Its disadvantage is the high tar concentration in the flue gas as some of the products of the drying and pyrolysis zone are released without undergoing second decomposition [I-39]. This makes updraft gasifiers unsuitable for high-volatility fuels [I-35].

In a downdraft gasifier (Figure I-13/B), the product gas is released at the bottom of the reactor while crossing the accumulated hot ash. The heat of the ash promotes the tar cracking into non-condensable gases [I-35]. As heat exchange with the feed cannot take place, the gases leave the reactor at high temperature (900-1000°C) and their heat energy is lost [I-34, I-37].

In a cross-draft gasifier (Figure I-13/C) the product gases leave on the side of the reactor. This design has a small reaction zone with low thermal capacity, but it is adequate to load changes.

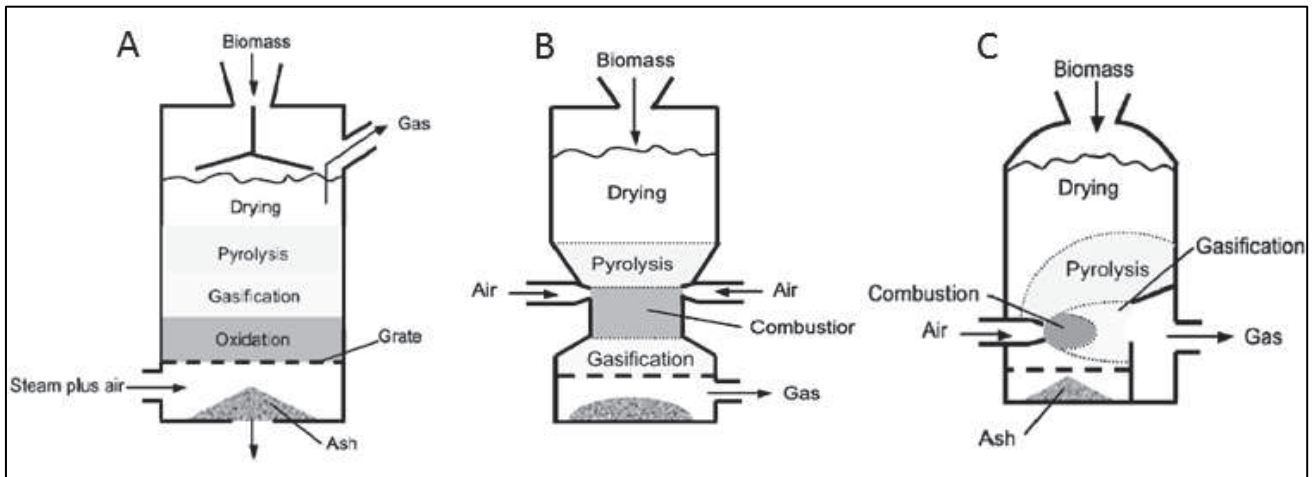


Figure I-13: Updraft (A), downdraft (B) and cross-draft (C) gasifier [I-35]

#### I.4.2 FLUIDIZED BED GASIFIER

In fluidized bed reactors the bed materials, usually inert heat resistant mineral particles, are kept in fluidized state by the gasifying medium [I-35]. The fluidization will be discussed in details in Chapter V. Due to the good mixing of the bed, the different zones (drying, pyrolysis, gasification and oxidation) cannot be differentiated [I-39]. Fluidized beds are annealing for biomass gasification because of the low process temperature (800 to 900°C), good material mixing, isothermal operating conditions and product gases with higher heating value [I-35, I-39, I-40]. The operating temperature of the fluidized bed can be controlled by the ratio of the gasifying agent and biomass feed [I-39]. The disadvantages of fluidized beds are the sensibility of fuel size and the high tar and dust concentration in the flue gas [I-39]. Regarding the tar production, fluidized bed is between the updraft (50 g/Nm<sup>3</sup>) and downdraft gasifiers (1 g/Nm<sup>3</sup>), it produces approximately 10 g/Nm<sup>3</sup> [I-35].

Fluidized bed gasifiers can be operated under autothermal and allothermal conditions [I-39]. In autothermal gasification the gasifying agent is air or oxygen and some part of the fuel is combusted to provide the necessary heat within the process [I-39]. In allothermal gasification the gasifying agent can be steam, and the required heat is supplied from external source [I-39].

The two main types of fluidized bed reactors are bubbling fluidised bed and circulating fluidised bed (see Figure I-14) [I-34, I-39]. Their hydrodynamics are very different as the fluidizing velocity can be five to ten times greater in a circulating bed (4.5-6.7 m/s) than in a bubbling fluidized bed (1.2 m/s) [I-35, I-41]. In consequence, in circulating fluidized bed the solids are dispersed all over resulting in a long residence time for gases and fine particles. The bed particles are recovered from the flue gas in a cyclone and fed back to the bottom of the reactor [I-35]. Owing to the high fluidization velocity, circulating bed can cope with greater biomass feed. While bubbling fluidized bed reactor is used up to 25 MW<sub>th</sub>, circulating bed is adequate in higher ranges as well [I-35].

During gasification the heat for the endothermic reactions is supplied by partial combustion of the biomass. For economic reasons, air is preferred to oxygen but using air results in a product diluted in nitrogen. The twin fluidized bed (also known as dual fluidized bed) solves this problem by separating the combustion and gasification in two reactors.

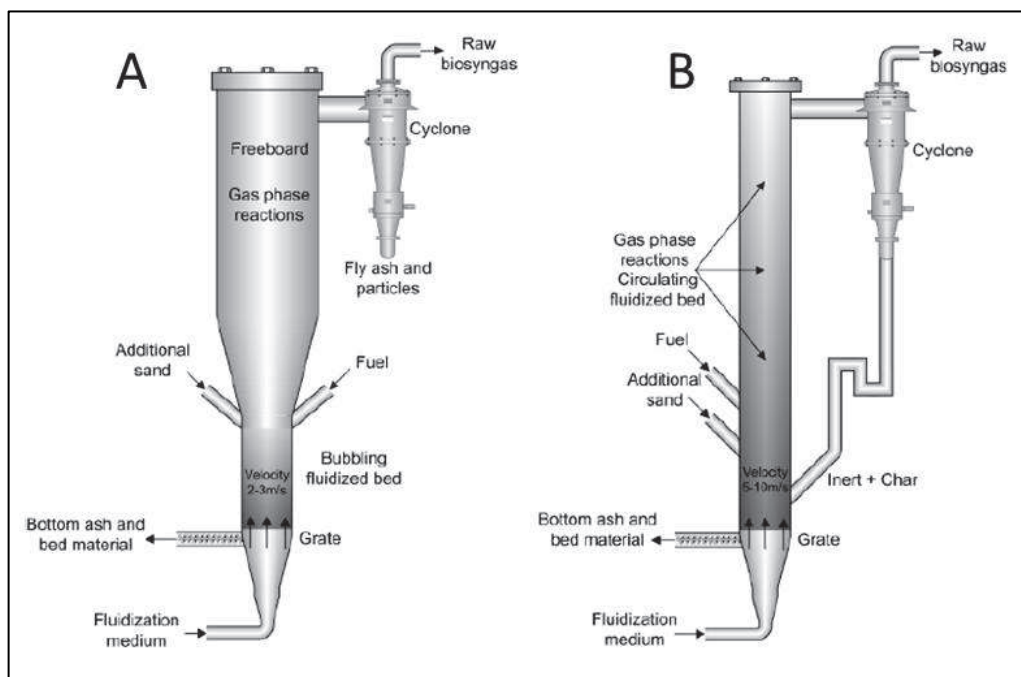


Figure I-14: (A) Bubbling and (B) circulating fluidized bed gasifier [I-39]

### I.4.3 ENTRAINED FLOW GASIFIER

In entrained flow gasifiers (Figure I-15) the pulverized fuel is injected at high speed at the top of the reactor and heated to high temperature ( $>1400$  °C) in the excess of oxygen resulting in  $H_2O$  and  $CO_2$ . As the oxygen is completely consumed at the feed, the residual char undergoes gasification in the  $H_2O$  and  $CO_2$  rich atmosphere at the downdraft part of the reactor. This design is mostly used for large scale coal, petroleum coke and refinery residues gasification [I-35], but its application for biomass gasification is becoming more and more common. As the reactor is operated at high pressure (30 to 80 bars), the product gas can be directly used in subsequent processes which further increases the efficiency of the process [I-42].

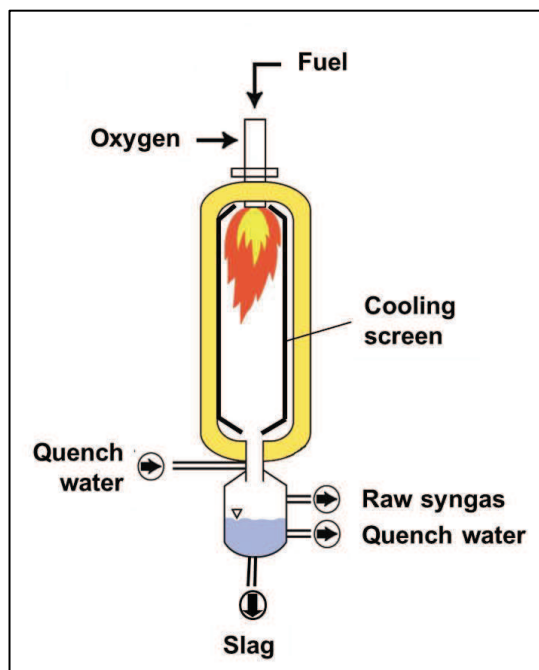


Figure I-15: Entrained flow gasifier [I-42]

#### I.4.4 CHALLENGES IN BIOMASS GASIFICATION IN FLUIDIZED BED

Despite the many advantages of fluidized bed for biomass gasification, many technical challenges have to be overcome. The main bottlenecks are related to the tar production, bed hydrodynamics and agglomeration [I-43].

Tar is mainly composed of aromatic compounds, acids and furans, which are generated during the pyrolysis of the char. These compounds are converted into smaller molecules and non-condensable gases ( $H_2$ ,  $CO$ ,  $CH_4$ ) by several heterogeneous and homogeneous reactions. The tar content of the syngas has to be minimized in order to avoid energy loss and cleaning costs. Tar can be decomposed by thermal or catalytic cracking. It is crucial to better understand the reaction kinetics of tar decomposition over different bed materials and the char [I-43].

The quality of the fluidization depends also on the biomass feed (shape, size and density). The costs can be lowered by enlarging the particle size flexibility of bubbling fluidized bed gasifiers. The current models have to be improved by taking into account the segregation and the attrition effects (fragmentation and abrasion) [I-43].

Agglomeration is related to the inorganic species present in the biomass. Lignocellulosic biomass contains high levels of alkalis and silica which form silicates and tends to melt below the process temperature. In consequence, the bed particles become sticky and form agglomerates. These agglomerates cannot be maintained by the gas flow, therefore the bed segregates and defluidizes [I-33]. The relative tendency of defluidization for some biomass

species in descending order is: miscanthus≈ straw≈ olive pomace > reed canary grass> lucerne>salix (willow)>birch [I-21].

The defluidization can be noticed by a sharp decrease in relative pressure drop and uneven heat distribution in the reactor [I-44, I-45]. Agglomeration highly depends on process temperature [I-21]: the higher the temperature in the reactor the more likely is the agglomeration [I-44, I-45]. The temperature gradient between a fuel particle and bed particle is also substantial as it can promote the transfer of volatized alkali from fuel to bed particle [I-21]. Agglomeration could be avoided by using lower operational temperature (<700 °C), but then other inconveniences, such as tar formation and char build-up would occur [I-21]. Increasing the gas velocity could break up the agglomerates but it would lead to char fly-out and energy loss. Although the operating temperature is an important factor, other parameters such as biomass or bed material composition also have to be taken into account [I-46].

## I.5 OBJECTIVES OF THE THESIS

The demand for energy diversification and the new objectives of the European Union and France highlight the interest in biomass sources and technology development. The advantage of using lignocellulosic biomass is that it does not compete with food resources and it is available in many forms such as forestry and agricultural residues or dedicated energy crops. Miscanthus is a perennial energy crop and it has been in the spotlights since early 90s due to its adoptability to different climates, high yields and low maintenance costs.

Gasification is a suitable technology for lignocellulosic biomass conversion. It produces syngas, the mixture of CO and H<sub>2</sub>, allowing a more versatile utilisation of the product as heat, electricity, chemical feedstocks or biofuel. Fluidized beds are well adapted to biomass gasification due to the good fuel mixing, relatively low temperature and medium scale application. However, the fluidized bed gasification of biomass is still facing some challenges. The ANR project GAMECO aims to improve the most important issues: hydrodynamic modelling, the tar reduction and bed agglomeration. The laboratory CEMHTI contributes to this project with its expertise on inorganic behaviour at high temperature.

This work studies the contribution of miscanthus ashes to fluidized bed agglomeration with a physicochemical approach. It examines the phase transformation in miscanthus ashes at high temperature and the interactions at the ash-bed particle interface with different bed materials. This thesis has double objectives: (1) understand the role of inorganics in agglomerate formation and (2) provide guideline for industrial applications in order to minimize the risks of agglomeration.

The first step towards these objectives is describing the transformation of inorganics at high temperature. The structure of miscanthus stem, the analysis of inorganic content and the phase transformation of these inorganic compounds are discussed in the next chapter.

## I.6 REFERENCES OF CHAPTER I

- [I-1] Heaton EA, Dohleman FG, Miguez AF, Juvik JA, Lozovaya V, Widholm J, et al. Miscanthus : A Promising Biomass Crop Biology. *Adv Bot Res* 2010;56:75–137.
- [I-2] Longwell HJ. *The Future of the Oil and Gas Industry : Past Approaches, New Challenges*. 2002.
- [I-3] Capros P, Mantzos L, Tasios N, De Vita A, Kouvaritas N. *EU energy trends to 2030-update 2009*. 2010.
- [I-4] Earth System Research Laboratory-Global Monitoring Division n.d.
- [I-5] Lambert F-M, Rohfritsch S. *La biomasse au service du développement durable*. 2013.
- [I-6] Basu P. Introduction (Chapter 1). *Biomass Gasif. Pyrolysis*. First Edit, © 2010 Elsevier Inc.; 2010, p. 1–25.
- [I-7] McKendry P. Energy production from biomass (part 1): overview of biomass. *Bioresour Technol* 2002;83:37–46.
- [I-8] Tumuluru JS, Sokhansanj S, Wright CT, Boardman RD, Yancey NA. A review on biomass classification and composition, co-firing issues and pretreatment methods. *Biofuels Bioprod Biorefining* 2011;5:683–707.
- [I-9] Naik SN, Goud V V., Rout PK, Dalai AK. Production of first and second generation biofuels: A comprehensive review. *Renew Sustain Energy Rev* 2010;14:578–97.
- [I-10] Cheviot trees. [Http://www.cheviot-trees.co.uk/products%20and%20services/trees\\_srf\\_energy\\_crops.html](http://www.cheviot-trees.co.uk/products%20and%20services/trees_srf_energy_crops.html)
- [I-11] Caslin B, Finnan J, McCracken A. *Short rotation coppice willow best practice guidelines*, 2011.
- [I-12] Ehleringer JR, Cerling TE. C3 and C4 Photosynthesis. *Encycl Glob Environmental Chang* 2002;2:186–90.
- [I-13] Basu P. Gasification Theory and Modeling of Gasifiers (Chapter 5). *Biomass Gasif. Pyrolysis*. First Edit, © 2010 Elsevier Inc.; 2010, p. 117–65.
- [I-14] Ruiz J a., Juárez MC, Morales MP, Muñoz P, Mendivil M a. Biomass gasification for electricity generation: Review of current technology barriers. *Renew Sustain Energy Rev* 2013;18:174–83.
- [I-15] Basu P. Biomass Characteristics (Chapter 2). *Biomass Gasif. Pyrolysis*. First Edit, © 2010 Elsevier Inc.; 2010, p. 27–63.
- [I-16] Basu P. Production of Synthetic Fuels and Chemicals from Biomass. *Biomass Gasif. Pyrolysis*. First Edit, © 2010 Elsevier Inc.; 2010, p. 301–23.
- [I-17] Sebestyén Z, Jakab E, May Z, Sipos B, Réczey K. Thermal behavior of native, washed and steam exploded lignocellulosic biomass samples. *J Anal Appl Pyrolysis* 2013;101:61–71.
- [I-18] Jørgensen U. Benefits versus risks of growing biofuel crops: the case of Miscanthus. *Curr Opin Environ Sustain* 2011;3:24–30.
- [I-19] Hodgson EM, Nowakowski DJ, Shield I, Riche a, Bridgwater a V, Clifton-Brown JC, et al. Variation in Miscanthus chemical composition and implications for conversion by pyrolysis and thermo-chemical bio-refining for fuels and chemicals. *Bioresour Technol* 2011;102:3411–8.

- [I-20] Werkelin J, Skrifvars B-J, Zevenhoven M, Holmbom B, Hupa M. Chemical forms of ash-forming elements in woody biomass fuels. *Fuel* 2010;89:481–93.
- [I-21] Liliedahl T, Sjöström K, Engvall K, Rosén C. Defluidisation of fluidised beds during gasification of biomass. *Biomass and Bioenergy* 2011;35:S63–S70.
- [I-22] ECN Phyllis database. <https://www.ecn.nl/phyllis2/Browse/Standard/ECN-Phyllis#miscanthus>
- [I-23] United States Department of Agriculture, ARS, National Genetic Resources Program. Germplasm Resour Inf Netw - [I-Online Database] Natl Germplasm Resour Lab Beltsville, Maryland
- [I-24] Lewandowski I, Clifton-brown JC, Scurlock JMO, Huisman W. Miscanthus: European experience with a novel energy crop 2008;19:209–27.
- [I-25] United States Department of Agriculture, Natural Resources Conservation Service-Plants profile. <http://plants.usda.gov/java/profile?symbol=MIGI2>
- [I-26] Pyter R, Voigt T, Heaton E, Dohleman F, Long S. Giant Miscanthus: Biomass Crop for Illinois 2007:39–42.
- [I-27] Kludze H, Deen B, Dutta A. Impact of agronomic treatments on fuel characteristics of herbaceous biomass for combustion. *Fuel Process Technol* 2013;109:96–102.
- [I-28] Michel R. Gazéification catalytique du Miscanthus X giganteus et vaporeformage d'un composé modèle: Production de gaz de synthèse. 2009.
- [I-29] McKendry P. Energy production from biomass (Part 2): Conversion technologies. *Bioresour Technol* 2002;83:47–54.
- [I-30] Melligan F, Aucaille R, Novotny EH, Leahy JJ, Hayes MHB, Kwapinski W. Pressurised pyrolysis of Miscanthus using a fixed bed reactor. *Bioresour Technol* 2011;102:3466–70.
- [I-31] Bridgwater a. V. Review of fast pyrolysis of biomass and product upgrading. *Biomass and Bioenergy* 2011:1–27.
- [I-32] Basu P. Pyrolysis and Torrefaction (Chapter 3). *Biomass Gasif. Pyrolysis*. First Edit, © 2010 Elsevier Inc.; 2010, p. 65–96.
- [I-33] Bartels M, Lin W, Nijenhuis J, Kapteijn F, van Ommen JR. Agglomeration in fluidized beds at high temperatures: Mechanisms, detection and prevention. *Prog Energy Combust Sci* 2008;34:633–66.
- [I-34] McKendry P. Energy production from biomass (Part 3): Gasification technologies. *Bioresour Technol* 2002;83:55–63.
- [I-35] Basu P. Design of Biomass Gasifiers (Chapter 6). *Biomass Gasif. Pyrolysis*. First Edit, © 2010 Elsevier Inc.; 2010, p. 167–228.
- [I-36] Campoy M, Gómez-Barea A, Vidal FB, Ollero P. Air–steam gasification of biomass in a fluidised bed: Process optimisation by enriched air. *Fuel Process Technol* 2009;90:677–85.
- [I-37] Kirkels AF, Verbong GPJ. Biomass gasification: Still promising? A 30-year global overview. *Renew Sustain Energy Rev* 2011;15:471–81.
- [I-38] Lamarche P. Contribution à l'étude expérimentale et à la modélisation de la gazéification étagée de la biomasse en lit fixe. 2011.

- [I-39] Obernberger I, Thek G. Combustion and gasification of solid biomass for heat and power production in Europe-State of the art and relevant future development. In: Cenertec P, editor. 8th Eur. Conf. Ind. Furn. Boil., Vilamoura, Portugal: 2008, p. 1–24.
- [I-40] Öhman M, Nordin A, Skrifvars B-J, Backman R, Hupa M. Bed Agglomeration Characteristics during Fluidized Bed Combustion of Biomass Fuels. *Energy & Fuels* 2000;14:169–78.
- [I-41] Peña JAP. Bubbling Fluidized Bed (BFB),When to use this technology? IFSA 2011, Ind. Fluid. South Africa, Johannesburg, South Africa: 2011, p. 1–12.
- [I-42] Helmholtz Virtual Institute for Gasification technology.  
<http://www.hvigastech.org/71.php>
- [I-43] GAMECO ANR Project: Gazéification AMéliorée pour des applications. Biomass 2010.
- [I-44] Olofsson G, Ye Z, Bjerle I, Andersson A. Bed Agglomeration Problems in Fluidized-Bed Biomass Combustion. *Ind Eng Chem Res* 2002;41:2888–94.
- [I-45] Lin W. Agglomeration in bio-fuel fired fluidized bed combustors. *Chem Eng J* 2003;96:171–85.
- [I-46] Li S, Shang L, Teng H, Lu Q. A model for agglomeration in bio-fuel fired fluidized bed. *J Therm Sci* 2010;19:451–8.
- [I-47] Weber R, Mancini M, Schaffel-Mancini N, Kupka T. On predicting the ash behaviour using Computational Fluid Dynamics. *Fuel Process Technol* 2013;105:113–28.



---

# CHAPTER II: CHARACTERISATION OF MISCANTHUS

---

## ABSTRACT

Miscanthus is an herbaceous biomass originated in Asia and has been successfully cultivated in Europe for the last 30 years. In thermal processes its inorganic composition is crucial; they can increase the product yield via their catalytic effect [II-1–3] but they can also lead to slagging, fouling and corrosion at the operating temperature.

Fluidized beds are well adapted for biomass combustion and gasification but they still need to overcome some challenges. One of the main bottlenecks of fluidized beds is the agglomeration of bed particles due to the ash melting at relatively low temperature.

The agglomeration of bed particles perturb the fluidized state, it can lead to defluidization and process shut down. To avoid the untimely amortization of the installation and the decline in efficiency it is essential to understand the transformation of inorganic phases and their role in agglomeration.

The main ash forming elements in biomass are K, Na, Ca, Mg, Fe, Al, Si, P, S, and Cl. They serve different functions in the plant, hence they can be found in different forms such as ions, bound to the organic structures or oxides [II-4]. Their chemical form is of great importance as it will affect how they are released during the thermal treatment.

Although many studies reported the inorganic composition of biomass samples and ashes after the thermal processes, only few of them gave detailed description of phase transformations as a function of temperature [II-5].

The aim of this chapter is double: (1) investigation of the thermal degradation of miscanthus stem with focus on the appearance of crystalline and amorphous inorganic phases and (2) study the phase transformation of inorganics between 400 to 1400 °C to understand the liquid phase formation and its role in agglomeration.

This study was carried out with different analytical methods such as scanning electron microscopy-energy dispersive X ray spectroscopy (SEM-EDX), inductive coupled plasma-mass spectroscopy (ICP-MS), thermogravimetric analysis (TGA), X-ray diffraction (XRD) and chemical fractionation analysis (CFA).

The effect of different harvest time and oxidizing/reducing atmosphere were investigated.

Below 750 °C the inorganics are mainly present as salts (KCl, K<sub>2</sub>SO<sub>4</sub>, Ca<sub>3</sub>PO<sub>4</sub>), carbonates (CaCO<sub>3</sub>, MgCO<sub>3</sub>) and oxides (SiO<sub>2</sub>). The ash starts to melt around 750 °C the liquid phase is composed of SiO<sub>2</sub>, K<sub>2</sub>O, CaO and MgO. At higher temperature the solid phase is enriched in calcium silicates and phosphates.

## II.1 INTRODUCTION

In energy applications, the ash composition is commonly expressed in the form of oxides. But this does not reflect the reality as the inorganics are present in different chemical forms (salts, carbonates and oxides) according to their functions. Their chemical form is of great interest as it will affect the way inorganics are released to the gaseous phase or associated in the reactor during the thermal treatment.

Identifying and quantifying the inorganics in biomass involves certain challenges due to the relatively low ratio of inorganics/organic content in the plant, the variety of inorganic compounds, and their appearance both in crystalline and amorphous form.

Although many studies reported the inorganic composition of biomass samples and biomass ashes after gasification and combustion, only few of them gave detailed description of phase transformations as a function of temperature[II-5].

The aim of this chapter is double; (1) investigation of the thermal degradation of miscanthus stem with focus on the appearance of crystalline and amorphous inorganic phases and (2) study the transformation of inorganics between 400 to 1400 °C to understand their role in agglomeration.

This chapter starts with a state of the art of the structure of the miscanthus stem and the role of inorganics. Understanding the way the inorganics are distributed in the organic matrix can help to describe the phase transformations of inorganics at high temperature. The focus of this study is on the miscanthus stem, as only this part of the plant is considered as energy source in industry (usually energy crops are harvested at late winter or early spring after the senescence of the leaves). The analysis of organic phases (degradation of lignin, cellulose and hemicellulose) is out of the frame of this study.

The characterisation of inorganics in miscanthus is divided in two parts.

The first part studies the evolution of inorganic phases with the thermal degradation of the organic structure. The analyses were carried out with SEM-EDX without major destructions of the organic matrix to be able to locate the main inorganic compounds in the stem.

The second part focuses on the phase transformation of miscanthus ashes between 400 and 1400 °C.

Although it was shown by Osman et al in 1983[II-6] and Bryers et al. [II-4] pointed out again that analysis on high temperature ashes (prepared above 250 °C) are not accurate to predict ash transformation due to the loss of alkalis, until now the CEN/TS 15403 ash preparation standard prescribes the fuel calcination at 550 °C and the ash fusion test is done on ashes prepared according to the standard method at 815 °C [II-7].

In this study, a relatively low temperature, 400 °C was chosen to prepare a start-up batch of miscanthus ashes considering two main limitations<sup>1</sup>. Firstly, the presence of organic carbon at low temperature which limits the characterisation methods and secondly the transformation and volatilisation of inorganics starting from 250-300 °C.

It was found that the heat-treatment of miscanthus at 400 °C in air can eliminate most of the organic part without major modification of the inorganic phases. The ash obtained this way can be easily handled in laboratory furnaces and the concentration of inorganics in the samples is sufficient to be analysed by different analytical methods (ash fusibility test, thermogravimetric analysis, X-ray diffraction, scanning electron microscopy, inductive coupled plasma-mass spectrometer).

The start-up batch was prepared in air, as at 400 °C the reducing atmosphere would result in big quantity of char making it impossible to analyse the inorganic content. The transformation as a function of temperature was studied in details in oxidizing atmosphere. Being aware of possible differences in the reducing atmosphere of gasification, supplementary tests were performed on the start-up batch in reducing atmosphere corresponding to the gasification conditions with regard to the concentration of O<sub>2</sub>, N<sub>2</sub>, CO<sub>2</sub>, H<sub>2</sub>, CO<sub>2</sub> and H<sub>2</sub>O.

As it was mentioned previously, energy crops are harvested at the end of winter to avoid high alkali concentration. In this study we investigated the inorganic composition of miscanthus stem collected in September, to see to what extent the harvesting period influences the chemical composition of the inorganics.

Beside the basic analytical techniques, a sequential leaching procedure, the chemical fractionation analysis (CFA) was used to determine the chemical form of inorganics and to predict their reactivity during gasification[II-1].

---

<sup>1</sup> The miscanthus could not been directly ashed for high temperature analysis as the relatively low concentration of inorganics (2.1%) requires crucibles with great volume and the interaction between the ashes and the ceramic crucible above 750°C has to be taken into account. (Not to speak about the safety regulations of ashing the organic matter inside a laboratory.)

## II.2 STATE OF THE ART

### II.2.1 THE STRUCTURE OF MISCANTHUS STEM

Miscanthus is a vascular plant, which means that it has lignified tissues serving the transport of water and nutrients. Characteristically to monocotyledons, these conducting tissues are arranged in vascular bundles scattered in the stem. Staining is a widely used technique in biology to study the different organs of the plant. Cellulose and lignin can be stained with different colorant resulting in a better contrast of the microstructure. Usually two staining agents having different affinities to the different tissues are used together. The staining method is detailed in Appendix-A1.

Figure II-1 represents the cross-section of stained miscanthus stem. Figure II-2 illustrates the structure of vascular bundles. The parts of the stem starting from outside are [II-8,II-9] listed below.

- **Epidermis** is the outer protective layer of the stem
- **Cortex** consists of elongated cells (chollenchyma cells) with thick cellulose walls and small central vacuoles which serve the strengthening of the plant
- **Pith** is the spongy centre of the stem, composed of parenchyma cells/ground tissue with thin but flexible cellulose cell walls. These cells serve the storage of the water and the photosynthesis products.
- The **vascular bundles** are evenly distributed in a circle around the ground tissue and they can also be found in the centre of the pith. They are composed of phloem, xylem and bundle sheath cells.

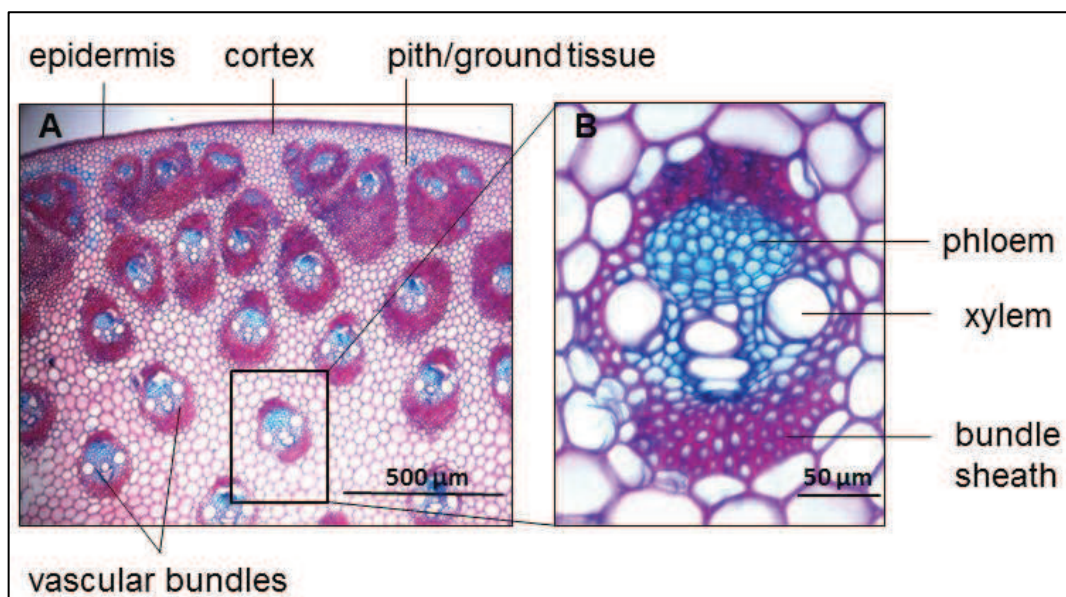


Figure II-1: Cross section of miscanthus stem (A), close-up of vascular bundle(B)  
(Images from Françoise Laurans INRA, Orléans)

- **Xylems** are thin tubes in the inner side of the vascular bundles which serve the transport of water and dissolved minerals from the roots to the leaves. Xylems are built up from dead hard walled hollow cells impregnated with lignin, called tracheids.
- **Phloem** is found in the outer part of the vascular bundle. It is built up of living cells (cellulose), so called sieve-tube members. These are connected by sieve plates with pores serving the transport of molecules. The phloems are responsible for the transport of the products of photosynthesis (carbohydrates-sucrose) from the leave to the roots.
- The vascular bundle is surrounded by **bundle sheath** for additional support.

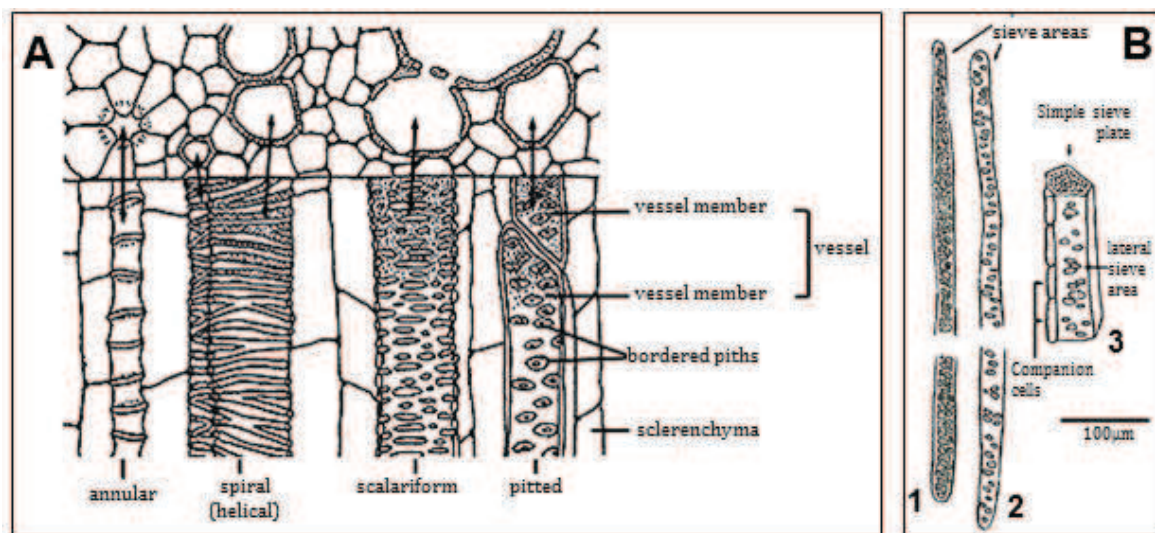


Figure II-2: Transverse and longitudinal view of xylem(A), longitudinal view of phloem(B) [II-10]

### II.2.2 THE ROLE OF INORGANICS

The main inorganics in lignocellulosic biomass are K, Na, Ca, Mg, Si, P, S and Cl. In small amount Al, Fe, Mn can be found as well. These inorganics serve different functions in the plant (support, transport, production), hence they are present in different forms. A summary of the different elements, their source and form is given in Table II-1.

According to the work of Bryers [II-4], sulfur can be found in organic compounds or in the form of sulphate in salts. Chlorine forms soluble salts as chloride ion. Phosphorus occurs as phosphate in soluble inorganic salts or in esters and pyrophosphates. Alkali metals, alkaline earth metals, aluminium, iron and manganese form soluble inorganic salts or they are present as free ions in solutions [II-4, II-11]. They can also be associated to the biomass fibres [II-4, II-11]. Silicon can have high deposition in the plant tissue providing enhanced strength and rigidity. It is not essential for the plant but it has beneficial effects on growing, development, yield and disease resistance [II-12]. The Si is taken up by the roots in the form of silicic acid and transported to the different part of the shoot by the xylem. It first forms colloidal silicic acid then polymerizes into silica gel ( $\text{SiO}_2 \cdot n\text{H}_2\text{O}$ ) [II-12]. In the stem, silica deposits can be found in the epidermis and vascular tissues [II-12]. As silicon is not mobile it accumulates with the aging of the plant [12].

Minerals can also derive from external source, from traces of soil or pollution during harvest and processing [13]. These minerals are usually in the form of oxides and they are less reactive than biomass derived inorganics having biological functions. Though, it is important to be aware of their presence as they can modify the ash behaviour, e.g. the aluminium silicates from the soil can bind the potassium and alter the ash melting tendencies [II-13, II-14].

*Table II-1: The source of minerals in the soil, their role and form in the plant [4]*

	Source	Role	Form
N	Organic (humus) or mineral ( $\text{NH}_4^+$ , $\text{NO}_3^-$ )	Protein formation	Organically bound
S	Atmospheric $\text{SO}_2$ , absorption from soil	Protein formation	organic sulfur or sulphates
Cl	Soil	Charge balance	Chloride ion
P	Soil, in the form of $\text{H}_2\text{PO}_4$	Energy transfer (ATP)	$\text{H}_2\text{PO}_4$ or esters, pyrophosphates
Si	Silicic acid $[\text{SiO}_x(\text{OH})_{4-2x}]_n$	Strengthening, resistivity	Silicic acid( $\text{SiO}_2 \cdot n\text{H}_2\text{O}$ ); or quartz
K	Soil	metabolic and transport roles	Potassium ion
Na	Soil	substitution for K, but toxic >2%	Sodium ion
Ca	Soil	cell wall stiffening, plant growth regulation	Organically bound
Mg	Soil	Photosynthesis	Organically bound
Al	Contamination	no biological function	Aluminium hydroxide or silicates
Fe	Soil	transport, reversible oxidation/reduction reactions	Chelates, mostly concentrated in leaves

### II.2.3 THE TRANSFORMATION OF INORGANICS AT HIGH TEMPERATURE

Many studies were dedicated to the characterization of biomass inorganic content and ash composition in gasification and combustion. As inorganic compounds can be found both in amorphous and crystalline phases, complementary analytical methods have to be used to be able to fully describe the ash composition. The methods used today were adopted from traditional coal characterisation at the end of 80s, beginning of 90s in the Scandinavian countries, where the residues of pulp and paper industry and wood manufacturing represent a significant energy source [II-15]. The two most utilised methods to characterise the biomass inorganic composition and to describe the ash transformation at high temperature are chemical fractionation analysis (CFA) and thermodynamic equilibrium calculations.

These methods had to be modified as the composition of coal ashes differs significantly from the one of biomass. Coal ash contains a lot of heavy metals (Fe, Al, Ti), sulfur, silicon, moderate amount of Ca and small amount of alkali metals. These elements are present as minerals. On the other hand, biomass ash is rich in alkalis, chlorine and phosphorus with complex chemical forms. Their form is of high interest as the way the elements are bound influences their volatilisation and melting behaviour.

The minerals can be grouped as [II-14];

- Salts
- Organically bound elements
- Minerals included in the fuel structure/minerals from external source

Chemical fractionation analysis (CFA) is a widely used method to determine the form of inorganics in the biomass feedstocks and ashes. CFA involves the consecutive leaching of samples in increasingly strong aqueous solvents.

It is considered that the distribution of the minerals in the different fractions can help to predict their behaviour at high temperature, namely the tendency to be released in the gas phase or remain in the bottom of the reactor [II-11].

Figure II-3 illustrates the different steps of the chemical fractionation analysis method. The biomass samples are first leached in water to dissolve alkaline salts and carbonates, then in 1 M ammonium acetate to dissolve organically bound alkaline and alkali earth metals. At last 1 M HCl solution is used to dissolve earth alkali sulphates and carbonates. The residue after the last washing step is composed of silicates and oxides.

Usually the original biomass or ash samples and the solid residues are digested in strong acid solution ( $\text{HNO}_3\text{-H}_2\text{O}_2$ ) and they are analysed along with leachates after each step by wet analytical methods (ICP-AES or ion chromatography) [II-11,II-15-17].

In the 2010s, many additional analytic techniques were developed to refine this method. Werkelin et al. measured the concentration of anionic groups in solid residues by methylene blue sorption [II-11]. Doshi et al. used the pH extraction analysis which determines the leachability curve of each element in the range of pH=2 and pH=12 [II-18]. Bonjoob et al.

developed a dynamic method using automated flow system with in situ pH detection and online monitoring by ICP-AES [II-19].

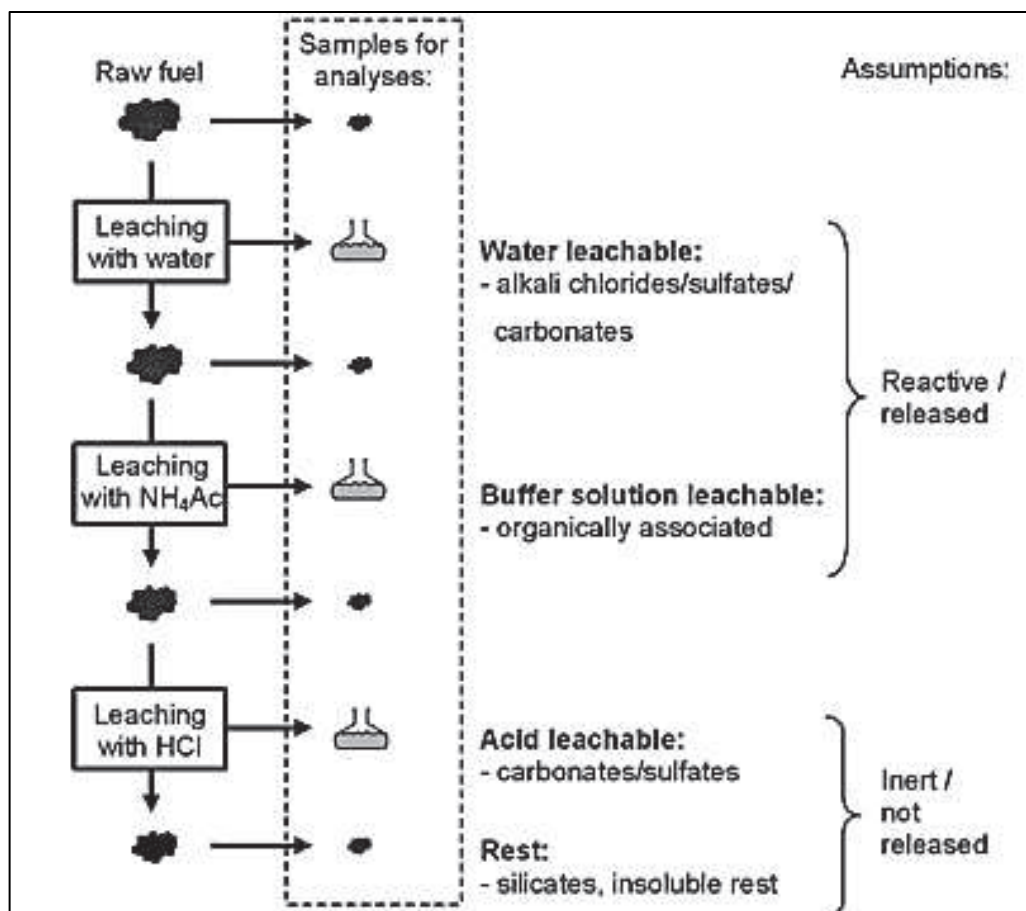


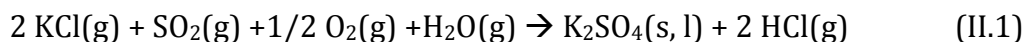
Figure II-3: Illustration of the chemical fractionation analysis (CFA) [II-20]

Werkelin et al. used the chemical fractionation analysis to describe the form of inorganics in woody biomass [II-11]. Jordan et al. completed this work with the analysis of fuel cane bagasse ashes after gasification experiments in an air-blown gasifier operated at 900 °C [II-1].

They found that the alkalis are present as water soluble salts ( $MCl$ ,  $M_2SO_4$ ,  $M_2PO_4$ ,  $M_2CO_3$ , where  $M=K, Na$ ) [II-11]. During gasification around 30% of alkalis are released into the gaseous phase; the rest remains in the bottom ash as salts [II-11]. The alkali earth metals are bound to the organic matrix [II-11]. Most of them are released into the gaseous phase; the rest forms oxides and silicates. Silica is present both in amorphous and crystalline phases in the biomass [II-11]. The amorphous phase is part of the biomass structure: the crystalline phase derives from soil pollution [II-11]. Only 15% of Si is released into the gaseous phase, most of it remains in the bottom ash and forms silicates with alkali and alkali earth metals [II-11].

Chlorine is a highly reactive element: 85 wt % of it volatilises. Sulfur is present as sulphate and organically bound sulfur in the biomass [II-11]. During gasification only 20 wt % is released into the gaseous phase; the rest of it transforms into organically bound sulfur [II-11].

It is important to note that the fate of sulfur changes during combustion. In oxidizing atmosphere the sulfur can capture the potassium and form  $K_2SO_4$  [II-17].



Based on many years of experience, Boström et al. proposed a simplified conceptual model to group the main reactions of ash transformation during biomass combustion [II-14]. They grouped the main reactions into primary and secondary ash transformation [II-14].

The primary ash transformation is related to the release of the elements from the organic matrix. They compared the affinity of the elements to oxygen and the affinity of oxygen to the carbon and hydrogen as a function of temperature. According to this approach the elements having high affinity to oxygen will stay in the form of oxides (Ca, Mg and Si). On the other hand, elements with lower affinity to oxygen than carbon or hydrogen will tend to stay unoxidized (K, Na, P, Cl) [II-14].

Therefore, it is likely that alkali earth metals appear as stable CaO and MgO and Si as  $SiO_2$ .

On the other hand, P, Cl, S, K and Na will tend to volatilise in the form of gaseous  $P_2O_3$ ,  $S_2$ ,  $H_2S$ ,  $SO_3$ ,  $Cl_2$ , HCl, KOH or NaOH. As these gaseous compounds are highly reactive, they will possibly reorganise.

The secondary ash transformation reactions include the reorganisation of the above mentioned oxides. As presented in Table II-2, these oxides can be divided in two groups: basic and acidic compounds. According to this approach, the formation of K-phosphates is the most probable. In case of K excess, K-sulphates will be formed, while the excess of phosphorus results in Na or Ca-phosphates [II-14].

High amount of K can lead to molten K-silicate phase incorporating alkali earth oxides at high temperature [II-14]. The excess of MgO and CaO can reduce the quantity of molten phase by the precipitation of Ca-Mg-silicates [II-14].

When the basic compounds are in surplus and the bed temperature is moderated the carbonate formation is favoured [II-14].

External minerals are stable compounds but their structure can be modified at high temperature and therefore can react with ash forming elements.

*Table II-2: Basic and acidic compounds in ash in order of their reactivity*

Basic compounds	Acidic compounds
KOH (l,g)	$P_2O_5$ (g)
NaOH(l,g)	$SO_2(g)/SO_3(g)$
CaO(s)	$SiO_2(g)$
MgO (s)	HCl(g), $Cl_2(g)$
$H_2O$ (g)	$CO_2$ (g)
	$H_2O(g)$

#### II.2.4 PREDICTION OF BIOMASS ASH BEHAVIOUR

The terms *sintering temperature* and *agglomeration temperature* are often alternately used in literature. Sintering temperature refers to the biomass ash melting and it is usually determined ex-situ with laboratory measurements. Agglomeration temperature is related to the fluidized bed processes and refers to the temperature when the bed defluidizes due to the ash melting and the accumulation of agglomerates. It is determined with in-situ measurements of pressure or temperature changes in the fluidized bed. As the bed material and process conditions (atmosphere, hot spots) play an important role, the agglomeration temperature is often lower than the sintering temperature.

Concerned about the ash related problems, many studies were performed to predict the fusion and volatilisation of inorganics in biomass feedstocks. Thermodynamic calculations, fuel ash characterisation methods, predictive indices are common methods to evaluate the ash behaviour.

Many studies use ***thermodynamic calculations*** to predict the inorganic phase transformation during different thermal processes [II-21–30]. Thermodynamic calculations are based on the minimization of Gibbs energy of the components at fixed pressure and temperature [II-21]. These calculations must be interpreted with care as there are certain limitations regarding the description of molten biomass ash. Comparing experimental results and calculations of liquidus temperature can show 200 °C difference [II-21, II-23]. The eligibility of thermodynamic calculations will be studied in Chapter III.

***Fuel ash characterisation methods*** are based on the change of certain physical parameters with the appearance of liquid phase upon heating the ash sample. The most common ash characterisation methods are the differential thermal analysis (DTA), the standard ash fusion test, dilatometry measurements, electrical resistance tests and the ash pellet compression test [II-31]. It has to be noted that these methods have limitations and the results always have to be handled with care. These measurements often treat already ashed samples, but the initial ashing temperature and the ash particle size can influence the sintering temperature, moreover, the heating rate of the sample also can alter the results [II-31]. These methods are ex-situ analyses and the atmosphere is usually different during combustion and gasification.

Ash fusibility test is a widely used method in industry to determine the sintering tendency of ashes. The standard ash fusion test consists of the preparation of an ash cone and the determination of four characteristic temperatures upon heating. The standard ash fusion test is not adequate to predict ash sintering tendencies as the ash samples used for this test are prepared at elevated temperature (550 to 815 °C according to different standards). As alkalis volatilise easily, their total concentration is not taken into account, and the sintering temperature is often overestimated with 150-200 °C [II-4, II-6].

During thermogravimetric analysis, the temperature difference of the ash samples and an inert material at constant heat flow is registered. The endothermic peaks of the registered curve refer to the decomposition, vaporization and melting of the ash.

The dilatometry or thermal mechanical measurement consists of measuring the expansion and contraction of the ash sample as a function of temperature. Upon heating, the ash first blows up then shrinks. This method determines the sintering temperature at the point where the sample starts to shrink.

The electrical conductance measurement is based on the principal that the conductance of the sample increases with the appearance of ionic liquid. The resistance of the ash sample is plotted versus temperature and the change of the slope indicates the melting of the ash.

For the compression strength measurement the biomass ash is pelletized, then the ash pastilles are heat-treated at different temperatures. After cooling down, the compression strength is measured in a standard device. A sharp increase in the measured strength values indicates the sintering temperature [II-31, II-32]. Skrifvars et al. compared the results of compression strength measurement with laboratory fluidized bed combustion tests for five different biomasses. They found only 20-50 °C difference compared to bed agglomeration temperature. The temperature which correspond to 3 N/mm<sup>2</sup> ash pellet strength showed even better agreement with fluidized bed tests [II-33].

**Predictive indices** compare the proportion of easily volatile (N, S, Cl), melt forming (K, Na) and stable (Ca, Mg) elements in the ash to evaluate the risk for aerosol emission, slagging, fouling, corrosion and agglomeration during energy conversion [II-34–39]. Many types of indices exist which consider different scenarios of ash behaviour. Industrials develop their own indices, as so far no equation exist which could be used for all kind of biomass fluidization [II-38]. Here, the most common indices are presented.

The molar alkali to sulfur and chlorine ratio (II.2) can give an estimation about the alkalis which will probably remain in the bed and cause agglomeration problems [II-34]. Alkalis favour to form salts with sulfur and chlorine which volatilise easily at the process temperature. If the amount of alkalis is higher than amount the amount of S and Cl, the risks of alkali induced agglomeration is present.

$$\frac{Na+K}{2S+Cl} > 1 \quad (II. 2)$$

The second index (II.3) considers the reaction between the silica sand bed and the alkali content of the fuel resulting in eutectic mixture of K<sub>2</sub>O-Na<sub>2</sub>O-SiO<sub>2</sub> with a lower melting point (<800 °C), than silica alone (1700 °C) [II-40].

$$\frac{K_2O+Na_2O}{SiO_2} > 1 \quad (II. 3)$$

The third index (II.4) considers that the ratio of Si and alkali earth metals can modify the ash melting and agglomeration tendencies. If Si is in excess, there is no sufficient amount of alkali earth metals to bind it in the form of stable Ca- or Mg-silicates.

Alkalis (Na and K) can be also added to this index as they further increase the agglomeration tendencies. The phosphorus (P) also has to be considered as many biomasses have high phosphorus concentration (sewage sludge). In the literature controversial approaches can be found for the effect of P in agglomerate formation. Sommersacher et al. found that high P content favours the ash melting; therefore they modified this index as [II-39]:

$$\frac{K+Na+Si+P}{Ca+Mg} > 1 \quad (\text{II. 4})$$

On the other hand, Visser et al. observed that phosphorus has an agglomeration lowering effect. During the fluidisation of silica sand bed, they observed double layer formation around the bed particles. The inner layer was rich in K, Na and Si, which result in sticky surface. The outer layer was composed of Ca, P, Mg having a higher melting temperature and disfavours the adhesion of silica sand particles [II-34]. Therefore they modified the index as:

$$\frac{K+Na+Si}{Ca+P+Mg} > 1 \quad (\text{II. 5})$$

The effect of P most probably depends on the form of P in the biomass and the availability of alkalis and alkaline earth metals. If P tends to associate with alkalis, it will lower the melting temperature while P bound to alkali earth metals will form solid phosphates.

The bed agglomeration index (BAI, II.6) considers that iron oxide can form  $K_2Fe_2O_4$  or  $Na_2Fe_2O_4$ , which have a higher melting point (1135 °C) than alkali silicates [II-31]. Fuels with lower values than 0.15 are considered to be problematic [II-37].

$$BAI = \frac{Fe_2O_3}{K_2O+Na_2O} \quad (\text{II. 6})$$

The base to acid ratio ( $R_{b/a}$ , II.7) evaluates the tendency of fouling. It calculates the ratio of basic and acidic oxides. In case of the excess of basic oxides, the risk of fouling is elevated. This index was modified by Kukla et al. for biomass ashes taking into account the fouling effect of  $P_2O_5$  [II-38].

$$R_{b/a} = \frac{Fe_2O_3+CaO+MgO+K_2O+Na_2O+P_2O_5}{SiO_2+TiO_2+Al_2O_3} > 1 \quad (\text{II. 7})$$

As the fuel composition and operating conditions can vary significantly, no general formula exists to describe agglomeration tendency for all cases. Most of the indices were studied in fixed beds or fluidized beds operated with silica sand. An alternative bed material which consists of different constituents than  $SiO_2$  can significantly modify the validity of these indices.

## II.3 STUDY OF THE INORGANICS IN MISCANTHUS STEM

The aim of Chapter II is to reveal the inorganic phase transformations in miscanthus stem at high temperature. This subsection investigates the degradation of organic part and the formation of new inorganic phases starting from ambient temperature up to the disappearance of organic residues (between 700 and 800 °C). These experiments were performed without destroying the fine structure of the organic network.

### II.3.1 COMPOSITION OF MISCANTHUS X GIGANTEUS

The miscanthus (specie *Miscanthus X Giganteus*) used in this study was harvested in April 2011 at La Ferté Chevresis, France (supplied by NovaBiom).

Table II-3 contains the ultimate analysis of miscanthus, the ash composition at 815 °C and the ash fusibility test of the ash at 815 °C. These analyses and characterisations were carried out by Socor Laboratory on the demand of Novabiom.

*Table II-3: Analysis of Miscanthus Giganteus X (April 2011, La Ferté Chevresis, France)*

<b>Miscanthus (La Ferté Chevresis)</b>	<b>Analyse by Socor</b>
Moisture content	15.1
Ash content at 815°C (%dry)	2.1
Carbon (wt %dry)	48.6
Oxygen (wt %dry)	43.0
Hydrogen (wt %dry)	5.8
Nitrogen (wt %dry)	< 0.3
Sulfur (mg/kg dry)	1669
Chlorine (mg/kg dry)	1002
Cellulose (wt %dry)	48.4
Hemicellulose (wt %)	23.9
Lignine (wt %brut)	10.9
Ash composition (wt %)	
SiO <sub>2</sub>	66
K <sub>2</sub> O	14.1
CaO	10.4
MgO	2.5
Na <sub>2</sub> O	1.1
P <sub>2</sub> O <sub>5</sub>	1.6
SO <sub>3</sub>	1.5
Al <sub>2</sub> O <sub>3</sub>	1.0
Fe <sub>2</sub> O <sub>3</sub>	1.1
TiO <sub>2</sub>	<0.1
MnO <sub>2</sub>	0.3

## II.3.2 PREPARATION OF SAMPLES FOR SEM-EDX ANALYSIS

As demonstrated in Figure II-4 and Figure II-5, small pieces of the dried stem were separated with a blade into the outer rigid part (cortex) and the inner spongy structure (pith).

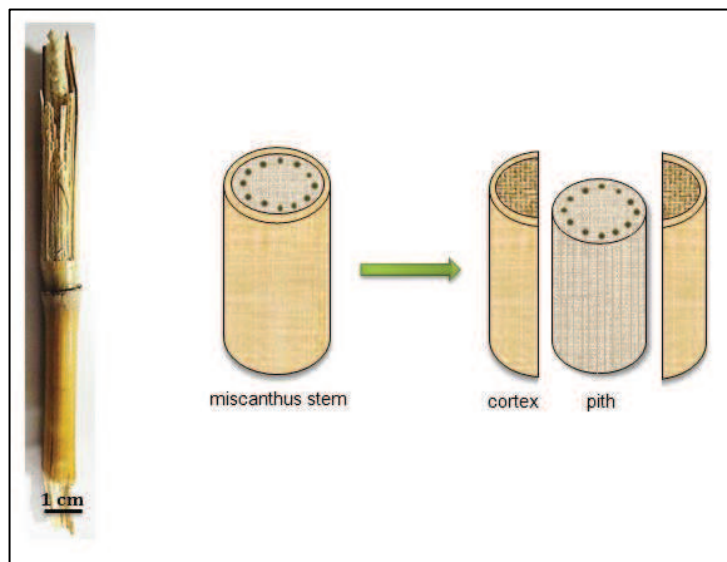


Figure II-4: Separating dried stem of miscanthus into the pith and cortex

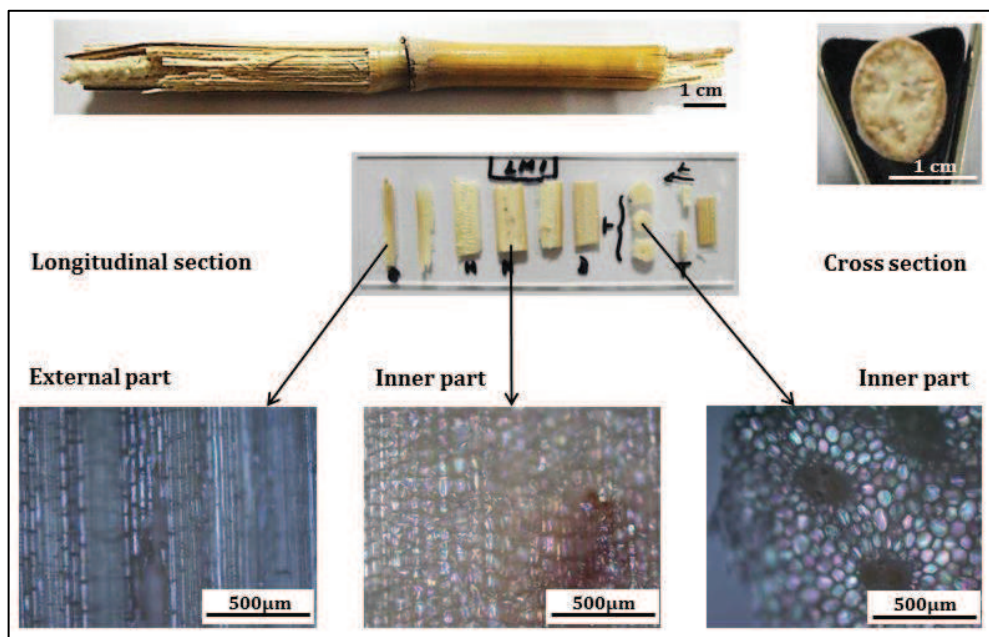


Figure II-5: Studying the different parts of miscanthus stem

These separated samples were heat-treated in air in laboratory furnace between 250 and 800 °C for two hours with a heating rate of 5 °C/min.

The morphology of the stem samples was studied by optical microscope (Olympus BX51) and scanning electron microscope (F.E.I., XL 40 TMP ESEM). The chemical composition was

determined by energy dispersive spectroscopy (SEM-EDX) with cobalt reference. The data were treated with the software of Oxford Instruments.

For imaging, low voltage (5kV) was applied in order to conserve the fragile structure of the samples. The stem pieces which were treated lower than 500 °C were not conductive and charged during the analysis; hence they had to be metalized by carbon or gold. It is important to note that the metallization by gold improves the image quality but inhibits the detection of small quantities of sulfur and phosphorus, as the signals of gold overlap with the signals of these elements.

For the qualitative elemental analysis 15kV electron beam was used. The pieces of the stem could not be embedded into resin and could not be polished due to their fine structure and fragility. Therefore, the qualitative analysis is only indicative as the samples do not have a plane surface (the electron beams scatter, and exact quantification is not possible). Nevertheless, this analysis is important as it offers an indication of elements and a rough estimate on their concentration in different parts of the stem. As the applied voltage during the qualitative analysis is higher than that during imaging, the electron beam penetrates the sample deeper. In case of thin layers, it often occurs that we do not see the same microstructure at a voltage of 5kV and 15kV. During the analysis the electron beams penetrate the sample in a drop shape of about  $1\mu\text{m}^3$ . Hence, it is possible that the analysis includes information of the material which is around the spot we want to observe.

## II.3.3 TRANSFORMATION OF INORGANICS AT LOW TEMPERATURE

Figure II-6 shows the miscanthus stem at room temperature.

In Figure II-6/A the cross section of a miscanthus stem is illustrated. In Figure II-6/B, the epidermis, cortex and vascular bundles can be observed. The cortex lies between the pith and epidermis; it is built up of elongated thick walled cells. Figure II-6/C shows one of the vascular bundles with the vessels of xylems and phloems surrounded by the ground tissue. The longitudinal view of a xylem vessel is shown in Figure II-6/F. The wall of the xylem vessel is composed of lignified scalariform tissue. Figure II-6/E shows the rectangular cells of the ground tissue of the pith. In Figure II-6/E the small pores on the cellwall can be observed. These cells serve the storage of water and carbohydrates, the pores insure the permeability of the cells.

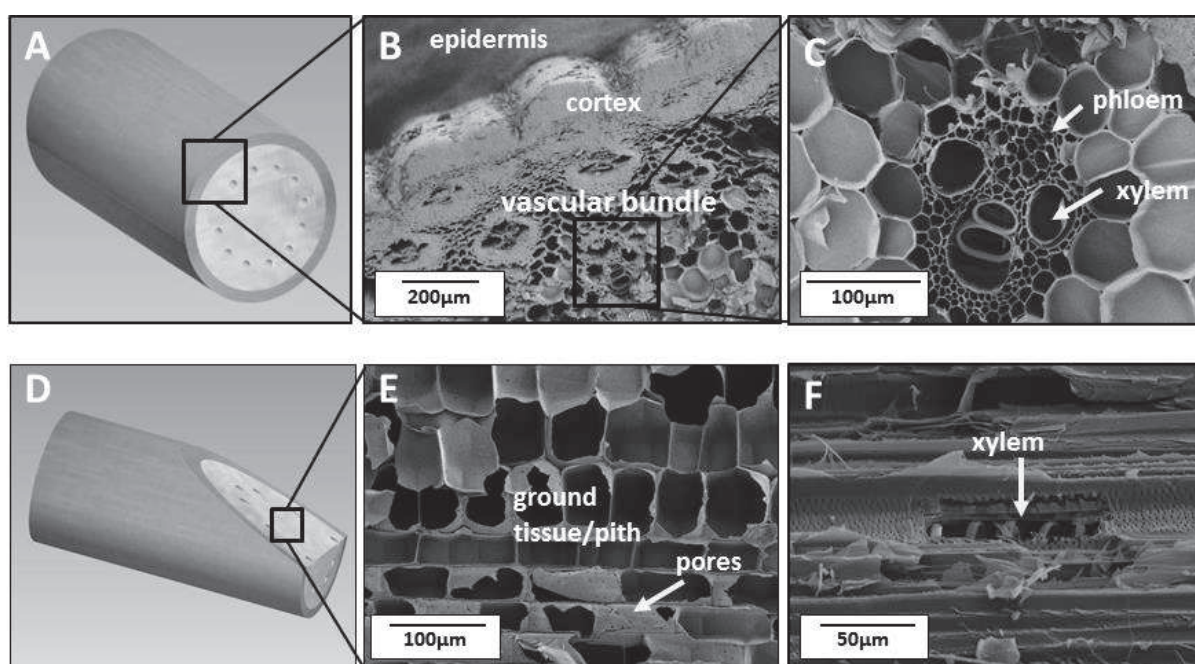
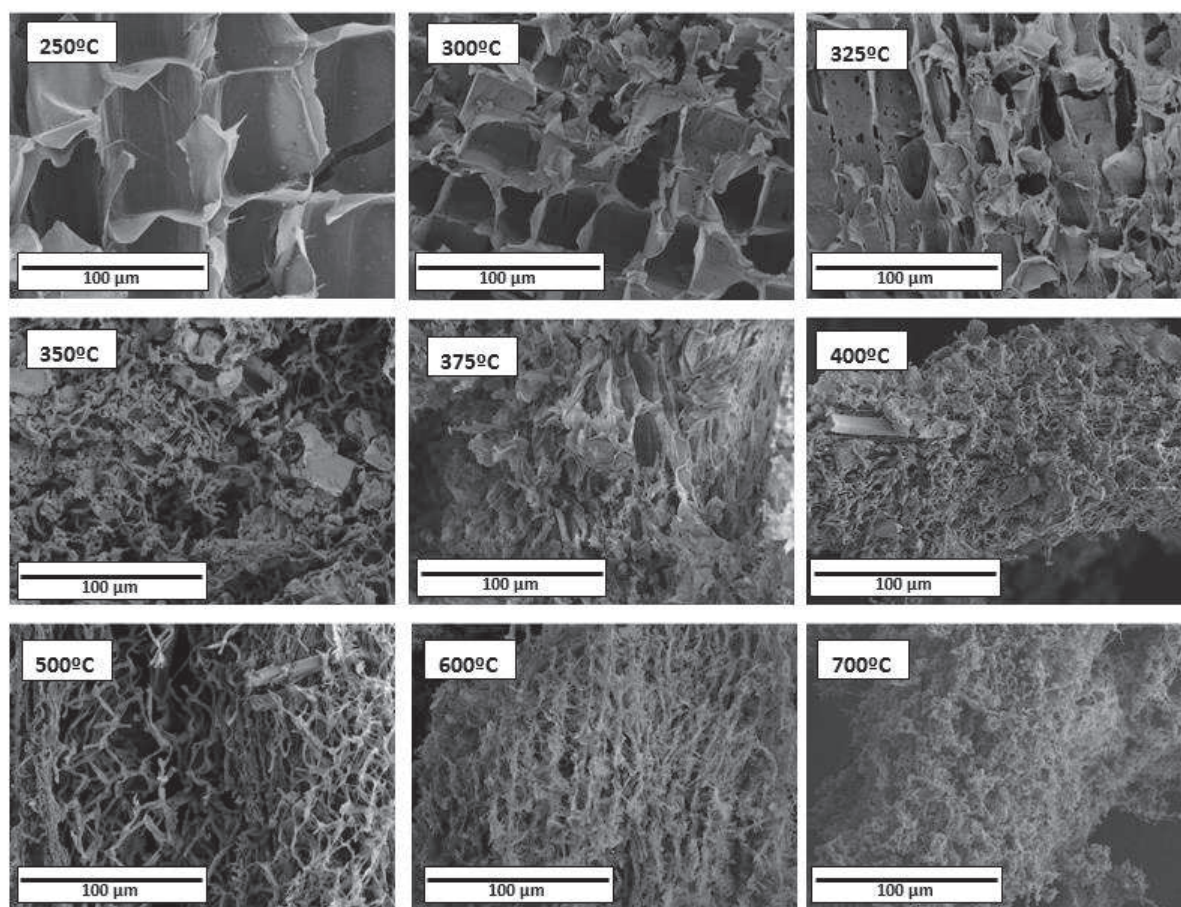


Figure II-6: Observation of miscanthus stem by SEM; above- cross section of the vascular bundle, below- longitudinal cut of the stem

Figure II-7 presents the thermal degradation of the pith between 250 °C and 700 °C.

The volume of the cells progressively decreases (to one quarter between 250 °C and 300 °C) and a cobweb-like structure develops between 325 and 375 °C. The molten residues of the cobweb-like structure can be still observed at 700 °C. Figure II-8 shows the thermal degradation of the outer part of the stem (cortex) up to 700 °C. The wrinkled structure is due to the vascular bundles lying underneath the cortex. At 325 °C, only small damages of the outer surface can be seen. At 500 °C we can still observe the original structure: the wrinkles are still visible, however the cortex is partly molten. The lignified tissue and the high Si concentration assure that the structure of the cortex is stable up to 500-700 °C. At 700 °C the

organic structure almost totally disappears and the cortex is completely melted. (The degradation of the stem observed with optical microscope is shown in Appendix-A2.)



*Figure II-7: SEM images of the thermal degradation of pith between 250 and 700 °C*

Below 250 °C, the inorganics are hardly detectable by SEM-EDX.

Figure II-9 shows the analysis of the cortex (A), pith (B) and the vascular bundle (C) at 250 °C. The cortex mostly contains silicon, while the vascular bundle and the pith are rich in potassium. Because of the organic matrix (peak of the carbon in the EDX), the potassium is hardly detectable. (The peaks of gold refer to the metallisation for better imaging).

Figure II-10 shows the SEM-EDX analysis of the stem and vascular bundle samples at 375 °C and the pith at 350 °C. The organic matrix has significantly decreased in each case (carbon signal is weaker). The cobweb-like structure of the pith has melted and gives a strong signal of potassium. The vascular bundle contains both silicon and potassium.

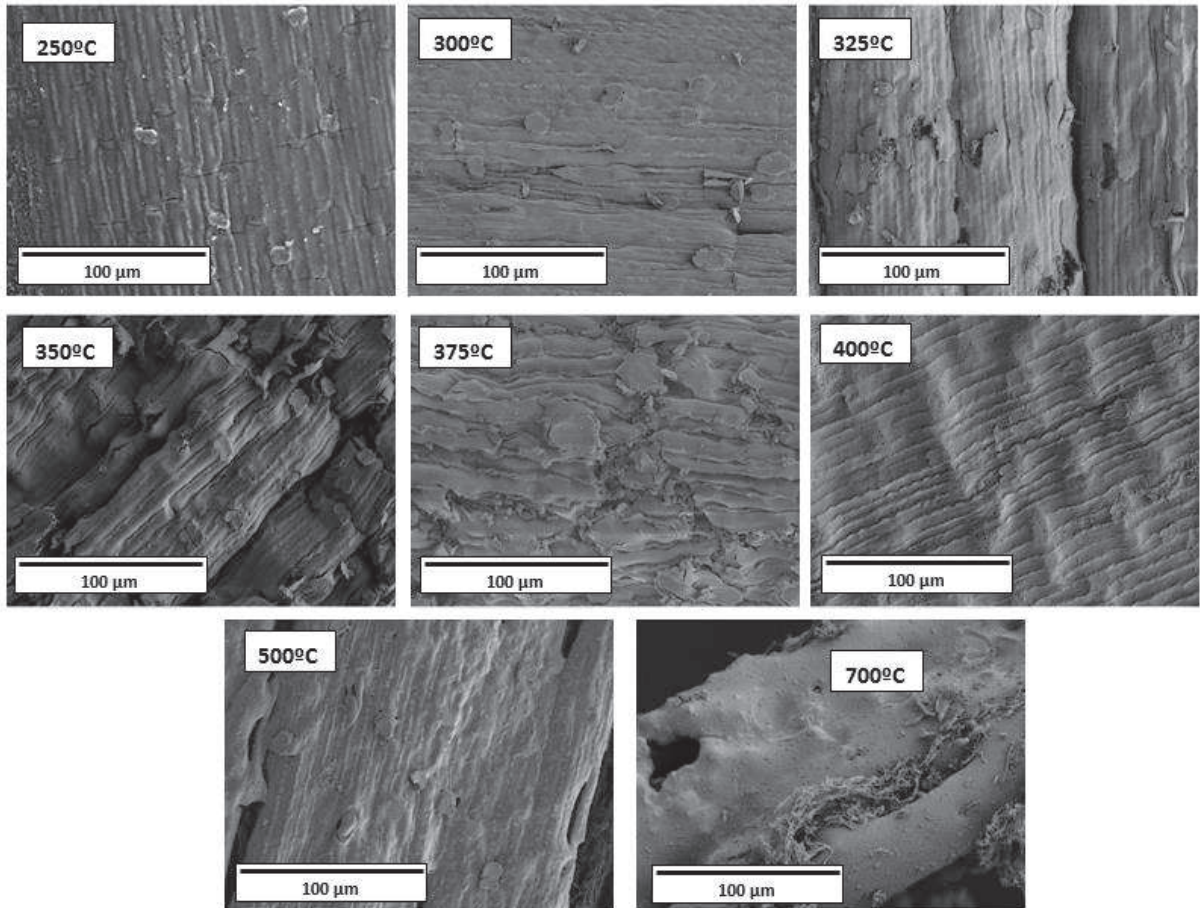


Figure II-8: SEM images of the cortex between 250 and 700 °C

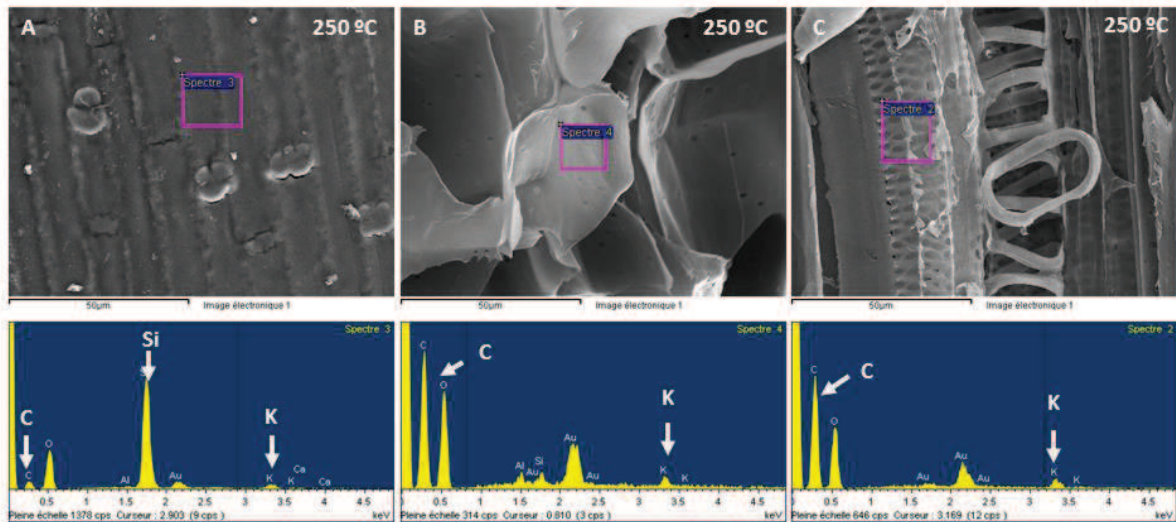


Figure II-9: SEM-EDX analysis of the stem, pith and the vascular bundle at 250 °C

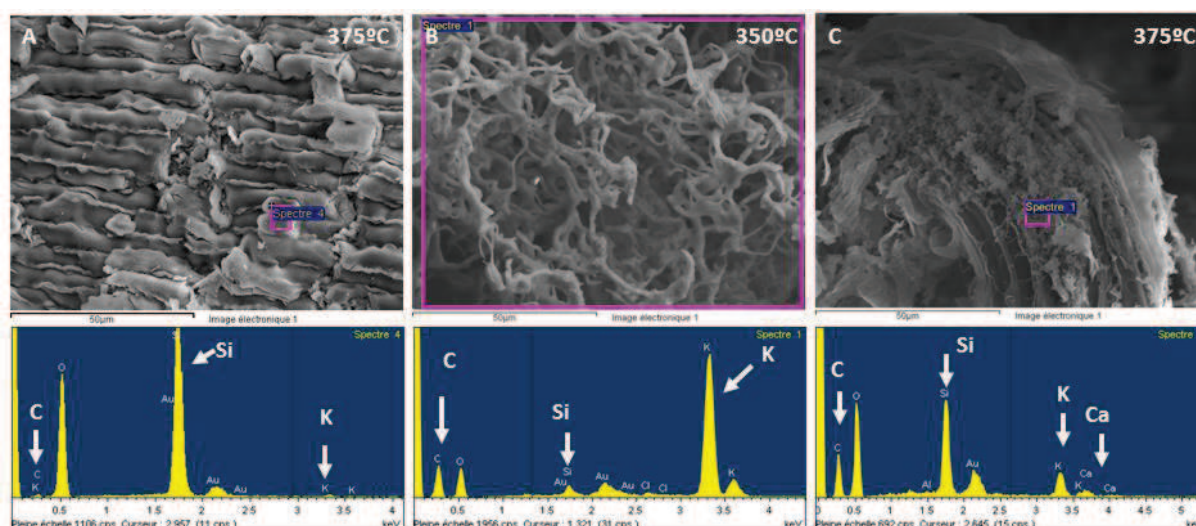


Figure II-10: SEM-EDX analysis of the stem, pith and the vascular bundle at 375 °C

A closer look at 375 °C shows the presence of small particles with a diameter of about 0.25  $\mu\text{m}$  just underneath the cortex (Figure II-11). These particles can also be observed in the vascular bundle (bended due to the heat shock) in Figure II-12. They are rich in Si and also contain some K, Ca and Mg. They most probably derive from the silica gel accumulated in the epidermis and the vascular bundle during the growth of the plant. The small amount of K, Ca, Mg comes from the degradation of the organic structure. In Figure II-12/2 the cross section of a vascular bundle can be observed which contains K and Si in the same order of magnitude.

In the fourth image of Figure II-12, small crystals of potassium containing a small amount of Si and Cl were observed on the cobweb-like pith.

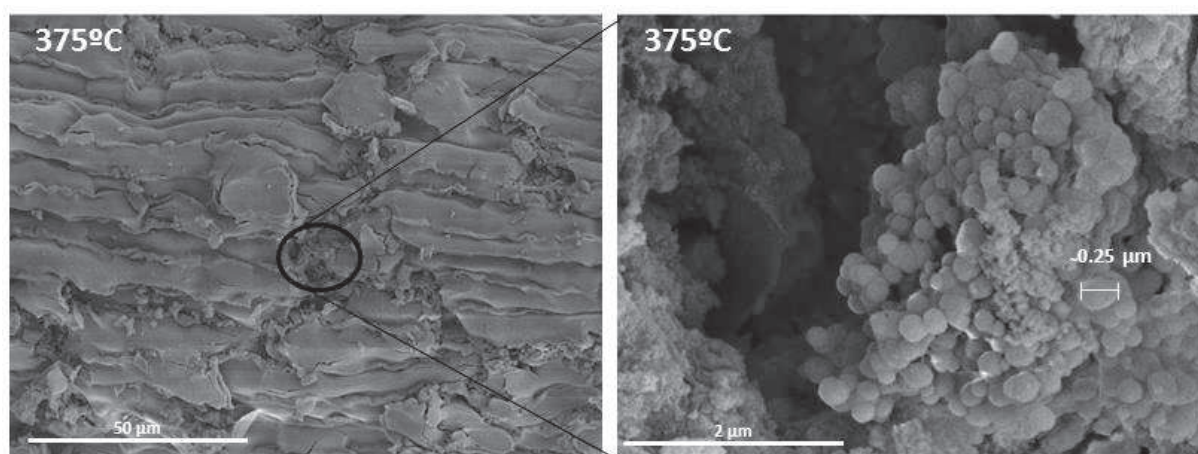


Figure II-11: Small particles underneath the cortex

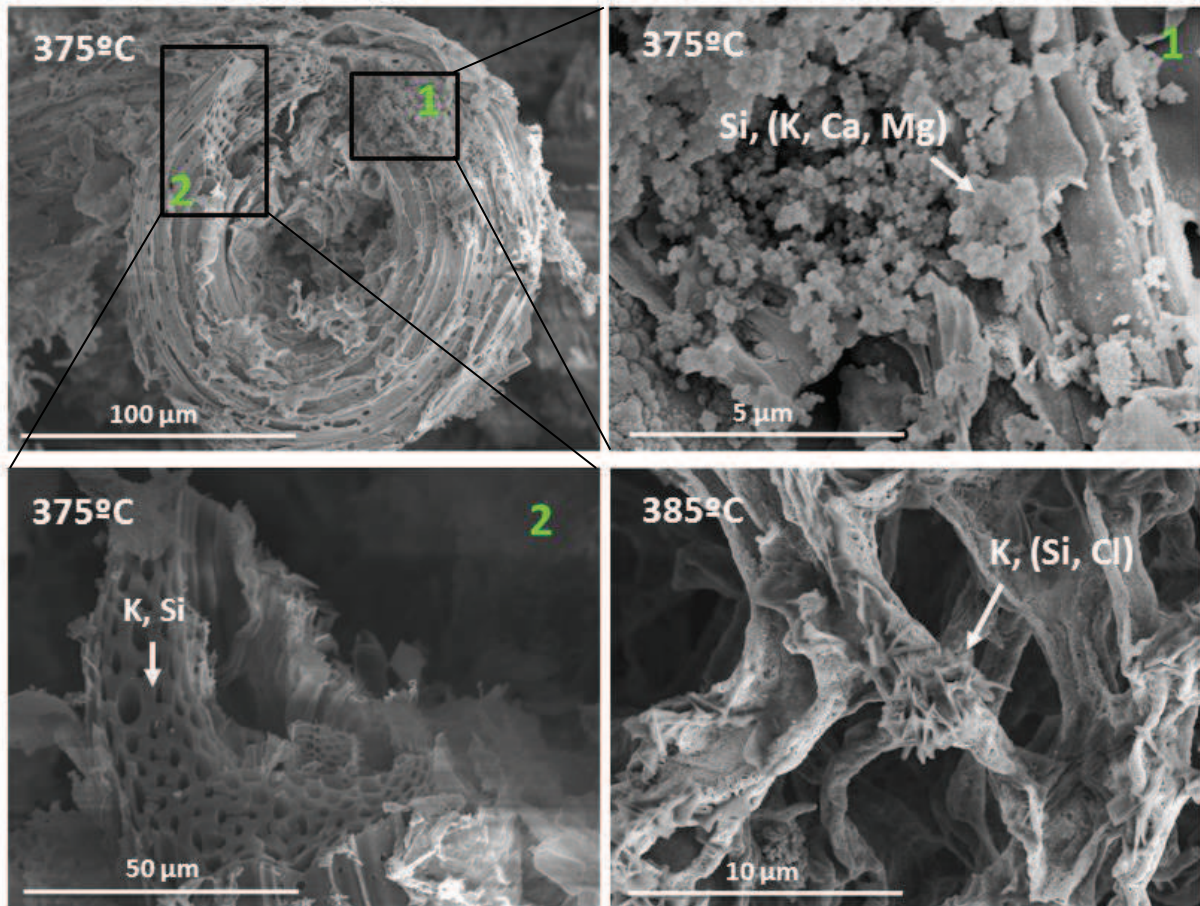


Figure II-12: Vascular bundle and pith heat-treated at 375 °C and 385 °C

Figure II-13 shows the cortex at 380 and 385 °C. Around this temperature, small crystals appear on the surface of the cortex. In Figure II-14 the crystals and partly molten structure on the two sides of the cortex can be observed even better at 400 °C.

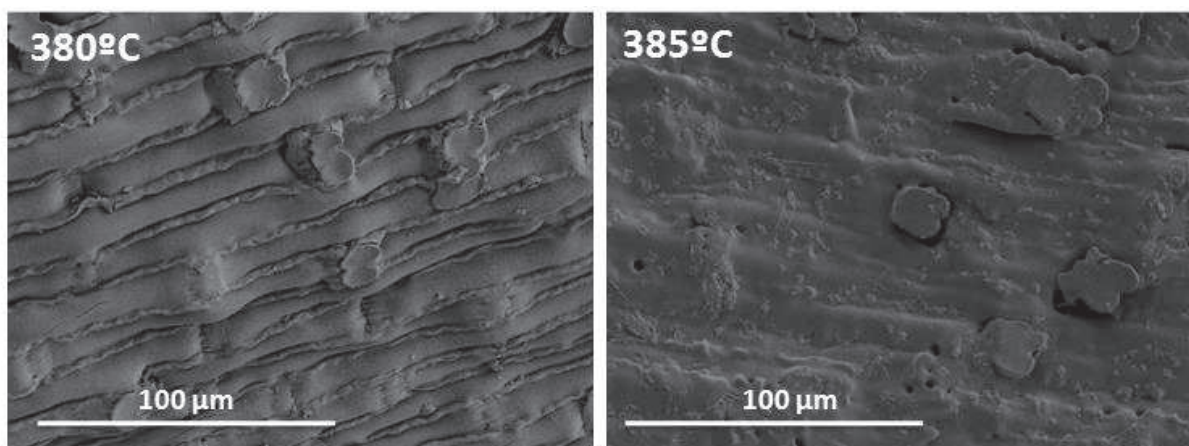


Figure II-13: Surface of the cortex at 380 °C and at 385 °C

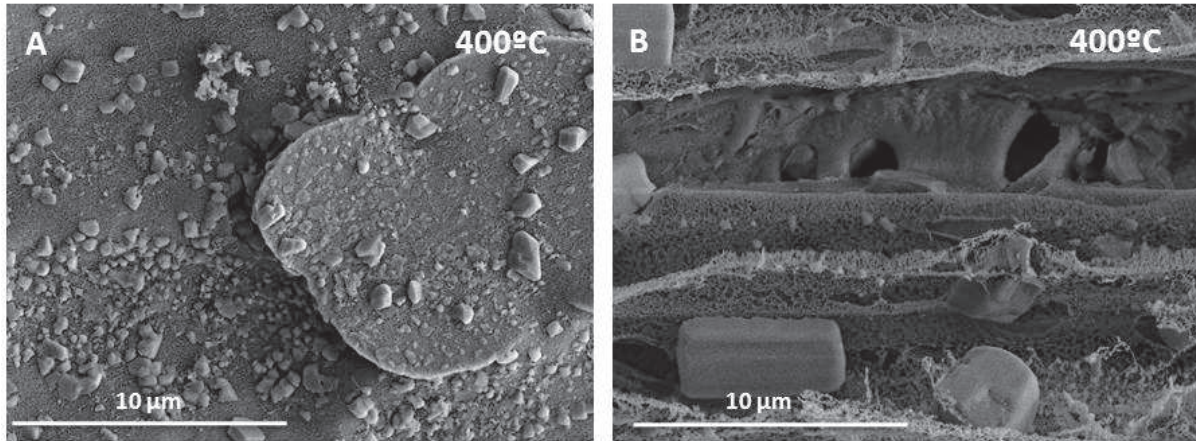


Figure II-14: Cortex from outside and from inside at 400 °C

As the degradation of the organic structure progresses, more and more ash forming elements become detectable by SEM-EDX analysis. Ca and Mg can be identified already around 375 °C, sulfur and phosphorus starting from 500 °C.

Figure II-15 shows the qualitative analysis of the cortex (A) and the pith (B) attached to the vascular bundle (C) at 500 °C. The stem is rich in Si and the signal of the K increased compared to lower temperatures. The pith is rich in Si with considerable amount of K and Cl. The analysis of the vascular bundle reveals high amount of Cl and K, possibly KCl crystals and a small amount of Si, Mg and Ca.

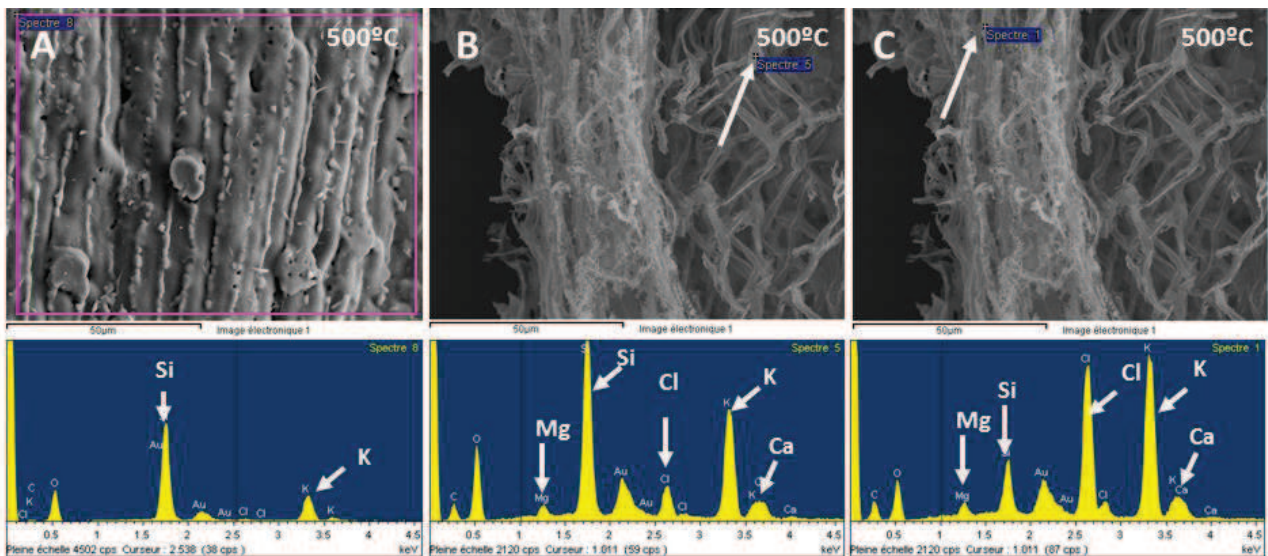


Figure II-15: SEM-EDX analysis of the stem heat-treated at 500 °C; a, pith; b, cortex; c, vascular bundle

Figure II-16 reveals the presence of small crystals in the cortex at 600 °C. The high magnification and the uneven sample surface increase the uncertainty of the analysis because of the pear-shape interaction volume of about  $1 \mu\text{m}^3$  and the scattering of electron beams. However, it can be evidenced that both the rectangular and spherical crystals are mostly

composed of Si and K. The fourth analysis point is in the inner side of the cortex which was bended back during the heat treatment. The SEM-EDX analysis displays moderate amount of sulfur.

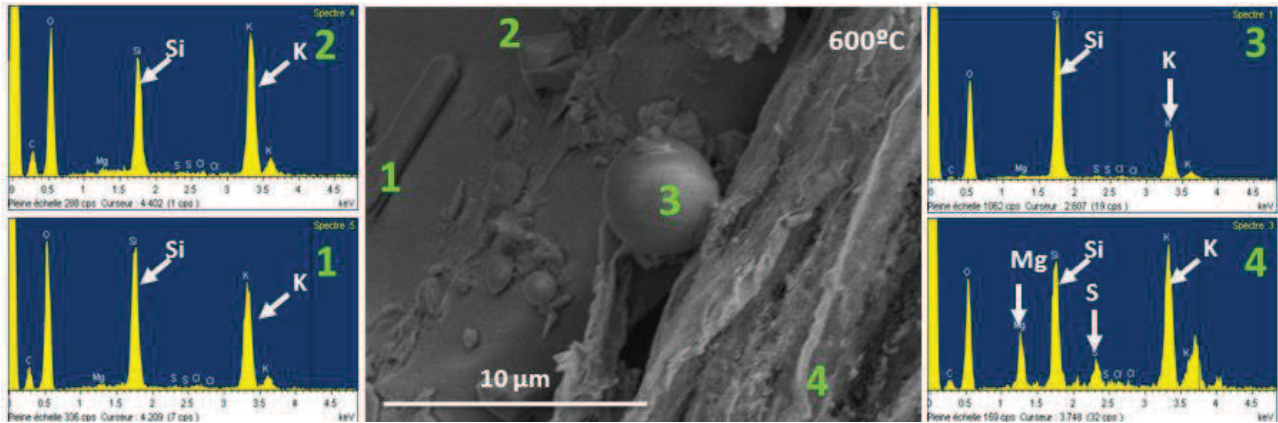


Figure II-16: SEM-EDX analysis of the cortex heat-treated at 600 °C

In Figure II-17 the residues of the molten cobweb-like structure and clusters of particles (already formed around 375 °C) can be observed. It seems like that these small particles ( $d=0.25 \mu\text{m}$ ) observed in Figure II-11 and Figure II-12 melted and accumulated into bigger grains of 7-8  $\mu\text{m}$ .

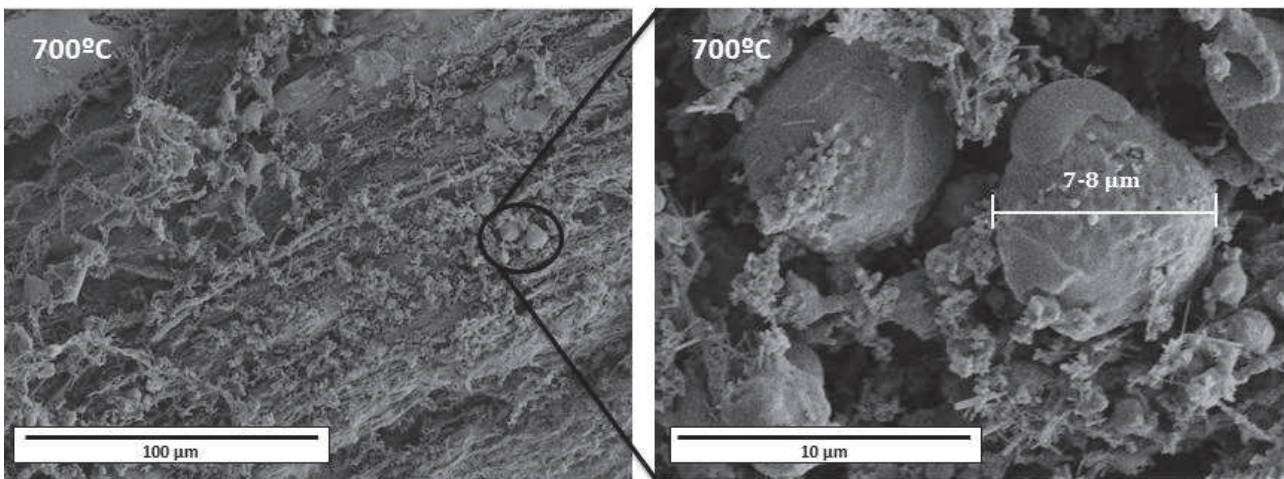


Figure II-17: Melted grains at 700 °C in the vascular bundle

Figure II-18A represents the cortex and the pith at 700 °C. Both the small crystals and the bulk of the cortex contain Si and K. The melted pith (Figure II-18/B) is mainly composed of K, but Na and Si were also detected in very small quantities.

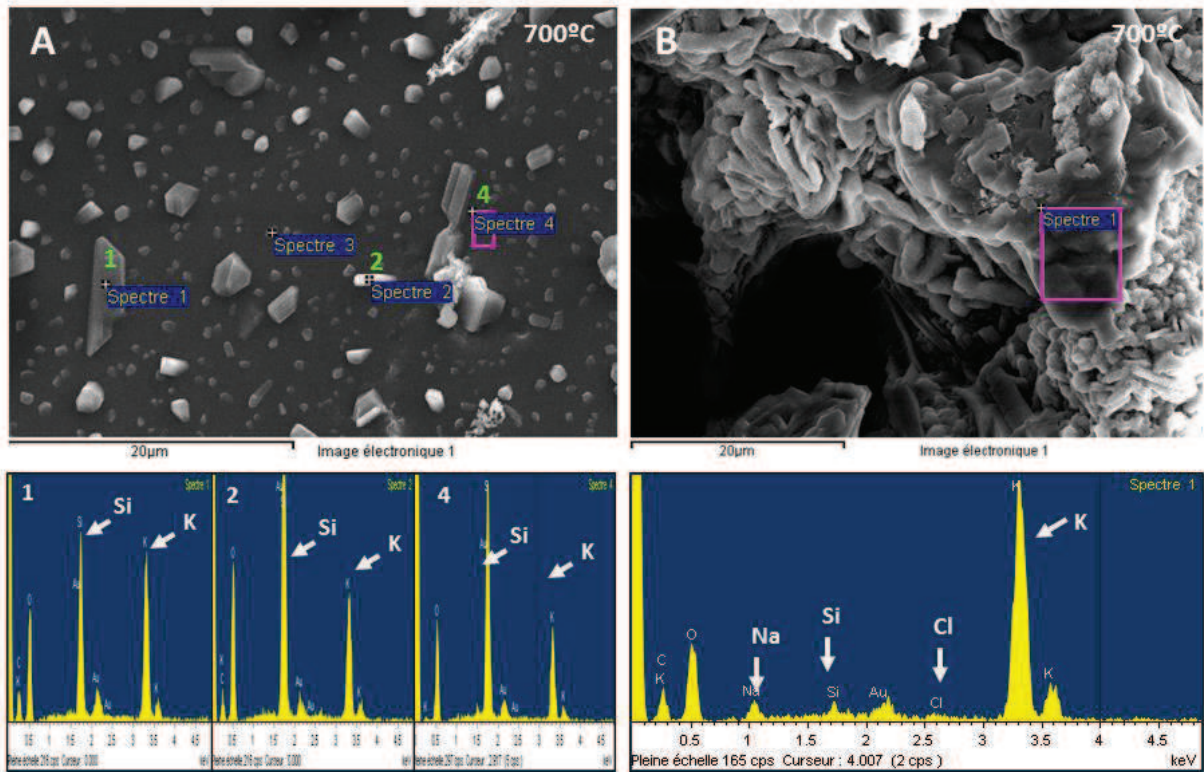


Figure II-18: SEM-EDX analysis of the cortex and vascular bundles at 700 °C

Figure II-In Figure II-19 the remaining vascular bundles can be recognised. Moderate amounts of Mg, Ca and P were detected with the degradation of the organic matrix.

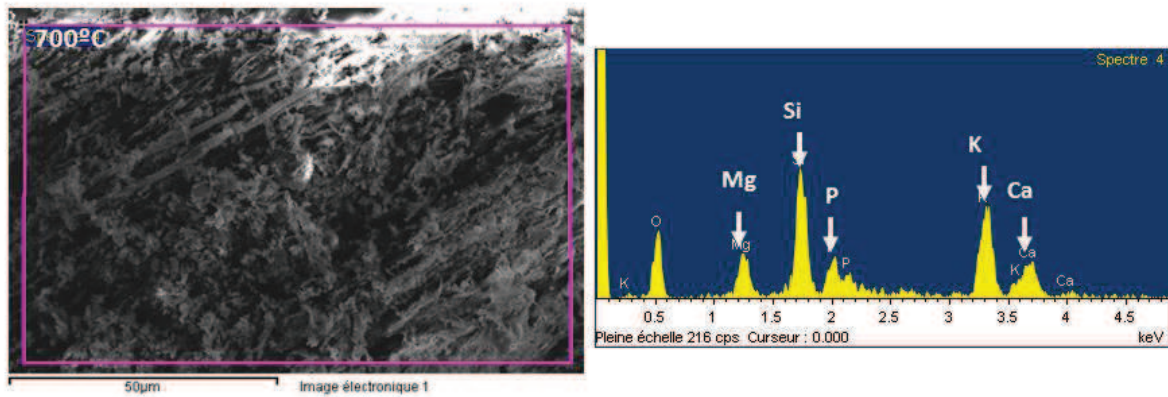


Figure II-19: SEM-EDX analysis of the vascular bundles and pith at 700 °C

#### II.3.4 DISCUSSION OF INORGANIC TRANSFORMATION AT LOW TEMPERATURE

In this subsection the structure of the miscanthus stem, its degradation as a function of temperature were studied focusing on the distribution of inorganics between the outer rigid part (cortex) and the inner spongy structure (pith). Subjected to heat-treatment, the pith degraded into a thin cobweb like structure starting from 325 °C and the outer part started to decompose around 390-400 °C. The formation of small crystals on the cortex was observed around 380-385 °C and the cobweb like structure started to melt around 350 °C.

The cortex is mainly composed of Si to reinforce its structure but Ca, Mg and K are also present. The inner part of the stem is built up of spongy structured cells and vascular bundles, these latter serving the distribution of water, nutrition and photosynthesis products into the different parts of the plant. The inner part of the stem is rich in K and Cl, but the vascular bundles contain Si, Mg, Ca, P, and S. Silicon and potassium can be detected starting from 250-300 °C, alkali earth metals (Ca and Mg) from 350-400 °C. Due to their low concentration Cl, P and S are only occasionally detectable below 600 °C but their presence can be evidenced at 700 °C. Na and Al were identified only occasionally in very small quantity, whereas Fe and Mn were not found at all.

This study revealed that it is possible to have an approximate qualitative analysis of the different elements in the miscanthus stem, but it is not possible to reliably analyse the inorganics by SEM-EDX without damaging the samples. The limits of the SEM-EDX techniques also have to be mentioned, namely the pear-shape interaction volume of 1µm<sup>3</sup>, which means that the surrounding matrix is also taken into account at high magnification. Moreover, hydrogen and nitrogen cannot be detected and the carbon content cannot be quantified.

In conclusion, subjected to heat-treatment the organic matrix starts to decompose between 350 °C and 400 °C and the inorganics start to crystallise around 400 and 500 °C. These reactions take place simultaneously; hence it is difficult to determine the exact temperature when the crystal formation starts and when the degradation of organic structure finishes. In general, the inorganics become detectable around 375-400 °C and the organic part totally decomposes between 700 and 800 °C. Due to the relatively low concentration of inorganics compared to the organic matrix, it is not possible to describe their modification without accumulating and homogenizing a decent amount of ash samples.

This study proved that 400 °C is an adequate temperature to accumulate miscanthus ashes using an oxidizing heating. These ashes can serve as a start-up batch for further studies of phase transformations at high temperature.

## II.4 STUDY OF THE ASH BEHAVIOUR AT HIGH TEMPERATURE

It is indispensable to study the phase transformation of miscanthus ashes as a function of temperature to evaluate the risks of bed agglomeration during fluidized bed gasification and combustion. In this subsection, the miscanthus ashes were subjected to heat-treatment between 400 and 1400 °C and were characterised by different analytical methods: thermoanalytic techniques (TGA, DTA), inductive coupled plasma-mass spectroscopy (ICP-MS), SEM-EDX and X-ray diffraction. These methods were complemented with the ASTTM/DIN ash fusion test and chemical fractionation analysis which are common methods to describe ash sintering and the chemical composition of biomass feedstock and ashes. For the experiments, the start-up samples were prepared in air at 400 °C in an open muffle furnace. This step was necessary to obtain sufficient amount of homogenous miscanthus ash sample without major modification of inorganic phases. This homogenous batch served as start-up sample for further high temperature experiments.

### II.4.1 PREPARATION OF START-UP BATCH FOR HIGH TEMPERATURE ANALYSIS

According to the analysis of Socor Laboratory, the miscanthus contains of 2.1 wt % ash on dry base at 815 °C. This means that a big quantity of dried plant is necessary to obtain sufficient amount of ash at high temperature. To obtain 1g of ash at 815 °C, about 50g of dried plant has to be burnt which has a volume of approximately 1 litre. In consequence, we face some limitations to perform the heat-treatments directly burning the miscanthus stem at high temperature.

These limitations are:

- The heat-treatment cannot be done inside the laboratory due to the smoke (degradation of organics) and the limited furnace capacity
- The dried miscanthus has to be burnt in a big crucible due to its volume, therefore we are limited to use alumina crucibles
- But at high temperature we risk the interaction between the ash and the alumina crucible, and the ash definitely sticks on the inner wall of the crucible. For this reason, above 700 -800°C it is better to use a sample holder made of platinum.
- Moreover, the laboratory furnace which enables us to study the transformation in reducing atmosphere, can handle only few grams of samples
- On the other hand, treating the miscanthus directly in reducing atmosphere would produce a big amount of char, and the inorganic content could not be studied by the available analytical techniques
- However, pre-ashing the miscanthus prior to further heat-treatment can alter its composition as alkali metals volatilize at relatively low temperature

Considering all these limitations, a moderate temperature, 400 °C, was chosen to obtain a homogenous batch of ash. As it was shown in the first part of this chapter, 400 °C allows eliminating most of the organic matrix without major modification of the inorganic phases.

To prepare this homogenous start-up batch, the miscanthus stem was dried at 105 °C and blended to a particle size less than 1 cm. Approximately 100 g of sample was placed in a Al<sub>2</sub>O<sub>3</sub> crucible at a time and calcined in an open muffle furnace (Parmilleux, type: FP 1200, Figure II-20) for 6 hours, which resulted in 2-2.5g ash.



*Figure II-20: Preparing miscanthus ashes at 400 °C in an open muffle furnace (Parmilleux, type: FP 1200)*

The ashes were homogenised in a mortar grinder (Fritsch Pulverisette, type 02.102) and were used as start-up batch for further high temperature experimentation.

For the high temperature analysis, approximately 0.45 g of ash was pressed into pastille, placed on a Pt-Rh support and heat-treated for 6 hours in a laboratory furnace (Nabertherm N7/H, heating rate 5 °C/min, air).

#### II.4.2 EXPERIMENTAL SETUP IN REDUCING ATMOSPHERE

Supplementary tests on ash samples were performed in reducing atmosphere to study the impact of gasification conditions.

The technology of EQTEC reactor (GAMECO project partner) uses limited air supply for biomass gasification (equivalent ratio ER=0.33). Thus the carbon is partially oxidized during the process and results in a reducing gas mixture (CO, CO<sub>2</sub>, H<sub>2</sub>, H<sub>2</sub>O) inside the reactor.

Therefore there are two possibilities to examine the transformation of ashes under similar conditions as the EQTEC technology: using air diluted with nitrogen or using a reducing gas mixture. It is important to note that both methods have their own drawbacks.

Firstly, the air should be diluted at such a certain extent what cannot be reliably controlled. Secondly, contrary to industrial gasifiers we are working with ash instead of biomass pellets and the carbon and hydrogen concentration in the ash samples are low (approximately 10 wt % of C and < 1 wt % of H<sub>2</sub>). Therefore, using diluted air would not be similar to the biomass gasification conditions.

For our trials the available reducing gases were CO<sub>2</sub> and H<sub>2</sub>, therefore we were limited by the gas shift reaction (CO<sub>2</sub> + H<sub>2</sub> ↔ CO + H<sub>2</sub>O) to create a reducing environment around the ash samples. The gas products of the trials were analysed by micro gas chromatography and were compared to thermodynamic calculation. The analysis showed that the injected gas mixture can reach the equilibrium state during the current experimental set up. The molar concentration of flow rates and the gas mixture in equilibrium is given in Table II-4.

Table II-4: Composition of input gas and equilibrium gas mixture at 900 °C

	Gas flow (L/h)	Input (% mol)	Equilibrium (% mol)
CO <sub>2</sub>	0.146*	1.77	0.6
H <sub>2</sub>	6**	2.95	1.78
CO	-	-	1.16
H <sub>2</sub> O	-	-	1.16
N <sub>2</sub>	-	95.3	95
<i>total</i>	<i>6.146</i>	<i>100</i>	<i>100</i>
*100%; **3% in N <sub>2</sub>			

The product gas mixture during industrial gasification is the result of many simultaneous chemical reactions, usually not in equilibrium, which influences the gas composition in the reactor. Although, it is not possible to simulate the exact ratio of CO, CO<sub>2</sub>, H<sub>2</sub>O and H<sub>2</sub> during gasification using only the gas shift reaction, the laboratory gas mixture contains the major gas components of gasification technology and the partial pressure of oxygen in the equilibrium gas mixture is in the same order of magnitude as in gasification (ppO<sub>2</sub>=10<sup>-15</sup>-10<sup>-20</sup> bar) The importance of oxygen partial pressure will be unfolded in Chapter III.

#### DESIGN OF THE CONTROLLED ATMOSPHERE DEVICE

The controlled atmosphere device used for the reducing atmosphere experimentation was set up at LTB-Liten (Atomic Energy Commission (CEA), Grenoble, France). As it is represented in Figure II-21 and Figure II-22 the setup can be divided into three parts: (A) the sample support, (B) «controlled atmosphere» device and (C) vertical tube furnace (Al<sub>2</sub>O<sub>3</sub> (C 530), *Nabertherm RT 50-250/13*, maximum temperature: 1300 °C).

The sample support (A) consists of three parts; two sample holders for the platinum cups and one to fix the thermocouples. These three parts are sustained with two aluminium oxide rods. The samples can be placed on the platinum cups and the temperature is monitored by three thermocouples.

The sample support is placed inside the «controlled atmosphere» device. The device is made of an Inconel 600 tube (d<sub>int</sub>= 25mm), the gas input tube (Inconel 4/6) is welded around it. The top of the device is closed by a plug with the gas outlet and the air-tight passage for the thermocouples.

The controlled atmosphere device is placed into the tubular furnace and it is closed by two *Macor* plug to avoid heat loss during the experiments.

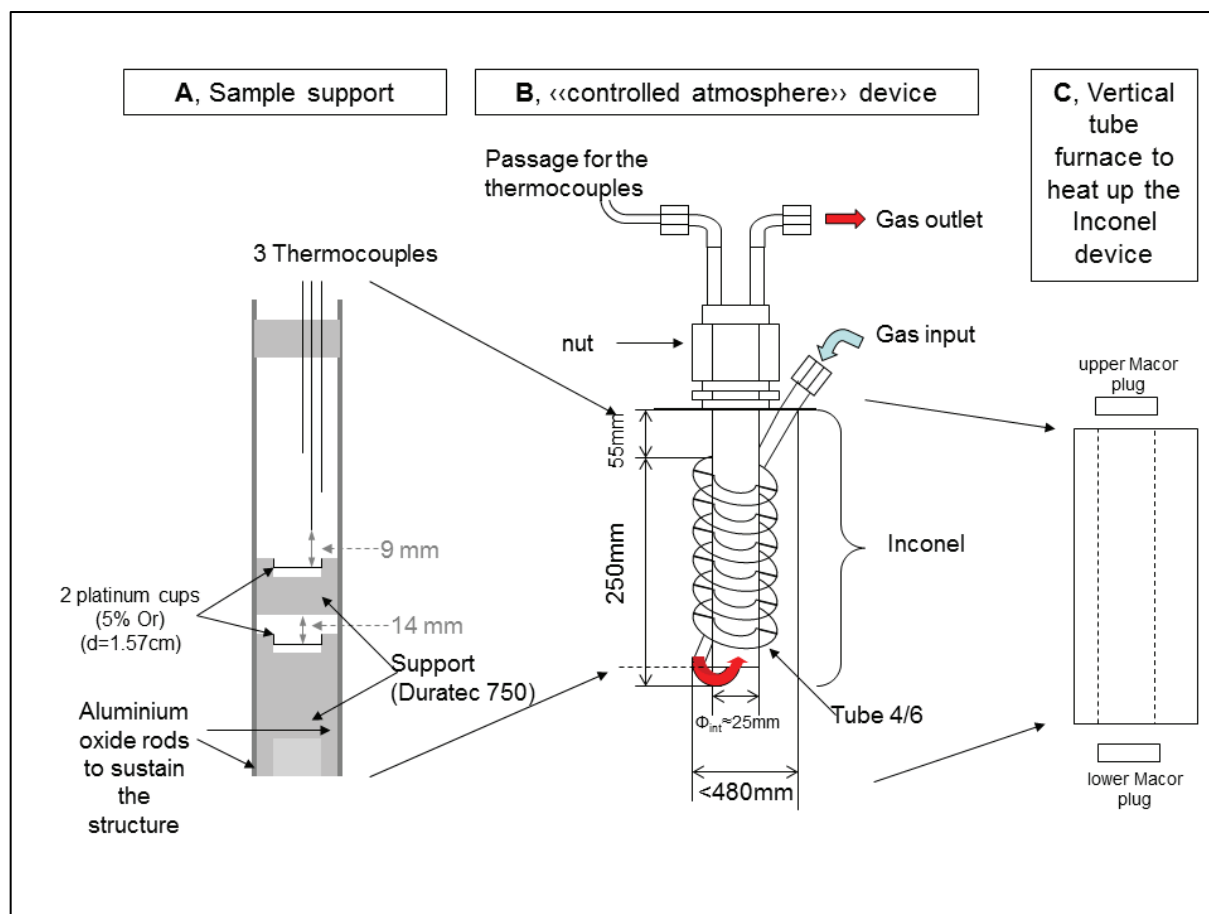


Figure II-2: Scheme of the «controlled atmosphere» device

### HEAT-TREATMENT OF ASH SAMPLES IN REDUCING ATMOSPHERE

Ash pastilles were placed on a Pt sample holder and closed into the chamber. The chamber was rinsed by  $N_2$  for 10 min. The samples were heated up to 900 and 1000 °C with 10 °C/min for 6 h under  $CO_2$ - $H_2$  flow. At the end of the trial, the samples were quenched by the following method: the inner chamber was taken out of the oven and placed on an iron triangle (Figure II-22) to cool down with an approximately 100 °C/min quenching rate. The  $CO_2$ - $H_2$  gas flow was maintained till the samples reached 400 °C, and then the chamber was rinsed by  $N_2$  till cool-down to room temperature.

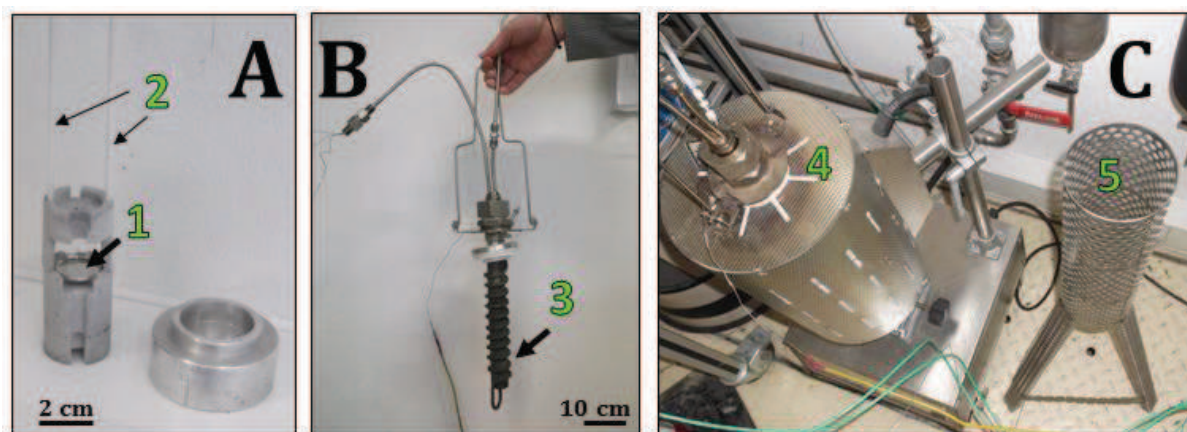


Figure II-22: The main components of controlled atmosphere device: sample support with Pt-Rh sample holder (A/1) and alumina rods(A/2) to place the sample holder into the device , chamber with gas input tube (B/3), tubular furnace (C/4) and iron triangle (C/5) for quenching

### II.4.3 CHARACTERISATION OF ASH SAMPLES

#### ELEMENTAL COMPOSITION

The elemental composition of miscanthus ash samples was determined by Laser Ablation Inductively Coupled Plasma Mass Spectrometry (LA-ICP-MS) in the laboratory IRAMAT, CNRS, Orleans. This technique couples a VG UV Laser probe laser ablation sampling device with a VG Plasma Quad PQXS Inductively Coupled Plasma Mass Spectrometer. The sample introduction by laser ablation allows the analysis of solid samples by creating fine particles with a focalised laser. These fine particles are ionized by inductive coupled plasma and separated in a mass spectrometer on the basis of their mass to charge ratio.

The miscanthus ash samples were grinded and compressed into pastilles prior to analysis. The grinding was necessary to obtain homogenous samples as the different chemical phases tend to segregate in the ashes after heat-treatment.

Sulfur could not be analysed due to the lack of reference standard materials with the same type of matrix as the ashes. Therefore, complementary SEM-EDX analyses were performed to determine the concentration of the sulfur.

#### THERMAL ANALYSIS

Miscanthus stem (LM1-harvested in April 2011) was analysed by Thermal Gravimetric Analysis (TGA) using a Setaram Setsys Evolution 2400 apparatus. Blended miscanthus stem (103 mg) was heated to 1000 °C with a heating rate of 5 °C/min both in air and oxygen flow (20 mL/min). It is possible to run the apparatus in simple TGA or differential thermal analysis (DTA), but also in coupled TGA-DTA mode.

The phase transformation of miscanthus ash (LM1, prepared at 400 °C) was followed by differential thermal analysis (TGA-DTA, Setaram, Setsys 2400) coupled to the thermal gravimetric analysis. The advantage of this coupled method is that the mass loss of the sample and the exothermic/endothemic peaks can be detected at the same time as a function of temperature.

#### ASH FUSION TEST

The ash fusibility test is a normalised test method which describes the ash fusion under well-defined conditions.

The atmosphere and the temperature of the furnace is controlled: the test are done either in reducing or oxidizing environment. During the test, the furnace is progressively heated and the deformation of the ash cone is detected in real time. The fusion of the ash is described with four characteristic temperatures presented in Figure II-23, namely:

1. Shrinkage temperature, when a small shrinkage of the sample is detected
2. Deformation temperature, when the edges of the sample become rounded
3. Hemisphere temperature, the sample becomes the shape of a hemisphere
4. Flow out temperature, when the quantity of liquid phase is sufficient to cause the spreading of sample on the sample holder

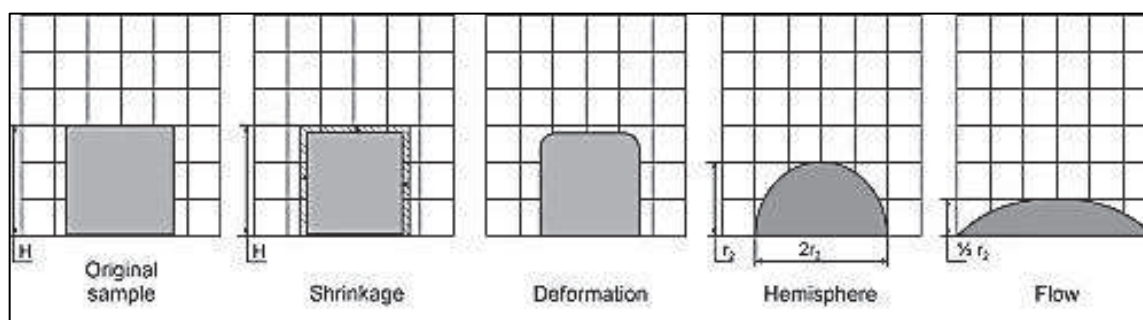


Figure II-23: Characteristic temperatures of the standard ash fusion test (CEN/TS 15370)

The ash fusion test of LM1 ashes was performed by Socor Laboratory according to the standard CEN/TS 15370-1 in oxidizing atmosphere with a start-up ash sample prepared at 815 °C.

#### MINERALOGICAL FORM OF MISCANTHUS ASHES

The crystalline phase of miscanthus ashes was analysed by powder X-ray diffraction. The diffractograms were recorded on a Bruker D8 Advance diffractometer (cathode Cu,  $K\alpha_1=1.5406 \text{ \AA}$ ,  $12-70^\circ$ , detector open at  $8^\circ$ , step  $0.0164^\circ$ , scan speed= $1\text{s}/\text{scan}$ ,  $30\text{kV}$ ,  $40\text{mA}$ , div split  $0.7$ , rotation  $15\text{mps}$ ).

The ash samples were first heat-treated then ground into fine flour consistency. Approximately  $0.5 \text{ g}$  of the ash was placed in the silicon sample holder and flattened with a microscopy glass.

The phase analysis was performed with the software DIFFRACplusEVA using the ICDD (International Centre for Diffraction Data) database.

#### CHEMICAL FRACTIONATION ANALYSIS (CFA)

Dried miscanthus and miscanthus ash samples prepared at different temperature were analysed by chemical fractionation analysis (CFA) described by Zevenhoven et al. [II-41]. The modification of sample analysis methods is presented in Figure II-24.

Instead of analysing the leachates after the washing steps, one part of the solid sample was taken aside. The solid samples were ashed at 400 °C and analysed by XRD, SEM-EDX and ICP-MS. The elemental analyses by ICP-MS and SEM-EDX provide information about the wash-out ratio of the different elements. Comparing the diffractograms after each leaching step reveals the exact chemical speciation of the leached-out compounds. The difference between the identified crystalline phases and the global elemental analysis gives information about the amorphous phase.

For the chemical fractionation analysis, the miscanthus stem was consecutively washed in ultrapure water, 1 M ammonium acetate solution (Fisher, prepared from powder) and 1 M HCl solution (Fisher, 33%).

The blended and dried miscanthus stem (70 g) was placed into a plastic vessel with 700mL of washing agent and agitated in a three dimension (rotation, translation and inversion) mixer (TURBULA T2F). Each washing step was repeated twice at room temperature to assure the complete washout of inorganics. The samples were filtered in a Buchner funnel after each leaching step. The solid residue was washed by ultrapure water and dried between the different washing agents.

In order to determine the remaining mineral matter, one part of the solid residue was retained after each step then burnt in a muffle furnace at 400°C. The elemental composition was determined by LA-ICP-MS and completed with SEM-EDX. The crystalline phases of solid samples were analysed by XRD.

In case of the heat-treated ash samples (1000 °C) the chemical fractionation analysis was slightly modified: the leaching step with ammonium acetate buffer solution was left out. According to the literature, the buffer dissolves elements attached to the organic structure in the ash [II-15]. As in oxidizing atmosphere no organic structure remains in the ash at 1000 °C, this washing step is not necessary. For the analysis of heat-treated ashes the finally grinded ash particles were consecutively washed in ultrapure water and 1 M HCl using 20ml solvent per 1 gram ash.

Similarly to the leaching procedure of the dried miscanthus stem, the ash samples were filtered and washed with ultrapure water after each step. One part of the ash was retained after each step for further analyses.

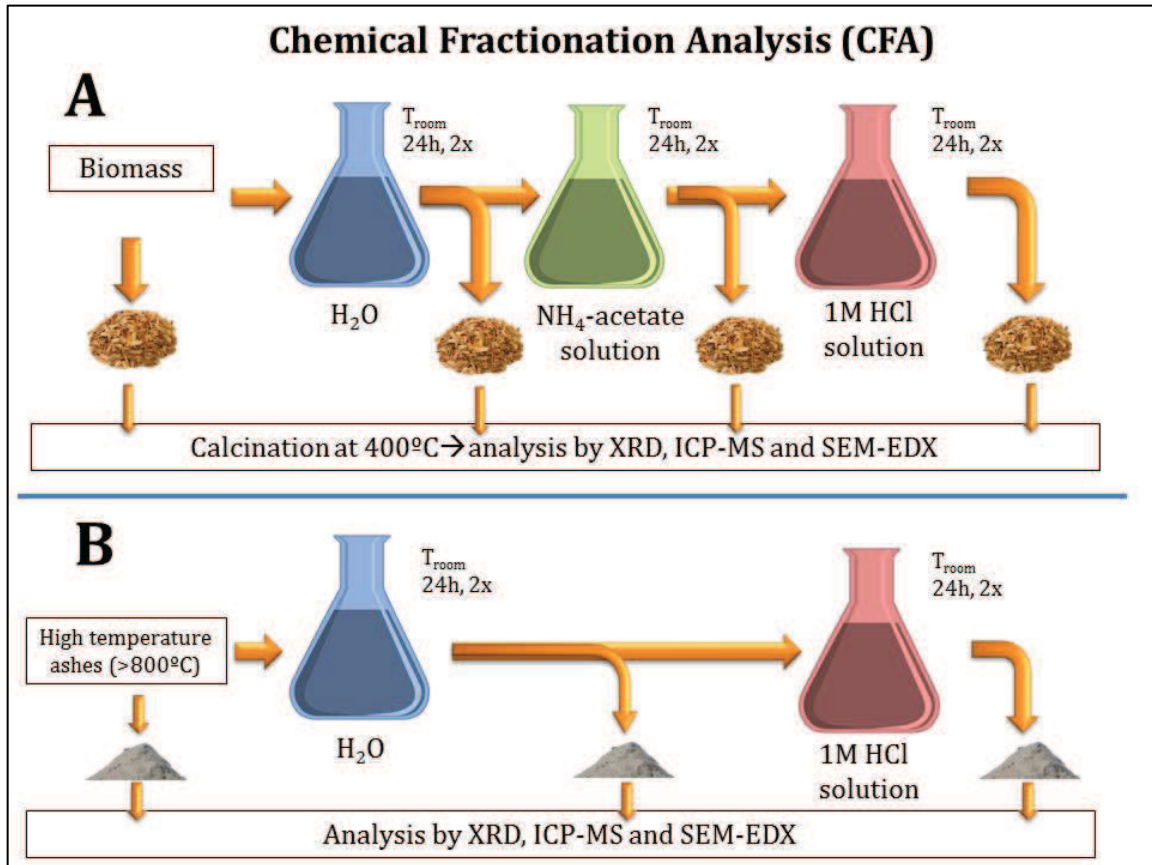


Figure II-24: Chemical Fractionation Analysis; A, method in case of dried biomass, B, method in case of high temperature ashes

## II.4.4 THERMAL ANALYSIS OF MISCANTHUS

Figure II-25 presents the thermogravimetric analysis of dried miscanthus stem in oxygen and in air. As expected, the decomposition of the organic structure is the faster in pure oxygen than air.

The first descent of the curve corresponds to the loss of water. The deep slope between 250 and 350 °C is due to the decomposition of hemicellulose and cellulose, and the slope between 350 and 600 °C correspond to the decomposition of lignin [II-42].

The main difference in mass loss is in the range of 250 and 550 °C; afterwards the curves approach each other and reach approximately the same value at 530 °C.

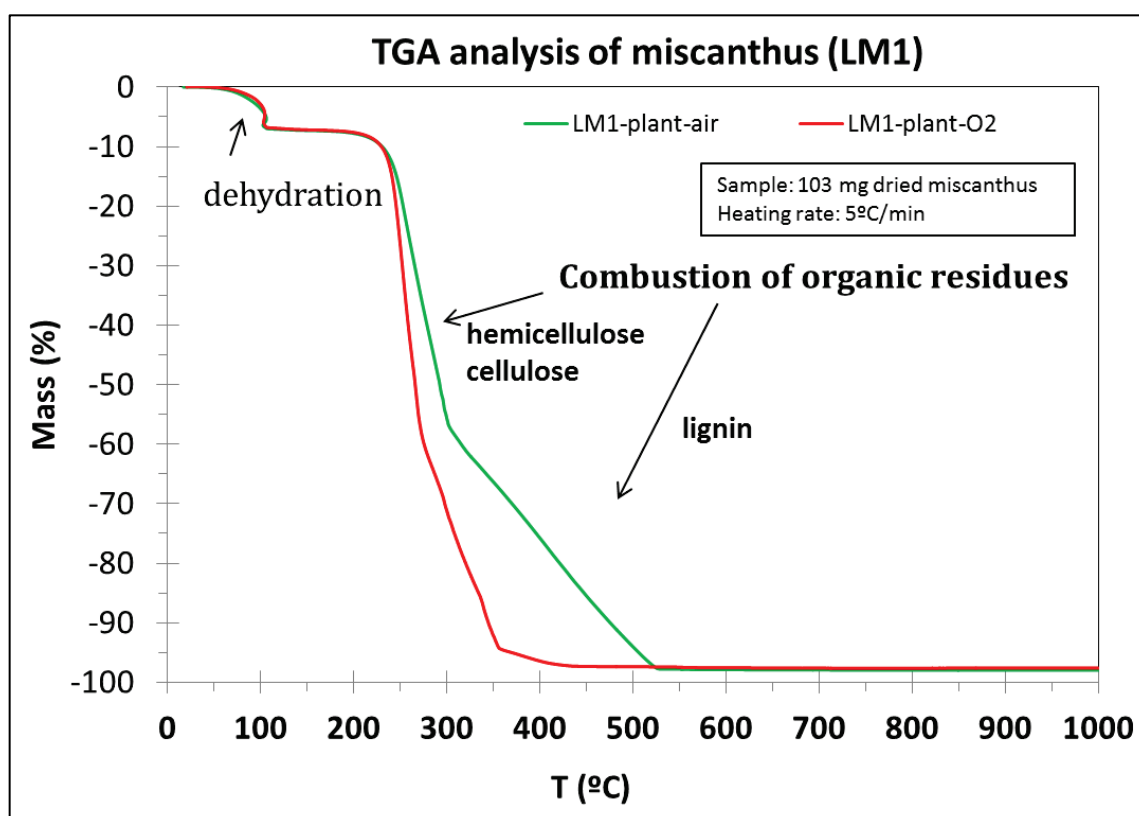


Figure II-25: TGA of LM1ash in O<sub>2</sub> and in air

The simultaneous TGA-DTA analysis of LM1 ash performed in air is presented in Figure II-26. The first endothermic peak at 150 °C is due to the dehydration. The exothermic reaction between 400-450 °C is most probably due to the oxidation of organic residue in the ashes. The endothermic peak and the mass loss at 750 °C are probably related to CO<sub>2</sub> release from the decomposition of carbonates [II-42, II-43]. The mass loss between 700 and 1000 °C can be due to the volatilisation of salts, while the endothermic peak between 1200 °C and 1300 °C can be attributed to sulphate decomposition [II-43]. The small exothermic peak around 850 °C could be related to the formation of alkali silicates [II-43]. The fusion of the ash cannot be defined. To justify the interpretation of the endothermic and exothermic peaks, elemental analysis, XRD measurement and thermodynamic calculation are necessary.

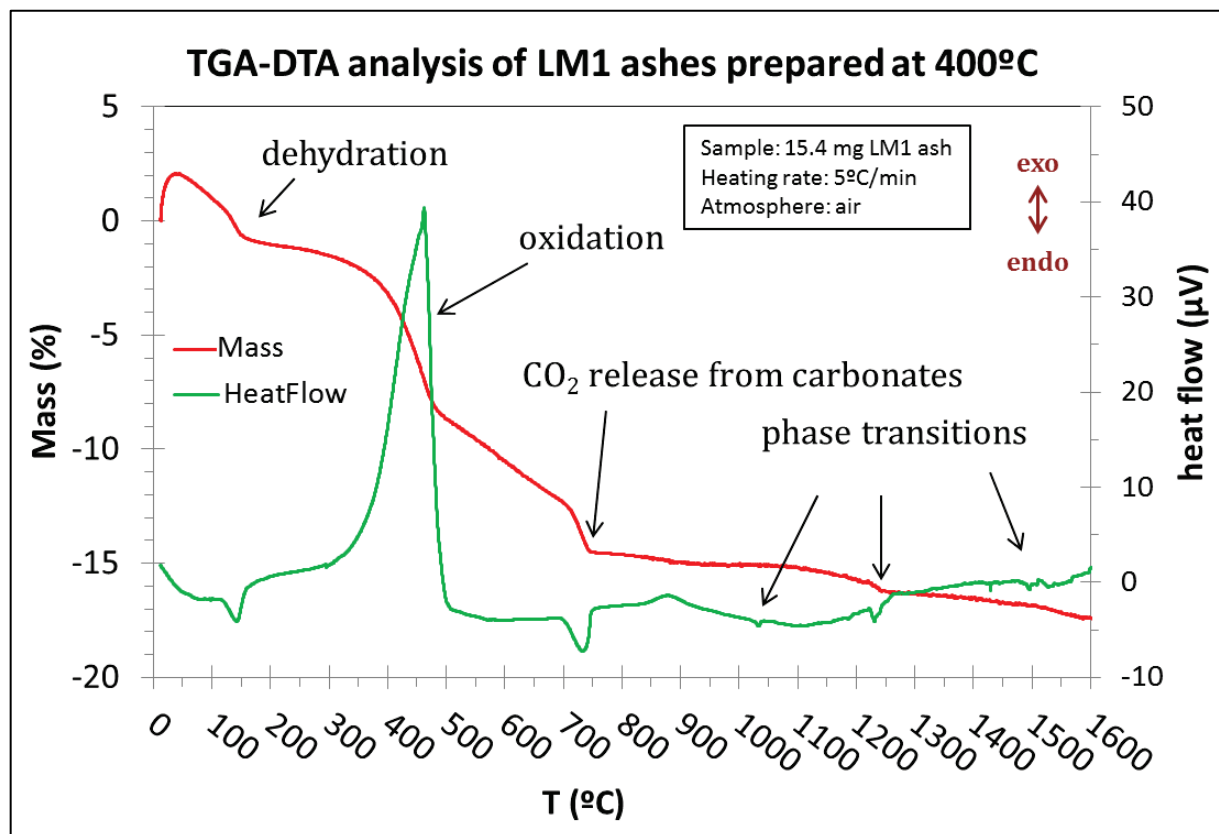


Figure II-26: TGA-DTA analysis of LM1 ash

#### II.4.5 ASH FUSIBILITY TEST

The ash fusibility test was done by Socor Laboratory according to the standard CEN/TS 15370-1 in oxidizing atmosphere on the ash prepared at 815 °C. The characteristic temperatures of ash fusibility test are presented in Figure II-27. We cannot gain reliable information about the sintering tendency of the ash as the initial ash sample was obtained at elevated temperature (815 °C). The DTA analysis of the LM1 showed that many phase transformations occur in the range of 400 and 800 °C, which are most likely related to the volatilisation of alkali metal oxides and salts. Due to the loss of alkalis the ash sintering temperature can be overestimated. Moreover, the formation of liquid alkali silicates is also possible below 815 °C.

As this test was done by an external company, we have no influence on the preparation method of the ash sample. Despite the uncertainty, this test gives an approximate estimation about the fusion of miscanthus ash. It is certain that most of the inorganics are molten at 1100 °C and that the ash completely melts around 1320 °C. To be able to precisely describe the ash melting, more accurate analysis and thermodynamic calculation are necessary.

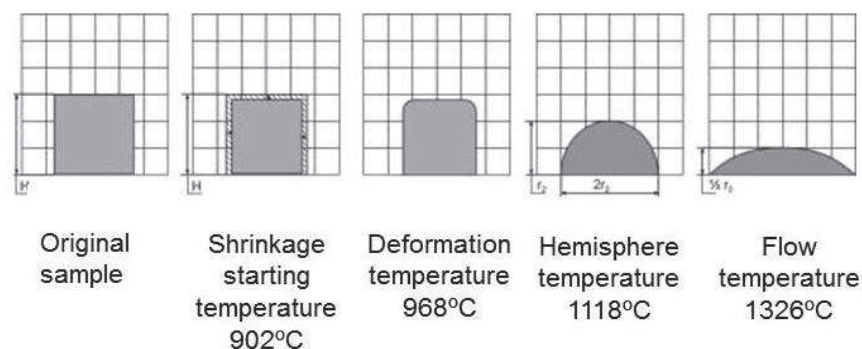


Figure II-27: Characteristic temperatures of LM1 miscanthus ash fusibility test (laboratory Socor)

#### II.4.6 INORGANIC COMPOSITION BASED ON THE CHEMICAL FRACTIONATION ANALYSIS

As the previous analyses show, the ash behaviour cannot be interpreted with thermal analysis or ash fusion test; these techniques have to be completed with more complex phase characterisation method.

The mineralogical form of the inorganics was analysed by XRD measurements. As the miscanthus ashes include many different elements in small quantities, the diffractograms dispose several small, often overlapping peaks, which make it difficult to determine the crystalline phases. Therefore, consecutive leaching analysis was used, which separates the water, acetate and acid soluble compounds resulting in clear diffractograms. The ICP-MS measurements after each leaching step complete the diffractograms with information about the amorphous phase.

Figure II-28 shows the ICP-MS analysis of the reference sample, and the residues after leaching in ultrapure water, ammonium acetate and hydrochloric acid. Most of the alkalis are washed out by pure water which means that these elements were in ionic form in the miscanthus stem. Some of the Mg and Ca were attached to the organic part as they are dissolved in the ammonium acetate solution. After washing the plant by HCl, only Si remains in the ash.

Figure II-29 shows the diffractograms of the samples after ashed at 400 °C. The diffractograms of the reference and the washed samples provide more complex information of the different crystalline phases in the ash. After leaching, the diffractograms have less and better differentiated peaks due to the clearance of some disturbing and overlapping phases and the appearance of so far hidden components.

According to the XRD analysis (Figure II-29) the inorganics are mostly present as salts: KCl,  $K_2SO_4$  and calcium phosphate which are washed away by the water. The diffractogram after washing by water shows the present of  $CaCO_3$  and  $MgCO_3$ , whose peaks disappear after washing by ammonium acetate. These carbonates derive from the Ca and Mg, originally attached to the organic structure then degraded into carbonates after the ashing at 400 °C (necessary step to be able to analyse the sample). No peaks remained after washing by ammonium acetate which means that the Si detected by ICP-MS is in amorphous form. The dome in the region of 15-35  $2\theta$  also refers to the presence of amorphous phase.

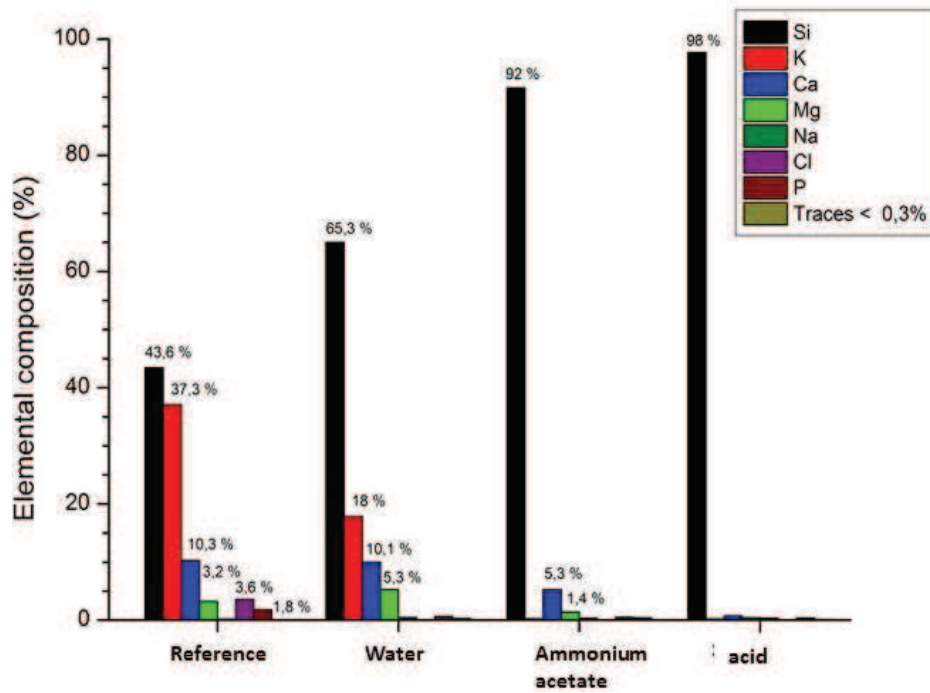


Figure II-28: ICP-MS analysis (wt %) of heat-treated (400 °C) residues of dried miscanthus after the different steps of CFA procedure

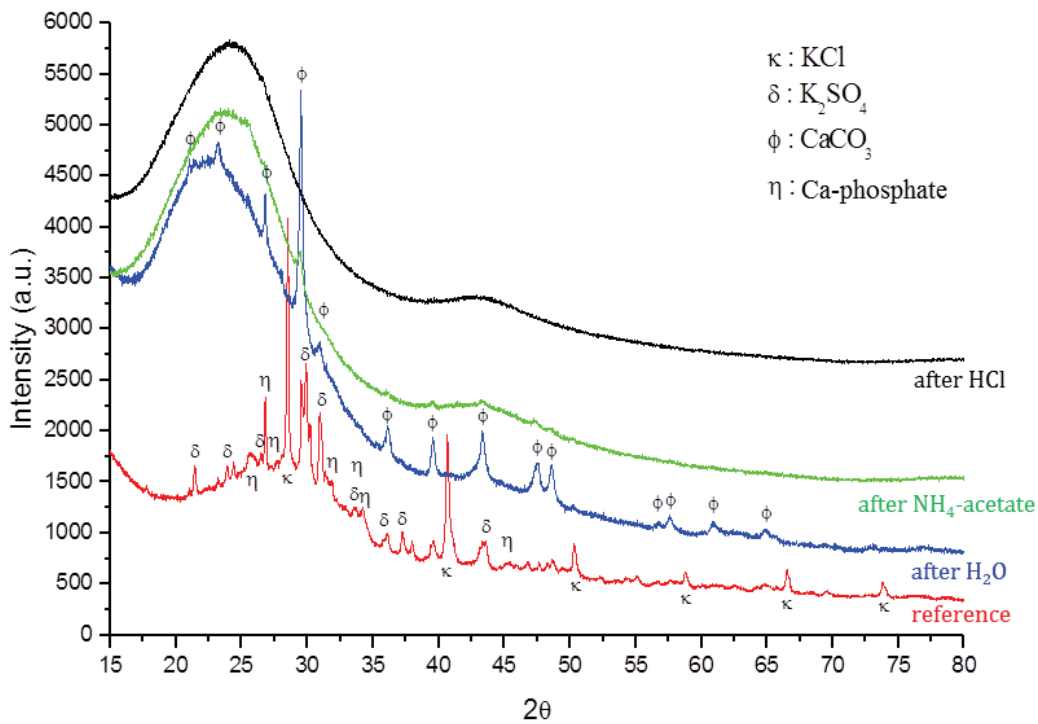


Figure II-29: X-ray diffractograms of heat-treated (400 °C) residues of dried miscanthus after the different steps of CFA procedure

Figure II-30 and Figure II-31 show the ICP-MS analysis and the diffractograms of the LM1 ash prepared at 1000 °C. This analysis proves that the form of the inorganics has been changed after the heat-treatment at 1000 °C. The ICP-MS analysis shows that only a small part of the alkalis can be washed out by water (KCl and K<sub>2</sub>SO<sub>4</sub> according to the diffractogram) but most of the elements remain even after the washing step with HCl.

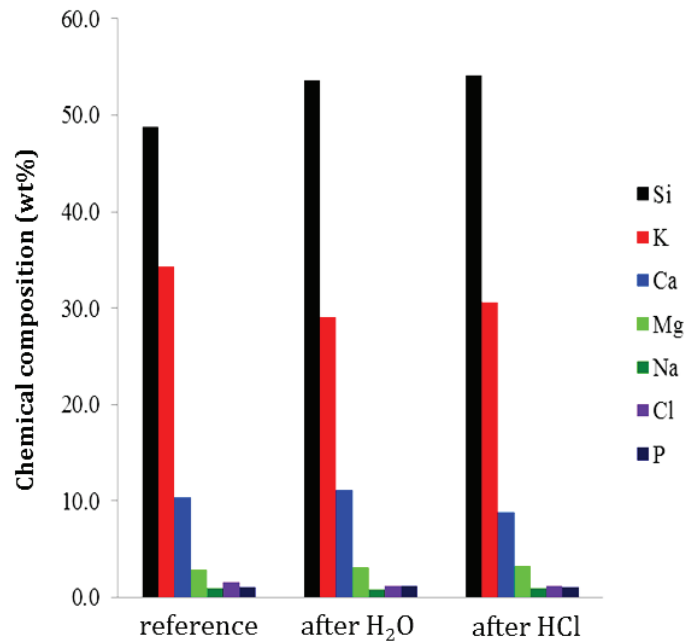


Figure II-30: ICP-MS analysis of high temperature ash leaching (1000 °C)

The X-ray diffractograms reveal the presence of Ca- and Mg-silicates (Figure II-31).

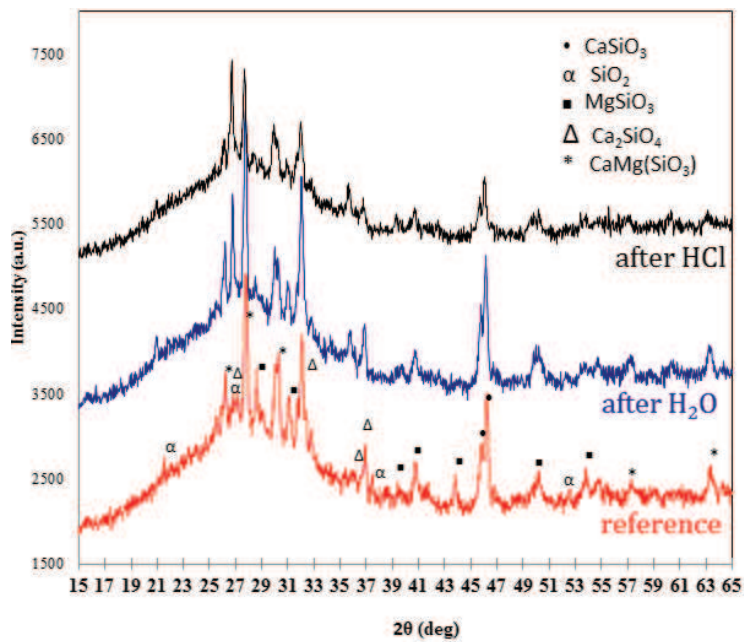


Figure II-31: X-ray diffractograms of ash leaching at 1000 °C

Though the presence of potassium is proved by ICP-MS, it cannot be detected in the X-ray diffractograms. This means that it was transformed into an insoluble vitreous phase after the heat-treatment at 1000 °C. The SEM-EDX analysis of the original ash sample (Figure II-32) demonstrates that most of the ash is molten and consists of silica, potassium and calcium oxides. Small crystals of Ca-silicate can be also detected. In some cases small crystals of Ca-phosphate were detected, but their quantity is so low that they cannot be always evidenced in the SEM analysis. The darker patches in the SEM image correspond to amorphous silica. These patches derive from the molten outer part of the stem, which contains a high amount of silicon in the form of silica gel which becomes amorphous silica (opal) at high temperature. (The small pieces of cortex structure are still visible after 10 minutes treatment at 1000 °C. The SEM image is shown in Appendix-A3.)

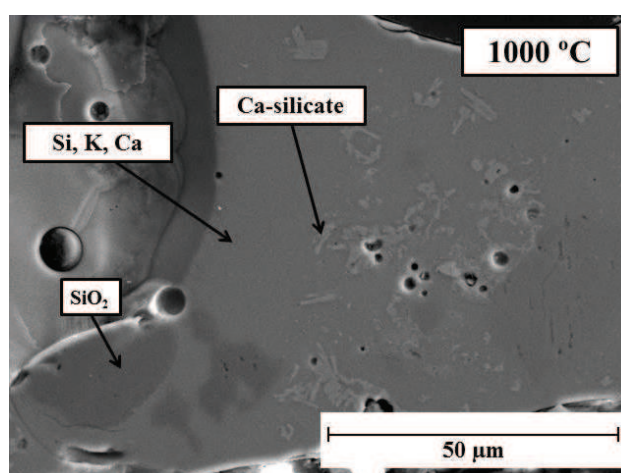


Figure II-32: SEM-EDS analysis of high temperature ash

#### II.4.7 TRANSFORMATION OF CRYSTALLINE PHASES

We already revealed that the inorganics form KCl, K<sub>2</sub>SO<sub>4</sub>, CaCO<sub>3</sub> and SiO<sub>2</sub> at low temperature. It was also shown that the ash at elevated temperature mostly contains Ca- and Mg-silicates and only a small amount of salts. The aim of this subsection is to describe the transformation of crystalline phases by X-ray diffraction. For this study, the start-up ash samples were pressed into 0.5g pellets and heat treated between 400 °C and 1400 °C in air.

Figure II-33 represents the transformation of miscanthus ashes (LM1 April 2011) as a function of temperature. Between 400 and 750 °C the samples look identical. Above 750 °C, the samples stiffen and their colour lightens as the carbon content of the samples decreases. Around 925-950 °C they lose the greyish tone. Above 900 °C due to the volatilisation of inorganics the ash pastilles blow up. The amount of liquid phase increases gradually: at 1100-1150 °C the ash pastille becomes rounded. Between 1200 and 1250 °C the ratio of liquid to solid increase significantly, the pastille does not keep its shape anymore and it flows. A small amount of solid phase is still present at 1300-1350 °C giving the sample an opalescent outlook. At 1400 °C the ash sample is considered to be completely molten.

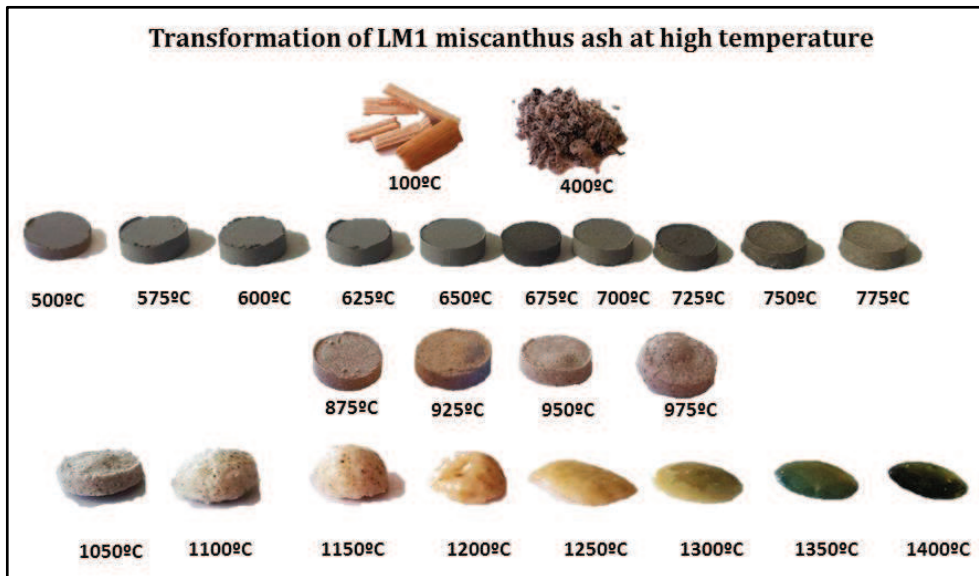


Figure II-33: Transformation of LM1 ashes as a function of temperature

These samples were ground into flour fine powder and analysed by XRD. The diffractograms are presented in Figure II-34, Figure II-35 and Figure II-36. In the range of 400 to 775 °C the main crystalline phases are KCl,  $K_2SO_4$ , hydrated Ca-phosphate and  $SiO_2$ . Formerly,  $SiO_2$  was detected in the amorphous phase (Ch II.4.6). It is possible that miscanthus ash contains both amorphous and crystalline  $SiO_2$  at low temperature. While amorphous silica derives from the silicic acid (one of the building block of the stem), crystalline silica most probably comes from external sources like soil.  $CaCO_3$  is detected up to 450 °C, the Ca-phosphate appears around 500-550 °C. A small amount of KCl can be still observed at 775 °C.

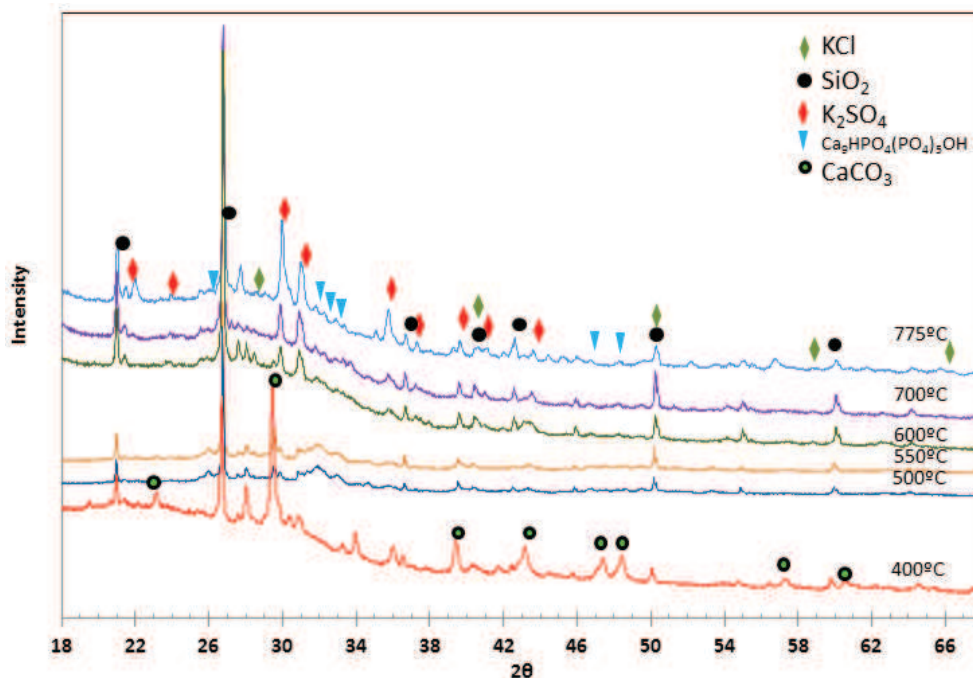


Figure II-34: X-ray diffractograms of LM1 ashes heat-treated in air for 6 hours (400 - 775 °C)

Around 850-875 °C, the hydrated Ca-phosphate transforms into  $\text{Ca}_3(\text{PO}_4)_2$  and a new silicate phase,  $\text{CaSiO}_3$  appears. Between 1100 and 1150 °C the  $\text{SiO}_2$  and  $\text{CaSiO}_3$  gradually decrease, at 1200 °C they cannot be detected. The  $\text{K}_2\text{SO}_4$  decomposes around 1200-1250 °C, at 1300 °C the only solid phase is  $\text{Ca}_3(\text{PO}_4)_2$ . At 1400 °C no crystalline phase can be detected.

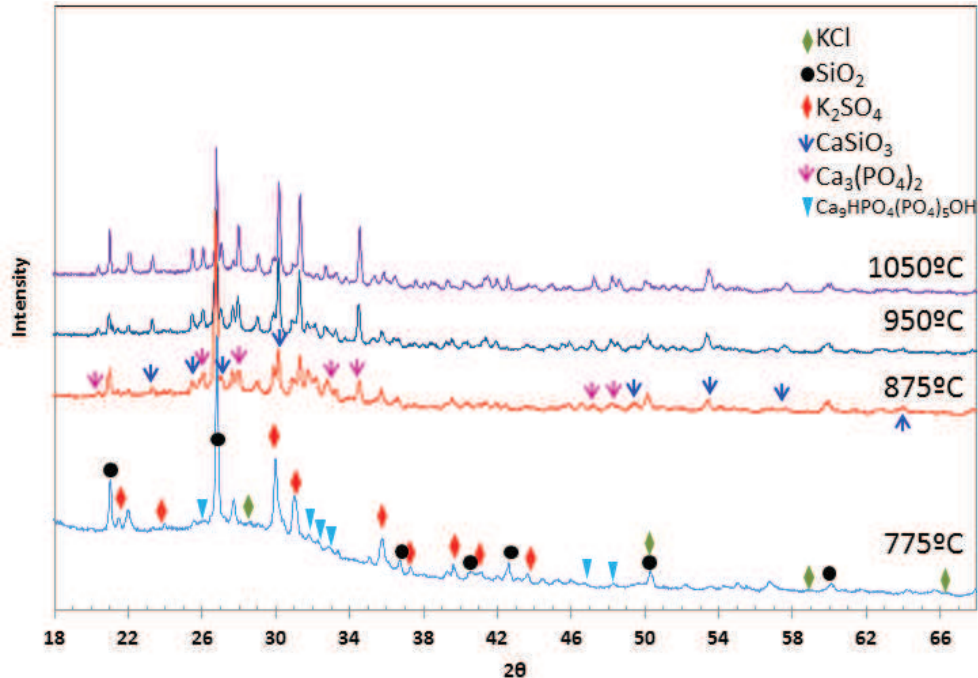


Figure II-35: X-ray diffractograms of LM1 ashes heat-treated in air for 6 hours (775 -1050 °C)

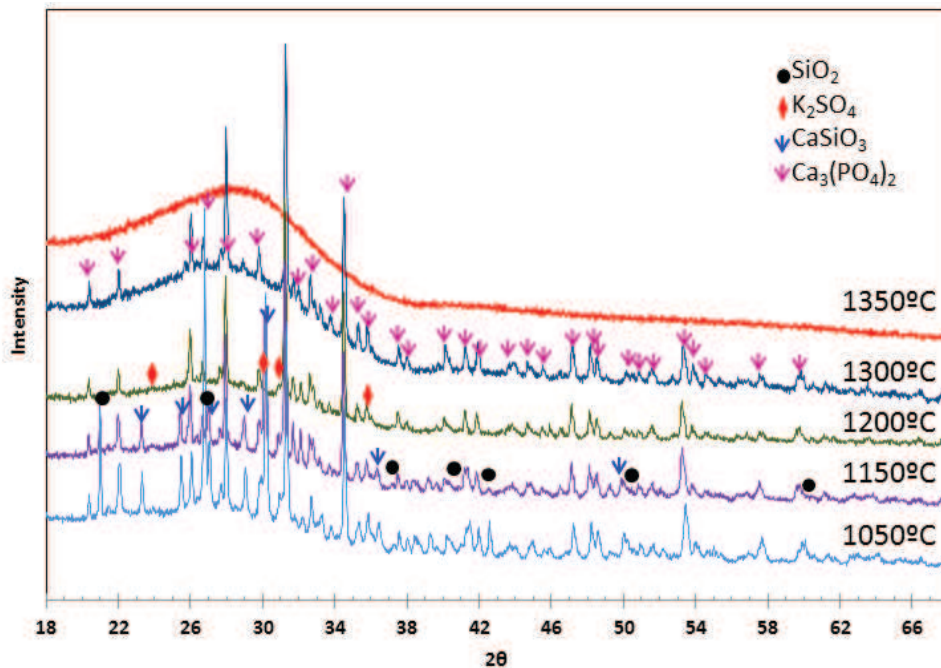


Figure II-36: X-ray diffractograms of LM1 ashes heat-treated in air for 6 hours (1050- 1350 °C)

Table II-5 summarizes the compounds detected by XRD analysis between 400 and 1400 °C. K-silicates could not be detected by XRD but they were observed with SEM-EDX analysis (Figure II-18).

Table II-5: Compounds identified by XRD analysis between 400 and 1350 °C (✓ the compound is present, ~ possible presence but the compound has weak signal or overlaps with other phases)

	400 °C	450 °C	500 °C	550 °C	600 °C	750 °C	775 °C	850 °C	875 °C	900 °C	1050 °C	1100 °C	1150 °C	1200 °C	1300 °C	1350 °C
<b>KCl</b> 00-04-0587*	✓	✓	✓	✓	✓	✓	✓									
<b>K<sub>2</sub>SO<sub>4</sub></b> 00-44-1414*	✓	✓	✓	✓	✓	✓	✓	✓	✓	✓	✓	✓	✓	✓		
<b>CaCO<sub>3</sub></b> 00-05-0586*	✓	✓														
<b>CaO</b> 00-28-0775*	~	~														
<b>Ca<sub>9</sub>HPO<sub>4</sub> (PO<sub>4</sub>)<sub>5</sub>OH</b> 00-46-0905*			✓	✓	✓	✓	✓									
<b>Ca<sub>4</sub>P<sub>2</sub>O<sub>9</sub></b> 00-11-0232*			~	~	~	~	~									
<b>Ca<sub>3</sub>(PO<sub>4</sub>)<sub>2</sub></b> 00-55-0898*									✓	✓	✓	✓	✓	✓	✓	
<b>SiO<sub>2</sub></b> 00-46-1045*	✓	✓	✓	✓	✓	✓	✓	✓	✓	✓	✓	✓	✓			
<b>CaSiO<sub>3</sub></b> 00-10-0487*								✓	✓	✓	✓	✓	✓			
<b>CaMg(SiO<sub>3</sub>)<sub>2</sub></b> 00-11-0654*												~	~	~		
<b>MgSiO<sub>3</sub></b> 00-76-6231*												~	~	~		
*JCPDS (Joint Committee on Powder Diffraction Standards) reference number																
✓ the compound is present, ~ possible presence but the compound has weak signals or the peaks overlap with other phases																

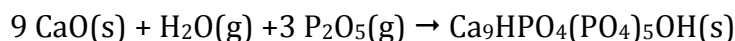
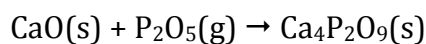
From these experimental data, the main crystalline and vitreous phase transformations in oxidizing atmosphere can be concluded as:

---

**400-500 °C**

---

- The decomposition of  $\text{CaCO}_3$  and the formation of hydrated Ca-phosphate

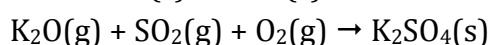
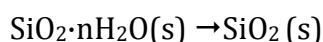


---

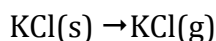
**500 and 750 °C**

---

- The amount of  $\text{SiO}_2$  and  $\text{K}_2\text{SO}_4$  increases as the silica gel decomposes



- Volatilisation of KCl



---

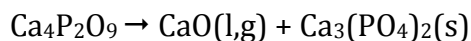
**775 and 875 °C**

---

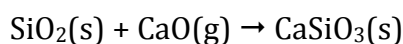
- The amount of sulphate and silica decreases



- The  $\text{Ca}_4\text{P}_2\text{O}_9$  decomposes and forms Ca-phosphate



- The silica and released CaO forms  $\text{CaSiO}_3$



---

**900 and 1000 °C**

---

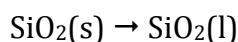
- The diminution of  $\text{K}_2\text{SO}_4$  and  $\text{SiO}_2$  continue, and the solid phase is enriched in  $\text{Ca}_3(\text{PO}_4)_2$  and  $\text{CaSiO}_3$ .
- Possible formation of Mg-silicates

---

**1150 and 1200 °C**

---

- Both  $\text{CaSiO}_3$  and the rest of the silica melt, only  $\text{Ca}_3(\text{PO}_4)_2$  and a small amount of  $\text{K}_2\text{SO}_4$  stay in the solid phase

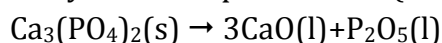


---

**1300 and 1350 °C**

---

- The only solid compound is  $\text{Ca}_3(\text{PO}_4)_2$  and at 1350°C the ash is completely molten



## II.4.8 EFFECT OF HARVEST TIME ON THE CHEMICAL COMPOSITION OF MISCANTHUS ASHES

As discussed previously, harvesting biomass before the winter results in 30-60% greater yield. Yet, biomass is usually collected early spring due to the lower moisture and alkali contents [II-44, II-45]. In the frame of the GAMECO research project, the biomass ash behaviour was studied with miscanthus collected in April 2011.

To evaluate the risks of an eventual late summer harvest, 5 kg of miscanthus was cut in September from the same plot of land as the April harvest (LM1). The collected miscanthus was defoliated and only the stems were compared to see the difference in the inorganic evolution in the stem. The LM2 ash samples were prepared the same way as LM1 samples: the stem was chopped, dried and ashed at 400 °C in an open muffle furnace. As the quantity of the LM2 lot was limited, only few characterisation tests were performed.

Table II-6 gives the composition of LM1 (April 2011) and LM2 (September 2011) ashes prepared at 400 °C. LM2 ash is richer in K, Cl and P than LM1. The complementary SEM-EDX analysis revealed that both samples contain approximately 1% of sulfur. As it can be seen in Figure II-37 the different chemical composition results in a different behaviour at high temperature. At 775 °C, the volume of LM2 ash pastille is reduced, it changes its colour after the thermal treatment and it easily absorbs the humidity of the air, which makes it difficult to analyse by SEM-EDX or XRD.

Table II-6: ICP-MS analysis (wt %) of pastilles of ash LM1 and ash LM2 prepared at 400 °C

LM1				LM2			
Oxides (wt %)		Elements (wt %)		Oxides (wt %)		Elements (wt %)	
		O	39.5			O	32.1
SiO <sub>2</sub>	56.2	Si	26.0	SiO <sub>2</sub>	37.2	Si	17.3
<b>K<sub>2</sub>O</b>	<b>27.0</b>	<b>K</b>	<b>22.3</b>	<b>K<sub>2</sub>O</b>	<b>48.6</b>	<b>K</b>	<b>40.3</b>
CaO	8.7	Ca	6.2	CaO	3.1	Ca	2.2
MgO	3.2	Mg	1.9	MgO	2.3	Mg	1.4
<b>P<sub>2</sub>O<sub>5</sub></b>	<b>2.5</b>	<b>P</b>	<b>1.1</b>	<b>P<sub>2</sub>O<sub>5</sub></b>	<b>4</b>	<b>P</b>	<b>1.7</b>
<b>Cl</b>	<b>2.7</b>	<b>Cl</b>	<b>2.2</b>	<b>Cl</b>	<b>4.6</b>	<b>Cl</b>	<b>4.6</b>
Na <sub>2</sub> O	0.1	Na	0.1	Na <sub>2</sub> O	0.1	Na	0.1
traces	0.20	traces	0.70	traces	0.01	traces	0.3
Complementary SEM-EDX analysis revealed approximately 1 wt % of S both in LM1 and LM2 ashes							



Figure II-37: LM1 and LM2 ashes heat treated in air at 775 °C for 6 hours

Table II-7 summarizes the main crystalline phases at 400 and 900 °C, the diffractograms are presented in Appendix-A4. Due to the elevated amount of K, Cl and P the ashes are mainly composed of salts: KCl, K<sub>2</sub>SO<sub>4</sub>, and possibly Mg<sub>2</sub>P<sub>2</sub>O<sub>7</sub>. Besides, potassium and calcium carbonates are also formed.

Potassium is also associated to silica and forms KHSi<sub>2</sub>O<sub>5</sub>. A very small amount of crystalline SiO<sub>2</sub> was also detected in the diffractograms but most of the silica is in the amorphous phase, which is indicated by a dome in the diffractogram.

The main crystalline phase at 900 °C is K<sub>4</sub>H<sub>2</sub>(CO<sub>3</sub>)<sub>3</sub>·1.5 H<sub>2</sub>O. KHCO<sub>3</sub> and K<sub>2</sub>SO<sub>4</sub> are still present but their quantities decrease. KCl is also detected but the intensity in the diffractogram is weaker. As KCl has a low volatilization temperature, usually it is not present at 900 °C in the ash samples. It is likely that the small amount of KCl derives from the deposits on the ash sample surface due to the very low air current in the furnace. At 900 °C, the KHSi<sub>2</sub>O<sub>5</sub> and SiO<sub>2</sub> are molten and only a very small amount of KHSi<sub>2</sub>O<sub>5</sub> could be identified in the diffractograms.

Table II-7: Mineralogical composition of LM2 ashes at 400 °C and 900 °C

LM2 (harvest September 2011)				
	Compounds	JCPDS reference	400 °C	900 °C
salts	KCl	41-1476	yes	yes, decreased
	K <sub>2</sub> SO <sub>4</sub>	44-1414	yes	yes, decreased
	K <sub>2</sub> Mg <sub>2</sub> (SO <sub>4</sub> ) <sub>3</sub>	21-1400	maybe	maybe
	Mg <sub>2</sub> P <sub>2</sub> O <sub>7</sub>	32-0626	maybe	maybe
carbonates	KHCO <sub>3</sub>	12-0292	yes	yes
	CaCO <sub>3</sub>	05-0586	yes	maybe
	K <sub>4</sub> H <sub>2</sub> (CO <sub>3</sub> ) <sub>3</sub> ·1.5 H <sub>2</sub> O	20-0886	yes	yes, increased
silicates	KHSi <sub>2</sub> O <sub>5</sub>	43-0629	yes	yes, decreased
	SiO <sub>2</sub>	46-1045	yes	maybe
	SiO <sub>2</sub> (s) amorphous	-	yes	yes

## II.4.9 EFFECT OF ATMOSPHERE ON THE CHEMICAL COMPOSITION OF MISCANTHUS ASHES

The effect of reducing atmosphere was tested by heat-treating the ash samples in the mixture of CO<sub>2</sub> and H<sub>2</sub> (1.77 mol % CO<sub>2</sub> and 2.95 mol % H<sub>2</sub> in N<sub>2</sub> as input, Table II-4). Figure II-38 shows the X-ray diffractograms of miscanthus ashes at 900 °C in oxidizing and reducing atmospheres. The main difference is the absence of K<sub>2</sub>SO<sub>4</sub> in reducing atmosphere. According to the work of Jordan et al. [II-1], only moderate amount of sulfur is released into the gaseous phase in reducing atmosphere; the rest is transformed from inorganic acid soluble fraction into organically bound sulfur. Although the presence of K<sub>2</sub>S cannot be proved by XRD, the SEM-EDX analysis (Figure II-39) showed the presence of potassium and sulfur attached to the organic residue in the molten ashes. (In the SEM-EDX analysis, some area rich in CaCO<sub>3</sub> were also detected.)

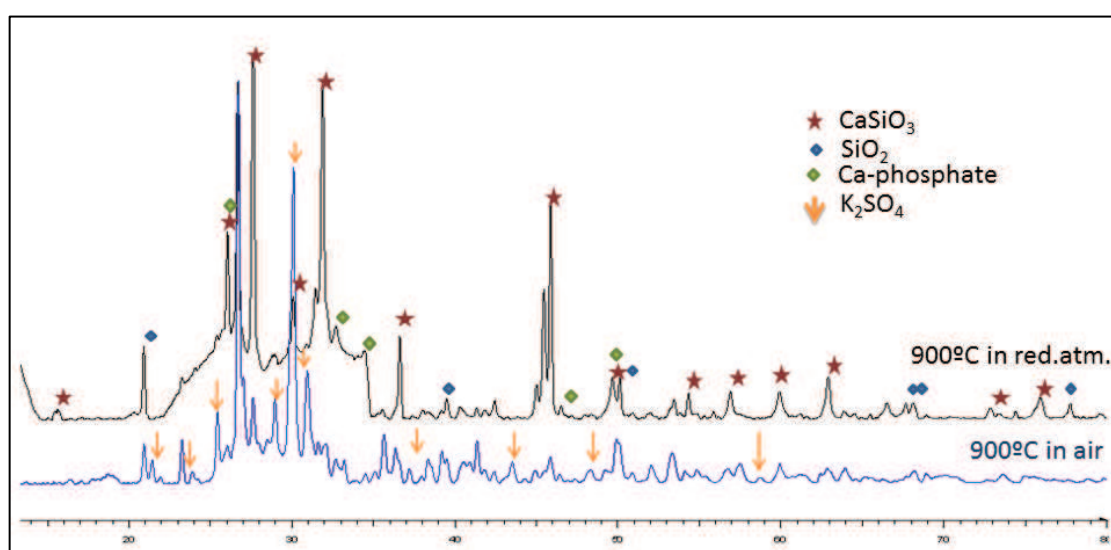


Figure II-38: diffractograms of LM1 ashes at 900 °C in oxidizing and reducing atmosphere

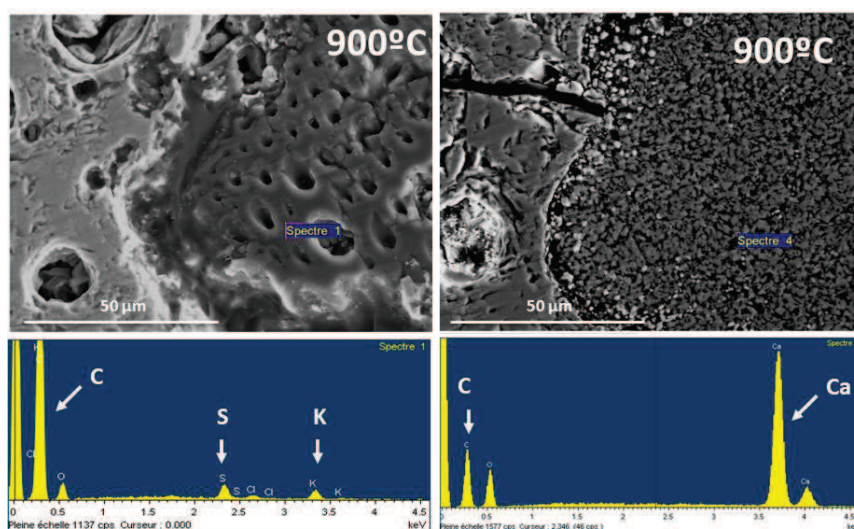


Figure II-39: SEM-EDX analysis of LM1 ashes prepared at 900° in reducing atmosphere

Figure II-40 presents the LM1 and LM2 ash samples after the heat-treatment in reducing atmosphere. While LM1 ash retains a lot of unburnt carbon, LM2 ash seems to be carbon free (carbon content cannot be determined by SEM-EDX analysis).

Earlier studies of Zhang et al. and Dupont et al. showed the catalytic effect of inorganics on biomass char gasification [II-2, II-3]. While potassium promotes the biomass char decomposition, silicon was found to be an inhibitor [II-2, II-3]. LM2 ash contains elevated level of potassium. While the K/Si ratio in the LM1 ash samples is 0.86, in case of LM2 the K/Si ratio is 2.3 (Table II-6), which explains the difference in the decomposition of carbon. As seen in Figure II-41, in contact with bed material the catalytic effect of K is not predominant due to the Si content of calcined olivine. (The same effect was found in contact with silica sand and olivine particles. Details on the ash/bed material interaction will be presented in Chapter IV.)

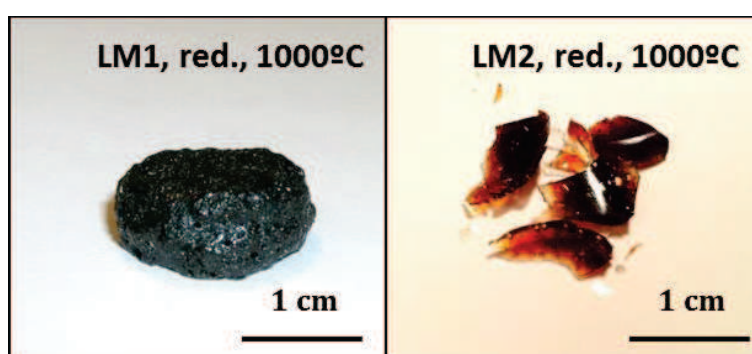


Figure II-40: LM1 and LM2 ashes in reducing atmosphere at 1000 °C for 6 h

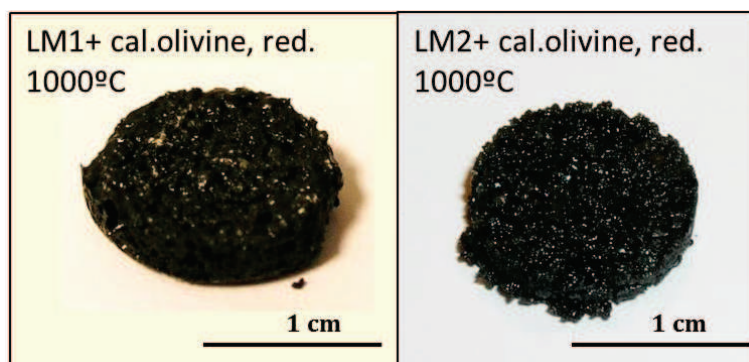


Figure II-41: LM1 and LM2 ashes with calcined olivine in reducing atmosphere at 1000 °C for 6 h

LM2 ashes are rich in chlorine and potassium. During the experiments we observed the deposition of KCl on the thermocouples (Figure II-42/A). (While pulling the sample holder out of the chamber, the KCl deposit fell back on the ash sample (Figure II-42/B)). The deposits were collected, dissolved in water and analysed by ion chromatography.

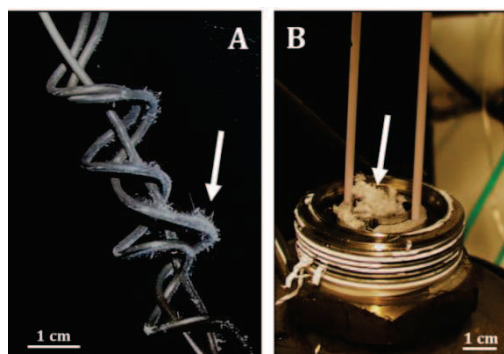


Figure II-42: KCl deposit on the thermocouples and the sample holder during the heat-treatment of LM2 ashes in reducing atmosphere

#### II.4.10 COMPOSITION OF LIQUID PHASES IN MISCANTHUS ASHES AT HIGH TEMPERATURE

For the SEM-EDX analysis of the liquid phase, the ash samples were heat-treated at 900 and 1000 °C for 6 h, then embedded in resin and polished. The SEM-EDX analysis was carried out at different points of the samples and an average elemental composition was calculated. Figure II-43 shows the composition of liquid phases in LM1 and LM2 ashes at 900 °C and 1000 °C. The liquid ashes mainly consist of SiO<sub>2</sub>, K<sub>2</sub>O and a small amount of CaO and MgO. The composition of liquid ash does not differ significantly in oxidizing and reducing atmosphere. In reducing atmosphere the sulfur forms gaseous H<sub>2</sub>S and does not bind the K as K<sub>2</sub>SO<sub>4</sub>, therefore the liquid phase contains more potassium. The liquid ashes of LM2 contain more potassium due to initially higher concentration in the plant. The amount of liquid phase cannot be determined by SEM-EDX analysis; it will be estimated by thermodynamic calculation in Chapter III.

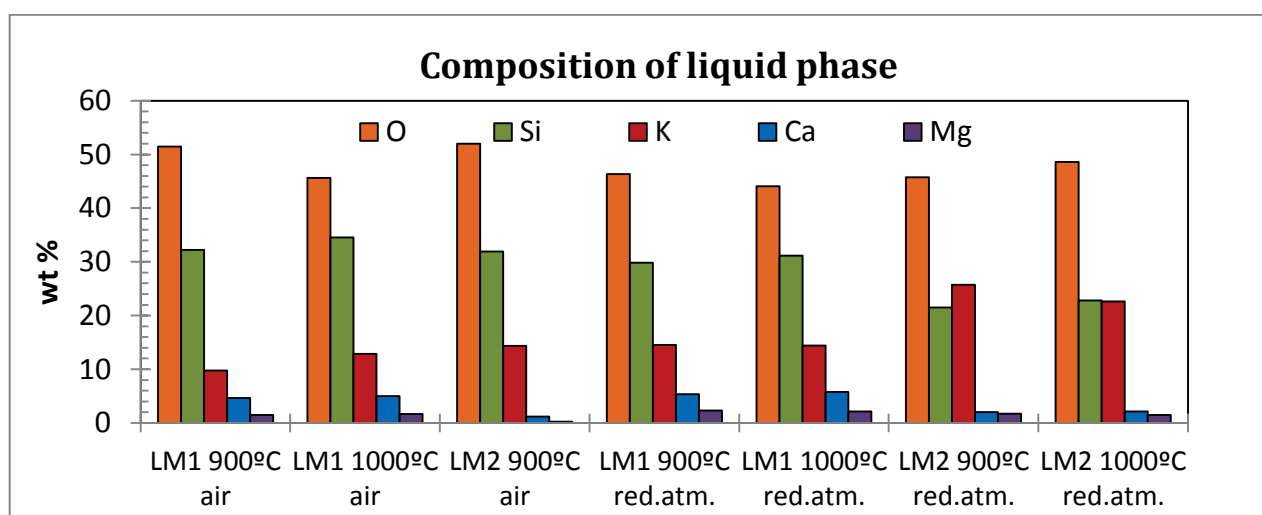


Figure II-43: Composition of liquid phases in LM1 and LM2 ashes in oxidizing and reducing atmosphere

## II.5 CONCLUSION

The aim of this chapter was to study the inorganic composition of miscanthus stem and to describe the phase transformations of miscanthus ashes as a function of temperature.

The characterisation of inorganics is challenging due to the variety and small quantity of compounds, which are present both in amorphous and crystalline phases in the organic matrix. The inorganic composition of miscanthus stem and miscanthus ashes was studied by chemical fractionation analysis and completed with ICP-MS, SEM-EDX and XRD measurements.

The main inorganics in miscanthus are Si, K, Ca, Mg, P, S, Cl and Na. Their distribution significantly varies between the outer and inner part of the stem. While the outer rigid part (cortex) is rich in silicon, the inner spongy part mostly contains potassium. Other inorganic elements are present in smaller quantities and therefore can be detected only after the degradation of the organic structure.

The chemical fractionation analysis showed that most of the inorganics are in reactive ionic form in the miscanthus and that the ashes heat-treated at high temperature (800 to 1000 °C) are mainly composed of silicates.

The detailed XRD analysis revealed the complex phase transformations of miscanthus ashes as a function of temperature. The main phase transformations in LM1 miscanthus ashes in oxidizing atmosphere are summarised in Figure II-43. At moderate temperature (<750 °C) most of the inorganics form salts, carbonates and silica. With increasing temperature the carbonates decompose, the chlorides volatilise and new silicate phases appear. Above 1000 °C the crystalline phase declines and the ash completely melts between 1300 and 1350 °C.

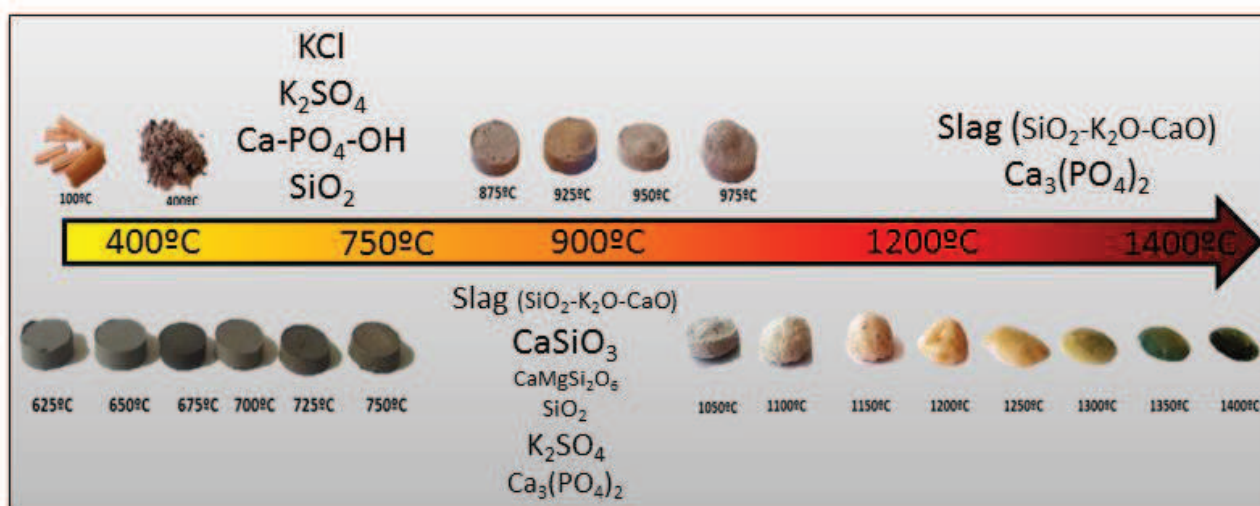


Figure II-44: Transformation of solid phases in LM1 ash in oxidizing atmosphere as a function of temperature

We found that the harvest time significantly modifies the composition of miscanthus ashes. Miscanthus harvested in September (LM2) contains almost twice as much potassium as the April harvest (LM1) resulting in the presence of potassium salts, carbonates and silicates both at 400 and 900 °C.

In the literature the phosphorus is mainly found in the form of potassium phosphate and sulfur can be found as  $\text{CaSO}_4$  [II-14]. However, in miscanthus ashes the formation of Ca- and Mg-phosphates is favoured and sulfur is always associated with potassium.

The main differences between oxidizing and reducing atmospheres are the presence of unburnt carbon and the form of sulfur. In reducing atmosphere  $\text{K}_2\text{SO}_4$  is not present but a small amount of  $\text{K}_2\text{S}$  can be detected with SEM-EDX analysis. While LM1 ash contains a lot of unburnt carbon in reducing atmosphere at high temperature (900 and 1000 °C), the LM2 ash has a glassy appearance with no or very small quantity of carbon; this is due to the catalytic effect of potassium on gasification rate.

The SEM-EDX analysis revealed that regardless the atmosphere and harvest time,  $\text{SiO}_2$  and  $\text{K}_2\text{O}$  are the major compounds of the molten ash phase and  $\text{CaO}$  and  $\text{MgO}$  are present in smaller quantity.

Due to the complexity of the ash samples, the exact solidus and liquidus temperatures and the amount of liquid phase could not be determined experimentally.

The ash fusibility test reported 902 °C as shrinkage starting temperature and 1326 °C as flow temperature. These results have to be handled with care, as this test was carried out with ashes prepared at 815 °C. The loss of volatile compounds, in particular the potassium, during the ash preparation can modify the ash melting tendencies.

The thermal analysis could not give adequate information about the ash melting either and it showed the complexity of the different exothermic and endothermic reactions between 400 and 1300 °C.

Considering all these difficulties, thermodynamic calculations can complement the experimentation. Moreover, they are useful tool to predict the solidus and liquidus temperature and the ratio of liquid and solid phases at elevated temperature. The comparison of calculations to experimental methods can also evaluate the adequacy and limitations of existing thermodynamic calculation tools.

## II.6 REFERENCES OF CHAPTER II

- [II-1] Andrea Jordan C, Akay G. Speciation and distribution of alkali, alkali earth metals and major ash forming elements during gasification of fuel cane bagasse. *Fuel* 2012;91:253–63.
- [II-2] Zhang Y, Ashizawa M, Kajitani S, Miura K. Proposal of a semi-empirical kinetic model to reconcile with gasification reactivity profiles of biomass chars. *Fuel* 2008;87:475–81.
- [II-3] Dupont C, Nocquet T, Da Costa JA, Verne-Tournon C. Kinetic modelling of steam gasification of various woody biomass chars: influence of inorganic elements. *Bioresour Technol* 2011;102:9743–8.
- [II-4] Bryers RW. Fireside slagging, fouling, and high-temperature corrosion of heat-transfer surface due to impurities in steam-raising fuels. *Prog Energy Combust Sci* 1996;22:29–120.
- [II-5] Vassilev S V., Baxter D, Andersen LK, Vassileva CG, Morgan TJ. An overview of the organic and inorganic phase composition of biomass. *Fuel* 2012;94:1–33.
- [II-6] Osman EA, Goss JR. Ash chemical composition, deformation and fusion temperatures for wood and agricultural residues. *Am Soc Agric Eng* 1983;83:3549–65.
- [II-7] Baxter XC, Darvell LI, Jones JM, Barraclough T, Yates NE, Shield I. Study of *Miscanthus x giganteus* ash composition – Variation with agronomy and assessment method. *Fuel* 2012;95:50–62.
- [II-8] Berg L. *Introductory Botany: Plants, People, and the Environment*. Second Edi. Thomson Brooks/Cole; 2008.
- [II-9] Ducreux G. *Introduction a la botanique*. Éditions Belin; 2002.
- [II-10] *Introduction to Plant Structure* n.d.
- [II-11] Werkelin J, Skrifvars B-J, Zevenhoven M, Holmbom B, Hupa M. Chemical forms of ash-forming elements in woody biomass fuels. *Fuel* 2010;89:481–93.
- [II-12] Ma JF, Yamaji N. Silicon uptake and accumulation in higher plants. *Trends Plant Sci* 2006;11:392–7.
- [II-13] Vassilev S V., Baxter D, Andersen LK, Vassileva CG. An overview of the composition and application of biomass ash. Part 1. Phase–mineral and chemical composition and classification. *Fuel* 2013;105:40–76.
- [II-14] Boström D, Skoglund N, Grimm A, Boman C, Ohman M, Brostrom M, et al. Ash transformation Chemistry during Combustion of Biomass. *Energy & Fuels* 2012;26:85–93.
- [II-15] Pettersson A, Zevenhoven M, Steenari B-M, Åmand L-E. Application of chemical fractionation methods for characterisation of biofuels, waste derived fuels and CFB co-combustion fly ashes. *Fuel* 2008;87:3183–93.
- [II-16] Piotrowska P, Zevenhoven M, Hupa M, Giuntoli J, de Jong W. Residues from the production of biofuels for transportation: Characterization and ash sintering tendency. *Fuel Process Technol* 2013;105:37–45.

- [II-17] Vainio E, Yrjas P, Zevenhoven M, Brink A, Laurén T, Hupa M, et al. The fate of chlorine, sulfur, and potassium during co-combustion of bark, sludge, and solid recovered fuel in an industrial scale BFB boiler. *Fuel Process Technol* 2013;105:59–68.
- [II-18] Doshi V, Vuthaluru HB, Korbee R, Kiel JH a. Development of a modeling approach to predict ash formation during co-firing of coal and biomass. *Fuel Process Technol* 2009;90:1148–56.
- [II-19] Boonjob W, Zevenhoven M, Hupa M, Ek P, Ivaska A, Miró M. Elucidation of associations of ash-forming matter in woody biomass residues using on-line chemical fractionation. *Fuel* 2013;107:192–201.
- [II-20] Frandsen FJ, van Lith SC, Korbee R, Yrjas P, Backman R, Obernberger I, et al. Quantification of the release of inorganic elements from biofuels. *Fuel Process Technol* 2007;88:1118–28.
- [II-21] Lindberg D, Backman R, Chartrand P, Hupa M. Towards a comprehensive thermodynamic database for ash-forming elements in biomass and waste combustion — Current situation and future developments. *Fuel Process Technol* 2013;105:129–41.
- [II-22] Petit M. Etude du comportement des espèces inorganiques dans une installation de gazéification de la biomasse: condensation des aérosols et dépôts. Nancy-Université-Ecole Doctorale EMMA, Laboratoire des Technologies de la Biomasse, Institut Jean Lamour, 2011.
- [II-23] Berjonneau J, Colombel L, Poirier J, Pichavant M, Defoort F, Seiler J-M. Determination of the Liquidus Temperatures of Ashes from the Biomass Gazification for Fuel Production by Thermodynamical and Experimental Approaches. *Energy & Fuels* 2009;23:6231–41.
- [II-24] Froment K, Defoort F, Bertrand C, Seiler JM, Berjonneau J, Poirier J. Thermodynamic equilibrium calculations of the volatilization and condensation of inorganics during wood gasification. *Fuel* 2013;107:269–81.
- [II-25] Evic N, Brunner T, Obernberger I. Prediction of biomass ash melting behaviour- correlation between the data obtained from thermodynamic equilibrium calculations and simultaneous thermal analysis (STA). 20th Eur Biomass Conf Exhib 2012.
- [II-26] Li H, Yoshihiko N, Dong Z, Zhang M. Application of the FactSage to Predict the Ash Melting Behavior in Reducing Conditions. *Chinese J Chem Eng* 2006;14:784–9.
- [II-27] Van Dyk JC, Melzer S, Sobiecki a. Mineral matter transformation during Sasol-Lurgi fixed bed dry bottom gasification – utilization of HT-XRD and FactSage modelling. *Miner Eng* 2006;19:1126–35.
- [II-28] Elled A, Åmand L, Steenari B. Composition of agglomerates in fluidized bed reactors for thermochemical conversion of biomass and waste fuels Experimental data in comparison with predictions by a thermodynamic equilibrium model. *Fuel* 2013;111:696–708.
- [II-29] Grimm A, Boström D, Lindberg T, Fredriksson A, Öhman M. Bed agglomeration characteristics during fluidized olivine bed combustion of typical biofuels. 19th Eur. Biomass Conf. Exhib. Berlin, Berlin, Germany: 2011, p. 1345–50.
- [II-30] Grimm A, Öhman M, Lindberg T, Fredriksson A, Boström D. Bed Agglomeration Characteristics in Fluidized-Bed Combustion of Biomass Fuels Using Olivine as Bed Material. *Energy Fuels* 2012;26:4550–9.

- [II-31] Bartels M, Lin W, Nijenhuis J, Kapteijn F, van Ommen JR. Agglomeration in fluidized beds at high temperatures: Mechanisms, detection and prevention. *Prog Energy Combust Sci* 2008;34:633–66.
- [II-32] Skrifvars B-J, Hupa M, Hiltunen M. Sintering of ash during fluidized bed combustion. *Ind Eng Chem Res* 1992;31:1026–30.
- [II-33] Skrifvars B-J, Ohman M, Nordin A, Hupa M. Predicting Bed Agglomeration Tendencies for Biomass Fuels Fired in FBC Boilers : A Comparison of Three Different Prediction Methods. *Energy & Fuels* 1999;13:359–63.
- [II-34] Visser HJM. The influence of fuel composition on agglomeration behaviour in fluidised-bed combustion. 2004.
- [II-35] Vamvuka D, Zografos D. Predicting the behaviour of ash from agricultural wastes during combustion. *Fuel* 2004;83:2051–7.
- [II-36] Jenkins BM, Baxter LL, Miles TRJ, Miles TR. Combustion properties of biomass. *Fuel Process Technol* 1998;54:17–46.
- [II-37] Mac an Bhaird ST, Walsh E, Hemmingway P, Maglinao AL, Capareda SC, McDonnell KP. Analysis of bed agglomeration during gasification of wheat straw in a bubbling fluidised bed gasifier using mullite as bed material. *Powder Technol* 2014;254:448–59.
- [II-38] Kupka T, Mancini M, Irmer M, Weber R. Investigation of ash deposit formation during co-firing of coal with sewage sludge, saw-dust and refuse derived fuel. *Fuel* 2008;87:2824–37.
- [II-39] Sommersacher P, Brunner T, Obernberger I. Fuel Indexes: A Novel Method for the Evaluation of Relevant Combustion Properties of New Biomass Fuels. *Energy & Fuels* 2012;26:380–90.
- [II-40] Basu P. *Combustion and Gasification in Fluidized Beds*. Taylor&Francis Group, LLC; 2006.
- [II-41] Zevenhoven-Onderwater M, Blomquist J-P, Skrifvars B-J, Backman R, Hupa M. The prediction of behaviour of ashes from five different solid fuels in fluidised bed combustion. *Fuel* 2000;79:1353–61.
- [II-42] Burhenne L, Messmer J, Aicher T, Laborie M-P. The effect of the biomass components lignin, cellulose and hemicellulose on TGA and fixed bed pyrolysis. *J Anal Appl Pyrolysis* 2013;101:177–84.
- [II-43] Du S, Yang H, Qian K, Wang X, Chen H. Fusion and transformation properties of the inorganic components in biomass ash. *Fuel* 2014;117:1281–7.
- [II-44] Prade T, Finell M, Svensson S-E, Mattsson JE. Effect of harvest date on combustion related fuel properties of industrial hemp (*Cannabis sativa* L.). *Fuel* 2012;102:592–604.
- [II-45] Van der Drift A, Olsen A. Conversion of biomass, prediction and solution methods for ash agglomeration related problems. 1999.

---

## CHAPTER III: THERMODYNAMIC CALCULATION

---

### ABSTRACT

As it was pointed out in the previous chapters, predicting the thermochemical reactivity of biomass ashes is crucial to be able to counteract operational problems such as slagging, fouling or agglomeration during biomass thermal conversion [III-1].

However, laboratory and pilot experiments are time consuming and expensive, moreover, due to the complex system, the physicochemical analysis of biomass ashes is challenging. Since the development of computational thermochemistry in the 1990s, many studies use thermodynamic equilibrium calculation to predict the inorganic phase transformation during different thermal processes [III-1–10]. These calculations are based on the global minimization of Gibbs energy at fixed pressure and temperature [III-2].

The aim of this chapter is to describe the biomass ash transformation using the thermochemical software package FactSage® and compare the calculations with laboratory experiments. The calculations were performed with FactPS, FToxid, FTsalt and GToxid databases under oxidizing and reducing conditions at atmospheric pressure. The results were validated with static laboratory experiments carried out at CEMHTI, CNRS (oxidizing conditions) and at the laboratory LTB-LITEN, CEA Grenoble (reducing conditions).

The calculations showed reasonably good agreement with the experiments, but it has to be noted that the choice of databases and solution phases can significantly influence the prediction of ash melting and the composition of the solid and liquid phases. Still, thermodynamic calculations remain one of the main predictive tools in biomass thermal conversion as they can estimate the liquid to solid ratio at high temperature and they can help to interpret experimental results.

## III.1 INTRODUCTION

The aim of this chapter is to describe the phase transformation of miscanthus ashes by thermochemical calculations under different conditions and to compare these calculations with laboratory experiments.

The calculations were performed with the software package FactSage 6.3<sup>®</sup>. The results were validated with static laboratory experiments on miscanthus ashes. The experiments in oxidizing atmosphere were performed at the laboratory CEMHTI, CNRS, while the experiments in reducing atmosphere were carried out in the laboratory *LTB-LITEN (Laboratoire des Technologies de la Biomasse-Laboratoire d'Innovation pour les Technologies et les Energies Nouvelles, CEA, Grenoble)*.

This chapter starts with an overview of the utilisation of thermodynamic calculations in biomass thermal conversion. The methodology section reasons the choice of input data, databases and solution phases.

The result section is divided into two parts.

The first part presents the transformation of miscanthus ashes under different conditions. For this calculation, the composition of 1 kg LM1 miscanthus was used. The calculations were performed both in the excess of oxygen and with restricted oxygen supply according to EQTEC gasification parameters (industrial partner of GAMECO project). The impact of elemental composition on liquid phase formation was also studied by varying the quantity of the different ash forming elements.

For the moment, the available data concerning alkali salt and alkali oxide systems in the thermodynamic databases are not complete. Therefore, beside using the salt database FTsalt, two oxide databases were compared: FToxid, the original oxide database available in FactSage package and GToxid database, developed by GTT Technologies in collaboration with the Jülich Research Center (FZJ) [III-11, III-12]. The GToxid database was provided to our disposition by LTB-LITEN laboratory. These two databases contain different solid silicates and solution phases. Our aim was to see the influence of the different databases on the prediction of miscanthus ash transformation and to determine the best adapted database.

In the second part of this chapter, the calculations were validated with laboratory experiments. In the experiments, the miscanthus ashes (prepared at 400 °C in air) were heat-treated under static conditions in different atmospheres. The oxidizing tests were performed in a regular laboratory furnace in air. The reducing tests were carried out in a laboratory furnace with controlled atmosphere (mixing H<sub>2</sub> and CO<sub>2</sub> gases) at the laboratory LTB-LITEN, CEA Grenoble. The ash samples were heat-treated at 900 °C and 1000 °C and analysed by XRD and SEM-EDX. The identified phases were compared to the calculations using FToxid, GToxid and FTsalt databases. In this case the composition of ashes prepared at 400 °C and the composition of the injected reducing gases were used as input data to better fit the experimental setup

## III.2 STATE OF THE ART

Many studies use thermodynamic equilibrium calculation to predict the ash behaviour during biomass thermal processes [III-1–10]. Thermodynamic calculations are based on the global minimization of Gibbs energy<sup>1</sup> of a system with given composition at fixed pressure and temperature [III-2].

Many thermodynamic softwares are available on the market, such as FactSage<sup>®</sup>, HSC Chemistry<sup>®</sup>, MTDATA<sup>®</sup>, MINGTSYS<sup>®</sup> [III-2]. This study was carried out with the software package FactSage<sup>®</sup>.

Factsage<sup>®</sup> was created in 2001 with combining two thermodynamic softwares, F\*A\*C\*T/FactWin and ChemSage [III-13]. It is used in many different fields such as materials science, metallurgy, glass technology, nuclear waste disposal, solar energy storage, combustion and ceramics [III-14].

FactSage<sup>®</sup> consists of different modules and enables among others to calculate phase diagrams, the concentration of chemical species in thermodynamic equilibrium or the surface tension, and viscosity [III-2, III-13].

FactSage<sup>®</sup> contains different databases [III-15]:

- *FToxid*- oxide database for slag<sup>2</sup>, glass, minerals, ceramics, refractories
- *FTsalt*- salt database of cations and anions
- *FThall*- Hall aluminium database
- *FThelg*- aqueous (Helgeson) database
- *FTmisc*-miscellaneous database for copper, nickel, lead, zinc, sulfides alloys
- *FTpulp*- pulp and paper database (corrosion and combustion in recovery boilers)
- *SGTE databases*- different alloy databases
- *TDNucl*- thermodata nuclear database

FTsalt database contains different liquid and solid solutions<sup>3,4</sup> of carbonates, chlorides and sulphates.

FToxid database consists of pure oxides and oxide solutions of 20 elements [III-15].

The liquid/glass solution phase (FToxid-Slag) also contains dilute solutions of S, SO<sub>4</sub>, PO<sub>4</sub>, H<sub>2</sub>O/OH, CO<sub>3</sub>, F, Cl, I, C, N and CN [III-13,15].

The right choice of solution phases is crucial as they can alter the composition of gaseous, liquid and solid phases at high temperature.

---

<sup>1</sup> Gibbs free energy or free enthalpy ( $\Delta G$  [J/mol]) is the thermodynamic potential of a system, which has a minimum in thermodynamic equilibrium

<sup>2</sup> Slag: mixture of oxides

<sup>3</sup> Solution: a homogenous mixture of two or more substances which is composed of one phase

<sup>4</sup> Solid solution: "a single crystalline phase which may be varied in composition within finite limits without the appearance of an additional phase" [23]

SlagA solution phase is the most commonly used liquid oxide solution [III-9, III-16], but calculation with SlagH (incorporating alkali halides in the oxide solution) was also published [III-1]. Calculations without selecting any liquid solutions are also found in the literature [III-7]. When the number of selected chemical elements is too important, using the solution phases can cause convergence problems during the calculations. Another special aim of not using solution phases can be the maximization of the alkali vapour pressure in the gaseous product to study the volatilisation and deposition of inorganics [III-4].

In any case, the results must be interpreted with care as the calculations regarding the molten biomass ash have certain limitations. The thermodynamic data and results have to be validated with literature data and experimentations. Comparing experimental results with liquidus temperature obtained by thermodynamic softwares can show 200 °C difference [III-2, III-3]. This uncertainty is first due to kinetic considerations: the software calculates the thermodynamic equilibrium considering infinite reaction time, while the residence time in industrial processes is too short (few seconds or minutes) [III-4, III-17]. As presented in Chapter II, the inorganics are present in different forms in the biomass such as ionic liquids (alkali salts of  $\text{Cl}^-$ ,  $\text{SO}_4^{2-}$ ,  $\text{CO}_3^{2-}$ ,  $\text{PO}_4^{3-}$ ), organically bonded alkali earth metals, sulfur or minerals. Their chemical form influences the formation of new solid phases or the rate of volatilization but the different form of elements cannot be taken into account in the calculations [III-2]. Solid-solid or solid-liquid phase reactions are in general slower than solid-gas, liquid-gas or gas-gas phase reactions [III-17]. Moreover, the organic matrix or the char can retard the reaction kinetics as diffusion and convection are slower than the actual chemical reaction [III-17]. While FactSage® only takes into account the equilibrium composition, some additional programs like DICTRA® can improve the calculations by taking into account the diffusion-control of the chemical reactions [III-2].

Another drawback using FactSage® is that not all the binary and ternary systems have been evaluated and optimized and these sub-systems are considered to be ideal solutions<sup>5</sup> or have been approximated [III-15].

The oxide solution phases were developed for metallurgical and coal ash slag ( $\text{Al}_2\text{O}_3\text{-CaO-FeO-Fe}_2\text{O}_3\text{-MgO-SiO}_2$ ) [III-5,18], which differs from the major component of biomass ash slag ( $\text{CaO-K}_2\text{O-SiO}_2\text{-MgO-NaO}$ ).

Though many binary and ternary systems have been recently evaluated ( $\text{Na}_2\text{O-SiO}_2$  [III-19],  $\text{K}_2\text{O-SiO}_2$  [III-19],  $\text{Na}_2\text{O-Al}_2\text{O}_3$  [III-20],  $\text{K}_2\text{O-Al}_2\text{O}_3$  [III-20],  $\text{K}_2\text{O-Na}_2\text{O-SiO}_2$  [III-21],  $\text{K}_2\text{O-Al}_2\text{O}_3\text{-SiO}_2$  [III-22]), the binary systems  $\text{K}_2\text{O-CaO}$  and  $\text{K}_2\text{O-MgO}$  have not yet been optimized [III-3]. Moreover, no accurate data are available for  $\text{K}_2\text{O-SiO}_2\text{-CaO}$  ternary system for the moment, which would be crucial to precisely describe the biomass molten ashes. Figure III-1 presents

---

<sup>5</sup> Ideal solution (containing A and B compounds) acts like ideal gases, the energy of A-B interaction is the same as A-A or B-B interactions, and therefore the enthalpy and volume are additives ( $\Delta G=0$ ,  $\Delta V=0$ )[26]. Whereas a non-ideal/real solutions can have volume change, and there is a possibility of immiscibility or partial immiscibility

the available literature data of the ternary phase diagram  $K_2O$ - $CaO$ - $SiO_2$  made by Morey et al in 1930 [III-23] Since the work of Morey, this ternary phase diagram has not been completed.

### $K_2O$ - $CaO$ - $SiO_2$

FIG. 391.—The high  $SiO_2$  corner of system  $K_2O$ - $CaO$ - $SiO_2$ .

G. W. Morey, F. C. Kracek, and N. L. Bowen, *J. Soc. Glass Technol.*, 14, 153 (1930).

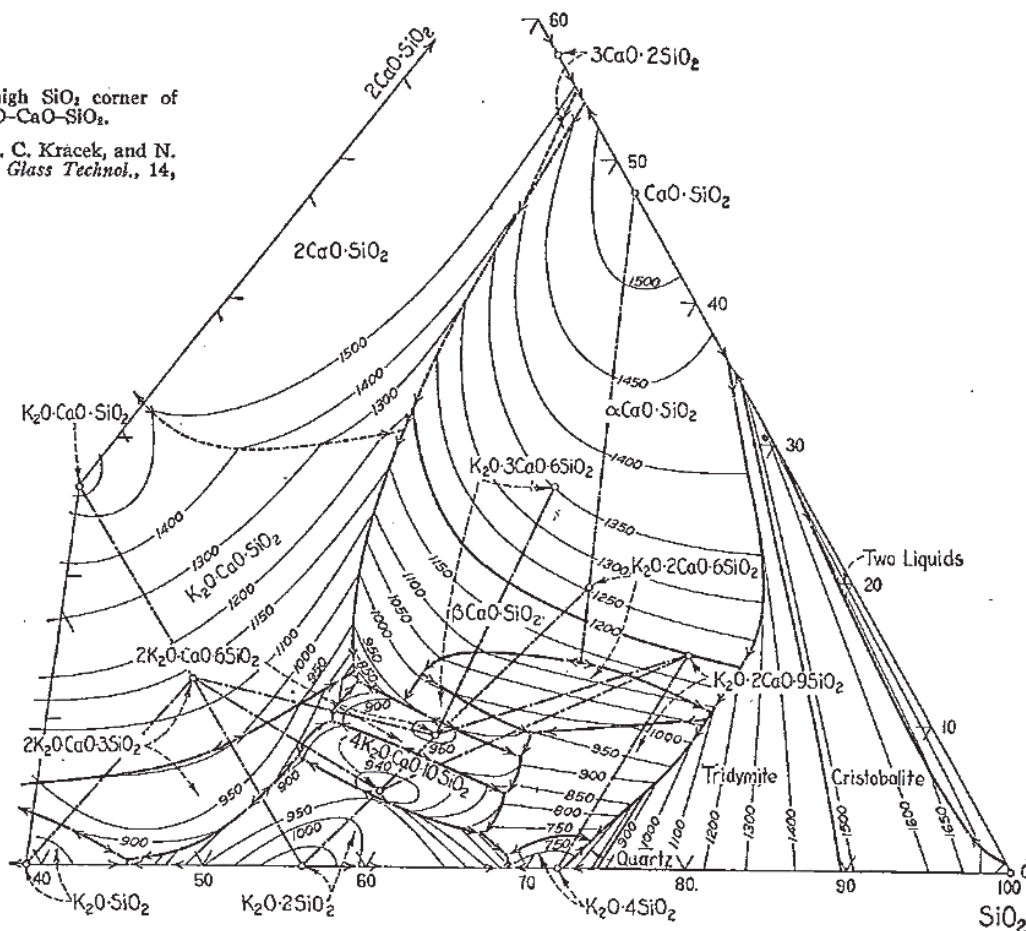


Figure III-1: The  $K_2O$ - $CaO$ - $SiO_2$  ternary phase diagram [III-23]

Salt databases are available for alkali (K, Na) salt mixtures only. According to a study in 2011, no database was available for the complex system containing Na, K, Ca, Mg, Zn, Pb salts, and calculations for the  $K^+$ ,  $Ca^{2+}$ // $SO_4^{2-}$ ,  $Cl^-$  system have only been performed recently [III-2]. The K-Ca-phosphate system for phosphorus rich biomasses (wheat, barley wastes, rapeseed cake) has also to be validated and the controversial results have to be clarified [III-2].

Recently, another oxide database has been developed in the collaboration of GTT Technology and Jülich Research Center (FZ) for refractory materials and metallurgical slag [III-11]. This thermodynamic database (further referred as GToxid) consists of the system  $CaO$ - $MgO$ - $Al_2O_3$ - $CrO_x$ - $FeO_x$ - $K_2O$ - $Na_2O$ - $SiO_2$  and it is based on experimental data on phase equilibria and thermodynamic properties [III-11]. It contains 175 stoichiometric compounds, 50 solid solutions and a liquid solution phase with 57 species and a gas phase [III-11]. In contrast to FToxid-Slag solution phase, the Gibbs-energy of the liquid phase is based on a non-ideal associate solution description [III-11], which might give better estimation on the properties of biomass ash liquid phase. Also, GToxid database contains solid phase Ca-K-silicates and Mg-K-silicates, which are not available in the FToxid database.

### III.3 MODELLING THE INORGANIC TRANSFORMATION IN MISCANTHUS

The aim of this study is to describe the transformation of inorganics in miscanthus and to estimate the melting behaviour of ashes in case of combustion and gasification. The gasification condition was chosen according to the EQTECH technology, one of the industrial partners of the GAMECO research project.

The calculations were performed with FactSage® version 6.3 and 6.4 selecting the FactPS, FToxid and FTsalt databases. We use the ultimate analysis data as start-up composition and to calculate the stoichiometric amount of air necessary to combust 1 kg of miscanthus. The calculations are performed at atmospheric pressure between 400 and 1400 °C. Two different air supplies were used: stoichiometric amount of air and limited amount of air (defined by our industrial partner). FToxid and FTsalt databases contain both liquid and solid solution phases. The solution phases have to be chosen with care, as they can significantly influence the results, the amount of liquid phase, the composition of liquid and solid phases and the vapour pressure of alkali compounds.

#### III.3.1 INPUT DATA FOR THERMODYNAMIC CALCULATIONS

##### FUEL COMPOSITION

One kg of miscanthus was used as fuel input. The composition of the biomass was adjusted from the standardized ultimate analysis provided by the analytic laboratory, SOCOR, France. The ultimate analysis of the miscanthus plant (LM1, April 2011) and the ash composition is presented in Table III-1 and Table III-2.

*Table III-1: Ultimate analysis of miscanthus*

Ultimate analysis of LM1 miscanthus	
	wt % on dry base
Ash content	2.1
C	48.6
H	5.74
N	<0.3
O	43
S	1669 mg/kg
Cl	1002 mg/kg
*prepared at 815 °C according to ISO 1171	

*Table III-2: ash composition of LM1 miscanthus (at 815 °C, ISO 1171)*

Ash composition at 815 °C (%wt)											
SiO <sub>2</sub>	Al <sub>2</sub> O <sub>3</sub>	Fe <sub>2</sub> O <sub>3</sub>	TiO <sub>2</sub>	CaO	MgO	Na <sub>2</sub> O	K <sub>2</sub> O	SO <sub>3</sub>	P <sub>2</sub> O <sub>5</sub>	MnO <sub>2</sub>	Total
66.0	1.0	1.1	<0.1	10.4	2.5	1.1	14.1	1.5	1.6	0.3	99.6

From the ultimate analysis of the miscanthus, a global organic formula was defined:  $\text{CH}_{1.42}\text{O}_{0.66}$  ( $M_{\text{CH}_{1.42}\text{O}_{0.66}}=23.98=24$  g/mol, 1 kg biomass 41.66 mol  $\text{CH}_{1.42}\text{O}_{0.66}$ ).

This formula was calculated via dividing the percentage of carbon, hydrogen and oxygen by their atomic mass. Then, the molar quantities of hydrogen and oxygen were normalized to the carbon.

$$\begin{array}{llll} \text{C:} & 48.6/12 = 4.05 & 4.05/4.05 \rightarrow 1 & \text{(III.1)} \\ \text{H:} & 5.74/1 = 5.74 & 5.74/4.05 \rightarrow 1.42 & \text{(III.2)} \\ \text{O:} & 43/16 = 2.69 & 2.69/4.05 \rightarrow 0.66 & \text{(III.3)} \end{array}$$

For the inorganic composition of the miscanthus only the main ash forming elements (K, Si, Mg, Ca, Na, S, P, Cl) were considered. Although they are indicated as oxides in the standard analysis (Table III-2), we preferred to use the form of pure elements, as they can be found in different forms in the biomass. (The form of oxides or pure elements does not influence the global equilibrium calculation. The calculation of elemental composition is found in Appendix A5.) The composition of 1 kg miscanthus (on dry base) is presented in Table III-3.

Table III-3: Composition of 1 kg dry miscanthus for the thermodynamic calculations

1 kg Miscanthus				
composition (dry) mass(g)				
Organic	$\text{CH}_{1.42}\text{O}_{0.66}$		973.4	
Inorganic	N	3	Mg	0.3
	S	1.7	K	2.5
	Cl	1	P	0.1
	Si	6.5	Na	0.2
	Ca	1.6	Other*	9.7
	total		1000	
* minor ash forming elements (Al, Fe, Ti, Mn), which were not taken into account in the calculation and the oxygen subtracted from the oxide form of the elements				

### ATMOSPHERE

The calculations were performed both in oxidizing and reducing atmosphere at atmospheric pressure. As presented in Chapter I.3.3, the oxygen requirement for the combustion of 1 kg of biomass, namely the *stoichiometric oxygen requirement* can be calculated from the ultimate analysis of the biomass by determining the oxygen needed to convert 1 kg of C into  $\text{CO}_2$ , 1 kg of H into  $\text{H}_2\text{O}$  and 1 kg of S into  $\text{SO}_2$  [III-24]. The oxygen already present in the biomass is subtracted.

In our case, for 1 kg of miscanthus (*C* 48.6 wt %, *H* 5.74wt %, *S* 0.167wt % and *O* 43wt % on dry base) the stoichiometric oxygen requirement is:

$$32/12 \cdot 0.486 + 8 \cdot 0.0574 + 0.0017 - 0.43 = \underline{\underline{1.327 \text{ kg O}_2 / \text{kg miscanthus}}} \quad (\text{III.4})$$

The gasification of the miscanthus is performed with limited oxygen supply. The *equivalent ratio* gives the ratio of the actual oxygen supply and the stoichiometric oxygen requirement. In EQTEC gasification technology the equivalent ratio is ER=0.33, which is equal to 444 grams O<sub>2</sub> for 1 kg miscanthus on dry base.

### III.3.2 CHOICE OF DATABASES AND SOLUTION PHASES

The appropriate databases have to be chosen for the thermodynamic calculations. *FactPS*, *FToxid* and *FTsalt* were selected as possible databases for biomass thermal conversion as they contain alkali and alkaline earth metal salts, oxides and silicates.

FactPS database contains more than 4000 pure substances in gaseous, liquid and solid phases, while FToxid, FTsalt and FTpulp are coupled compound and solution databases for solid and liquid phase [III-13]. FactPS is the only one out of the four databases which contains compounds in gaseous phase; therefore it always has to be selected when performing the calculations.

FToxid consists of compounds and solutions of alkali oxides and silicates and FTsalt consists of compounds and solutions of alkali chlorides, sulphates, carbonates, nitrates and hydroxides. The possible solution phases for the miscanthus are summarized in Appendix A6.

To compare the three databases, different preliminary calculations were performed in the equilibrium module both for combustion (ER>1) and gasification (ER=0.33) in the range of 400 and 1000 °C. The calculations are presented in Appendix A7. As a result, the following solution phases were selected:

<u>FToxid solid solution phases:</u>	FToxid-WOLLA wollastonite (CaSiO <sub>3</sub> , MgSiO <sub>3</sub> ), FToxid-cPyrA clinopyroxene (CaMgSi <sub>2</sub> O <sub>6</sub> , Mg <sub>2</sub> Si <sub>2</sub> O <sub>6</sub> )
<u>FToxid liquid solution phase:</u>	FToxid-SlagA alkali and alkaline earth metal oxides diluting sulphides (for reducing atmosphere) FToxid-SlagB alkali and alkaline earth metal oxides diluting sulphates (for oxidizing atmosphere)
<u>FTsalt solid solution phases:</u>	FTsalt-ACl_A solid chloride solution of alkali and alkaline earth metal FTsalt-CSOB solid alkali sulphate/carbonate solution FTsalt-SCMO solid binary solution of MgSO <sub>4</sub> and CaSO <sub>4</sub>
<u>FTsalt liquid solution phases:</u>	FTsalt-SALTF liquid solution of alkali salts

### III.3.3 TRANSFORMATION OF MISCANTHUS ASHES

After selecting the databases and solution phases, the transformation of miscanthus ash was described both in oxidizing and reducing atmosphere in the range of 400 to 1400 °C.

The aim of this study was firstly to determine the amount of liquid phase as a function of temperature and secondly to compare the ash behaviour in oxidizing and reducing environment.

The liquid to liquid plus solid ratio ( $L/(L+S)$ (wt %)) is presented in Figure III-2.

The ratio of liquid phase significantly differs between 770 and 900 °C in case of gasification and combustion. While only 6% of liquid phase is predicted at 800 °C and 30% at 900 °C in oxidizing atmosphere, in reducing atmosphere the amount of liquid phase is significantly higher: it is about 50% in the range of 800 to 900 °C. The two curves equalize at 1000 °C and reaches 95% at 1300 °C. The liquidus temperature of miscanthus ash is 1703 °C in case of combustion and 1495 °C in case of gasification.

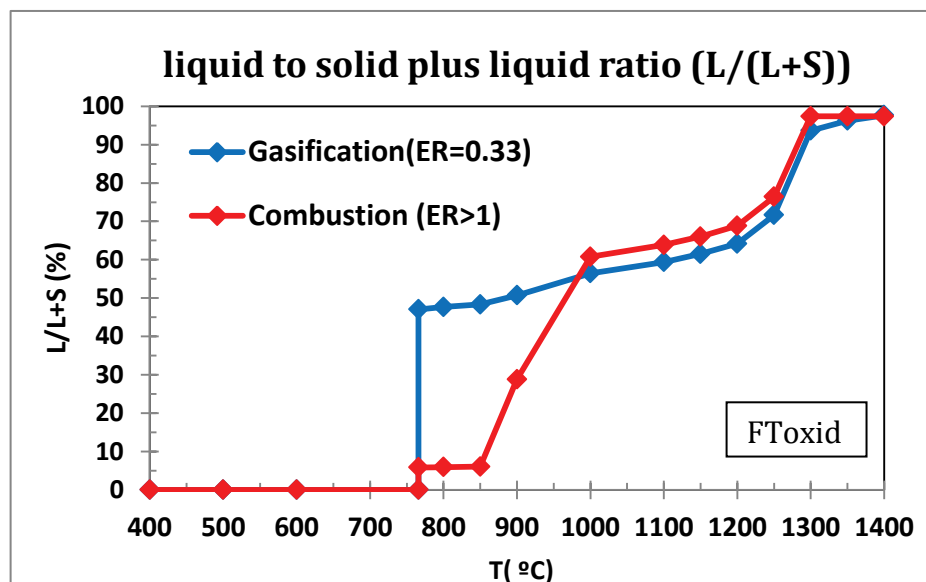


Figure III-2: liquid to liquid plus solid ratio in gasification ( $ER=0.33$ ) and combustion ( $ER>1$ ) in miscanthus ashes calculated with FToxid database

To understand the differences in liquid phase formation, the ash behaviour is detailed in the range of 400 to 1400 °C. The amount and composition of solid and liquid phases and the viscosity of the liquid phase in combustion and gasification are detailed in Appendix A8.

Figure III-3 and Figure III-4 illustrate the distribution of the condensed and volatilised compounds of LM1 ashes in oxidizing and reducing atmospheres. At low temperature (<750 °C) the ash is composed of salts (KCl,  $K_2SO_4$ ,  $CaSO_4$ , Ca-phosphates) and silicates ( $SiO_2$ ,  $CaSiO_3$ ,  $CaMgSiO_3$ , Na-Ca-silicate and a small amount of  $K_2Si_4O_9$ ). With increasing temperature the KCl volatilises, the  $CaSO_4$  and the  $K_2SO_4$  decompose. The S is released into the gas phase, while Ca forms solid silicates and K participates in the liquid phase formation.

The liquid phase appears above 750 °C and it consists of  $K_2O$ ,  $SiO_2$ ,  $CaO$  and a small amount of  $NaO$ . The amount of liquid phase increases gradually with increasing temperature. The ratio of the three main liquid components changes at elevated temperature as the solid silicates melt at 1300 °C, the amount of  $CaO(l)$  increases significantly with the melting of  $CaSiO_3(s)$ . With the melting of  $CaMgSi_2O_6$ ,  $MgO(l)$  also appears in the slag. The amount of  $K_2O(l)$  slightly decreases as more and more  $K$  volatilises. The only solid phase above 1300 °C is  $Ca_3(PO_4)_2$ .

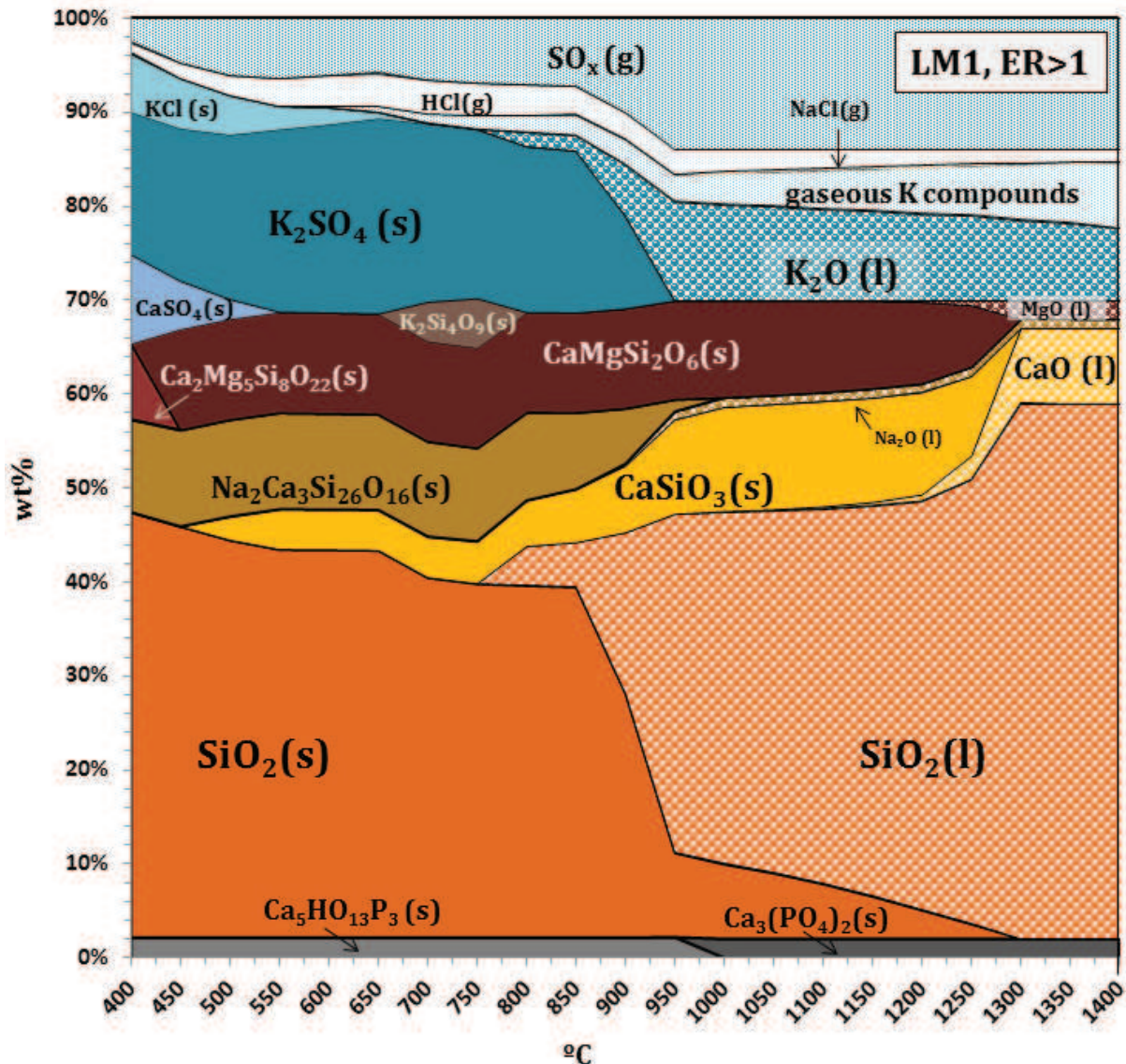


Figure III-3: Distribution of solid, liquid and gaseous compounds in miscanthus ashes as a function of temperature in case of combustion ( $ER > 1$ ) using FToxid database

In reducing atmosphere two main differences can be observed. The  $S$  does not form alkali salts but it is present in different gaseous compounds (mainly  $H_2S$  and  $COS$  and a small amount of  $HS$  and  $SO_x$ ). In consequence, greater amount of potassium silicates is formed. As  $K$ -silicate has low melting point (around 750 °C), the amount of liquid phase in the range of 750-900 °C is significantly greater than in combustion.

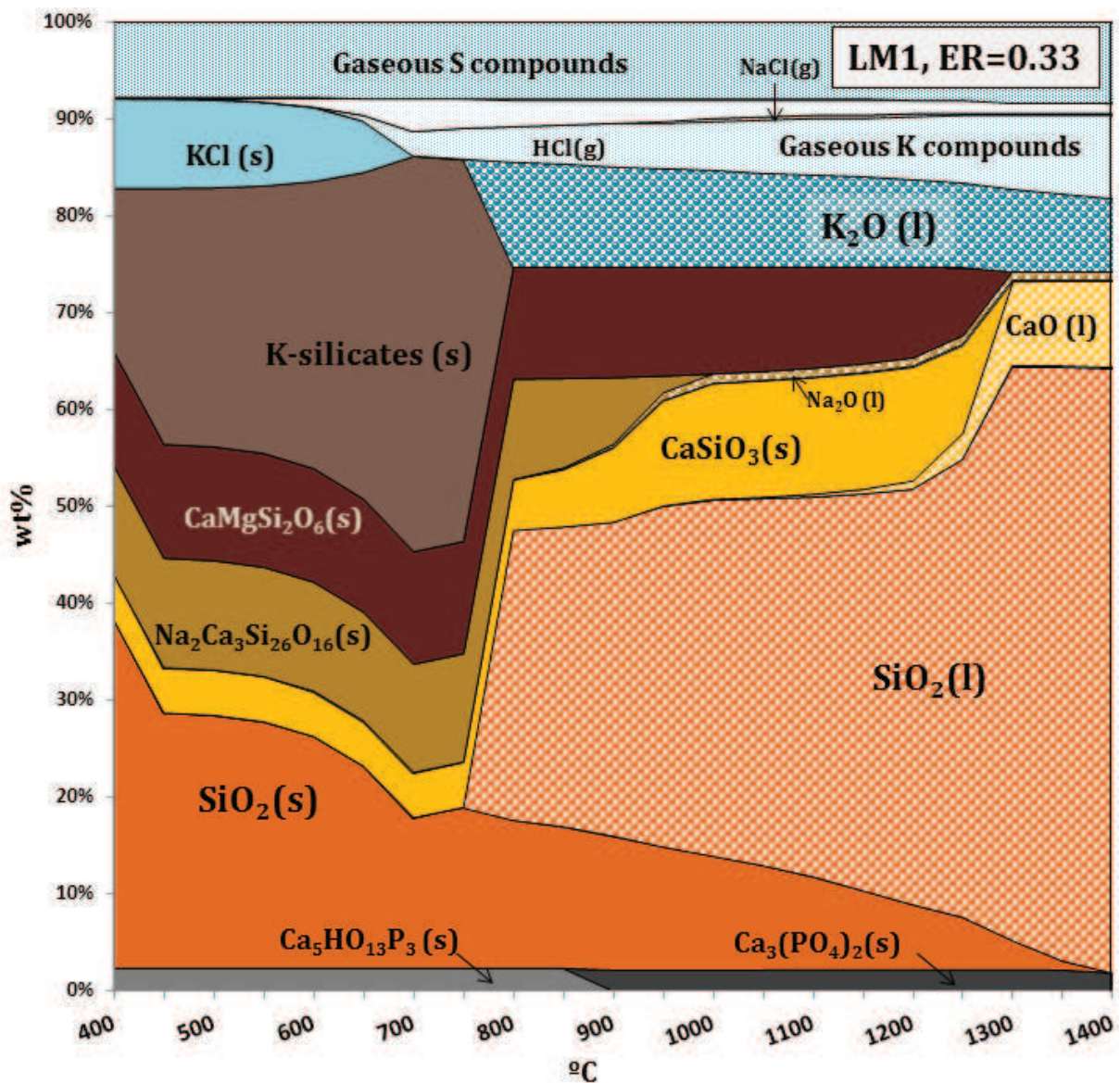


Figure III-4: Distribution of solid, liquid and gaseous compounds as a function of temperature in miscanthus ashes in case of gasification ( $ER=0.33$ ) using FToxid database

Figure III-5 presents the distribution of S, Si and K in the solid, liquid and gaseous phases during gasification and combustion. The main difference is summarised in Table III-4.

In case of combustion, potassium forms potassium silicate and potassium sulphate. Potassium silicate melts below 800 °C but  $K_2SO_4$  is stable in solid phase up to 1000 °C. During gasification, the formation of KCl and K-silicate is favoured, both of which are sensitive to heat. KCl is released into gas phase while  $K_2Si_4O_9$  melts and at 770 °C, which results in a higher liquid ratio below 900 °C.  $K_2SO_4$  melts above 900 °C thus the amount of liquid phase almost equalize in gasification and combustion.

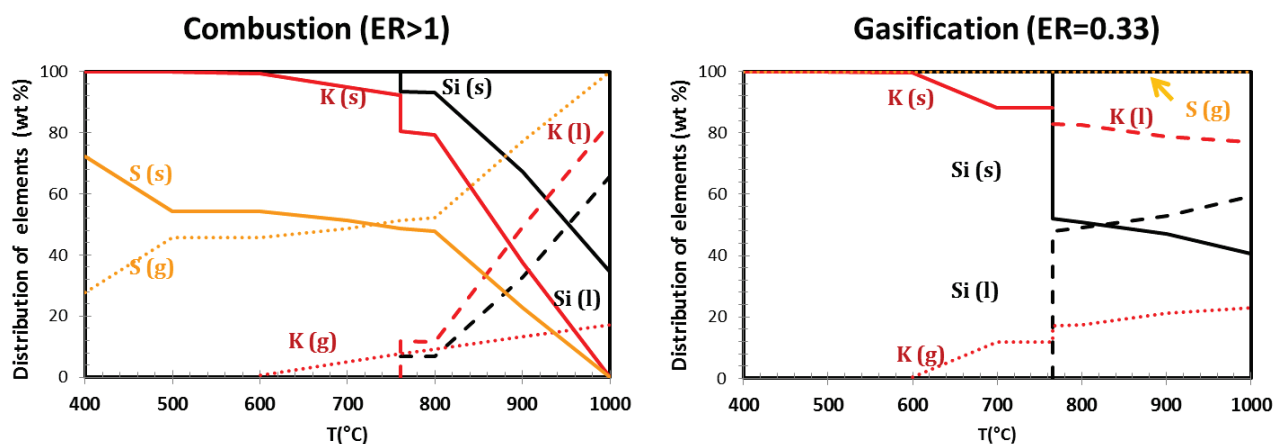


Figure III-5: Distribution of S, K and Si in gasification( $ER=0.33$ ) and combustion( $ER>1$ ) using FToxid database

Table III-4: Form of sulfur and potassium phases in case of gasification and combustion

	Gasification ( $ER=0.33$ )	Combustion ( $ER>1$ )
sulfur	$H_2S(g)$	$SO_2(g)$ , $K_2SO_4(s)$
potassium	$KCl(s,g)$ , K-silicate	$KCl(s,g)$ , K-silicate, $K_2SO_4(s)$

In summary, the nature of sulfur during gasification or combustion influences the  $L/(S+L)$  ratio by keeping a part of potassium in solid phase as  $K_2SO_4$ . This also means that the ash melting tendency can be lowered by reducing the quantity of potassium in the molten phase. This can be achieved either by decreasing the alkaline concentration in the biomass (washing with water or solvents) or by adding new components which promote the formation of new phases with higher melting point. It is known that while alkalis promote the liquid phase formation, elevated level of alkaline earth metals increase the ash melting temperature. In thermal conversion, biomass treatments or additives are often used to modify the ash melting behaviour (more detailed explanation will be provided in Chapter IV).

Another calculation series was performed to investigate the effect of the concentration of main ash forming elements on the amount of liquid phase. Aluminium was also added to the calculation. Although it has no biological role in the plant but it can be present as soil contamination and it is often used as additive in thermal processes (see Chapter IV.2.3).

The elements S, Ca, Mg, K, P, Na, Cl and Al were chosen as variables and Si as fix component. The calculation were carried out at 900 °C at 1 atm in combustion ( $ER>1$ ) and gasification( $ER=0.33$ ).

As 1 kg miscanthus contains 6.5g Si (analysed by Laboratory SOCOR), the quantity of the variables was chosen between 0 and 6.5g. The original amount of elements and their ratio to Si are given in Table III-5 .

Table III-5: amount of chosen elements in 1 kg of miscanthus and their ratio to Si

	Mass (g)	X*/Si
S	1.7	0.26
Ca	1.6	0.25
Mg	0.3	0.05
K	2.5	0.38
P	0.1	0.02
Cl	1	0.15
Na	0.2	0.03
Al	-	-
X*= S, Ca, Mg, K, P, Cl, Na and Al		

The tendencies in case of the different elements are presented in Table III-6. More details and figures are available in Appendix A9.

Table III-6: Main profile of liquid phase formation with increasing concentration of elements in case of combustion (ER>1) and gasification (ER=0.33)

	ER>1	ER=0.33
K	→	→
Na	→	→
Mg	↘	↘
Ca	↘	↘
P	→	→
S	→	→
Cl	↘	↘
Al	↘	↘

The main findings are:

- The increase of elements basically has the same effect on liquid phase formation in combustion and gasification
- The amount of P and S has no influence on liquid phase formation in gasification (ER=0.33) but their concentration between certain range can decrease the amount of liquid phase in combustion (ER=1.01)
- The increase of Mg and Ca overall has positive effect on decreasing the liquid phase
- Increasing amount of alkalis (K, Na) significantly increases the amount of liquid phase
- Cl promotes the volatilisation of alkalis. Although the amount of liquid phase decreases, the corrosion and deposition risks increase significantly
- Al as additive decreases the amount of liquid phase

### III.3.4 COMPARISON OF FTOXID AND GTXID DATABASES

As it was already mentioned, the calculations with FToxid databases have to be handled with care, as the solution phases had not been optimized for biomass ash, in particular for the  $\text{SiO}_2\text{-K}_2\text{O-CaO}$  system. Recently, another database was developed by GTT Technology for oxide systems. In this subsection, the miscanthus ash behaviour was studied with the two different oxide databases (FToxid and GTXid) to compare the differences.

In case of FToxid, the slagA liquid solution phase was chosen, the GTXid database contains only one liquid solution phase, GTXid-LIOX. The main difference in using the two databases is the form of solid silicates. While FToxid database contain K-silicate and Ca-Mg-silicates, GTXid database contains K-Mg-silicates and K-Ca-silicates. Na-Ca-silicates can be found in both databases but in different form.

In GTXid database all solution phases were selected to see which one can be present in the equilibrium. Beside the oxide databases, FTsalt liquid solution phases were also selected. Using FToxid database no liquid salt solution was calculated while in case of GTXid, liquid salt can be present at 900 °C which results in the presence of sulfur in the liquid phase. (The list of calculated solid and liquid compounds is given in Appendix 10.)

The solidus temperatures of miscanthus ashes (LM1-April 2011) for the different cases are compared in Table III-7. While FToxid gives similar value for the formation of liquid phase in combustion and gasification, GTXid database shows a difference of 250 °C. Comparing FToxid and GTXid, there is a difference of 90 °C for combustion and 166 °C difference for gasification.

*Table III-7: Calculated solidus temperature of miscanthus ashes (LM1 April2011) in combustion and gasification using FToxid or GTXid databases*

	FToxid	GTXid
Combustion (ER>1)	761 °C*	850 °C
Gasification (ER=0.33)	766 °C	600 °C
*calculated using slagB solution phase. The difference between slagA and slagB solution phases for the current system is negligible (see Appendix A7)		

The ratio and the quantity of liquid and solid phases as a function of temperature are compared in Figure III-6. Despite of the difference in the values of solidus temperature, the formation of liquid phase shows the same trend in case of combustion. In case of gasification, much more liquid is formed with FToxid in the range of 766-950 °C. Although the liquid phase appears at lower temperature with GTXid, its quantity stays below 10% until 850 °C, then significantly raises, catches up and exceeds the amount of liquid at 1000 °C using FToxid.

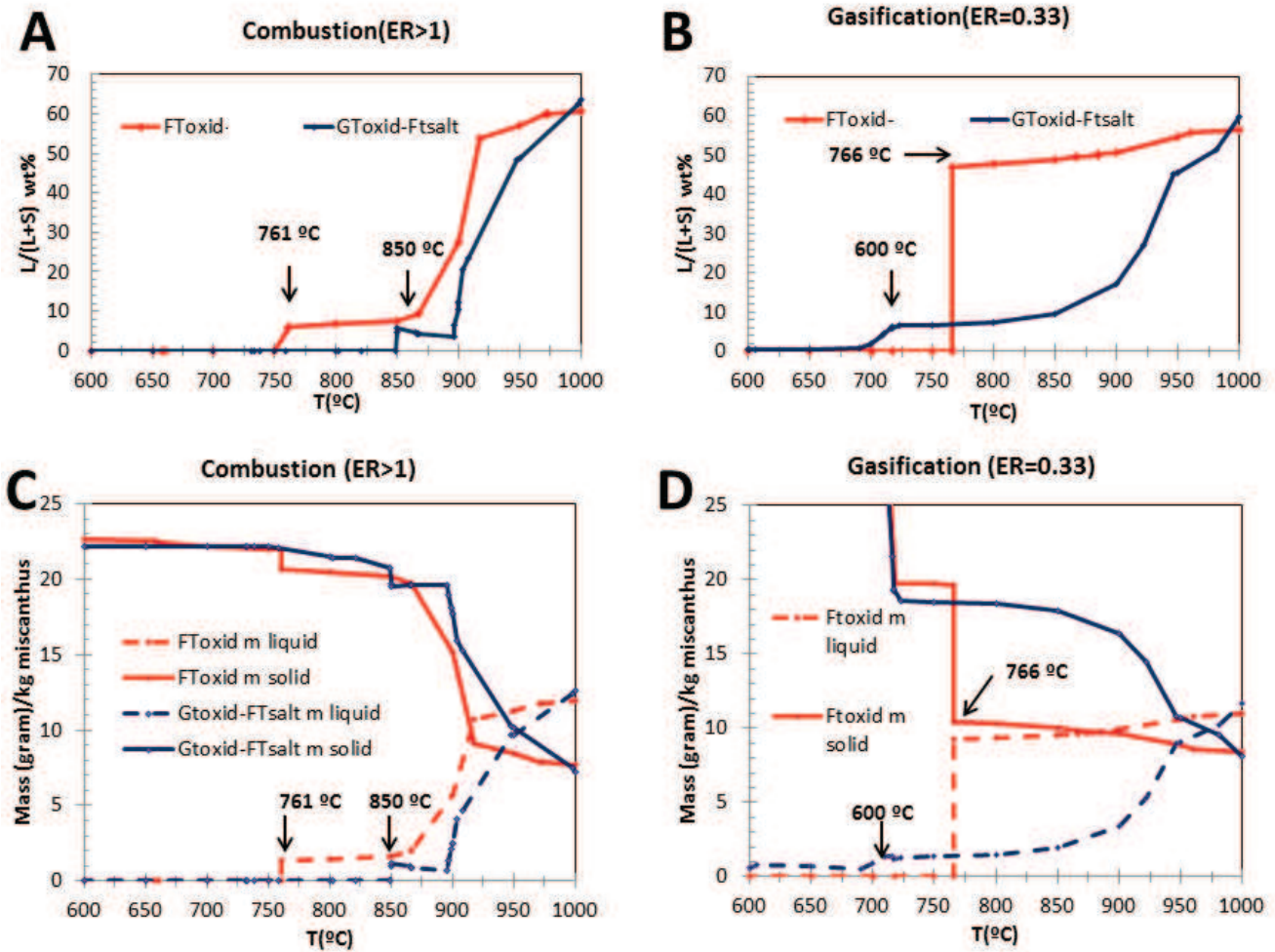


Figure III-6: liquid to liquid plus solid ratio ( $L/(L+S)$ ) in combustion (A) and in gasification (B); the quantity of liquid and solid phases of miscanthus ashes as a function of temperature in combustion (C) and in gasification (D) calculated with FToxid or GToxid databases

Figure III-7 and Figure III-8 show the composition of solid and liquid phases in miscanthus ash in case of gasification using FToxid and GToxid databases. A liquid salt phase is present between 600 and 700 °C in the case of GToxid-Ftsalt databases. Liquid silicates start to form at 700 °C but the quantity is lower than the corresponding FToxid-SlagA, because the potassium is kept in the solid phase by the formation of  $K_2Si_5MgO_{12}$ . Once  $K_2Si_5MgO_{12}$  decomposes at 910 °C the quantity of liquid phase levels off. K-Mg silicate cannot be found in FToxid database, K is present as  $K_2Si_4O_9$  and it melts at 766 °C.

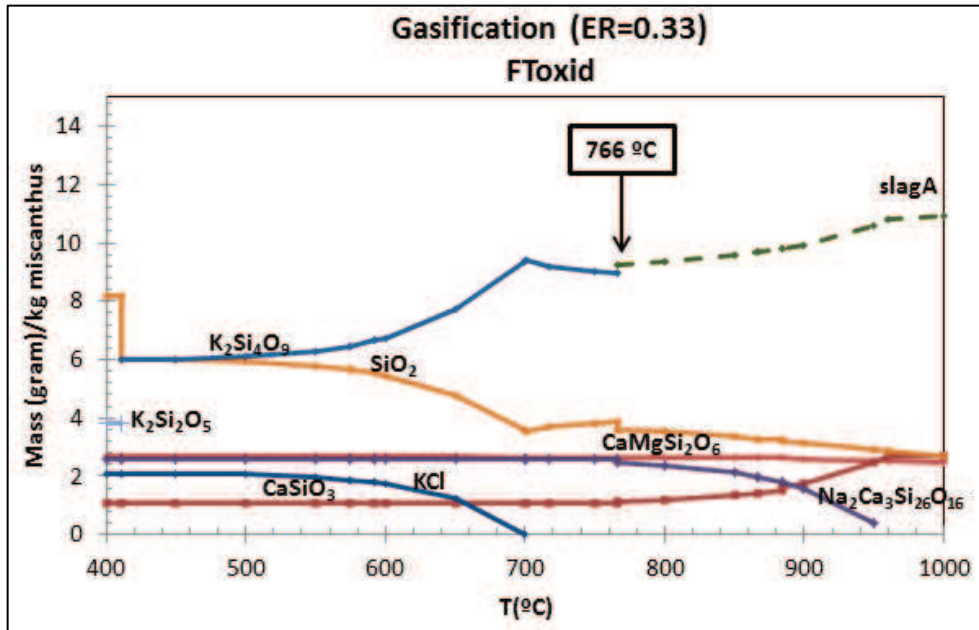


Figure III-7: Composition of condensed phases as a function of temperature in gasification using FToxid databases in miscanthus ashes

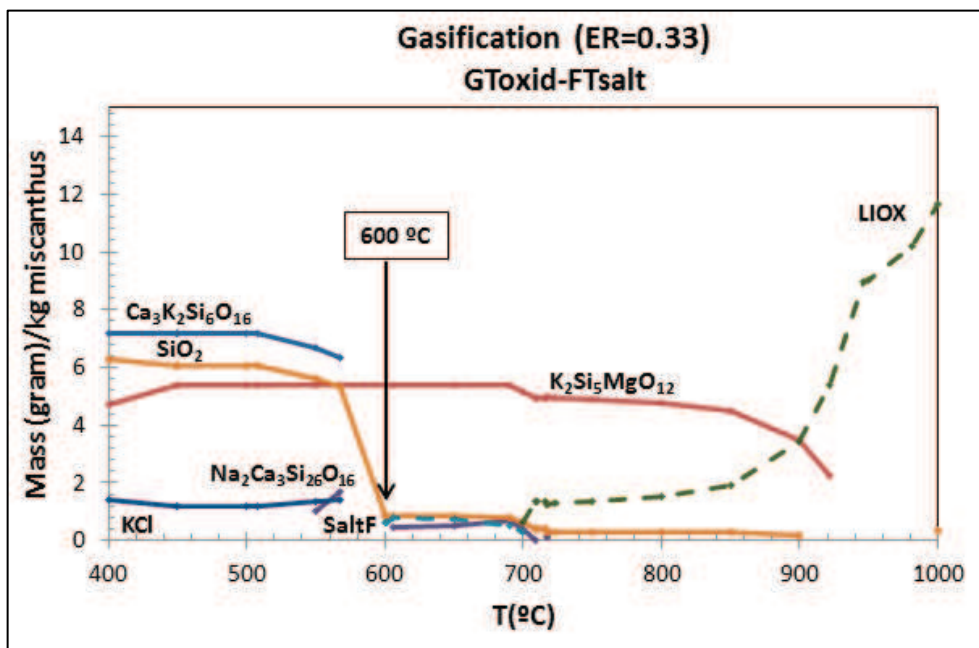


Figure III-8: Composition of condensed phases as a function of temperature in gasification using GToxid databases in miscanthus ashes

Figure III-9 and Figure III-10 show the composition of solid phases in combustion using FToxid and GToxid databases. The difference in the solidus temperature is due to the same reason as in case of gasification. In GToxid database, the formation of K-Mg silicates ( $K_2Si_{12}Mg_5O_{30}$  and  $K_2Si_5MgO_{12}$ ) keeps the K in the solid phase. As in combustion K is also present as solid  $K_2SO_4$ , the molten salt solution can form only at higher temperature compared to gasification (850 °C)

after the decomposition of solid sulphates. As the solid  $K_2SO_4$  decomposes at 850 °C, the molten salt phase appears and a new solid K-Mg-silicate forms with higher amount of K.



$K_2Si_5MgO_{12}$  is stable up to 910 °C, above this temperature the molten salt phase disappears and the alkalis form liquid silicate solution (GToxid-LIOX).

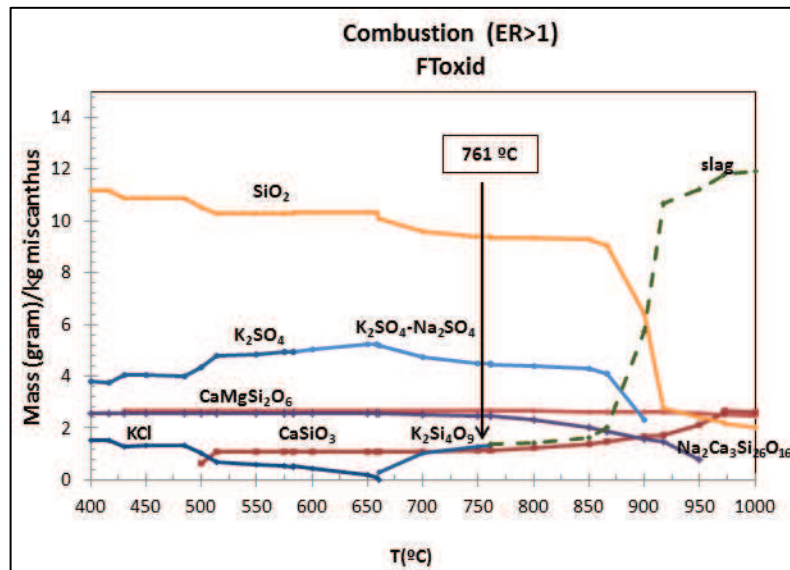


Figure III-9: Composition of condensed phases as a function of temperature in combustion using FToxid databases in miscanthus ashes

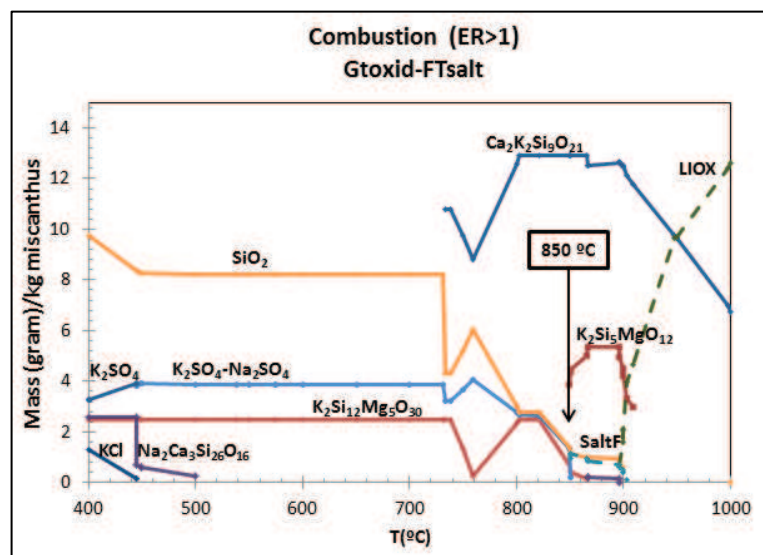


Figure III-10: Composition of condensed phases as a function of temperature in combustion using GToxid databases in miscanthus ashes

Figure III-11 and Figure III-12 represent the elemental composition of liquid phase of miscanthus ashes at 900 °C and 1000 °C in oxidizing (ER>1) and reducing (ER=0.33) atmospheres using the FToxid or GToxid databases. Liquid salt can be present at 900 °C in case of GToxid, which results in the presence of sulfur and elevated quantity of sodium in the liquid phase.

Beside the presence of salts, no major difference was found comparing different atmospheres or different temperatures. In FToxid database the main slag forming species are K<sub>2</sub>O and SiO<sub>2</sub> and a small amount of Na<sub>2</sub>O is present at 1000 °C. In GToxid database, in addition to K<sub>2</sub>O, SiO<sub>2</sub>, Na<sub>2</sub>O, the presence of CaO and MgO were calculated in the liquid phase.

In oxidizing atmosphere, liquid salt solution (K<sub>2</sub>SO<sub>4</sub>-Na<sub>2</sub>SO<sub>4</sub>) can be present at 900 °C resulting in elevated level of Na and S in the liquid phase.

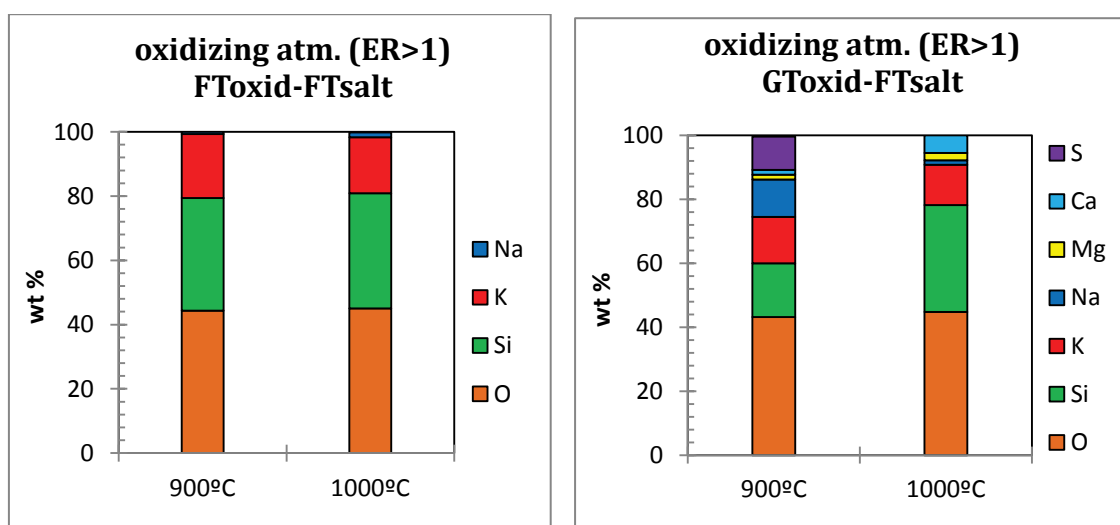


Figure III-11: Comparison of elementary liquid phase composition at 900 °C and at 1000 °C in miscanthus ashes using FToxid or GToxid in oxidizing atmosphere (ER>1) (1kg of miscanthus)

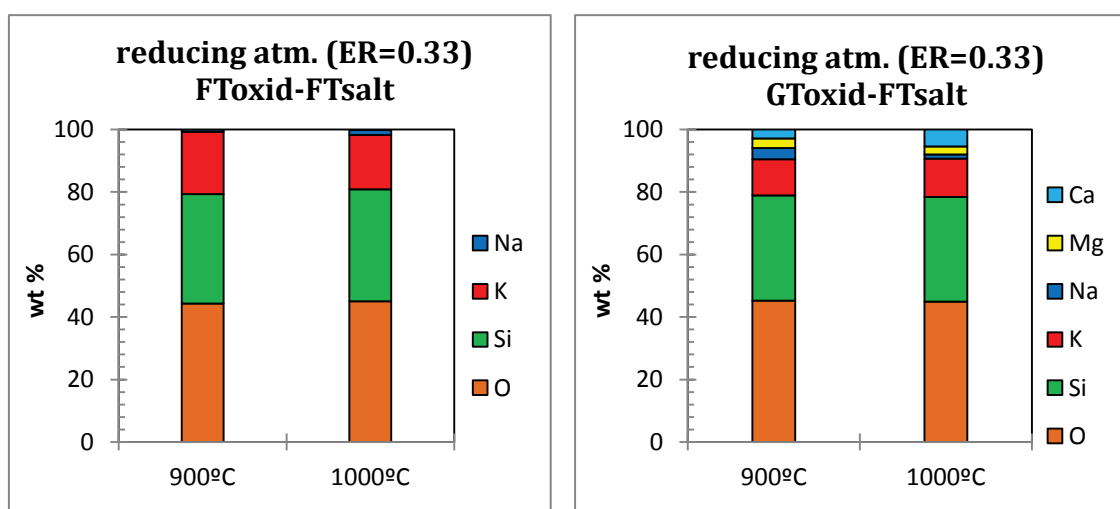


Figure III-12: Comparison of elementary liquid phase composition at 900 °C and at 1000 °C in miscanthus ashes using FToxid or GToxid in reducing atmosphere (ER=0.33) (1kg of miscanthus)

In summary, there is great difference in the solidus temperature and the amount of liquid phases using FToxid or GToxid databases. GToxid database predicts higher solidus temperature both in combustion and gasification because of the formation of solid K-Mg-silicate which is more stable than K-silicate.

Using GToxid database, molten salt solution is also present. It can be due to the lack of available  $\text{SiO}_2$  to form liquid silicate solutions, as the silica is kept in solid phase in the K-Mg-silicate. Therefore the solid  $\text{K}_2\text{SO}_4\text{-Na}_2\text{SO}_4$  solution in case of combustion and the solid  $\text{KCl-NaCl}$  solution in case of gasification can melt and form molten salt solution until the  $\text{SiO}_2$  is released with the decomposition of  $\text{K}_2\text{Si}_5\text{MgO}_{12}$ . This results in completely different liquid phase composition at 900 °C in FToxid and GToxid databases.

The choice of the most adapted database for equilibrium phase prediction will be presented in the next part (III.4.4) based on the comparison of experiments with calculations.

### III.4. VALIDATION OF THE THERMODYNAMIC MODEL WITH LABORATORY EXPERIMENTS

To validate the thermodynamic model, the calculations have been compared with experimental data. The experiments were carried out on miscanthus ashes (prepared at 400 °C in air) under static conditions. For the validation of calculations in oxidizing atmosphere, the ashes were heat-treated in a standard laboratory furnace in air. For the reducing atmosphere, the ash samples were heat-treated in a controlled atmosphere device with CO<sub>2</sub> and H<sub>2</sub> gas flow. (The description of the device can be found in Chapter II.) The microGC analysis proved that the injected gases reach equilibrium inside the furnace. The partial pressure of oxygen during the experiments in reducing atmosphere is 10<sup>-17</sup> bar.

According to the approach of Petit et al. [III-10], the partial pressure of oxygen is the main driving force of ash behaviour in different thermal processes and the effect of the different gasifying agents (like O<sub>2</sub>, CO<sub>2</sub> or steam) can be compared based on the oxygen partial pressure in the equilibrium. Figure III-13 illustrates the oxygen partial pressure versus the amount of different gasifying agent. The curve can be divided into three main parts; the pyrolysis zone, the gasification/partial oxidation zone and the combustion zone [III-10].

When no gas or very little amount of gas is introduced-in the pyrolysis zone- the oxygen partial pressure is constant at about 10<sup>-20</sup> bar. In the gasification zone, with increasing amount of gasifying agent, the oxygen partial pressure increases gradually. At a certain amount of gasifying agent the oxygen partial pressure rises suddenly and its value becomes almost constant at about 10<sup>-1</sup> bar, indicating the zone of combustion.

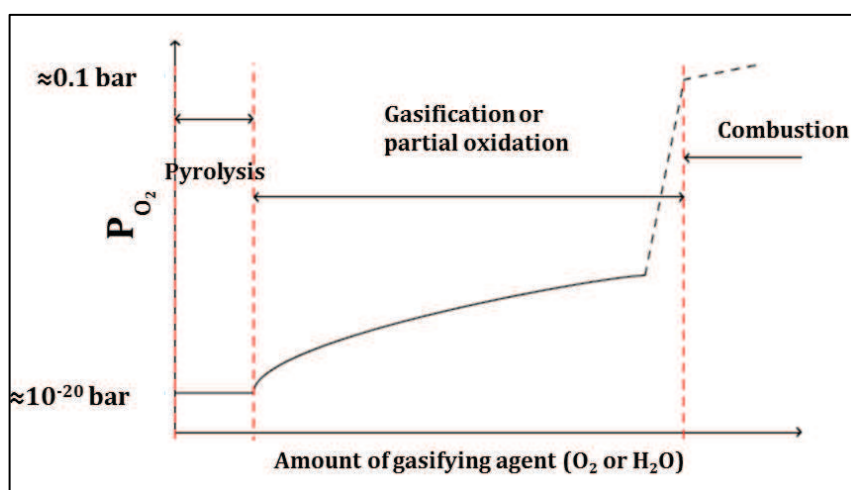


Figure III-13: Illustration of oxygen partial pressure versus the amount of gasifying agent [III-10]

Figure III-14 shows the evolution of the oxygen partial pressure in case of air as gasifying agent with 1 kg miscanthus. The amount of added air is expressed in the form of equivalent ratio (added O<sub>2</sub> (kg)/ stoichiometric oxygen requirement (kg)).

The calculations showed that the oxygen partial pressure during the laboratory experiments is in the same order of magnitude as the calculated values in case of biomass gasification with the EQTEC technology (ER=0.33) and combustion (ER>1).

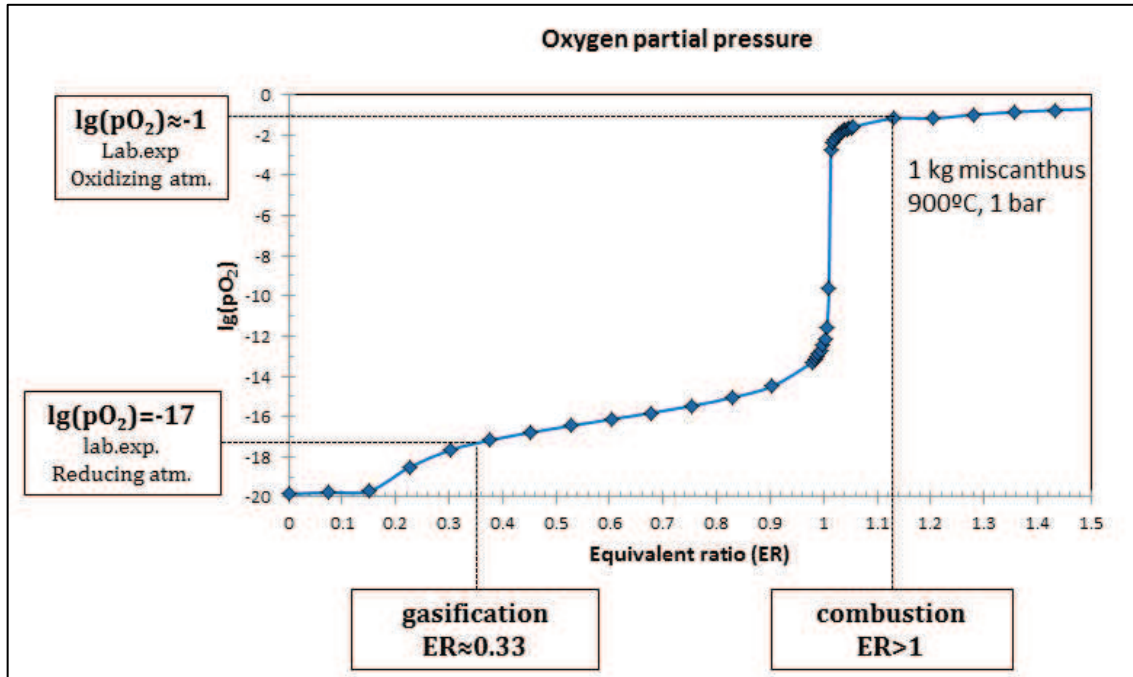


Figure III-14: Oxygen partial pressure versus amount of oxygen expressed as equivalent ratio: comparison of laboratory experiments with industrial conditions

To compare the thermodynamic calculations with the laboratory experiments (qualitative), the input data of the calculations were chosen to fit the laboratory experimental set-up. The elemental composition of the ashes prepared at 400 °C was determined by SEM-EDX analysis. For reducing atmosphere, the equilibrium composition of the injected gas mixture (H<sub>2</sub>, CO<sub>2</sub>, N<sub>2</sub>) was used. For oxidizing atmosphere, the same method, an excess amount of air was used.

The only exception is the comparison of the liquid phase formation with the ash fusibility test. As the ash fusibility test was performed with ashes prepared at 815 °C (ISO 1171 utilised by Laboratory Socor), the characteristic temperatures based on the Socor analysis were compared directly with the calculations of 1 kg miscanthus.

III.4.1 COMPARISON: LIQUID TO LIQUID PLUS SOLID ( $L/(L+S)$ ) WITH ASH FUSIBILITY TEST

The liquid to liquid plus solid ratio ( $L/(L+S)$  wt %) calculated with FToxid and GToxid databases is compared to the characteristic ash fusion temperatures in Figure III-15. The evolution of the liquid phase using the FToxid database can be divided into four zones and attributed to the characteristic temperatures. Around 25% of liquid phase corresponds to the first characteristic temperature (shrinkage 902 °C). Between 950-1100 °C the amount of liquid phase is around 60%. This zone fits well the deformation temperature (968 °C). Between 1100 and 1250 °C the amount of liquid reaches 75%, which correspond to the hemisphere temperature (1118 °C).

At 1250-1300 °C the amount of liquid exceeds 95%. This zone can be attributed to the characteristic flow temperature (1326 °C).

The calculated  $L/(L+S)$  ratio using GToxid calculations is shown between 800 °C and 1000 °C. In GToxid database the evolution of liquid phase is slower. The liquid phase appears at 850 °C (3%) and reaches 20% at 905 °C, which is good correlation with the shrinkage temperature (908 °C). At 950 °C it reaches 50% and it exceeds 60% at 1000 °C. This increase fits well the deformation temperature (968 °C).

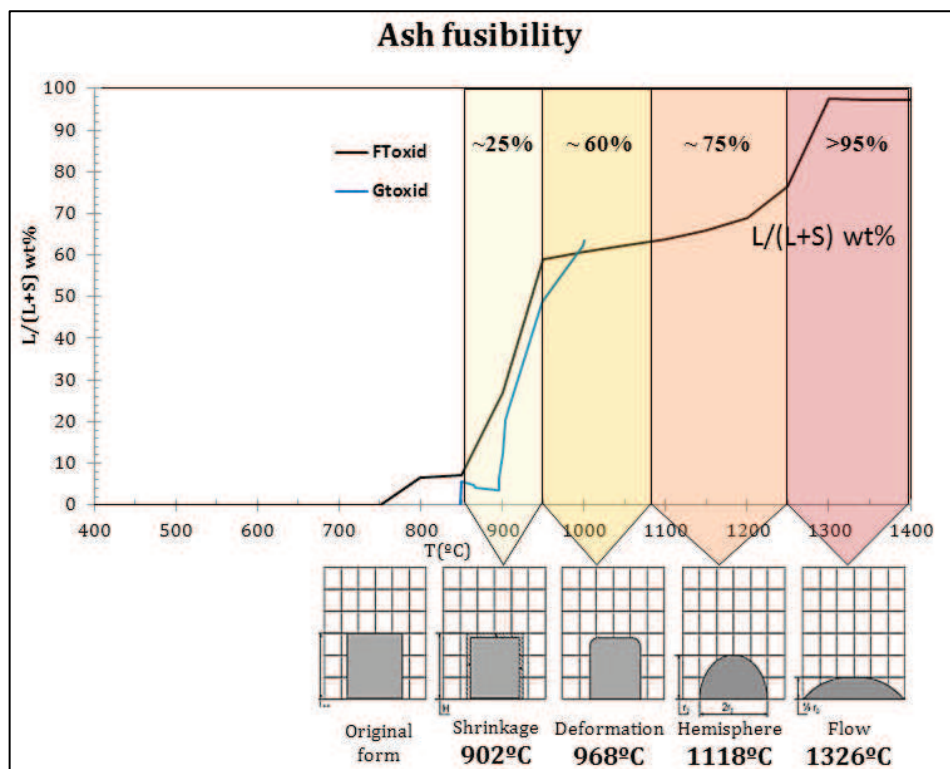


Figure III-15: Comparing ash fusibility test with calculated liquid to liquid plus solid ratio ( $L/(L+S)$  wt %)

### III.4.2 COMPARISON OF EQUILIBRIUM SOLID PHASES WITH X-RAY DIFFRACTION

Table III-8–12 compare the XRD analysis and the calculations with FToxid and GToxid databases. LM1 ashes were studied in details in oxidizing atmosphere (Chapter II.4.2); therefore the comparison could be completed in the whole range of 400 to 1400 °C (Table III-8). In reducing atmosphere only few experiments were performed; the comparison is limited to the compounds present at 900 °C (Table III-9). In case of LM2 ashes (harvest September 2011), the comparison could be only performed at 400 and 900 °C in oxidizing atmosphere (Table III-10 and Table III-11) and at 900 °C in reducing atmosphere (Table III-12).

Regarding the X-ray diffractograms, it is quite difficult to describe the evolution of ash composition as the ash contains several inorganic compounds in small quantities and in amorphous form. However, some tendencies can be drawn for the main compounds and the results can be compared with thermodynamic calculation.

At low temperature (<750 °C), the main crystalline phases are KCl, K<sub>2</sub>SO<sub>4</sub>, SiO<sub>2</sub> and Ca<sub>9</sub>HPO<sub>4</sub>(PO<sub>4</sub>)<sub>5</sub>OH. Potassium silicates were not found in the diffractograms but they were identified with SEM analysis (Chapter II.3.2, Figure II-18). At higher temperatures (800 to 1200 °C) the main compounds are K<sub>2</sub>SO<sub>4</sub>, Ca<sub>3</sub>(PO<sub>4</sub>)<sub>2</sub> and alkaline earth silicates. The diffractograms of high temperature ashes (800-1000 °C) show the presence of CaSiO<sub>3</sub>, CaMgSi<sub>2</sub>O<sub>6</sub>. The K-Ca-silicates and K-Mg-silicates of GToxid databases (Ca<sub>2</sub>K<sub>2</sub>Si<sub>9</sub>O<sub>21</sub>, K<sub>2</sub>Si<sub>5</sub>MgO<sub>12</sub>) were not identified in the diffractograms.

Two main differences can be observed between the laboratory experiments and the thermodynamic calculations. Firstly, the alkali salts are present at higher temperature in laboratory experiments. KCl is still present at 800 °C (versus volatilisation above 600 °C in the calculation) and K<sub>2</sub>SO<sub>4</sub> is present at 1200 °C (versus 1000 °C). It is possible that the volatilised compounds condensed on the surface of the ash sample, or the way the sample was prepared (pressed in pastille) influenced the volatilisation of the salts.

The second difference is the formation of alkali and alkaline earth minerals. In the X-ray diffractograms, they appear starting from 800-850 °C, while in the calculations they are present already at 400 °C. As it was already pointed out in the introduction, the formation of new mineral phases depends on the availability and chemical form of inorganics in the biomass. In the miscanthus stem silicon is present as silica gel (SiO<sub>2</sub>·nH<sub>2</sub>O) and the alkali earth metals are bond to the organic matrix. For the formation of new silicates, firstly the lignin and cellulose have to be decomposed and the organically bonded Ca and Mg have to form carbonates. The typical decomposition of cellulose is around 350 °C and the lignin around 350 to 500 °C, while the carbonates will form oxides only in the range of 650-800 °C. Moreover, the elements have to be able to reach each other. Often, the diffusion of elements is slower than the chemical reaction itself [III-17]. The diffusion can be accelerated by the apparition of liquid phase (around 750-800 °C typically for biomass ash). Considering the hydrodynamics and the residence time in fluidized beds, the reactions are further limited.

Table III-8: Comparing the different compounds in LM1 ashes in XRD and thermodynamic calculation in oxidizing atmosphere

<b>LM1 (April 2011) in oxidizing atmosphere</b>			
Compounds	XRD	FToxid-FTsalt	GToxid-FTsalt
KCl (s)	400-800 °C	400-600 °C	400-600 °C
K <sub>2</sub> SO <sub>4</sub> (s)	400-1200	400-1000 °C	400-1000 °C
CaCO <sub>3</sub> (s)	450 °C	✗	✗
Ca <sub>3</sub> (PO <sub>4</sub> ) <sub>2</sub> (s)	500-1300 °C	400-1400 °C	400-1400 °C
SiO <sub>2</sub> (s)	400-1150 °C	400 °C	✗
K-silicate (s)	SEM	600-700 °C	✗
CaSiO <sub>3</sub> (s)	850-1150 °C	400-1200 °C	950-1050 °C
MgSiO <sub>3</sub> (s)	?	700-1200 °C	950-1050 °C
CaMgSi <sub>2</sub> O <sub>6</sub> (s)	?	400-1200 °C	750-950 °C
Mg <sub>2</sub> SiO <sub>4</sub> (s)	?	✗	600-700 °C
Na-Ca-silicate (s)	?	400-900 °C	400-550 °C
Ca-K-silicate (s)	?	✗	400-950 °C
Mg-K-silicate (s)	?	✗	400-950 °C
✓ present; ? cannot be defined/not sure; ✗ not present			

In reducing atmosphere at 900 °C the main difference between the experiments and the calculations is the presence of unburnt organic carbon in case of LM1 ashes, which can retain other inorganic elements such as Cl or S. The SEM-EDX analysis proved the presence of K<sub>2</sub>S, CaS and small amount of alkali chlorides in the ash.

Table III-9: Comparing the different compounds in LM1 ashes in XRD and thermodynamic calculation in reducing atmosphere at 900 °C

<b>LM1 (April 2011) at 900 °C in reducing atmosphere</b>			
Compounds	XRD	FToxid-FTsalt	GToxid-FTsalt
Ca <sub>3</sub> (PO <sub>4</sub> ) <sub>2</sub> (s)	✓	✓	✓
Ca <sub>5</sub> HO <sub>13</sub> P <sub>3</sub> (s)	✗	✗	✓
SiO <sub>2</sub> (s)	✓	✗	✗
CaSiO <sub>3</sub> (s)	✓	✓	✗
MgSiO <sub>3</sub> (s)	maybe	✓	✗
CaMgSi <sub>2</sub> O <sub>6</sub> (s)	maybe	✓	✓
Ca-K-silicate (s)	✗	✗	✓
Mg-K-silicate (s)	possible	✗	✓
CaCO <sub>3</sub> (s)	SEM	✗	✗
K <sub>2</sub> S, CaS (s)	SEM	✗	✗
✓ present ; ✗ not present			

In case of LM2 (September 2011) in oxidizing atmosphere both at 400 and 900 °C the presence of salts is in good agreement with the experiments. Similarly to the case of LM1 ashes, there is a difference between the presence of Ca-carbonates and silica in the diffractograms compared to the equilibrium prediction of alkali earth silicates.

Analysing the diffractograms of LM2 ashes at 900 °C in reducing atmosphere is very challenging because of the presence of hygroscopic salts and amorphous phase. The presence of the predicted compounds is possible but cannot be totally evidenced.

*Table III-10: Comparing the different compounds in LM2 ashes in XRD and thermodynamic calculation in oxidizing atmosphere at 400 °C*

<b>LM2 (Sept 2011) at 400 °C in oxidizing atmosphere</b>			
Compounds	XRD	FToxid-FTsalt	GToxid-FTsalt
K <sub>2</sub> CO <sub>3</sub> (s)	KHCO <sub>3</sub> (s), K <sub>4</sub> H <sub>2</sub> (CO <sub>3</sub> ) <sub>3</sub> ·1.5H <sub>2</sub> O (s)	✓	✓
CaCO <sub>3</sub> (s)	✓	✗	✗
K <sub>2</sub> SO <sub>4</sub> (s)	✓	✓	✓
KCl (s)	✓	✓	✓
Mg <sub>3</sub> P <sub>2</sub> O <sub>8</sub> (s)	Mg <sub>2</sub> P <sub>2</sub> O <sub>7</sub> (s)	✓	✓
Ca <sub>3</sub> (PO <sub>4</sub> ) <sub>2</sub> (s)	✗	✓	✓
SiO <sub>2</sub> (s)	✓	✗	✗
K-silicate (s)	KHSi <sub>2</sub> O <sub>5</sub> (s)	✓	✓
Mg <sub>2</sub> SiO <sub>4</sub> (s)	✗	✓	✓
MgK <sub>2</sub> SiO <sub>4</sub> (s)	✗	✗	✗
CaK <sub>4</sub> Si <sub>3</sub> O <sub>9</sub> (s)	✗	✗	✓
✓ present ; ✗ not present			

*Table III-11: Comparing the different compounds in LM2 ashes in XRD and thermodynamic calculation in oxidizing atmosphere at 900 °C*

<b>LM2 (Sept 2011) at 900 °C in oxidizing atmosphere</b>			
Compounds	XRD	FToxid-FTsalt	GToxid-FTsalt
K <sub>2</sub> CO <sub>3</sub> (s)	KHCO <sub>3</sub> (s), K <sub>4</sub> H <sub>2</sub> (CO <sub>3</sub> ) <sub>3</sub> ·1.5H <sub>2</sub> O (s)	✓	✓
CaCO <sub>3</sub> (s)	?	✗	✗
K <sub>2</sub> SO <sub>4</sub> (s)	✓	✓	✓
KCl (s)	✓ (small amount)	✗	✗
Mg <sub>3</sub> P <sub>2</sub> O <sub>8</sub> (s)	?	✓	✓
Ca <sub>3</sub> (PO <sub>4</sub> ) <sub>2</sub> (s)	?	✓	✓
K-silicate (s)	✓ (small amount)	✓	✓
Mg <sub>2</sub> SiO <sub>4</sub> (s)	✗	✓	✓
MgK <sub>2</sub> SiO <sub>4</sub> (s)	✗	✗	✓
CaK <sub>4</sub> Si <sub>3</sub> O <sub>9</sub> (s)	✗	✗	✗
? cannot be defined/not sure; ✓ present ; ✗ not present			

Table III-12: Comparing the different compounds in LM2 ashes in XRD and thermodynamic calculation in reducing atmosphere at 900 °C

LM2 (Sept 2011) reducing atm. 900 °C			
Compounds	XRD	FToxid-FTsalt	GToxid-FTsalt
Mg <sub>3</sub> P <sub>2</sub> O <sub>8</sub> (s)	possible	✓	✗
Ca <sub>3</sub> (PO <sub>4</sub> ) <sub>2</sub> (s)	possible	✓	✓
Ca <sub>5</sub> HO <sub>13</sub> P <sub>3</sub> (s)	possible	✓	✗
K <sub>2</sub> HPO <sub>4</sub> (s)	K-phosphate	✗	✓
Mg <sub>2</sub> SiO <sub>4</sub> (s)	possible	✗	✓
K <sub>2</sub> Si <sub>2</sub> O <sub>5</sub> (s)	✗	✗	✓
MgK <sub>2</sub> SiO <sub>4</sub> (s)	possible	✗	✓
✓ present ; ✗ not present			

### III.4.3 Comparison of equilibrium liquid phases with SEM-EDX analysis

Figure III-16 and Figure III-17 compare the equilibrium compositions of molten phases in LM1 and LM2 ashes with the SEM-EDX analysis at 900 °C in oxidizing and reducing atmospheres. For the SEM-EDX analysis the ash samples were heat-treated for 6 hours, then embedded in resin and polished. The SEM-EDX analysis was carried out at different points of the samples and an average elemental composition was calculated. In GToxid database, in the case of using the composition of LM1 ashes (prepared at 400 °C) as input data, no liquid phase was calculated for oxidizing atmosphere at 900 °C. In this case, the data obtained from 1kg miscanthus (analysis by Laboratory Socor) was used. In the case of using GToxid together with FTsalt database, the presence of molten salts (FTsalt-SaltF solution phase) was predicted at 900 °C in oxidizing atmosphere. On the other hand, liquid salts were not found experimentally. The liquid oxide solution phase (GToxid-LIOX) contains Mg and Ca, which gives better description of the experimentally observed phases.

In overall, GToxid database gives closer values to the experimental ones both in oxidizing and reducing atmosphere. FToxid database predicts two main components; K<sub>2</sub>O, SiO<sub>2</sub> and a very small quantity of Na<sub>2</sub>O (<1 wt %). GToxid database predicts the presence of MgO and CaO, which were also detected by SEM-EDX. In GToxid database, 2-4 wt % Na is calculated, however almost no Na was found in the SEM analysis.

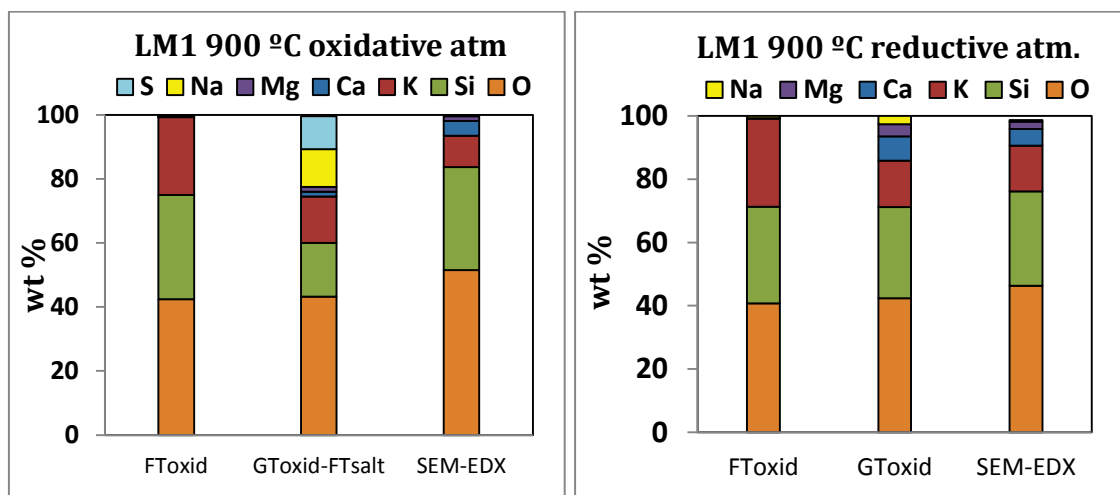


Figure III-16: Comparison (FToxid, GToxid, SEM analysis) of liquid phase composition of LM1 ashes at 900 °C

In case of LM2 ashes, the differences between the equilibrium phases and experiments are more significant. In case of using GToxid database, no liquid oxide solution is present at 900 °C in oxidizing atmosphere, only the partial melting of the salts ( $K_2SO_4$ , KCl and  $K_2CO_3$ ) is predicted. According to the SEM-EDX analysis the liquid phase is composed of  $K_2O$ ,  $SiO_2$ , CaO and MgO. Neither sulfur nor chlorine was detected by SEM-EDX. The XR-diffractogram showed the presence of crystalline K-carbonate and a small amount of  $K_2SO_4$  and KCl. Although the samples were quenched after heat-treatment, it is possible that some crystallisation occurred modifying the composition of liquid phase. In reducing atmosphere, the calculations are closer to the experimentally observed molten phase. Both in the case of FToxid and GToxid databases the  $SiO_2$ - $K_2O$  liquid oxide system is predicted. Experimentally, a small amount of Mg and Ca were also detected but their signals can derive from small crystals in the molten phase.

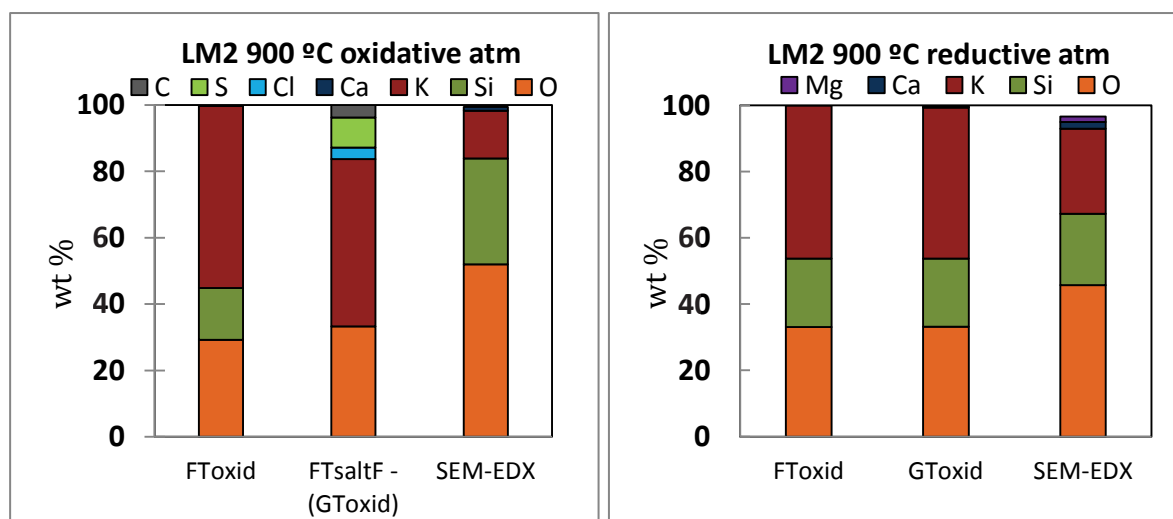


Figure III-17: Comparison (FToxid, GToxid, SEM analysis) of liquid phase composition of LM2 ashes at 900 °C

As the results show, the description of ash behaviour is limited both regarding the experiments and the thermodynamic calculations. For the experiments, more complex analysis has to be done on miscanthus ashes or model compositions. Precisely described circumstances should be used to evaluate the accuracy of the databases. Regarding the thermodynamic databases, there is still a lack of fundamental knowledge about the inorganic system in biomass ashes. The databases have to be completed and validated to assure their pertinence.

## III.4 CONCLUSION

Thermodynamic calculations were carried out to describe the miscanthus ash transformation under different conditions. The calculations were compared with laboratory experiments (XRD, SEM-EDS and ash fusibility test) both in oxidizing and reducing atmospheres.

The characterisation of biomass ash is challenging. It is difficult to interpret the thermogravimetric analysis as it contains many simultaneous phase transformations. The solidus temperature cannot be certainly measured as it is in the same range as the decomposition of the alkali carbonates.

The evaluation of crystalline phases in X-ray diffractograms is not evident because of their richness in small and overlapping peaks. Moreover, the samples contain organic carbon and amorphous phases and in the case of LM2 ashes the crystalline phases are hygroscopic.

In summary, the calculations regarding the formation of liquid phase corresponds reasonably well to the experimental data. FToxid database determines well the solid compounds, while the composition of liquid phase is more adequate using GToxid databases.

Equilibrium calculations can be used to estimate the biomass ash melting behaviour and as a complementary tool to interpret the experiments. However, these results have to be handled with care, as thermodynamic calculations have certain limits; the available databases are not complete and not all the data were validated with experiments. Moreover, the equilibrium state usually cannot be reached during industrial processes.

In the future, it is necessary to complete the existing databases in order to be able to use thermodynamic calculations as efficient predictive tools. For the biomass gasification, the moisture content of the fuel has to be taken into account as it can influence the phase transformation of ashes, in particular the release of potassium via the formation of gaseous KOH, HCl, H<sub>2</sub>S [III-25].

### III.5 REFERENCES OF CHAPTER III

- [III-1] Evic N, Brunner T, Obernberger I. Prediction of biomass ash melting behaviour-correlation between the data obtained from thermodynamic equilibrium calculations and simultaneous thermal analysis (STA). 20th Eur Biomass Conf Exhib 2012.
- [III-2] Lindberg D, Backman R, Chartrand P, Hupa M. Towards a comprehensive thermodynamic database for ash-forming elements in biomass and waste combustion — Current situation and future developments. *Fuel Process Technol* 2013;105:129–41.
- [III-3] Berjonneau J, Colombel L, Poirier J, Pichavant M, Defoort F, Seiler J-M. Determination of the Liquidus Temperatures of Ashes from the Biomass Gazification for Fuel Production by Thermodynamical and Experimental Approaches. *Energy & Fuels* 2009;23:6231–41.
- [III-4] Froment K, Defoort F, Bertrand C, Seiler JM, Berjonneau J, Poirier J. Thermodynamic equilibrium calculations of the volatilization and condensation of inorganics during wood gasification. *Fuel* 2013;107:269–81.
- [III-5] Li H, Yoshihiko N, Dong Z, Zhang M. Application of the FactSage to Predict the Ash Melting Behavior in Reducing Conditions. *Chinese J Chem Eng* 2006;14:784–9.
- [III-6] Van Dyk JC, Melzer S, Sobiecki a. Mineral matter transformation during Sasol-Lurgi fixed bed dry bottom gasification – utilization of HT-XRD and FactSage modelling. *Miner Eng* 2006;19:1126–35.
- [III-7] Elled A, Åmand L, Steenari B. Composition of agglomerates in fluidized bed reactors for thermochemical conversion of biomass and waste fuels Experimental data in comparison with predictions by a thermodynamic equilibrium model. *Fuel* 2013;111:696–708.
- [III-8] Grimm A, Boström D, Lindberg T, Fredriksson A, Öhman M. Bed agglomeration characteristics during fluidized olivine bed combustion of typical biofuels. 19th Eur. Biomass Conf. Exhib. Berlin, Berlin, Germany: 2011, p. 1345–50.
- [III-9] Grimm A, Öhman M, Lindberg T, Fredriksson A, Boström D. Bed Agglomeration Characteristics in Fluidized-Bed Combustion of Biomass Fuels Using Olivine as Bed Material. *Energy Fuels* 2012;26:4550–9.
- [III-10] Petit M, Froment K, Patisson F, Seiler J-M, Defoort F. Relation between oxygen partial pressure in the syngas and inorganic releases during biomass gasification. 17th Eur. Biomass Conf. Exhib. Hambg., 2009.
- [III-11] Hack K, Jantzen T, Müller M, Yazhenskikh E, Wu G. A novel thermodynamic database for slag systems and refractory materials. 5th Int. Congr. Sci. Technol. Steelmak., Dresden: 2012.
- [III-12] Yazhenskikh E, Hack K, Muller M. Thermodynamic Assessment of the System Al<sub>2</sub>O<sub>3</sub>-K<sub>2</sub>O-Na<sub>2</sub>O-SiO<sub>2</sub>-CaO-MgO. vol. 2. Julich: 2011.
- [III-13] Bale CW, Belisle E, Chartrand P, Decterov SA, Eriksson G, Hack K, et al. FactSage Thermochemical Software and Databases-Recent Developments. *Calphad-Computer Coupling Phase Diagrams Thermochem* 2009;33:295–311.

- [III-14] Bale CW, Belisle E, Chartrand P, Decterov SA, Eriksson G, Hack K, et al. FactSage Thermochemical Software and Databases-Recent Developments. *Calphad-Computer Coupling Phase Diagrams Thermochem* 2009;33:295–311.
- [III-15] [Http://www.crct.polymtl.ca/fact/documentation/](http://www.crct.polymtl.ca/fact/documentation/). FactSage Database Documentation
- [III-16] Petit M. Etude du comportement des espèces inorganiques dans une installation de gazéification de la biomasse: condensation des aérosols et dépôts. Nancy-Université-Ecole Doctorale EMMA, Laboratoire des Technologies de la Biomasse, Institut Jean Lamour, 2011.
- [III-17] Zevenhoven-Onderwater M, Backman R, Skrifvars B, Hupa M. The ash chemistry in fluidised bed gasification of biomass fuels. Part I: predicting the chemistry of melting ashes and ash-bed material interaction. *Fuel* 2001;80:1489–502.
- [III-18] Jak E. Prediction of coal ash fusion temperatures with the F\*A\*C\*T thermodynamic computer package. *Fuel* 2002;81:1655–68.
- [III-19] Yazhenskikh E, Hack K, Müller M. Critical thermodynamic evaluation of oxide systems relevant to fuel ashes and slags. Part 1: Alkali oxide–silica systems. *Calphad* 2006;30:270–6.
- [III-20] Yazhenskikh E, Hack K, Müller M. Critical thermodynamic evaluation of oxide systems relevant to fuel ashes and slags Part 2: Alkali oxide–alumina systems. *Calphad* 2006;30:397–404.
- [III-21] Yazhenskikh E, Hack K, Müller M. Critical thermodynamic evaluation of oxide systems relevant to fuel ashes and slags. Part 3: Silica–alumina system. *Calphad* 2008;32:195–205.
- [III-22] Yazhenskikh E, Hack K, Müller M. Critical thermodynamic evaluation of oxide systems relevant to fuel ashes and slags, Part 5: Potassium oxide–alumina–silica. *Calphad* 2011;35:6–19.
- [III-23] Levin EM, Robbins CR, McMurdie HF. Phase diagrams for ceramists. Columbus, Ohio 43214: The American Ceramic Society; 1964.
- [III-24] Basu P. Production of Synthetic Fuels and Chemicals from Biomass. *Biomass Gasif. Pyrolysis*. First Edit, © 2010 Elsevier Inc.; 2010, p. 301–23.
- [III-25] Sommersacher P, Brunner T, Obernberger I. Fuel Indexes: A Novel Method for the Evaluation of Relevant Combustion Properties of New Biomass Fuels. *Energy & Fuels* 2012;26:380–90.
- [III-26] Atkins P, De Paula J. *Atkins' Physical Chemistry*. Oxford, Great Britain: Oxford University Press; 2006.

---

# CHAPTER IV: INTERACTION BETWEEN MOLTEN MISCANTHUS ASHES AND BED PARTICLES

---

## ABSTRACT

Beside the importance of hydrodynamics in a fluidized bed, several other factors contribute to the agglomeration phenomenon, namely the amount and composition of molten ashes and the chemical reactivity of bed particles at high temperature. Although many studies have been conducted about the agglomeration mechanism using silica sand, olivine is only mentioned as an alternative bed material and its interaction with biomass ash is not deeply examined [IV-1, IV-2].

The aim of this chapter is to investigate the agglomeration of miscanthus ashes with different bed materials under static conditions, focusing on physicochemical aspects; wettability, adhesion, phase transformation and chemical interactions.

The mixture of ash and bed material was heat-treated in oxidizing and reducing atmospheres. The pastilles were characterized by scanning electron microscope (SEM-EDX) and X-ray diffraction (XRD).

It was found that regardless of atmosphere the molten ash phase is mainly composed of  $\text{SiO}_2$  and  $\text{K}_2\text{O}$ , causing the adhesion of bed particles. In contact with silica sand particles only physical adhesion was observed. In the case of olivine, the diffusion of Fe and chemical interaction between the liquid ash phases and calcined olivine surface occurred.

## IV.1 INTRODUCTION

The agglomeration during fluidized bed gasification and combustion is due to the melting of biomass ashes at relatively low temperature (<850 °C). The molten ash acts like glue and attach the bed particles upon collision, leading to the formation of agglomerates. Elevated amount of agglomerates can perturb the fluidized state, worsen the productivity and increase the maintenance costs. To provide a solution to this phenomenon, firstly the nature of the interaction has to be revealed and the physicochemical mechanisms have to be understood.

Many researchers studied the interaction between silica sand and wooden or more “risky” biomasses such as wheat straw [IV-1–5]. Although the catalytic effect of olivine in tar decomposition is well-known, its effect on agglomeration has not been revealed in details [IV-1].

In this chapter the interaction between miscanthus ashes and bed materials was studied under static conditions (without macroscopic movement of matter, in laboratory furnace). The aim of this work was to reveal the role of the key parameters on the agglomeration:

➤ ***the composition of miscanthus ashes***

Depending on the harvest time the composition of miscanthus ashes, particularly the concentration of potassium, can significantly vary. The effect of elevated amount of potassium was studied with a second batch of miscanthus ash harvested at the end of summer and consisting of 20% more potassium.

➤ ***phase transformation of bed material***

Silica sand is the most typical bed material due to its availability and good mechanical properties at high temperature. Often, olivine is favoured due to its catalytic effect in tar decomposition. However, olivine is not an inert mineral; it undergoes several modifications as a function of temperature, particularly the formation and migration of iron oxide to the surface. The iron can diffuse into the molten ash and modify the adhesion forces of molten ash layers.

➤ ***atmosphere***

As it was previously presented in Chapter II.4.1, the atmosphere influences the reactivity of potassium. Oxidizing atmosphere favours the formation of stable  $K_2SO_4$  while reducing atmosphere favours the formation of K-silicates with low melting point.

➤ ***contact time***

The contact time affects the thickness of molten ash layers and can alter adhesion force of molten ashes.

➤ ***temperature***

The typical operating temperature of fluidized bed gasification or combustion is 750-900 °C. The static tests were performed at 900 °C, which is the operating temperature chosen in the frame of GAMECO research project. A somewhat elevated temperature, 1000 °C was also investigated to better evidence the physicochemical interactions.

This chapter begins with an overview of the agglomeration phenomenon related to biomass ashes in fluidized bed gasification and combustion and a state of the art of the possible countermeasures to avoid agglomeration.

The section “Materials and methods” summarises the different methods used for the bed material characterisation and the laboratory experimental setup of static interaction tests.

The “Result” section is divided into three parts:

- The first part describes the transformation of olivine as a function of temperature using *in situ*-XRD and Raman measurements.
- The second part studies the wettability of olivine by molten ash at high temperature.
- The third part describes the characteristics of ash-bed material interaction observed by SEM-EDX analysis, focusing on the influence of the above mentioned parameters.

The chapter is closed with an overall conclusion about agglomeration mechanism of bed materials by miscanthus ashes.

## IV.2 STATE OF THE ART

One of the main bottlenecks of fluidized bed processes is the agglomeration of bed particles due to the transformation of biomass mineral matter at high temperature and the formation of low melting point silicates.

Agglomeration depends on (1) operation conditions (temperature, gas velocity, particle size), (2) particle hydrodynamics in a fluidized bed and (3) material properties [IV-6]. This overview focuses on this latter, more particularly the physicochemical interaction between molten ashes and bed particles and the influence of the chemical composition on agglomerate formation.

The state of the art summarizes the two main mechanisms of agglomeration, the influence of biomass and bed material on agglomeration and gives an overview of possible countermeasures to avoid agglomeration in regard to alternative bed materials, additives and fuel treatments.

### IV.2.1 AGGLOMERATION MECHANISM

At the beginning of 1990s, Skrifvars and al. already studied the agglomeration phenomenon in coal fluidized bed combustion of different type of coals. He established three main reasons for agglomeration, namely partial melting with non-viscous flow, partial melting with viscous flow and gas-solid chemical reaction [IV-7].

At the beginning of 2000s, as the use of short rotation coppice and herbaceous biomasses became more popular, more scientific work started to deal with fluidization problems related to the high alkali content of biomass ash.

The high alkali content led to the defluidization of silica sand beds below the optimal operating temperature of fluidized beds (800-850 °C) [IV-4]. However the melting point of quartz is 1725 °C, it forms low melting point eutectics with alkalis (Chapter III, Figure III-1) [IV-IV-1, IV-4].

Lin et al. observed the agglomeration phenomenon during wheat straw pellet combustion [IV-8]. They found that the burning char collects bed particles at around 720 °C. Due to the higher temperature of char particles compared to their environment, the molten inorganic compounds in the char diffuse to the surface resulting in sticky particles. Upon collision, char particles glue together the bed particles and form agglomerates. With the increase of temperature to 920 °C, the black core of agglomerates disappears and a liquid layer rich in Si and K is formed around the silica sand particles. With increasing process time, the agglomerates become hollow due to the ash volatilization.

Chirone et al. also remarked the cluster formation of silica sands by sticky char particle. With the burn off of organic matter, the structure of clusters is reinforced by K and Na rich neck formation and sintering as shown in Figure IV-1 [IV-9].

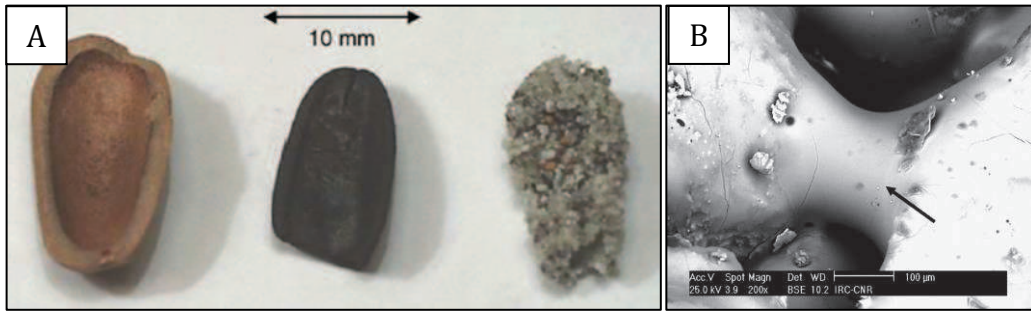


Figure IV-1: (A) Silica sand cluster on sticky char particle and (B) neck formation between silica grains during biomass combustion [IV-9]

The agglomeration depends on fundamental force balance. When the adhesive forces between two colliding particles are greater than the impact force of the collision, the particles will stick together. The key parameter of particle adhesion is the wettability of bed materials by molten ashes. In the case of good wettability, the molten ash creates viscous liquid bridges between the bed particles which influence the outcome of the force balance [IV-10]. The most important adhesive forces due to the presence of liquid bridges are the, cohesion forces, capillary forces and surface tension forces [IV-10].

Several publications deal with the mechanism of agglomeration during fluidized bed gasification and combustion of biomass fuel. The most accepted and most cited theory is the work of Öhman et al [IV-1,3,11]. According to Öhman, the two most important mechanisms are the melt-induced/direct and the initial layer formation/subsequent agglomeration [IV-3,12]. The first case is a non-reactive mechanism, when bed particles are glued together by small pieces of molten ash or char (Figure IV-3/A). The second case is a reactive mechanism: it consists of an initial layer formation by the deposition of gaseous inorganic compounds (alkali hydroxides, chlorides, sulphates) or molten ash particles on the bed particles (Figure IV-3/B). This layer can be homogenised and strengthened by different type of sintering: viscous flow (silicate melt) sintering, reactive liquid (salt melt) sintering or chemical reaction sintering [IV-11].

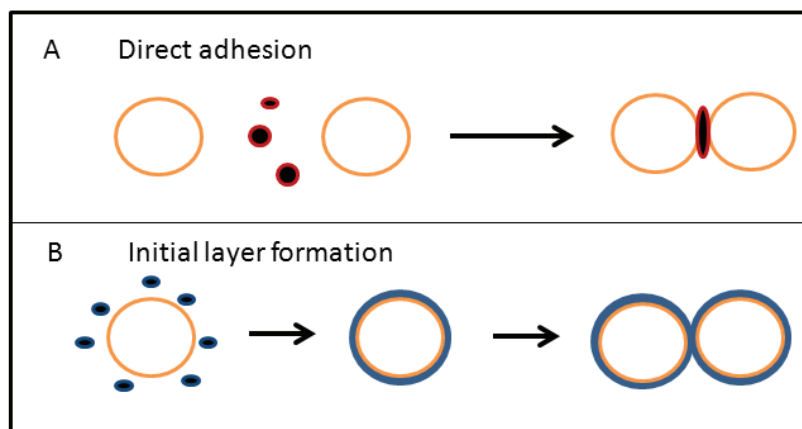


Figure IV-2: Mechanism of agglomeration: (A) melt induced/direct adhesion and (B) initial layer formation with subsequent adhesion

The exact composition of layers depends on the type of biomass and bed material. The coating can contain different ratios of K, Ca, Fe, Al and Na in the form of silicates. Öhman et al. found that the main contributor to the layer formation is the ternary system  $K_2O-CaO-SiO_2$  [IV-11]. Sulphates and chlorides were not found to participate in layer formation [IV-11].

The thickness of the layer depends on the operation time and ash content of the biomass. Depending on operating time (8 to 30 hours), 10-50  $\mu m$  thick layer was formed around bed particles [IV-11].

Often multiple layers are observed; a thicker homogenous inner layer due to sintering and a heterogeneous outer layer [IV-1,2,12]. An example of the work of Visser et al. is shown in Figure IV-3.

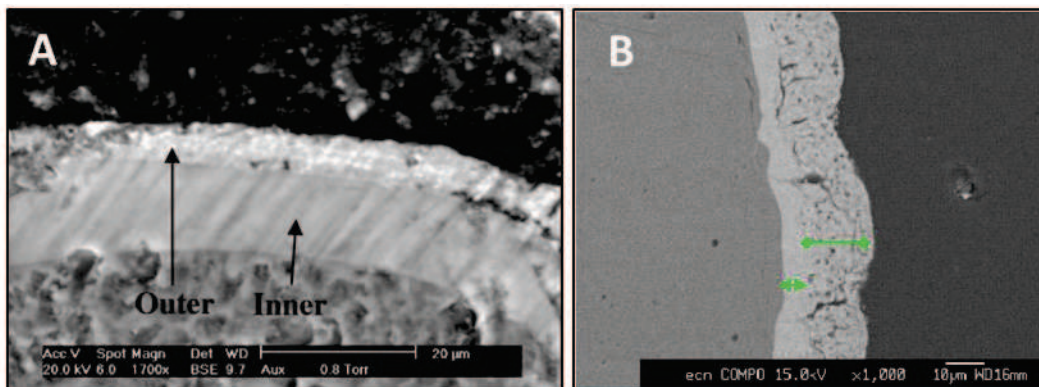


Figure IV-3: Multiply layer formation around silica sand bed particle: (A) combustion of olive residue [IV-13] and (B) combustion of wood mix [IV-2]

The composition of the inner layer depends both on the bed material and fuel properties while the composition of the outer layer is defined by the fuel composition [IV-11, IV-12]. For example, in the case of wood combustion using silica sand, Visser et al. observed a homogenous inner layer composed of Ca- and K-silicate and an outer layer consisting of Mg, P, Ca, Fe [IV-2]. Using olivine sand for the same trials resulted in a different inner layer composition; Ca-Mg-silicates [IV-2].

Considering the critical layer thickness, some scientists think that 10-50  $\mu m$  is enough to cause sticky adhesive layer, others consider somewhat thicker layer between 20-100  $\mu m$  [IV-14, IV-15].

The type of agglomeration mechanism depends both on the type of biomass and type of bed material used in the process [IV-16].

Depending on the alkali and silica content of the biomass, bed material can play a passive or active role in agglomeration. In the case of biomass with low alkali and silica content (woody biomass), bed material plays an active role in agglomeration [IV-12]. In this case, the silica content of the bed particles interacts with the gaseous alkali and alkali earth species and a low melting point silicate layer is formed around the bed particle [IV-16]. In the case of alkali and silica rich fuels, agglomeration is caused by partly melted ash droplets attaching the bed particles directly to each other [IV-16].

According to Fryda et al. it is the bed temperature that influences which mechanism will take place. Direct adhesion by molten ash or char particles can arrive at once at elevated operation temperature or in the high temperature zones. On the other hand, layer formation demands certain residence time. In the case of elevated temperature, the agglomerates will form by direct adhesion resulting in defluidization before there is time for layer formation [IV-17]. Testing different herbaceous plants, they found that agglomeration was due to direct adhesion and the SEM-EDX measurements did not indicate any chemical interaction between molten ash and quartz or olivine sand [IV-17].

Similar results were reported in the work of Brus et al [IV-13]. They found layer formation in the case of woody biomass and the diffusion of Ca into the quartz resulting in Ca-silicates [IV-13]. The inner layer grew inwards due to the chemical attack of olive residue ashes. In the case of herbaceous biomass direct adhesion by molten K-silicates was observed [IV-13].

In general, herbaceous biomass has higher level of potassium and silica; therefore the agglomeration occurs faster and at relatively lower temperatures. The bed collapses before chemical reaction could occur. In contrary, in the case of woody biomass, the main mechanism is the layer formation as less K and more Ca permits longer residence time and the formation of sticky layers before defluidization.

### IV.2.3 COUNTERACTING AGGLOMERATION

As it is shown in Figure IV-4, the two main ways to counteract agglomeration are either changing the process parameters or alter biomass inorganic matter. As this work is focusing on the physicochemical aspects of agglomeration, the following review only concerns the effect of using alternative bed materials, additives or modifying the inorganic composition of the fuel.

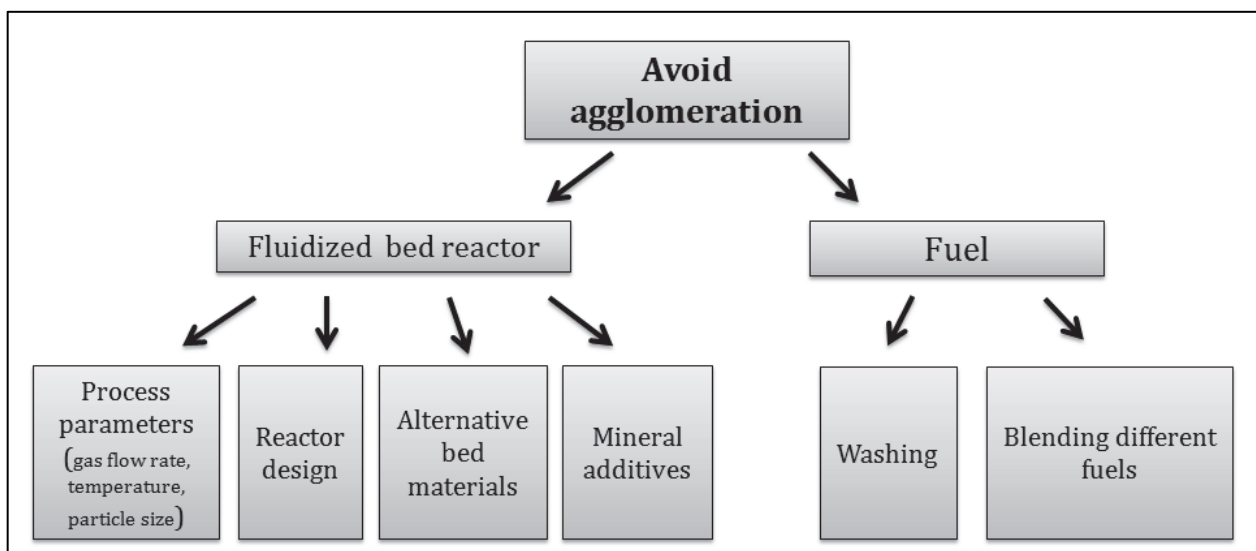


Figure IV-4: Different ways to counteract agglomeration

ALTERNATIVE BED MATERIALS AND ADDITIVES

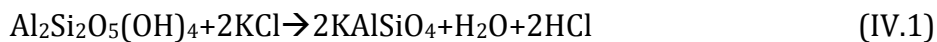
Although silica sand has many advantages (availability, stability at high temperature), many fluidized bed experiments reported agglomeration related problems using it as bed material. The main reason is the formation of potassium and calcium silicate liquid phase on the surface of sand particles. The most common countermeasure in industry to avoid agglomeration is the regeneration of bed after a certain operation time [IV-15]. As the costs of bed material regeneration are high, many attempts were made to use other alternatives: new type of bed materials or additives. It depends on the availability, cost and physical properties (grindable or resistant to abrasion) of the alternative mineral if it is used as bed material or additive. Minerals resistant to abrasion are usually used as alternative bed materials, while grindable minerals are pulverised and mixed to the bed [IV-1].

Their role is to increase the melting temperature of the liquid phase by modifying the liquid phase composition. The most common additives are aluminium silicates, alkali earth oxides and alkali earth carbonates. Minerals containing Ca, Mg, Fe or Al such as olivine ((MgFe)<sub>2</sub>SiO<sub>4</sub>), dolomite (CaMg(CO<sub>3</sub>)<sub>2</sub>), limestone (CaO), mullite (3·Al<sub>2</sub>O<sub>3</sub>,2SiO<sub>2</sub>) are good candidates as they generate high melting point silicates [IV-1].

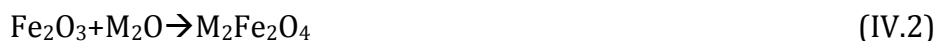
According to Ergudenler et al. [IV-4] using mullite instead of silica sand allows 120 °C higher operating temperature (from 800 to 920 °C) for straw gasification. Davidsson et al. [IV-18] reported improved agglomeration temperatures with blast furnace slag and olivine.

Alkali earth oxides can attach to the sticky sand surface and increase the sintering temperature of the eutectics. 60 °C higher operating temperature was reached by adding 2% of dolomite to the fuel feed [IV-19]. While dolomite is usually used as additive, magnesium oxide, magnesite and calcite were proposed as alternative bed materials [IV-1].

Aluminium silicates like common clay or kaolin (Al<sub>2</sub>Si<sub>2</sub>O<sub>5</sub>(OH)<sub>4</sub>) interact with molten ash and form Al-K-silicates according to the following mechanism [IV-18, IV-20–22].



Using ferric oxide (Fe<sub>2</sub>O<sub>3</sub>) instead of silica sand can increase the agglomeration temperature of the bed from 700 to 900 °C in fluidized bed combustion. As discussed previously, Fe binds alkaline and form oxides with high melting point [IV-1]:



These additives were tested for silica bed material in the case of combustion. In the case of gasification, only a few tests have been carried out in industrial scale [IV-23]. In the frame of GAMECO research project, olivine is used as bed material at more elevated temperature between 800-900 °C. The effect of these additives has to be validated for the project conditions.

### MODIFICATION OF BIOMASS ASHES

Alkali metals are the main responsables for agglomeration via formation of low melting point silicates. Potassium and sodium are present as salts in the biomass which makes them very reactive. The elimination of alkalis or the modification of their chemical form can reduce agglomeration.

Washing the biomass with water or other solvents prior to conversion can reduce the alkali content and reduce the risk of agglomeration [IV-24]. Arvelakis and al [IV-25] tested the washing of olive oil residues prior to gasification with silica bed with promising results. They reported seven to ten times longer operating time using washed samples.

Another possibility in order to avoid agglomeration is blending potentially dangerous biomass with other fuels. Blending can reduce the average alkali concentration or it can attach the reactive alkalis by new chemical bonds. For example, co-firing with sewage sludge reduces alkali volatilization by forming sulphates with the sulphur present in the added fuels [IV-26].

The influence of harvest time was tested with woody biomass [IV-2]. It was found that winter harvest (before the growing of leaves) has a less dangerous ash composition in regard of agglomeration. The concentration of critical elements in summer harvest can double. Therefore it is worth to optimize costs by mixing herbaceous crops or summer harvest wood with low alkali content biomass such as winter harvest wood or cocoa bean [IV-2].

## IV.3 MATERIALS AND METHODS

### CHARACTERISATION OF BED MATERIALS AND ADDITIVES

Three bed materials were used in this study: silica sand, olivine and calcined olivine. Sand and olivine are coming from Aheim, Norway (Sibelco). The calcined olivine was obtained by heat-treatment of the olivine particles at 1400 °C for 4 h in a laboratory furnace.

Kaolin (type Kerbrient) and dolomite (Neau, France) were tested as additives to prevent the agglomeration.

The main crystalline phases of crude minerals and samples heat-treated at 900 °C for 6 h in laboratory air circulation furnace (Nabertherm C 290) were analysed by X-ray diffraction (XRD, Bruker D8 Advance diffractometer, Cu-K $\alpha$ ).

The transformation of crystalline phases in olivine as a function of temperature was studied by optical microscope (Olympus BX51), *in-situ* X-ray diffraction in air (XRD, Bruker D8 Advance diffractometer, Cu-K $\alpha$ ) and Raman spectroscopy (InVia Reflex Renishaw, 633 nm laser wavelength, 13mW laser output) [IV-27].

For the visual observation, olivine samples were heat-treated in the temperature range of 400 to 1400 °C (heating rate 5 °C/min, annealed for 1 min), then embedded in resin and polished.

For *in-situ* XRD measurement, the olivine was finely ground and placed in a platinum plate in a HTK16 Anton Paar chamber. The sample was heated with 5 °C/min heating rate. The diffractograms have been determined for temperature steps of 20 °C. During the measurement, the sample was kept at constant temperature for 30 min [IV-27].

For the phase analysis by Raman mapping, small pieces of olivine rocks were heat-treated at 1400 °C for 4 hours, then embedded in epoxy resin and polished. The mapping was carried out with a holographic grating of 600 grooves/mm under x20 and x100 microscope objectives equipped with a charge coupled device (CCD) camera [IV-27].

### WETTING OF BED MATERIALS BY MISCANTHUS ASH

The wetting of olivine, calcined olivine and dolomite by molten miscanthus ash at high temperature was *in-situ* studied by optical dilatometer (Linseis L74 CTE) with sessile drop technique. Small olivine squares (1x1 cm) were obtained from an olivine bulk mineral with a table top cut off machine (Struers, Secotom 10). For calcined samples, the olivine squares were annealed at 1400 °C for 4 h in air. The dolomite substrate was prepared from fine ground powder with a pelletizer (d=41mm). The wetting tests were performed by placing the ash pastilles (d=5mm, batch: LM1/winter harvest, ashing temperature: 400 °C) on the different substrates and heated up to 1500 °C in air with a heating rate of 5 °C/min. The wetting of the substrates was *in-situ* filmed with a high resolution CCD camera.

The contact angle was determined at characteristic temperatures showing the characteristic changes in contact angle between 750 and 1200 °C. The cross section area of the ash pellet was also measured and compared to the size of the original pastille.

SAMPLE PREPARATION FOR STATIC INTERACTION TESTS

The interaction of miscanthus ashes and bed materials was studied in oxidizing and reducing atmospheres.

Pastilles of the mixture of miscanthus ashes and sand, olivine, calcined olivine were prepared with a pelletizer (50-50 wt% of ashes and bed materials, pastille d=13mm) and annealed for 6 and for 72 h at 900 and 1000 °C (heating rate 5 °C/min). For oxidizing atmosphere a laboratory air circulation furnace (Nabertherm C 290) was used.

The impact of reducing atmosphere on ash-bed material interaction was studied by applying the gasification conditions around the ash particle in a controlled atmosphere device with CO<sub>2</sub> and H<sub>2</sub> gas flow diluted with N<sub>2</sub> (input gas contains 2 mol% CO<sub>2</sub> and 3 mol% H<sub>2</sub>, experimental setup is described in Chapter II.4.2).

The heat-treated pastilles were mounted in epoxy resin (Epofix Kit, Struers) and polished with water free lubricants (DP Lubricant Brown and Yellow, Struers). The polished samples were metalised by carbon and analysed by scanning electron microscope measurements (Hitachi S4500, FEG, 15kV, 80sec/analyse).

## IV.4. PHASE TRANSFORMATION OF OLIVINE AT HIGH TEMPERATURE

Olivine is a natural mineral with a general composition of  $(\text{Mg}_{0.92}\text{Fe}_{0.08})_2\text{SiO}_4$ . It consists of two main crystalline phases: forsterite ( $\text{Mg}_2\text{SiO}_4$ ) and fayalite ( $\text{Fe}_2\text{SiO}_4$ ), whose ratio varies with the locality of the olivine. Beside the main compounds, other impurities, such as Na, Ca, Mn, Al, Cr and Ni can also be found. The name olivine derives from its green colour due to Ni impurities.

Olivine is often used as bed material in fluidized bed gasification as it has catalytic effect in tar decomposition [IV-28, IV-29]. This effect is due to the presence of iron. In order to increase the catalytic efficiency, olivine can be subjected to heat-treatment at elevated temperatures (900 °C to 1600 °C). The calcination of olivine promotes the migration of Fe to the surface [IV-29]. Regarding the agglomeration phenomenon, the presence of iron and other impurities (Ni, Cr) can modify the agglomeration mechanism as new phases can be formed in contact with the molten ash.

As calcined olivine is often used, it is important to understand how the heat treatment affects the surface characteristics of an olivine particle. The aim of this study is to reveal the phase transformation of olivine at elevated temperatures focusing on the transformation of the main phases, fayalite and hematite. Two complementary techniques were used; *in situ*-XRD and Raman spectroscopy.

*In situ*-XRD allows the precise description of crystalline phase transformation as a function of temperature. However, it is inefficient to describe the crystalline form of Fe in calcined olivine as the peaks of the different iron oxides ( $\text{Fe}_2\text{O}_3$ ,  $\text{Fe}_3\text{O}_4$ ,  $\text{MgFe}_2\text{O}_4$ ) are weak and overlap with the other crystalline compounds [IV-27].

In Raman spectroscopy the characteristic peaks of hematite ( $\text{Fe}_2\text{O}_3$ ) and magnetite ( $\text{Fe}_3\text{O}_4$ ) differ, therefore Raman analysis can complement the interpretation of diffractograms [IV-27]. The mapping mode makes it possible to detect the distribution of the different compounds on the particle surface.

The composition of olivine was analysed in order to quantify the impurities but their chemical form is not studied in depth.

### CHEMICAL COMPOSITION

The chemical composition of olivine was determined by LA-ICP-MS and it is presented in the form of oxides in Table IV-1. Beside the elements (Mg, Si and Fe) it contains a small amount (<1 wt%) of Al, Ca, Mn, Cr and Ni.

Table IV-1: Composition of olivine analysed by LA-ICP-MS

	wt %
MgO	45.3
SiO <sub>2</sub>	45.3
Fe <sub>2</sub> O <sub>3</sub>	7.71
Al <sub>2</sub> O <sub>3</sub>	0.56
CaO	0.11
MnO	0.11
Cr <sub>2</sub> O <sub>3</sub>	0.39
NiO	0.41

### PHASE TRANSFORMATION

Figure IV-5 shows the optical microscope images of olivine grains heat-treated in the range of 400-1400 °C. Olivine preserves its natural green colour up to 600 °C. At 700 °C the phase transformation is already visible, the grains successively become red. Deep red areas start to appear around 1200 °C, and they become dominant at 1400 °C. Moreover, starting from 1200 °C dark red veins can be also observed.

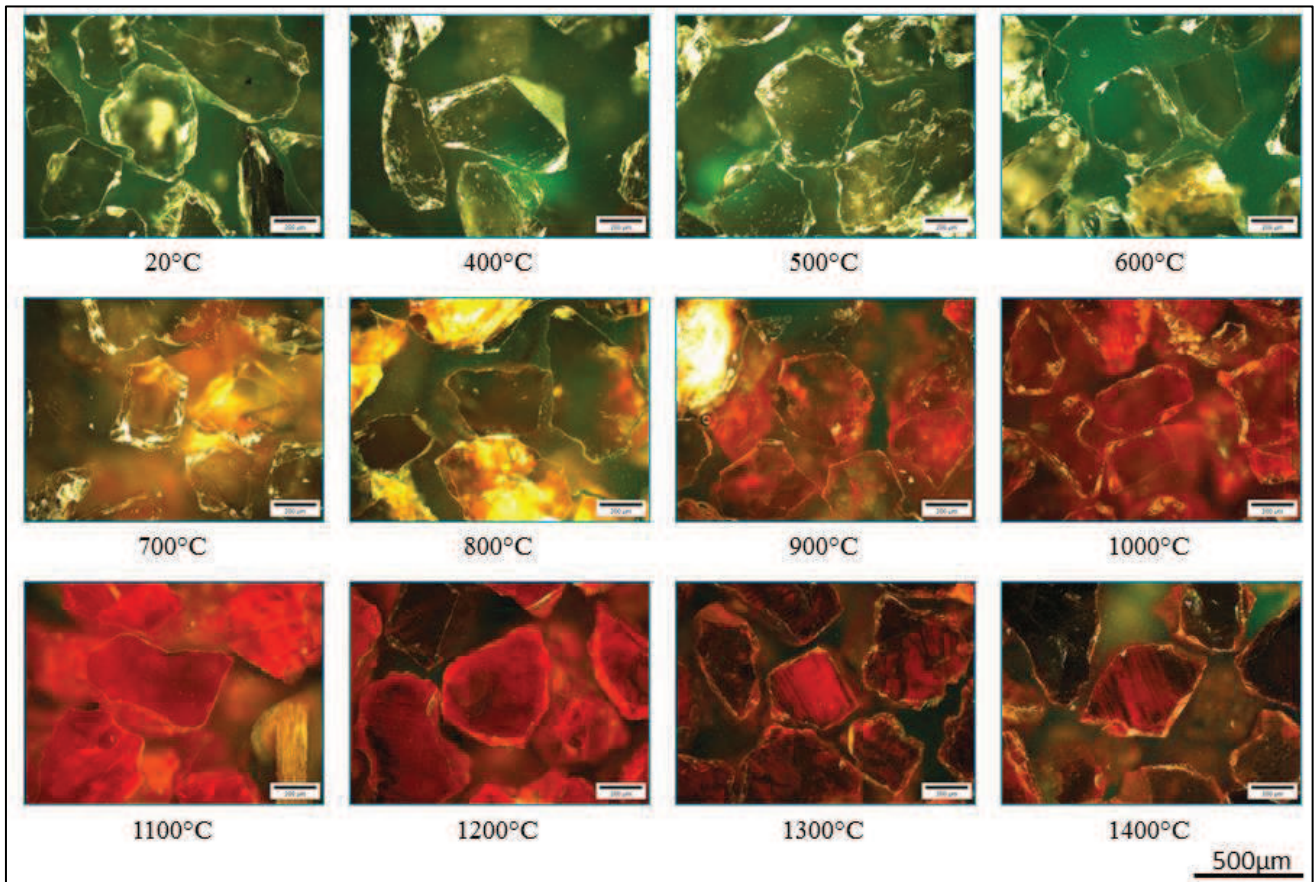


Figure IV-5: Phase transformation of olivine grains as a function of temperature

Figure IV-6 shows the diffractograms of *in situ*-XRD measurements between 25 and 1400 °C in the range of 22-34° (characteristic range for forsterite, serpentine and quartz and enstatite).

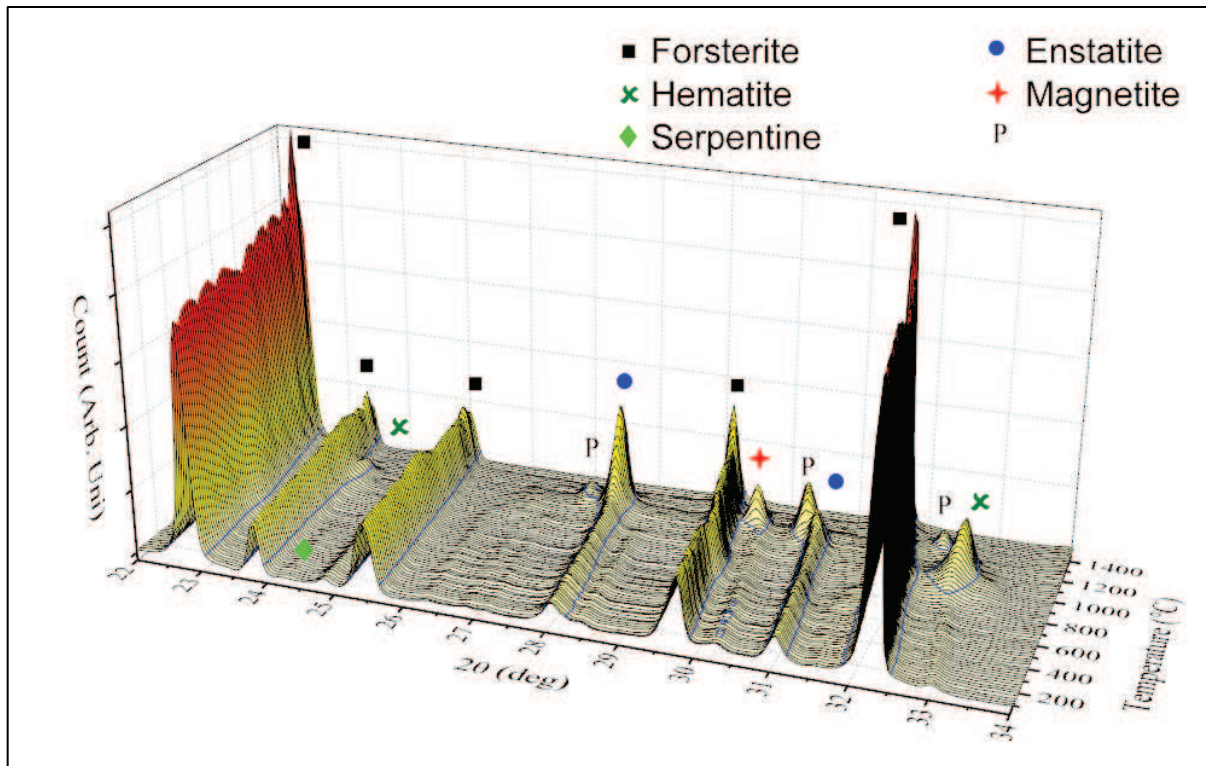
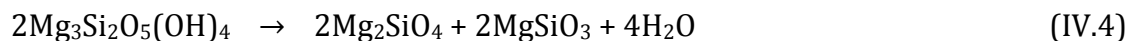


Figure IV-6 : *In situ* diffractograms of olivine between 25 and 1400 °C [IV-30]

The XRD analysis reveals the decomposition of serpentine into forsterite and enstatite around 600 °C.



Around 1030 °C forsterite reacts with quartz and forms enstatite.



Between 725 and 1150 °C fayalite oxidizes and forms either hematite or magnetite.



As the peaks of different iron oxides overlap, complementary methods are necessary to determine the nature of iron oxide.

In Raman spectroscopy, hematite and magnetite can be differentiated [IV-27]. Figure IV-7 shows the optical microscope image of calcined olivine in bright and dark field mode. A 1x1 cm zone was selected to perform the Raman analysis. In mapping mode, the spectra were collected

point by point with 1.6  $\mu\text{m}$  resolution. The spectra were undertaken to principal component analysis (PCA) [IV-27], which detected three compounds: forsterite ( $\text{Mg}_2\text{SiO}_4$ ), magnetite ( $\text{Fe}_3\text{O}_4$ ) and hematite ( $\text{Fe}_2\text{O}_3$ ).

Afterwards, the distribution of these three compounds was calculated with Direct Classical Least Squares (DCLS) method [IV-27]. The distribution of the three main compounds is shown in Figure IV-7/A-C with the corresponding Raman spectra (Figure IV-7d-f). The Raman analysis revealed that the dark veins mainly contain magnetite. Hematite can be found both in a small amount in the dark veins and in small areas on the grain.

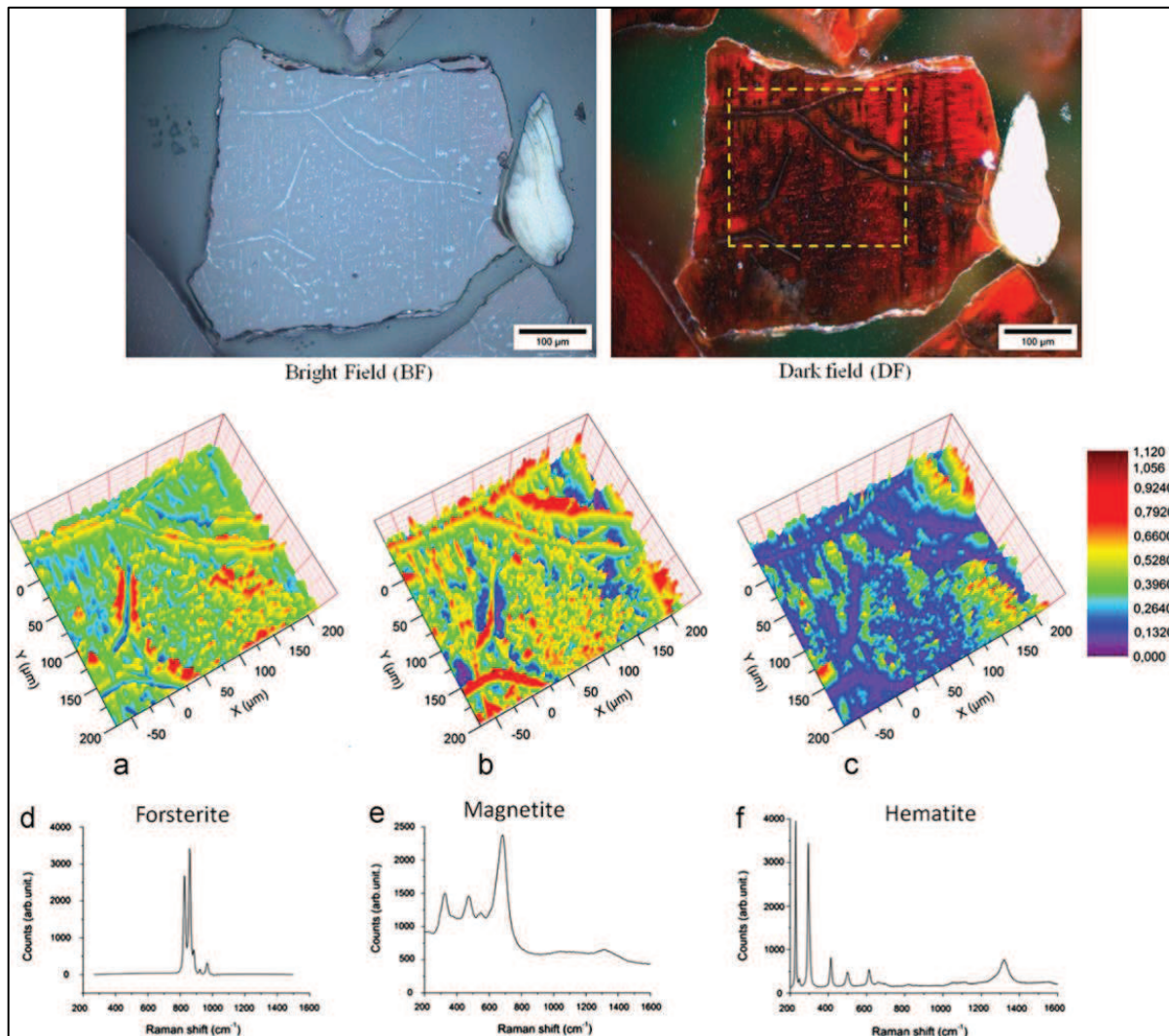


Figure IV-7: Raman mapping of calcined olivine sample; distribution of forsterite, magnetite and hematite [IV-27]

In summary, olivine is a common bed material in biomass thermal conversion due to its catalytic effect in tar decomposition. Olivine is a magnesium iron silicate with a general formula  $(\text{Mg,Fe})_2\text{SiO}_4$ , containing Cr and Al impurities. The main crystalline phases in the raw material are forsterite ( $\text{Mg}_2\text{SiO}_4$ ) and fayalite ( $\text{Fe}_2\text{SiO}_4$ ), which latter undergoes phase transformation at high temperature. It decomposes into magnetite ( $\text{Fe}_3\text{O}_4$ ) and hematite ( $\text{Fe}_2\text{O}_3$ ) turning the colour of the mineral red.

## IV.5 WETTABILITY OF BED MATERIALS BY MOLTEN ASHES

Agglomeration depends on the force balance of adhesion between sticky bed particles and collision kinetics of particles in fluidized bed. It has been previously shown that the mechanism of agglomeration includes sticky layer formation around the bed particles[IV-2]. The principal requirement of layer formation is the wettability of bed particles by the molten ashes.

Figure IV-8 presents a SEM image of agglomerate formed during miscanthus gasification in the pilot bubbling fluidized bed (laboratory LRGP, CNRS Nancy). The olivine particles are completely coated by molten ash. The thickness of the molten ash layer around the olivine particles is 10-40  $\mu\text{m}$ .

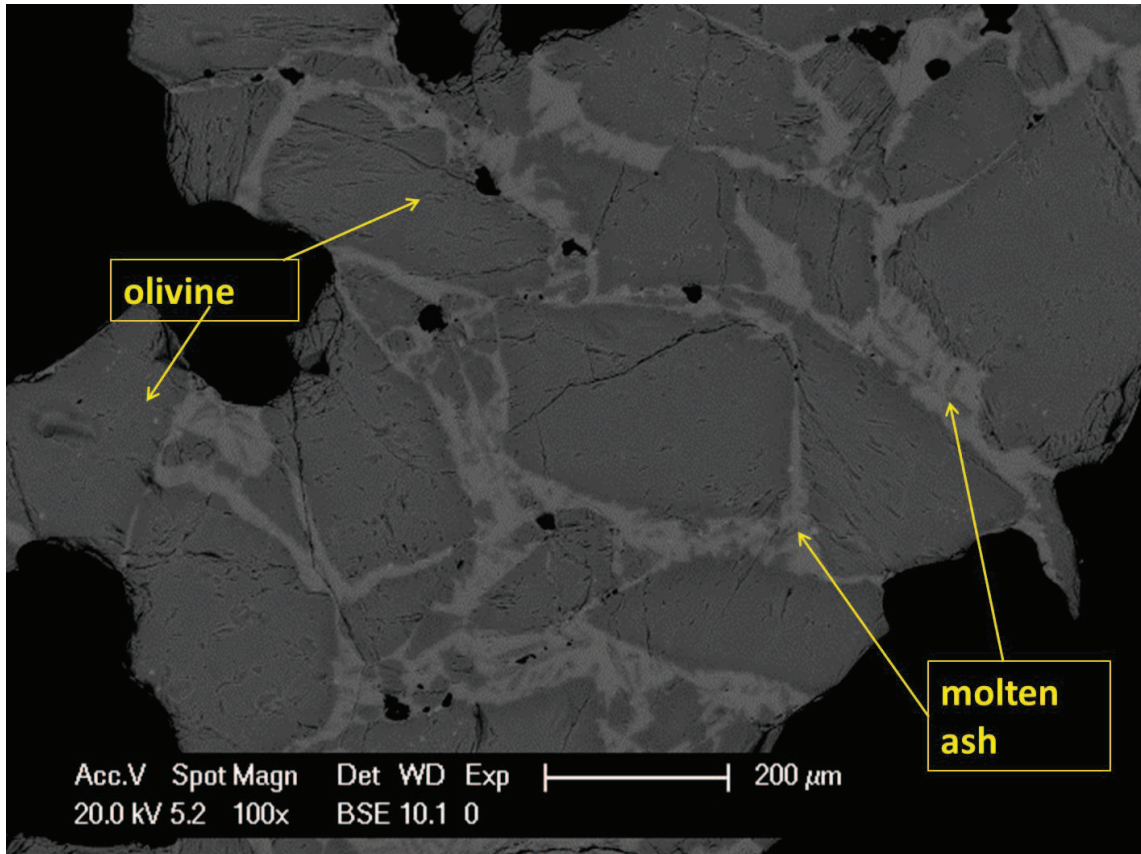


Figure IV-8 : SEM image of agglomerate deriving from miscanthus gasification in pilote fluidized bed (laboratory LRGP)

The wettability of a solid surface depends on the equilibrium of the surface tensions between the solid, liquid and gaseous phases (Figure IV-9). The equilibrium is expressed in the Young equation[IV-31]:

$$-\gamma_{SV} + \gamma_{SL} + \gamma_{LV} \cdot \cos\theta = 0 \quad (\text{IV.7})$$

- $\gamma_{SV}$  (J/m<sup>2</sup>) is the surface tension between solid and gaseous phase
- $\gamma_{SL}$  (J/m<sup>2</sup>) is the surface tension between solid and liquid phase
- $\gamma_{LV}$  (J/m<sup>2</sup>) is the surface tension between liquid and gaseous phase
- $\theta$  (°) is the contact angle of liquid phase on the solid surface

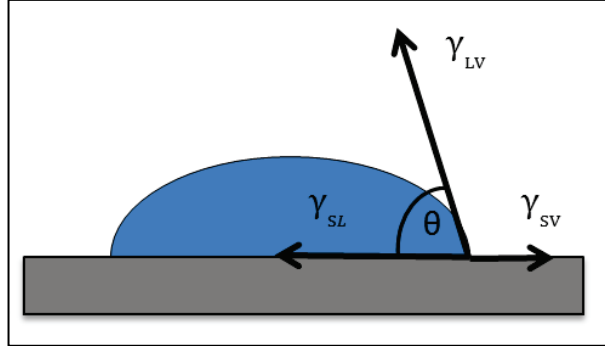


Figure IV-9: Equilibrium of surface tensions

A contact angle greater than 90° indicates non-wetting liquid, while less than 90° refers to good wetting[IV-31].

The energy needed to separate the liquid and solid phases is expressed in the adhesion work ( $W_a$ ) in the Dupré equation[IV-31]:

$$W_a = \sigma_{LV} + \sigma_{SV} - \sigma_{LS} \quad (IV.8)$$

- $\sigma_{LV}$  (J/m<sup>2</sup>) is the liquid-vapour surface energy
- $\sigma_{SV}$  (J/m<sup>2</sup>) is the solid-vapour surface energy
- $\sigma_{LS}$  (J/m<sup>2</sup>) is the solid-liquid interfacial energy

Combining the Dupré and Young equation, the adhesion work can be expressed as [IV-31]:

$$W_a = \cos\theta \cdot \sigma_{LV} + 1 \quad (IV.9)$$

Namely, the adhesion work ( $W_a$ ) can be calculated by measuring the contact angle and the liquid-vapour surface energy.

The contact angle of molten ash on olivine, calcined olivine (calcination at 1400 °C) and dolomite was measured in an optical dilatometer with sessile drop technique.

The liquid surface energy was taken from literature data [IV-31]. As it was shown in the previous chapter, the main components of molten ash are K<sub>2</sub>O and SiO<sub>2</sub>. Therefore, the surface energy of molten ash can be estimated with the data of glassy silicate systems.

To estimate the adhesion work of miscanthus ash on the olivine substrate, the surface energy of the system K<sub>2</sub>O-2 SiO<sub>2</sub> was used ( $\sigma_{LV} = 0.22 \text{ J/m}^2$  at 1045 °C) [IV-31].

Figure IV-10 shows the contact angle on the bed materials as a function of temperature. The contact angle on olivine is around 90° below 1000 °C and it decreases above 1000 °C. Above 1100 °C the contact angle decreases, at 1170 °C the molten ash is completely spread on the surface. The same mechanism was observed in the case of calcined olivine with somewhat higher contact angles below 1000 °C. In the case of dolomite, the ash is non-wetting, contact angles between 160 and 170° were observed below 1000 °C. The contact angle starts to decrease at 1100 °C and complete wetting occurs at 1200 °C.

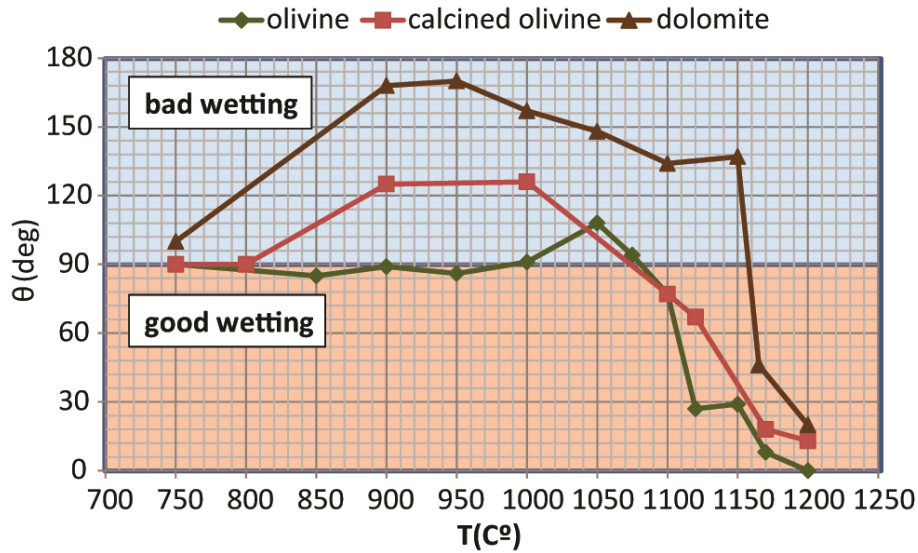


Figure IV-10: Contact angle of LM1 ash on olivine, calcined olivine and dolomite as a function of temperature

Figure IV-11, Figure IV-12 and Figure IV-13 present few images of miscanthus ash wetting on olivine, calcined olivine and dolomite in the range of 900 °C and 1200 °C.

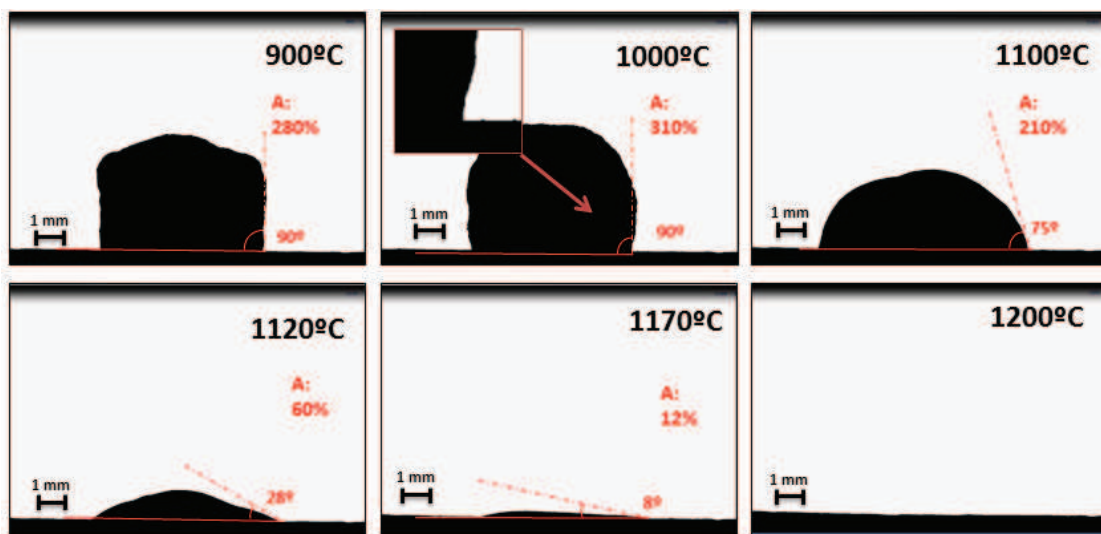


Figure IV-11: Wetting of olivine by miscanthus ash as a function of temperature

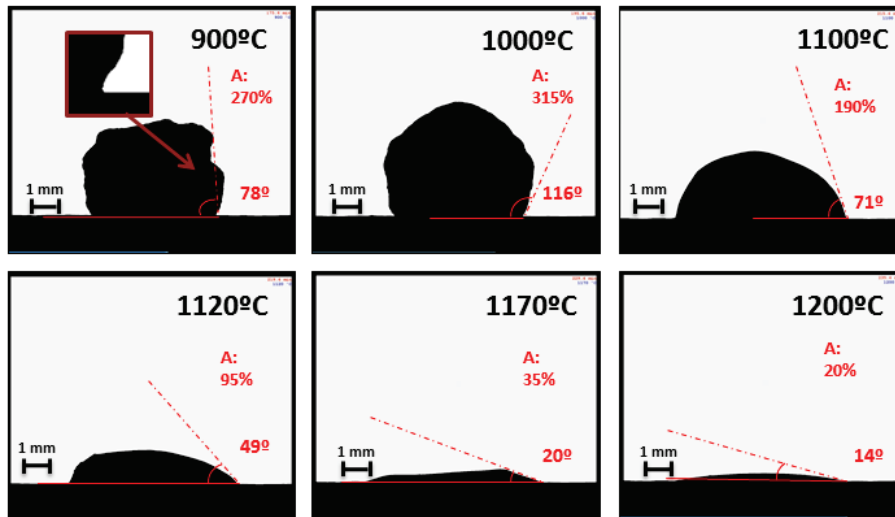


Figure IV-12: Wetting of calcined olivine by miscanthus ash as a function of temperature

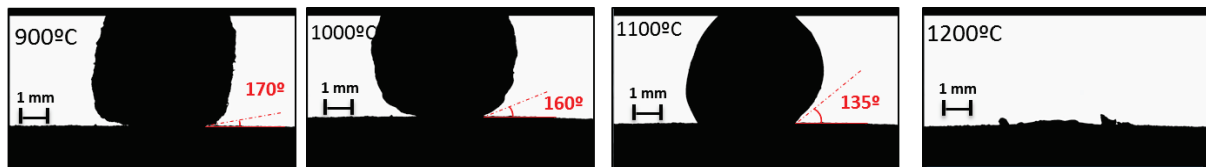


Figure IV-13: Wetting of dolomite (pastille) by miscanthus ash as a function of temperature

Figure IV-14 reports the estimated adhesion work between miscanthus ashes and bed materials as a function of temperature. The adhesion work is in the range of 80 to 100 mN/m below 1000 °C. Above 1000 °C the adhesion work increases and reaches 120 mN/m. It is proved in the Ph.D work of Michael Balland [IV-32] that the adhesion work between the molten miscanthus ashes and bed particles is sufficient to agglomerate the olivine particles at the operating temperature of the fluidized bed reactor.

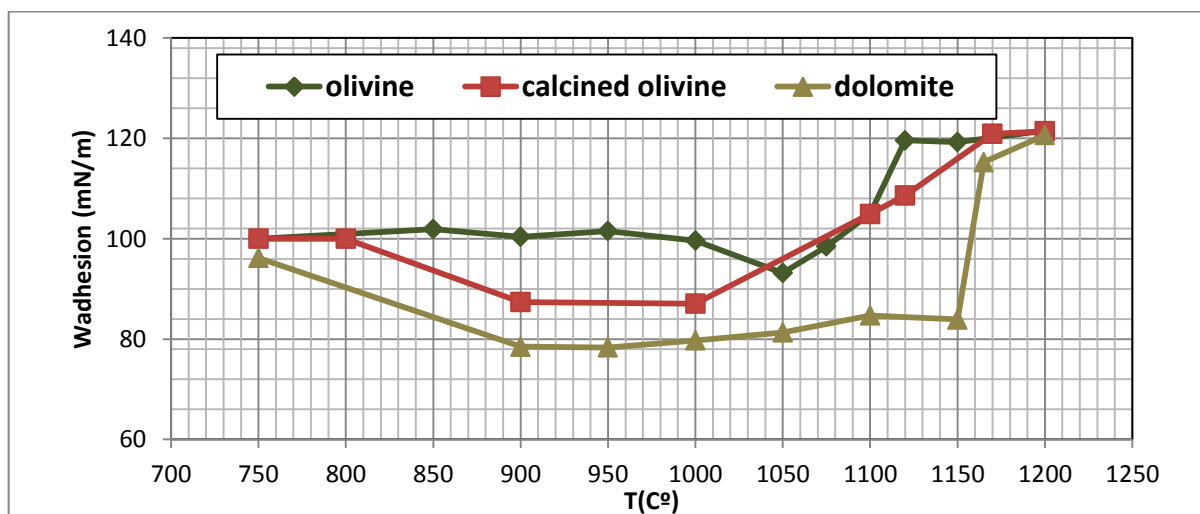


Figure IV-14: estimated work of adhesion versus temperature

Figure IV-15 shows the substrates after the wetting test (1200 °C in the case of olivine and 1500 °C in the case of calcined olivine and dolomite substrates). In the case of olivine, the ash is spread on the surface at 1200 °C, it is possible that it partially impregnated into the substrate but this could not be determined. In the case of the calcined olivine square and dolomite pastille, where the experiments were carried out up to 1500 °C, the molten ash impregnates into the solid support.



Figure IV-15: Olivine, calcined olivine and dolomite pastille after the wetting test

When interpreting these observations, it has to be considered that miscanthus ash, olivine and dolomite all undergo phase transformation at high temperature. Moreover, chemical interactions at the ash-mineral interface are also possible.

The ash pastille is a complex system which contains unburnt char, salts and silicates. In the temperature range of 400 to 1200 °C the main reactions are the thermal decomposition of carbonates, the volatilization of inorganic salts, and the formation of liquid silicates.

In consequence, viscosity of ash alters as a function of temperature. Moreover, the formation of gaseous species results in the swelling of the ash pastilles and the continuous changing of the pastille volume.

The molten biomass ash can be considered as molten glass, i.e. a mixture of oxides with good wetting ability of solid oxides [IV-31]. Molten glasses are highly viscous liquids ( $\eta > 10$  Pa.s) resulting in long spreading time (the time under the drop reaches its equilibrium shape on a given surface) [IV-31]. It would take several minutes or hours at a certain temperature to reach the thermodynamic equilibrium and to measure the equilibrium contact angle. Therefore, the results above are mostly indicative.

Miscanthus ashes showed good wetting both on natural and calcined olivine at high temperatures. Although good wetting of bed particles is essential for the formation of agglomerate, other aspects should also be considered to better estimate the interfacial bonding forces [IV-33], such as:

1. the capillary forces due to the liquid bridges between the particles<sup>1</sup> which can lead to solid bridge formation as shown in Figure IV-16 [IV-34]
2. the mineral surface topography (roughness)
3. the chemical reaction between ashes and bed material at the interface
4. the diffusion of phase components

The focus of the next subsection is on the diffusion of phase components and chemical interaction at the interface. The effect of surface roughness is concerned in the case of the calcined olivine whose surface is modified due to the thermal treatment at elevated temperature.

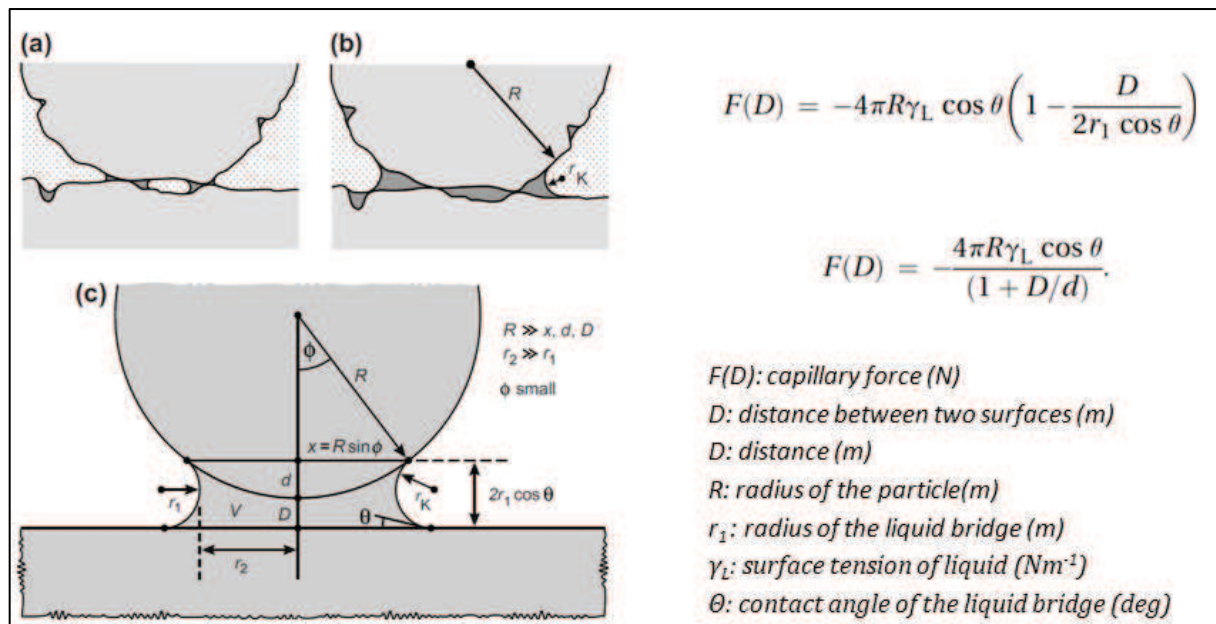


Figure IV-16: (a) formation of liquid contact points, (b) in the case of good wetting and sufficient amount of liquid, the voids are filled with the liquid, (c) model of capillary forces between particle and flat surface [IV-34]

<sup>1</sup> The capillary forces are inversely proportional to the liquid layer thickness between the particles and they can be increased with surface roughness [IV-34]

## IV.6 BED MATERIALS AND MISCANTHUS ASH INTERACTION TESTS

This subsection discusses the results of interaction tests between bed materials and miscanthus ashes under static conditions. Static condition means that the miscanthus ashes (prepared at 400 °C) are brought in contact with bed particles without macroscopic movement of the bed, focusing on the physicochemical aspects of adhesion and reactivity. The aim of this study is to reveal the adhesion mechanism of molten ashes on different bed particles, namely the occurrence of chemical interaction or diffusion of components at high temperature.

The typical operating temperature of bubbling fluidized bed is between 800 and 900 °C. Most of our laboratory tests are performed at 900 °C, the operating temperature chosen in the frame of GAMECO research project. The static experiments were carried out for 6 hours as preliminary studies proved that this time is adequate to examine the ash transformations and interaction with bed materials taking into account the high viscosity of molten ashes and the kinetics of chemical reactions.

Beside, further studies have been conducted with LM1 ash both at elevated temperature (1000 °C) and longer contact time with bed particles (72 h) to better evidence the physicochemical phenomena of agglomeration. LM2 ash-bed material interaction was only studied at 900 °C for 6 and 72 h.

As it was discussed in the literature overview, ash from woody biomass interacts with silica sand and form double layers around the silica particles. The inner layer has a composition similar to the bed material, while the composition of the outer layer is more close to the inorganic content of the biomass ash. In the case of herbaceous biomass, direct adhesion is observed [IV-13].

Olivine is a favoured bed material for its catalytic effect in tar decomposition but the interaction between biomass ashes and olivine was not studied in details. As it was shown earlier, the calcination of olivine significantly modifies its surface structure by accumulating  $\text{Fe}_2\text{O}_3$  and  $\text{Fe}_3\text{O}_4$  in dark veins. As Fe is more available after calcination, it can diffuse into the molten ash and/or form new phases.

This subsection aims to answer the following questions:

1. does miscanthus ash form silicates with silica sand?
2. does diffusion or chemical interaction occur in contact with olivine particles?
3. how does the elevated Fe concentration affect the adhesion; does it reduce the amount of liquid phase or strengthen the adhesion?
4. how does the contact time and temperature influence the layer formation?
5. what is the effect of harvest time of miscanthus on interaction (LM1-after winter harvest, LM2-late summer harvest)?
6. how does the reducing atmosphere influence the agglomeration mechanism?

IV.6.1 EFFECT OF BED MATERIAL

Miscanthus ashes (LM1-April 2011, LM2-September 2011) in contact with silica sand, olivine and calcined olivine were heat treated at 900 °C for 6 hours in air. In all cases, good adhesion is observed between the molten ash and the bed materials; SEM images are presented in Appendix A-12. Figure IV-17 shows the SEM-EDX analysis of ash-bed material interfaces.

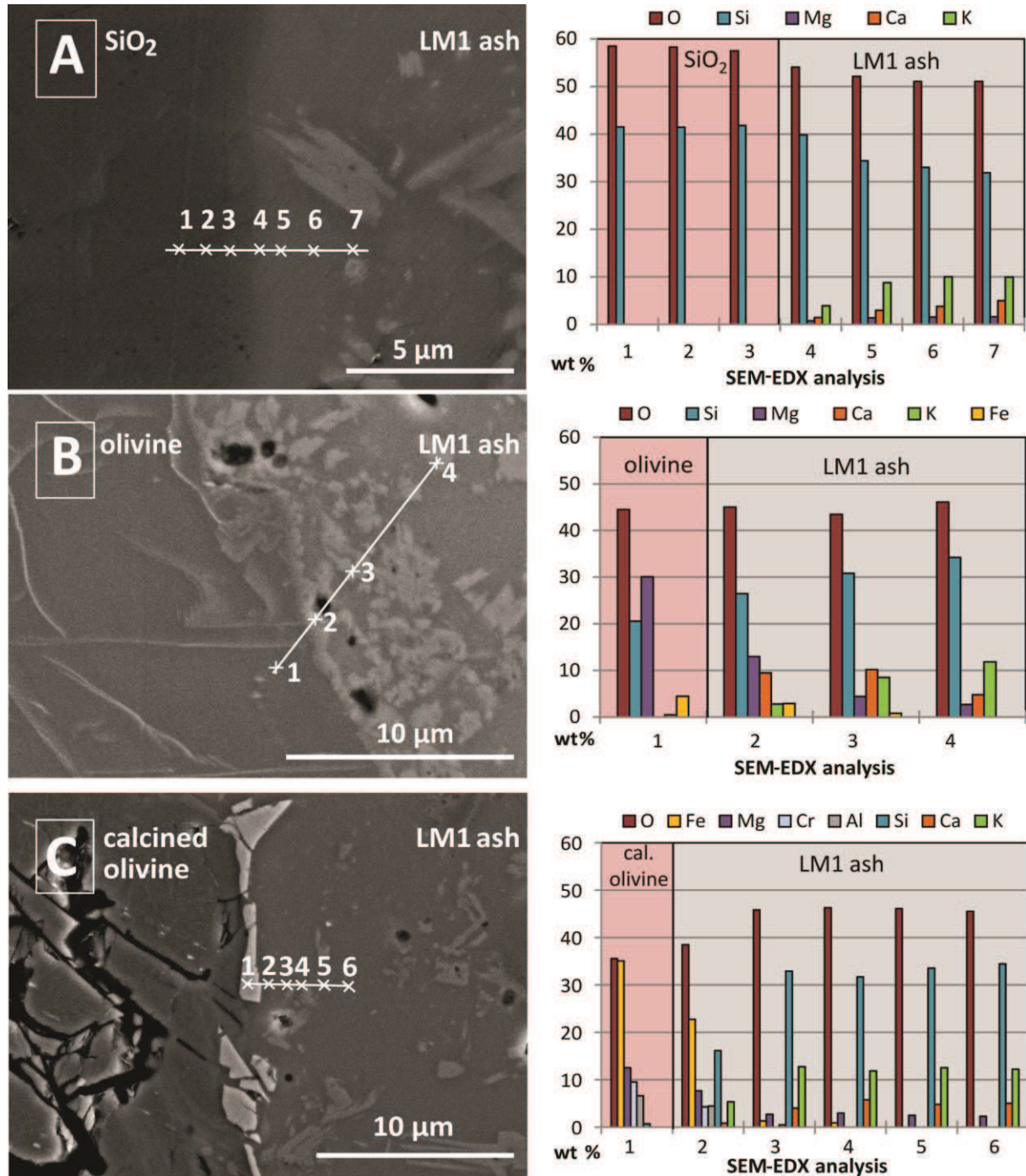


Figure IV-17: SEM-EDX analysis of LM1 miscanthus ash in contact with silica sand (A), olivine (B) and calcined olivine (C) after heat-treatment at 900 °C in air for 6 hours

In contact with silica sand ( $\text{SiO}_2$ ), the point by point analysis indicates a sharp cut in the values of K, Ca and Mg at the interface, the molten ash do not diffuse into or interact with the silica sand. In this case the adhesion is caused by the good wetting ability of the molten ash.

In contact with olivine and calcined olivine, a thin bright inner layer is observed at the interface. The EDX measurement indicates the accumulation of Ca at the interface. As the layer is very thin ( $\sim 0.5\text{-}1\ \mu\text{m}$ ), it is difficult to determine the exact composition. The Ca can be in the form of  $\text{CaSiO}_3$  or  $\text{CaMgSi}_2\text{O}_6$ . It can crystallize from the molten ash ( $\text{SiO}_2\text{-K}_2\text{O-CaO-MgO}$ ) or it can be formed in contact with enstatite ( $\text{MgSiO}_3$ ) from the olivine:



Beside the thin layer formation, the point-by point analysis proved the diffusion of iron into the molten ash and the migration of a very small amount of K and Ca into the olivine particle both in contact with olivine and calcined olivine.

#### IV.6.2 EFFECT OF MISCANTHUS HARVEST TIME

The effect of harvest time on the ash composition was studied in Chapter II. It was found that late summer harvest results in significantly greater amount of K, Mg and Cl, therefore the risk of agglomeration is higher.

The static interaction tests with late summer harvest miscanthus ashes (LM2) were performed under the same conditions as with LM1 ash ( $900\ \text{°C}$ , 6 h, in air). Figure IV-18 shows the SEM-EDX analysis of LM2/calcined olivine interface. In comparison with LM1 two main differences can be observed. Firstly, the bulk phase of the ash is more homogeneous. Secondly, the formation of  $\text{K}_2\text{MgSiO}_6$  instead of calcium silicate was observed at the interface.

LM2 ash contains more K than LM1 ash resulting in significantly higher amount of liquid phase at  $900\ \text{°C}$ .

The crystals observed at the interface can derive from the ash via crystallization or can be formed from molten ash ( $\text{K}_2\text{O-SiO}_2$ ) and enstatite ( $\text{MgSiO}_3$ ) interaction:



The small white crosses in the bottom part of the image (Figure IV-18, point 3) correspond to iron oxide.

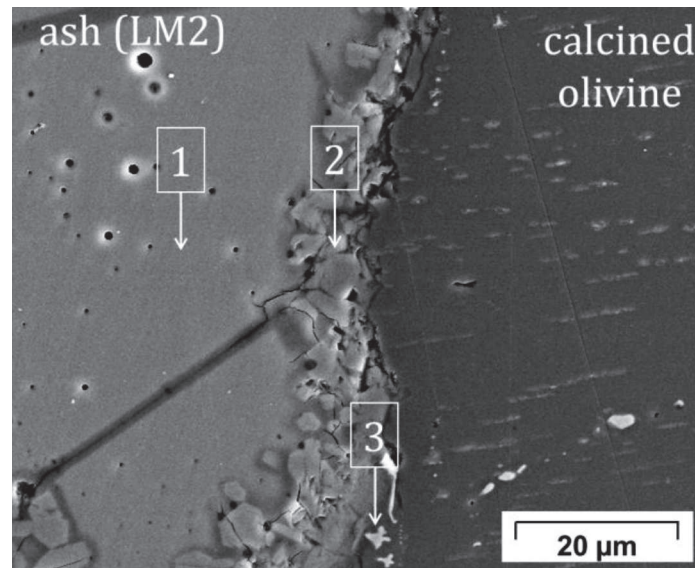


*Figure IV-18: Interaction between LM2 ashes (September 2011) and calcined olivine (900 °C, air)*

The diffusion of alkali metals and iron was studied by SEM-EDX analysis. Figure IV-19 shows the SEMEDX analyses of LM2 ash/bed material interfaces.

The LM2/silica sand interface is completely smooth; the LM2 ash is perfectly wetting the silica surface. The point by point analysis indicates a small amount of K diffused into the silica sand (Figure IV-19/A, point 6). As the K concentration at point 6 is very weak and the analysis point is close to the interface, the diffusion of K has to be proved by analysing samples which were heat-treated for elongated contact time or at elevated temperature.

At the LM2/olivine and LM2/calcined olivine interface the accumulation of magnesium silicates can be observed. In the case of olivine the point by point analysis shows weak diffusion of Fe into the ash and K into the olivine.

The EDX analysis of LM2/calcined olivine interface reveals approximately 2-3 wt % Fe diffused into the ash (Figure IV-19/C, points 3-7). The diffusion of a small amount of K into the olivine particles can be observed as well (Figure IV-19/C-points 8, 9, and 10).

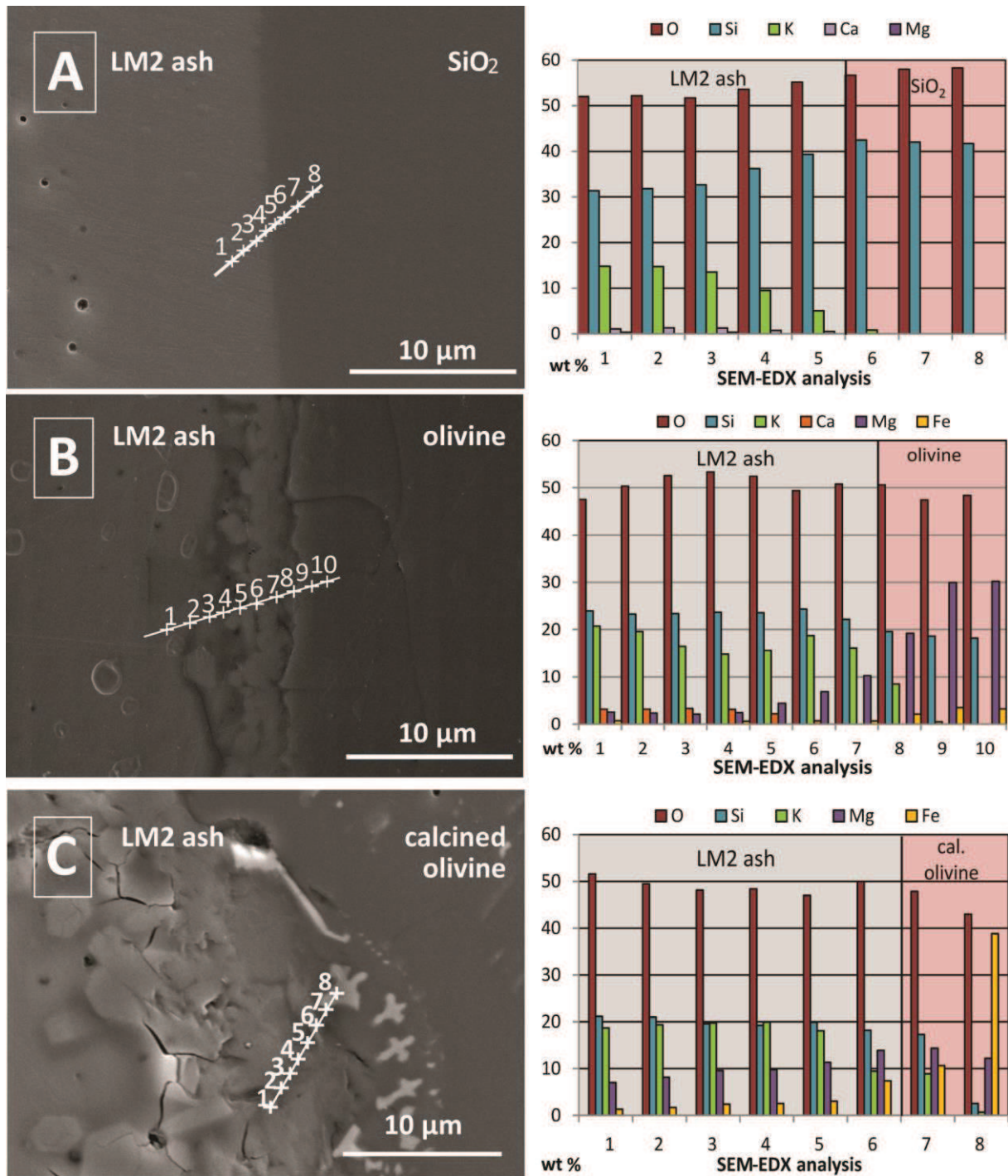


Figure IV-19: SEM-EDX analysis of LM2 miscanthus ash in contact with silica sand (A), olivine (B) and calcined olivine (C) after heat-treatment at 900 °C in air for 6 hours

## IV.6.3 EFFECT OF ELEVATED TEMPERATURE AND CONTACT TIME

Further studies were carried out with LM1 ashes both at elevated temperature (1000 °C) and longer contact time with bed particles (72 hours) to better evidence the nature of interaction. LM2 ash/bed material interaction was only studied at 900 °C for 6 and 72 hours.

In the case of the LM1/silica sand and LM2/silica sand tests the interface remains smooth, neither the elevated temperature nor the longer contact time initiated chemical interaction or diffusion.

In contact with olivine and calcined olivine, the thickness of the inner layer (calcium silicate in the case of LM1 and potassium magnesium silicate in the case of LM2) increases with time and temperature. Figure IV-20 shows the development of the inner layer at elevated temperature (900 and 1000 °C) and contact time (6 and 72 hours).

In the case of LM1 ash, the thickness of the calcium silicate layer increases moderately and remains relatively thin (~1 µm) in all cases. The inner layer is significantly thicker in the case of LM2 (4-8 µm), and in contact with calcined olivine its thickness doubles at elevated contact time.

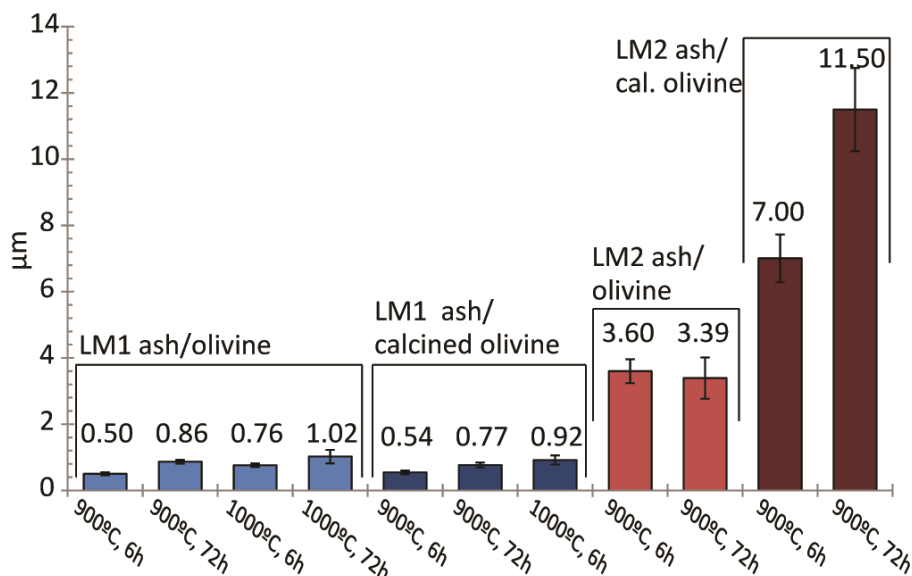


Figure IV-20: Inner layer thickness at the ash/olivine and ash/calcined olivine interface

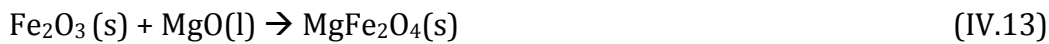
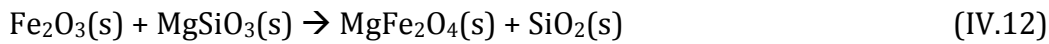
The point by point SEM-EDX analysis showed that the iron diffuses into the ash. With elevated contact time and temperature, the depth of diffusion slightly increases; in the case of heat-treatment at 1000 °C for 72 hours the depth of iron diffusion is approximately 15 µm around the particles. The concentration of iron in molten ash is 2-3 wt % in the case of olivine and somewhat lower, about 1 wt % in the case of calcined olivine.

In olivine, Fe is present in the form of fayalite ( $\text{Fe}_2\text{SiO}_4$ ). As it was discussed in section IV.4.1, it decomposes into iron oxide and silica starting from 725 °C and forms dark veins at the particle surface. In contact with molten ash, some part of the iron diffuse directly into the liquid phase,

while in the case of calcined olivine the previously formed iron oxide tends to stay on the olivine surface.

Contrary to olivine, at the LM1/calcined olivine interface the inclusion of magnesium ferrite ( $\text{MgFe}_2\text{O}_4$ ) into the molten ash was observed (Figure IV-21). The magnesium ferrite crystals contain a small amount of Cr (~4 wt %), Al (~2 wt %) and in some cases Ni (~1%). Their size increases with longer contact time and higher temperature from few micrometres up to twenty micrometres.

The source of these crystals has to be clarified. Formerly, the Raman analysis of the calcined olivine did not show the presence of magnesium ferrite. However, they were identified in calcined olivine particles by SEM-EDX analyses recently (see Appendix A13). As olivine is a natural mineral, the impurities of particles of the same source or batch are possible. The increase of the size of magnesium ferrite at the ash/calcined olivine interface can be due to the accumulation of oxides on the surface of olivine particles or to further chemical reactions with the molten ashes. There are two possible ways of  $\text{MgFe}_2\text{O}_4$  formation; (1) in contact with enstatite ( $\text{MgSiO}_3$ ) during the calcination of olivine or (2) in contact with MgO in molten biomass ashes.



In both cases, the calcination of olivine results in a roughened surface rich in ferrous oxides. The roughened surface increases the adhesion of molten ashes.

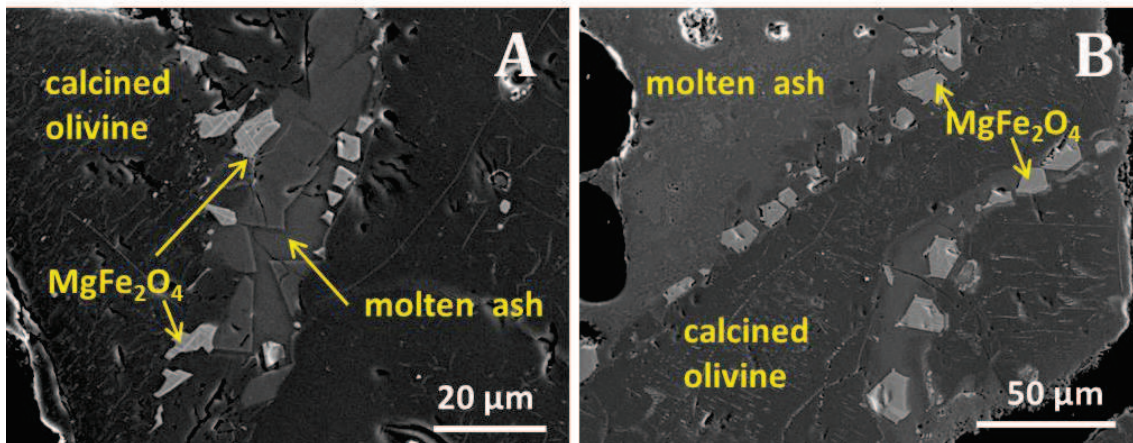


Figure IV-21:  $\text{MgFe}_2\text{O}_4$  crystals at LM1/calcined olivine interface after 72 hours heat-treatment at 900 °C (A) and 1000 °C (B)

Beside magnesium ferrite, other ferrous oxides were found. Figure IV-22 shows two examples. In Figure IV-22/A, the formation of a 100 µm wide  $\text{Fe}_2\text{O}_3$  crystal at elongated contact time (1000 °C, 72 h) was observed. The liquid phase around the  $\text{Fe}_2\text{O}_3$  crystal contains 6 wt % of Fe. Figure IV-22/B shows the Fe-Cr crystals. The bright lamellas (Figure IV-22/B, point 1) contain 55 wt % of Fe and 10 wt % of Cr, the somewhat darker area (Figure IV-22/B, point 2) contains 10 wt % of Fe and 40 wt % of Cr.

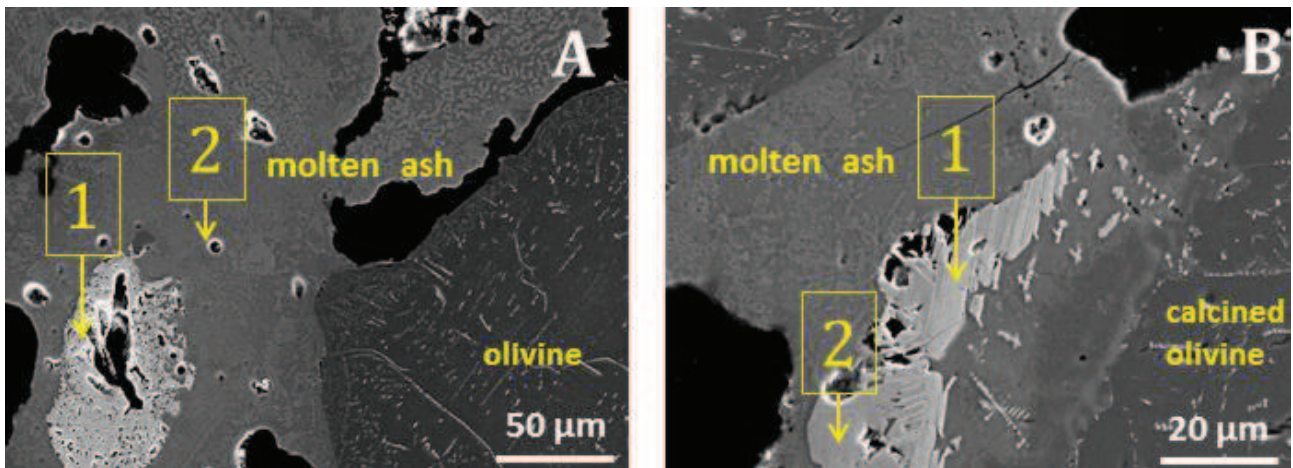


Figure IV-22: (A) LM1 ash/olivine interface after heat-treatment at 1000 °C for 72 hours, (B) LM1 ash/calcined olivine interface after heat-treatment at 1000 °C for 72 hours

#### IV.6.4 EFFECT OF REDUCING ATMOSPHERE

To study the effect of reducing atmosphere, the LM1/bed material pastilles were heat-treated in a reducing gas mixture (2 mol % of CO<sub>2</sub> and 3 mol % of H<sub>2</sub> diluted in N<sub>2</sub>) for 6 hours at 900 and 1000 °C.

Figure IV-23 shows the ash/olivine interface at 900 °C. Similarly to oxidizing atmosphere, a thin bright inner layer around the olivine particle can be observed in reducing conditions as well (Figure IV-23, point 1). The point by point SEM-EDX analysis showed the diffusion of Fe (in few micrometres depth) into the molten ash.

In contact with olivine, the sulfur deriving from the biomass ash forms FeS (Figure IV-23, point 3) and it migrates into the molten ash. Around the FeS 'islands' the liquid phase contains great amount of Fe (approximately 15 wt %, Figure IV-23, point 5).

At the ash/calcined olivine interface, FeMg<sub>2</sub>O<sub>4</sub> was observed (Figure IV-24, point 1). The erosion of calcined olivine occurred both at 900 and 1000 °C (Figure IV-24, point 2).

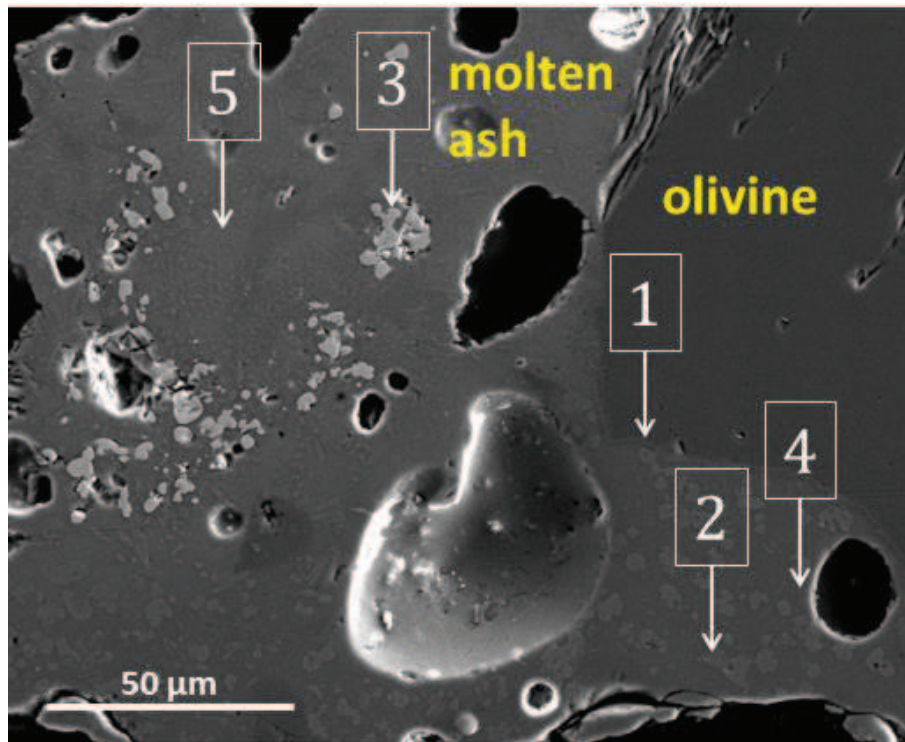


Figure IV-23: LM1 ashes/olivine interface (900 °C, 6h reducing gas mixture)

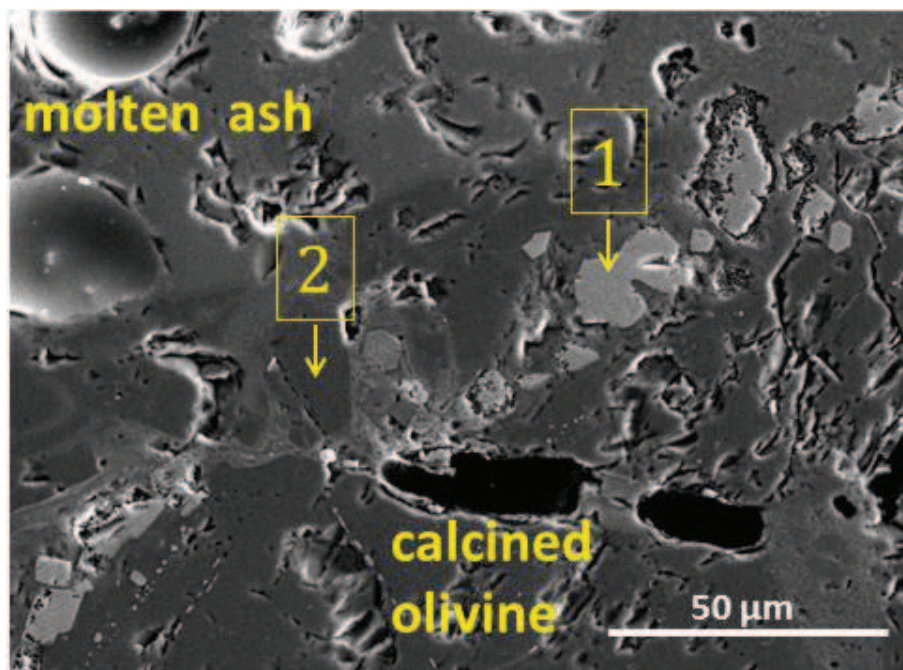


Figure IV-24: LM1 ashes/calcined olivine interface (900 °C, 6h reducing gas mixture)

As it is shown in Figure IV-25 (point 1), the molten ash incorporates small parts of calcined olivine. In reducing atmosphere two immiscible liquid phases are present: CaO-MgO-Fe<sub>2</sub>O<sub>3</sub>-SiO<sub>2</sub> with small amount of Al (Figure IV-25, point 2) and K<sub>2</sub>O-MgO-Fe<sub>2</sub>O<sub>3</sub>-SiO<sub>2</sub> (Figure IV-25, point 3). At some areas, the presence of Fe/Al/Mg-containing oxides (Figure IV-26, points 1, 3, and 4) and Fe/Mg/Al-containing silicates (Figure IV-26, point 2) were also observed.

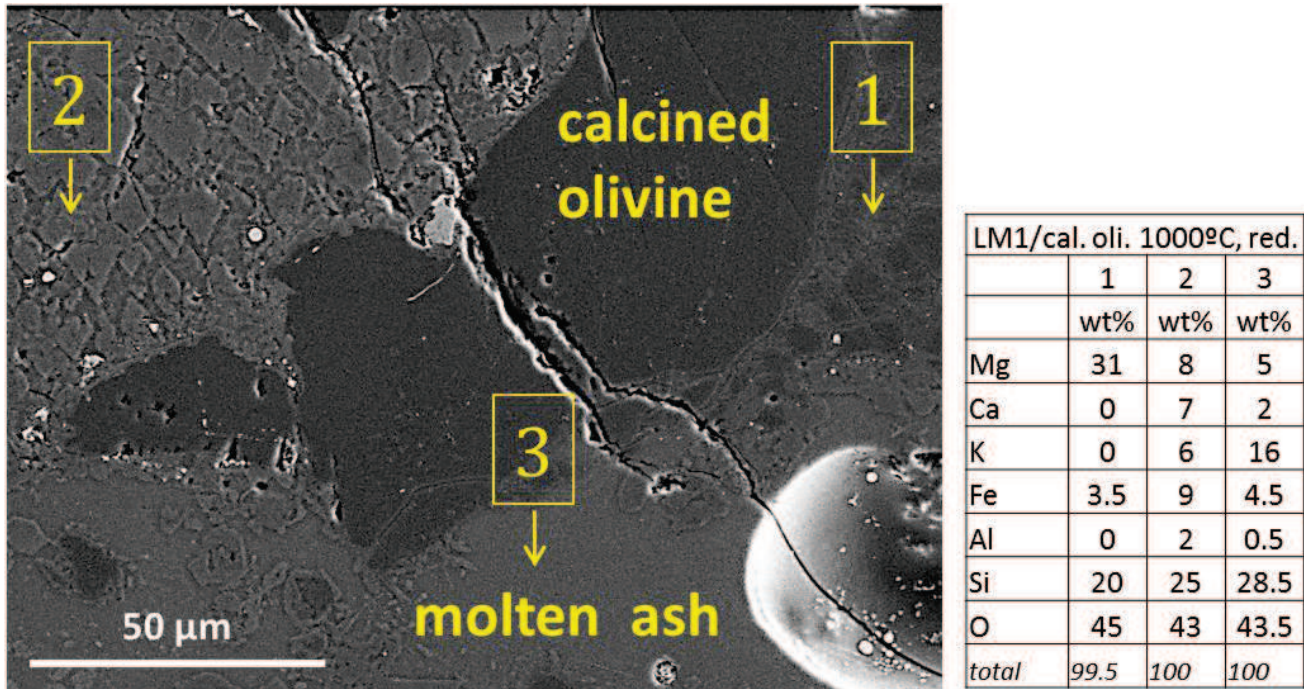


Figure IV-25: LM1 ashes/calcined olivine interface at 1000 °C in reducing gas mixture for 6 hours

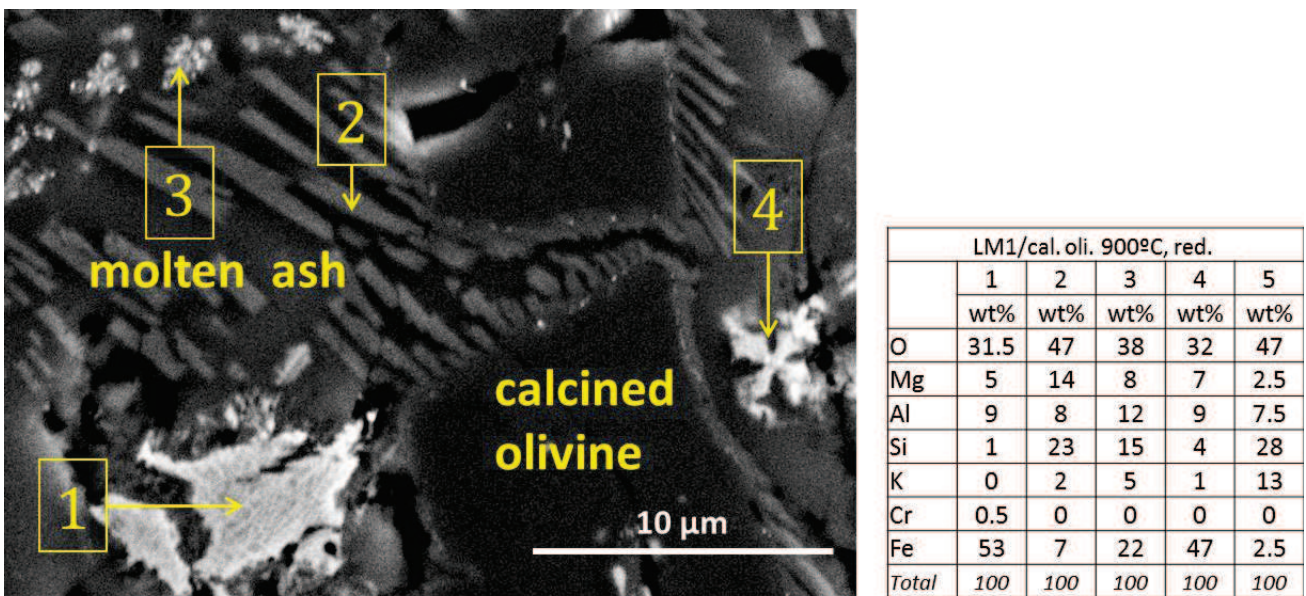


Figure IV-26: LM1 ashes/calcined olivine interface at 900 °C in reducing gas mixture for 6 hours

Table IV-2 summarises the findings of the static interaction tests. In contact with silica sand only physical adhesion was observed. In the case of olivine and calcined olivine, the diffusion of Fe (possibly iron oxide) into the molten ash was evidenced. The surface of olivine particles were roughened and enriched in iron oxide and magnesium ferrite due to calcination at 1400 °C.

We found that the reducing atmosphere has no influence on the ash/silica sand interaction. On the other hand, in contact with olivine, the molten ash is enriched in iron, and the presence of two immiscible phases is possible. In reducing atmosphere the agglomerates contain unburnt char, whose role in agglomeration has to be revealed in the future.

*Table IV-2 : Summary of ash/bed material interaction*

	Oxidizing atmosphere	Reducing atmosphere
Silica sand	<ul style="list-style-type: none"> <li>➤ Good wetting, adhesion</li> <li>➤ no chemical interaction</li> <li>➤ liquid phase SiO<sub>2</sub>-K<sub>2</sub>O-CaO</li> </ul>	No influence
Olivine	<ul style="list-style-type: none"> <li>➤ Good wetting, adhesion</li> <li>➤ diffusion of Fe into slag</li> <li>➤ liquid phase SiO<sub>2</sub>-K<sub>2</sub>O-CaO, 2-3 wt % of Fe around the bed particles</li> <li>➤ Ca accumulated at ash/olivine interface in the case of LM1</li> <li>➤ K, Mg accumulated at ash/olivine interface in the case of LM2</li> </ul>	At some areas two immiscible liquid phases, one richer in Fe Formation of FeS
Calcined olivine	<ul style="list-style-type: none"> <li>➤ Good wetting, adhesion</li> <li>➤ diffusion of Fe into slag</li> <li>➤ liquid phase SiO<sub>2</sub>-K<sub>2</sub>O-CaO, 1-2 wt % of Fe around the bed particles</li> <li>➤ roughened particle surface, inclusion of MgFe<sub>2</sub>O<sub>4</sub> into the slag</li> </ul>	At some areas two immiscible liquid phases, one richer in Fe

## IV.7 CONCLUSION

This chapter discussed the interaction between miscanthus ashes and bed materials under static conditions in regard of the physico-chemical aspects of agglomeration phenomenon. This study focused on (1) the phase transformation of olivine at high temperature, (2) the wetting ability of miscanthus ash on bed materials and (3) the nature of interaction at the ash-bed particle interface.

Three bed materials (sand, natural olivine and calcined olivine) were tested in contact with miscanthus ashes (LM1 winter harvest, LM2 summer harvest) in oxidizing and reducing atmosphere at elevated temperatures (900 °C-1000 °C).

The phase transformation of olivine at high temperature was studied in depth by Michel et al [IV-27]. Two complementary techniques, the *in situ*-XRD and Raman mapping revealed that fayalite ( $\text{Fe}_2\text{SiO}_4$ , one of the two main components of olivine) decomposes into  $\text{Fe}_2\text{O}_3$  and  $\text{SiO}_2$  above 725 °C, and  $\text{Fe}_2\text{O}_3$  oxidizes and forms dark  $\text{Fe}_2\text{O}_3$  veins on the particle surface above 1100 °C.

It was shown that the key parameter of agglomerate formation is the wetting of bed particles by molten ash and the adhesion work between sticky particles. As it is shown in Figure IV-27, good wetting results in viscous liquid film around the particles. These “sticky” particles can collide and liquid bridges can be formed in between them. If the adhesion energy is greater than the kinetic energy of the particle collision, the particles will form agglomerates.

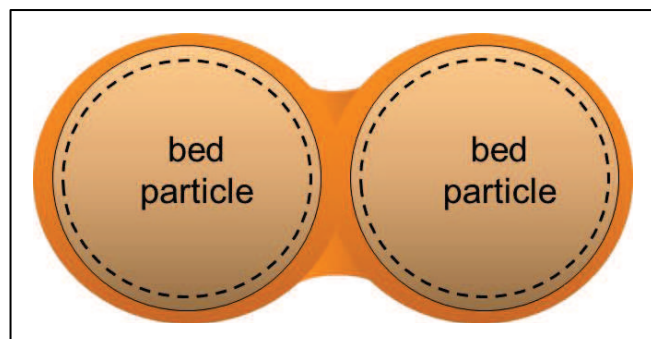


Figure IV-27: Agglomerate formation due to sticky viscous layer and liquid bridge formation

The interparticle forces between sticky particles can be enhanced by chemical interaction or increased surface roughness, therefore it is indispensable to study the nature of ash-bed material interaction.

In the case of woody biomass, the literature often describes double layers in contact with silica sand, where the inner layer is rich in Ca and K silicates. As miscanthus ashes are rich in K and Si they did not form double layers around silica sand, the agglomeration is due to direct sticking, as it was reported for the case of other herbaceous biomasses.

In contrary to silica sand, in the case of olivine and calcined olivine, a thin inner layer rich in Ca-silicate or K-Mg-silicates (depending on the harvest time) and the diffusion of Fe into the

molten ash were observed. The concentration of iron oxide in molten ash is relatively low (2-3 wt%), the contact time increases its diffusion to 10-15 $\mu\text{m}$  into the ash.

In contact with calcined olivine, magnesium ferrite ( $\text{MgFe}_2\text{O}_4$ ) was observed at the ash-bed particle interface. With increased contact time and temperature the crystal size reached 10 to 20 $\mu\text{m}$ . As illustrated in Figure IV-28), these crystals act like jigsaw teeth at the interface and reinforce the adhesion due to the surface roughness. Further investigations are necessary to determine if chemical reaction between the ferrous oxides and the molten ash occurs.

The impact of surface roughness and  $\text{MgFe}_2\text{O}_4$  inclusion on agglomeration will be studied under dynamic conditions in Chapter V.

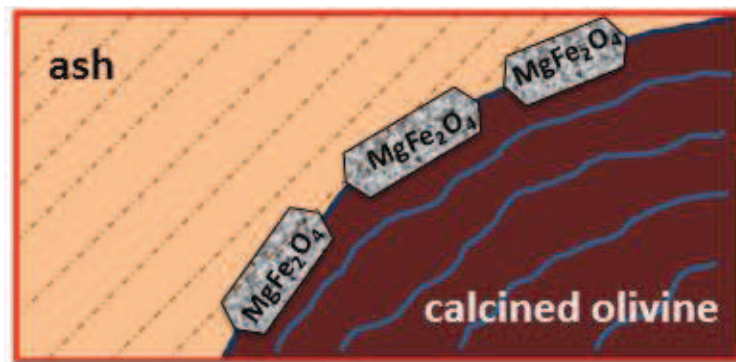


Figure IV-28: Formation of magnesium ferrite ( $\text{MgFe}_2\text{O}_4$ ) at ash-calcined olivine interface

The harvest time has significant effect on the agglomeration mechanism; LM2 ashes in contact with olivine and calcined olivine form a thick and compact inner layer of  $\text{K}_2\text{MgSi}_2\text{O}_6$  contrary to the thin Ca-silicate layer in the case of LM1 ashes.

The reducing atmosphere did not influence the wettability of bed materials.

Regarding the mechanism of agglomeration no difference was observed in the case of silica sand.

In the case of olivine and calcined olivine, the diffusion of Fe into the ash and the formation of thin Ca rich inner layer were also observed. The main difference compared to oxidizing atmosphere is the presence of FeS crystals in the molten ash, and the formation of two non-miscible liquid phases.

Considering all these observations, the following conclusion can be drawn:

1. the wetting ability of ash on bed material is the key parameter of the agglomeration
2. The adhesion between miscanthus ash and bed materials increase in the following order: sand $\rightarrow$ olivine $\rightarrow$ calcined olivine
3. The harvest time can significantly modify the ash composition, thus the nature of interaction
4. There is no significant difference in the agglomeration mechanism in oxidizing or reducing atmosphere

## IV.8 REFERENCES OF CHAPTER IV

- [IV-1] Bartels M, Lin W, Nijenhuis J, Kapteijn F, van Ommen JR. Agglomeration in fluidized beds at high temperatures: Mechanisms, detection and prevention. *Prog Energy Combust Sci* 2008;34:633–66.
- [IV-2] Visser HJM. The influence of fuel composition on agglomeration behaviour in fluidised-bed combustion. 2004.
- [IV-3] Brus E, Öhman M, Nordin A. Bed Agglomeration during Combustion of Biomass Fuels - Mechanism and Measures for Prevention n.d.;46:9195.
- [IV-4] Ergudenler A, Ghaly AE. Agglomeration of alumina sand in a fluidized bed straw gasifier at elevated temperatures. *Bioresour Technol* 1993;43:259–68.
- [IV-5] Steenari B-M, Lundberg A, Pettersson H, Wilewska-Bien M, Andersson D. Investigation of Ash Sintering during Combustion of Agricultural Residues and the Effect of Additives. *Energy & Fuels* 2009;23:5655–62.
- [IV-6] Khadilkar A, Rozelle PL, Pisupati S V. Models of agglomerate growth in fluidized bed reactors: Critical review, status and applications. *Powder Technol* 2014.
- [IV-7] Skrifvars B-J, Hupa M, Hiltunen M. Sintering of ash during fluidized bed combustion. *Ind Eng Chem Res* 1992;31:1026–30.
- [IV-8] Lin W. Agglomeration in bio-fuel fired fluidized bed combustors. *Chem Eng J* 2003;96:171–85.
- [IV-9] Chirone R, Miccio F, Scala F. Mechanism and prediction of bed agglomeration during fluidized bed combustion of a biomass fuel: Effect of the reactor scale. *Chem Eng J* 2006;123:71–80.
- [IV-10] Khadilkar A, Rozelle PL, Pisupati S V. Models of agglomerate growth in fluidized bed reactors: Critical review, status and applications. *Powder Technol* 2014.
- [IV-11] Öhman M, Nordin A, Skrifvars B-J, Backman R, Hupa M. Bed Agglomeration Characteristics during Fluidized Bed Combustion of Biomass Fuels. *Energy & Fuels* 2000;14:169–78.
- [IV-12] Öhman M, Pommer L, Nordin A. Bed Agglomeration Characteristics and Mechanisms during Gasification and Combustion of Biomass Fuels. *Energy & Fuels* 2005;19:1742–8.
- [IV-13] Brus E, Öhman M, Nordin A. Mechanisms of Bed Agglomeration during Fluidized-Bed Combustion of Biomass Fuels. *Energy & Fuels* 2005;19:825–32.
- [IV-14] Liliedahl T, Sjöström K, Engvall K, Rosén C. Defluidisation of fluidised beds during gasification of biomass. *Biomass and Bioenergy* 2011;35:S63–70.
- [IV-15] Brus E, Öhman M, Nordin A, Skrifvars B, Backman R. Bed Material Consumption in Biomass Fired Fluidised Bed Boilers Due to Risk of Bed Agglomeration - Coating Formation and Possibilities for Regeneration. *IFRF Combust J* 2003.
- [IV-16] De Geyter S, Öhman M, Boström D, Eriksson M, Nordin A. Effects of Non-Quartz Minerals in Natural Bed Sand on Agglomeration Characteristics during Fluidized Bed Combustion of Biomass Fuels. *Energy & Fuels* 2007;21:2663–8.
- [IV-17] Fryda LE, Panopoulos KD, Kakaras E. Agglomeration in fluidised bed gasification of biomass. *Powder Technol* 2008;181:307–20.

- [IV-18] Van der Drift A, Olsen A. Conversion of biomass, prediction and solution methods for ash agglomeration related problems. 1999.
- [IV-19] Davidsson KO, Åmand L-E, Steenari B-M, Elled a.-L, Eskilsson D, Leckner B. Countermeasures against alkali-related problems during combustion of biomass in a circulating fluidized bed boiler. *Chem Eng Sci* 2008;63:5314–29.
- [IV-20] Steenari B-M, Lindqvist O. High temperature reactions of straw ash and the anti-sintering additives kaloin and dolomite. *Biomass and Bioenergy* 1998;14:67–76.
- [IV-21] Campoy M, Gómez-Barea A, Vidal FB, Ollero P. Air–steam gasification of biomass in a fluidised bed: Process optimisation by enriched air. *Fuel Process Technol* 2009;90:677–85.
- [IV-22] Llorente MJF, Arocas PD, Nebot LG, García JEC. The effect of the addition of chemical materials on the sintering of biomass ash. *Fuel* 2008;87:2651–8.
- [IV-23] Corella J, Toledo JM, Padilla R. Olivine or Dolomite as In-Bed Additive in Biomass Gasification with Air in a Fluidized Bed : Which Is Better ? *Energy* 2004;2000:713–20.
- [IV-24] Davidsson KO, Korsgren JG, Pettersson JBC, Jaglid U. The effects of fuel washing techniques on alkali release from biomass. *Fuel* 2002;81:137–42.
- [IV-25] Arvelakis S, Gehrman H, Beckmann M, Koukios EG. Agglomeration problems during fluidized bed gasification of olive-oil residue: evaluation of fractionation and leaching as pre-treatments. *Fuel* 2003;82:1261–70.
- [IV-26] Davidsson KO, Åmand L-E, Elled A-L, Leckner B. Effect of Cofiring Coal and Biofuel with Sewage Sludge on Alkali Problems in a Circulating Fluidized Bed Boiler. *Energy & Fuels* 2007;21:3180–8.
- [IV-27] Michel R, Ammar MR, Poirier J, Simon P. Phase transformation characterization of olivine subjected to high temperature in air. *Ceram Int* 2013;39:5287–94.
- [IV-28] Devi L, Ptasiński KJ, Janssen FJJG, van Paasen SVB, Bergman PCA, Kiel JHA. Catalytic decomposition of biomass tars: use of dolomite and untreated olivine. *Renew Energy* 2005;30:565–87.
- [IV-29] Devi L, Craje M, Thüne P, Ptasiński KJ, Janssen FJJG. Olivine as tar removal catalyst for biomass gasifiers: Catalyst characterization. *Appl Catal A Gen* 2005;294:68–79.
- [IV-30] Michel R, Ammar MR, Veron E, Simon P, Poirier J. Investigating the mechanism of phase transformations and migration in olivine at high temperature. *RSC Adv* 2014;4:26645–52.
- [IV-31] Eustathopoulos N, Nicholas MG, Drevet B. Wettability at high temperature. Kidlington, Oxford OX5 1GB, UK: Elsevier Science Ltd; 1999.
- [IV-32] Balland M. Etude de l'influence des cendres de biomasse sur le phénomène d'agglomération en réacteur à lit fluidisé. thesis INP Lorraine at CEA Grenoble/Liten, supervisors Jacques Poirier and Karine Froment, to be defended in 2016.
- [IV-33] Drelich J, Miller JD. A critical review of wetting and adhesion phenomena in the preparation of polymer-mineral composites. *Miner Metall Process* 1995;12:197–204.
- [IV-34] Israelachvili JN. Intermolecular and Surface Forces. Third Edit. Santa Barbara, CALIFORNIA, USA: Elsevier Inc.; 2011.

---

# CHAPTER V: ASH-BED MATERIAL INTERACTION UNDER DYNAMIC CONDITIONS

---

## ABSTRACT

The aim of this chapter is to study the interaction between the miscanthus ashes and bed materials under dynamic conditions in two different scales: a bench scale high temperature device installed at CEMHTI, CNRS and a laboratory fluidized bed gasifier pilot (7.5 kW) installed at LRGP, CNRS, Nancy.

The bench scale device allows observing the agglomeration tendencies with miscanthus ashes and bed materials in oxidizing atmosphere. A systematic experimentation was performed to determine the agglomeration ratio, namely the mass ratio of the agglomerated bed and original bed. Different parameters were investigated: (1) the type of bed material (silica sand, olivine, calcined olivine), (2) the operating temperature (750 to 900 °C), (3) the ash/bed material ratio (0.25 to 4 wt %), (4) the operating time (10 to 300 minutes) and (5) the air flow rate (4 to 15 NL/min). In the case of olivine, the effect of additives (kaolin, dolomite) and the pre-treatment of biomass were also tested.

The bench scale interaction test results were compared to the trials of the laboratory fluidized bed gasification at LRGP, Nancy. In this case, the gasification experiments were carried out using miscanthus pellets and natural olivine. The experiments were performed in reducing atmosphere using diluted air. Samples were taken during the trials and the bed was completely recovered afterwards. After the experiments, the segregation of the bed was observed. While the upper part of the bed became rich in unburnt char, big agglomerates were found close to the grid. The SEM-EDX analysis of the agglomerates revealed that the molten ash got enriched in Fe and Cr, which indicates possible abrasion of the reactor wall.

## V.1 INTRODUCTION

As discussed previously, the agglomeration of fluidized bed depends on the balance of interfacial adhesive forces between sticky particles and the kinetic energy of particles impact. Good wetting of particles is the essential element of interfacial bindings. The adhesion can be further increased by capillary forces, diffusion of phase compounds, electrostatic or chemical interactions and surface topography [V-1]. The magnitude of the kinetic energy of a bed particle with a given mass mainly depends on the velocity of the fluidizing gas.

The Ph.D work of M. Balland [V-2] revealed that the work of adhesion and capillary forces between ash covered bed particles are sufficiently great to cause agglomeration. In Chapter IV, we carried out an extensive physicochemical investigation of agglomeration studying the wettability, diffusion and chemical interaction of compounds at the ash/bed particle interface.

It was shown that the adhesion in contact with different bed particles increases in the following order: silica sand, olivine and calcined olivine due to the difference in interfacial binding forces. While only physical adhesion was observed in the case of silica sand, the SEM-EDX analysis revealed the diffusion of Fe in the case of olivine and chemical interaction in the case of calcined olivine.

Chapter IV studied the ash/bed particle interaction under static conditions, namely without any macroscopic movement of matter. The miscanthus ash and bed particles were brought in contact in the form of gently pressed pastilles and annealed in a laboratory furnace.

The aim of chapter V is to study the interactions under dynamic conditions, namely assuring the continuous movement and mixing of the bed and ash particles by gas flow. This chapter begins with a short overview of fluidization theory focusing on the determination of minimum fluidization velocity.

The experimental section is divided into two parts:

The first part discusses the results of agglomeration tests, which were performed in a high temperature quartz device developed at CEMHTI-CNRS. The purpose of this device is to study the interaction between the ashes and bed particles and to visualize the agglomeration phenomenon at elevated temperature in real time. The agglomeration tests were performed between miscanthus ashes ( $T_{\text{ashing}}=400\text{ }^{\circ}\text{C}$ ) and bed materials using air as fluidizing agent. There are three main reasons to use ash instead of biomass pellets. Firstly security reasons, as the experiments were carried out inside the laboratory with limited possibility of collecting the developing gases. Secondly the continuous fuel feed is not feasible and the materials have to be added at the beginning of the experiments. As the ash content of the biomass is relatively low in regard of the size of the quartz reactor, it would be not possible to add sufficient amount of biomass

pellets. Thirdly the developing char and tar would damage the wall of the quartz reactor and the visualization of the agglomeration would not be possible any more.

During the experiments different parameters were tested: the choice of bed material, operating time, temperature and fluidization velocity. Besides, the effect of additives (dolomite, kaolin) and biomass pre-washing was also tested. The impact of these parameters was quantified via sieving the bed and determining the agglomeration ratio (A% (wt %)), the ratio of the weight of agglomerates and the initial bed. Only few experiments were carried out with silica sand and calcined olivine, the focus of this study was more on the olivine, which is the target bed material of the GAMECO project.

The second part of this chapter discusses the results of the laboratory fluidized bed pilot (7.5kW) installed at *LRGP, Nancy (Laboratoire Réactions et Génie des Procédés)*. This device was designed and constructed in the frame of the GAMECO research project for the purpose of studying tar kinetics, product yield and agglomeration during miscanthus gasification. These agglomeration tests permit the validation of the static and dynamic bed material/miscanthus ash interaction tests performed at CEMHTI.

The fluidized bed was set up during the year of 2013 and the first experiments were conducted at the beginning of 2014. These first trials served for security evaluation and functional testing such as the elimination of occurring dysfunctions (gas leakage) and the experimentations with process parameters (bed size, gas velocity, temperature).

In this chapter, the agglomerates of two of the first trials are characterised. The agglomerates were sieved and analysed by SEM-EDX. This characterisation will serve to provide suggestions to improved process parameters in regard of agglomeration.

The chapter is enclosed with an overall conclusion on dynamic interaction tests and with guidelines for future work with the laboratory and industrial fluidized beds.

## V.2 A SHORT OVERVIEW OF FLUIDIZATION THEORY

In fluidization, the solid particles are transformed into a fluid-like state through contact with a gas or a liquid [V-3]. The different steps of fluidization are shown in Figure V-1. In a fluidized bed reactor the bed particles are placed on a perforated plate and brought into movement by a gasifying agent entering at the bottom of the bed. At slow gas velocity the bed stays stationary (fixed bed reactors). With increasing gas velocity the bed expands and at one point, at the minimum fluidization velocity and it gets suspended by the gas flow. Further increase of the gas velocity will change the fluidization regimes from bubbling to turbulent then to fast fluidization [V-3]. At very high gas velocities the bed particles are entrained from the reactor [V-3, V-4].

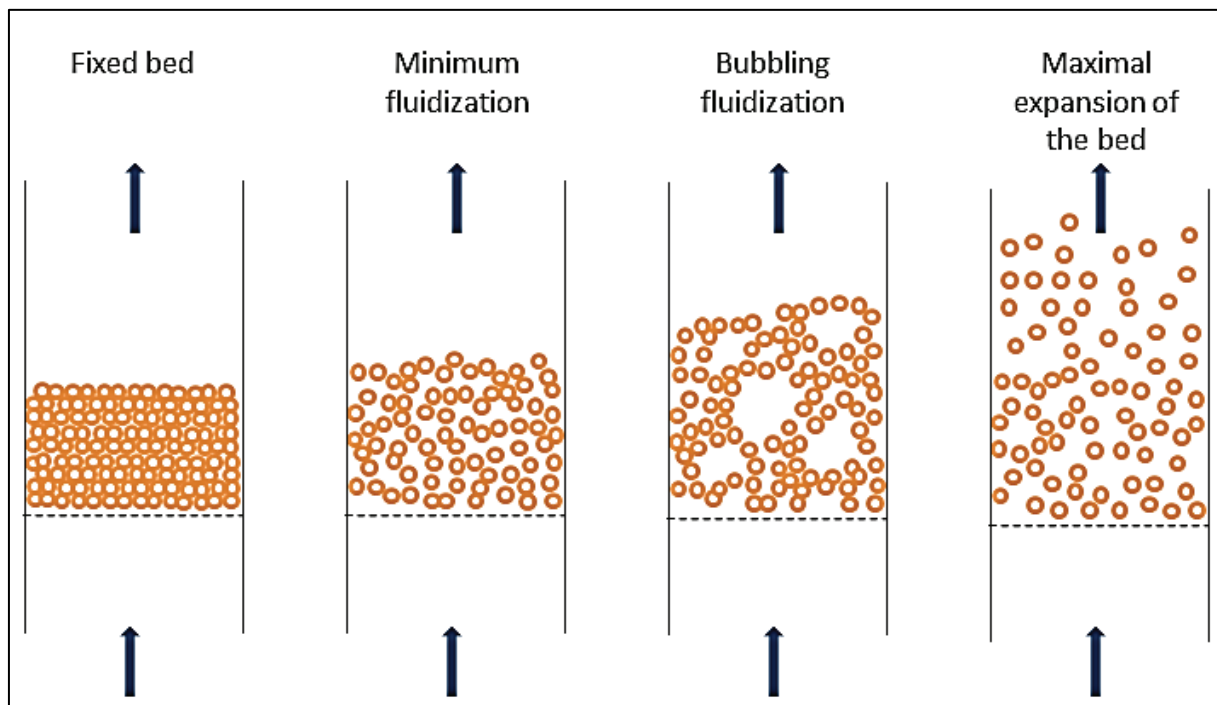


*Figure V-1: Illustration of fluidization regimes: fixed bed, minimum fluidization, bubbling fluidization and maximal expansion of the bed*

The fluidization can be presented by plotting the gas velocity versus the pressure drop over the bed as illustrated in Figure V-2.

With increasing velocity, the pressure drop increases till the point of reaching the fluidized state. In a fluidized bed, the pressure drop is constant. Elevated gas velocity leads to the entrainment of the bed and a sharp decrease in the pressure drop.

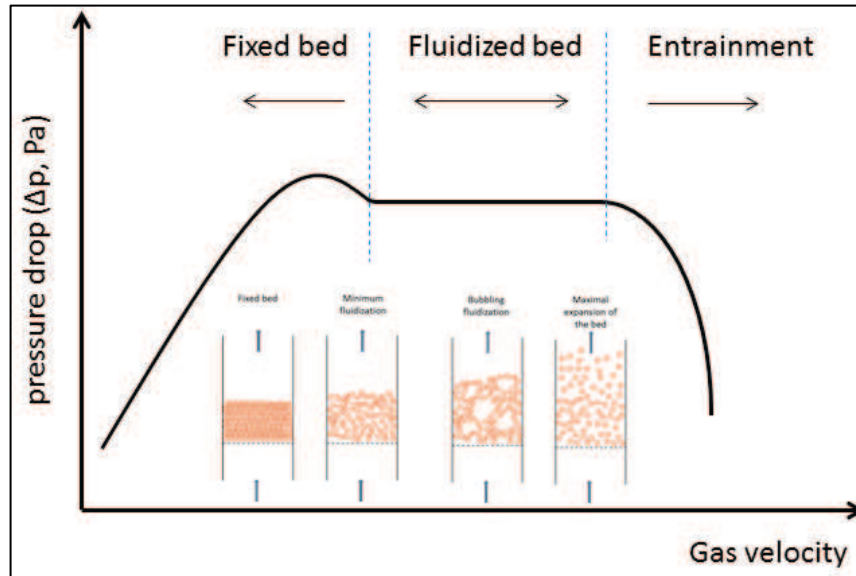


Figure V-2: The pressure drop of the bed versus gas velocity

### MINIMUM FLUIDIZATION VELOCITY

Regarding the hydrodynamics of a fluidized bed, the ratio of the fluidizing gas velocity and the minimum fluidization velocity ( $U/U_{mf}$ ) is an indispensable parameter. In order to provide good mixing of the biomass pellets and bed material, the  $U/U_{mf}$  has to be sufficiently high, but too elevated gas velocities can lead to the entrainment of the bed particles and insufficient carbon conversion, resulting in weak conversion efficiency [V-3].

Ergun et al. [V-4] established the following semi-empiric formula to determine the minimum fluidization velocity:

$$(1 - \varepsilon_{mf}) \cdot (\rho_s - \rho_g) \cdot g = 150 \cdot \frac{(1 - \varepsilon_{mf})^2}{\varepsilon_{mf}^3} \cdot \frac{\mu_g \cdot U_{mf}}{(\Phi_s \cdot d_p)^2} + 1.75 \cdot \frac{(1 - \varepsilon_{mf})}{\varepsilon_{mf}^3} \cdot \frac{\rho_g \cdot U_{mf}^2}{(\Phi_s \cdot d_p)} \quad (V.1)$$

$\varepsilon_{mf}$ (-)	porosity or void fraction <sup>1</sup> at the minimum fluidization
$\rho_s$ (kg/m <sup>3</sup> )	volumetric mass density of solid
$\rho_g$ (kg/m <sup>3</sup> )	volumetric mass density of gas
$g$ (m/s <sup>2</sup> )	acceleration unit from earth gravitation
$\mu_g$ (Pa·s)	dynamic viscosity of the gas
$U_{mf}$ (m/s)	minimum fluidization velocity (superficial <sup>2</sup> )
$\Phi_s$	sphericity factor <sup>3</sup>
$d_p$ (m)	particle parameter

<sup>1</sup> The void (empty) space between the particles of the bed: the ratio of the void volume and the total volume of the bed

<sup>2</sup> Superficial velocity: hypothetical velocity, considers that the gasifying medium is the only phase present, ignores other particles and porous materials [V-3]

<sup>3</sup> "The ratio of the surface area of a sphere -with the same volume as the particle- to the surface area of the particle" [V-11]

Using the Archimedes number ( $Ar$ ) and the Reynolds number at the point of minimum fluidization ( $Re_{mf}$ ), the minimum fluidization velocity can be expressed as:

$$Ar = \frac{\rho_g \cdot (\rho_s - \rho_g) \cdot d_p^3 \cdot g}{\mu_g^2} \quad (V.2)$$

$$Re_{mf} = \frac{\rho_g \cdot U_{mf} \cdot d_p}{\mu_g} \quad (V.3)$$

The correlation between  $Re_{mf}$  and  $Ar$  is:

$$\frac{1.75}{\varepsilon_{mf}^3 \cdot \Phi_s} \cdot Re_{mf}^2 + 150 \cdot \frac{(1 - \varepsilon_{mf})^2}{\varepsilon_{mf}^3 \cdot \Phi_s^2} \cdot Re_{mf} = Ar \quad (V.4)$$

Between the 1950s and 1980s several correlations were established to calculate the minimum fluidization from the Reynolds number [V-5]. Based on the agreement with the other partners in the GAMECO research project, the correlation of Wen et Yu[V-4] was used in our calculation:

$$Re_{mf} = \sqrt{(33.7^2 + 0.0408 Ar)} - 33.7 \quad (V.5)$$

This correlation is valid for  $0.001 < Re < 4000$  for a void fraction of  $\varepsilon = 0.38 - 0.45$  [V-4].

## V.3 DYNAMIC INTERACTION TESTS IN LABORATORY FLUIDIZED BED

### V.3.1 BED MATERIALS AND FUEL

For the laboratory tests, miscanthus ash was obtained by ashing the dried miscanthus (LM1 –April 2011) at 400 °C in an open muffle furnace (Parmilleux, type: FP 1200) for 6 h in air.

Three different bed materials with a particle size fraction between 400 and 500 µm were used: silica sand (Sibelco, Norway), natural olivine (Sibelco, Norway) and calcined olivine (Sibelco, Norway, olivine was calcined at 1400 °C for 4 hours in air at CEMHTI-CNRS).

### V.3.2 DESCRIPTION OF LABORATORY HIGH TEMPERATURE DEVICE

A bench scale high temperature device was designed at CEMHTI-CNRS to study and visualise the agglomeration between ashes and bed materials (Figure V-3). It consists of an secondary aluminium stand (Figure V-3/1), a tubular furnace (Figure V-3/2) and a quartz reactor (Figure V-3/3). The furnace is moveable both vertically and horizontally. Once the reactor is heated up, the furnace can be momentanesously opened, allowing the in-situ observation of the fluidization (Figure V-4). During the systematic experimentation campaign, the tubular furnace is closed around the quartz reactor to avoid the temperature fluctuation.

The quartz device is composed of two parts, being 60 cm and 40 cm long and 50 mm in inner diameter. The two parts are separated with a porous quartz grid (Figure V-3/5, pore DIA 50µm). The two parts of the quartz reactor are attached by ceramic pliers and ceramic screws (Figure V-3/4) and the joints are reinforced with high temperature grease (Marly Ceramic Paste) to avoid any leakage.

The air is injected at the bottom of the reactor and the gas flow is controlled with a rotameter (Platon, 2 - 25 NL/min).

The temperature of the bed is controlled with a thermometer (Carbolite VST 12/300). Porous alumina ceramics with high heat capacity are placed inside the bottom part of the reactor to preheat the air before reaching the bed material. The pressure drop during fluidization can be measured with a liquid column manometer.

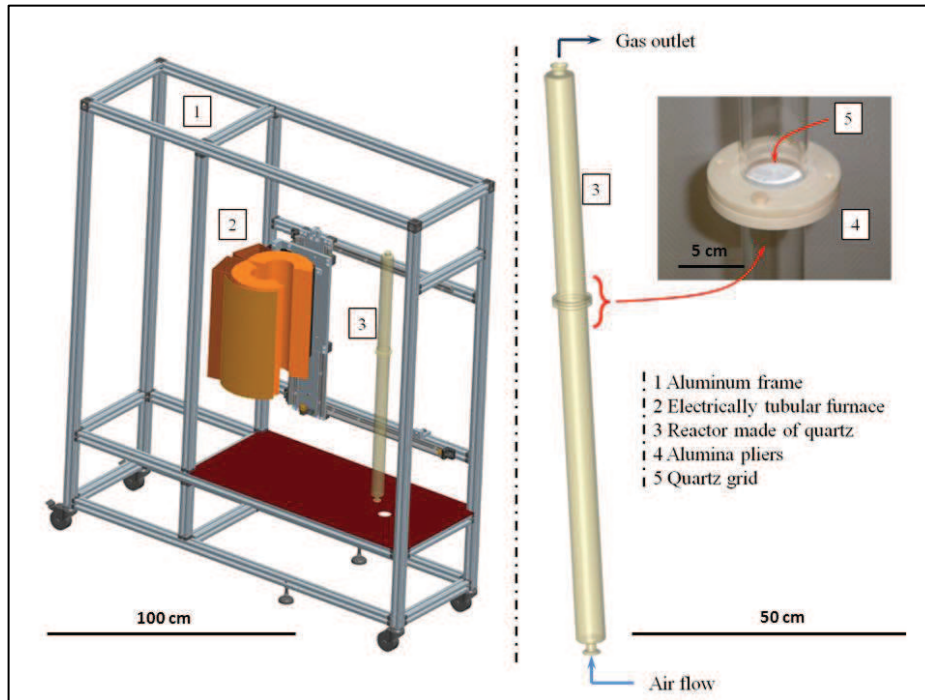


Figure V-3: Design of the laboratory quartz fluidized bed device

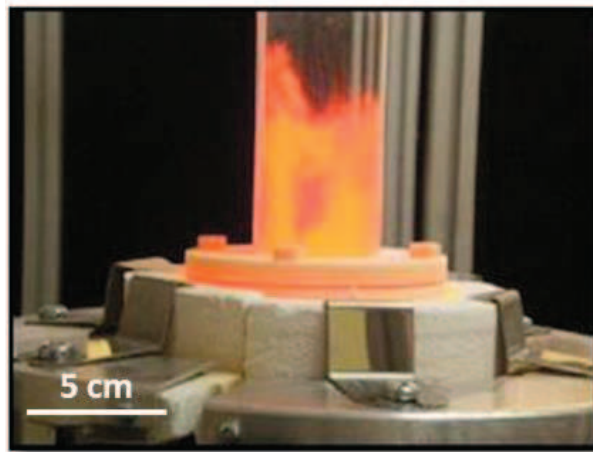


Figure V-4: Observing bed fluidization and agglomeration in real time

### V.3.3 DETERMINING THE MINIMUM FLUIDIZATION VELOCITY ( $U_{MF}$ )

The minimum fluidization rate of the bed was determined both experimentally and via calculation using the correlation of Wen and Yu [V-4].

To measure the pressure drop of the bed, two iron pipes ( $d=0.5$  mm,  $l=80$  cm) were connected to the liquid column and inserted into the reactor from the top and from the bottom, 5 cm far from the grid each side (Figure V-5). (As the reactor is made of quartz, the conventional pressure valves could not be built in the wall.)

The pressure drop can be determined from the hydrostatic pressure equation:

$$\Delta p = p_1 - p_2 = (h_1 - h_2) \cdot \rho \cdot g \quad (\text{V.6})$$

$\Delta p$	pressure drop
$p_1$	pressure under the grid [V-N/m <sup>2</sup> , Pa]
$p_2$	pressure above the bed [V-N/m <sup>2</sup> , Pa]
$h_1, h_2$	the height or depth of the column [V-m]
$g$	gravitational constant [V-m/s <sup>2</sup> ]
$\rho$	volumetric mass density of the liquid [V-kg/m <sup>3</sup> ]

First, the pressure drop of the grid was determined without adding bed material in the reactor (Figure V-5/A). The reactor was heated to elevated temperatures (750, 800, 900 °C), and the gas flow was gradually increased while noting the difference in the height of the liquid column ( $h_1$  and  $h_2$ ). Secondly, the pressure drop was determined by introducing 80 g of bed into the reactor (Figure V-5/B). The difference of the two measurements gives the pressure drop of the bed.

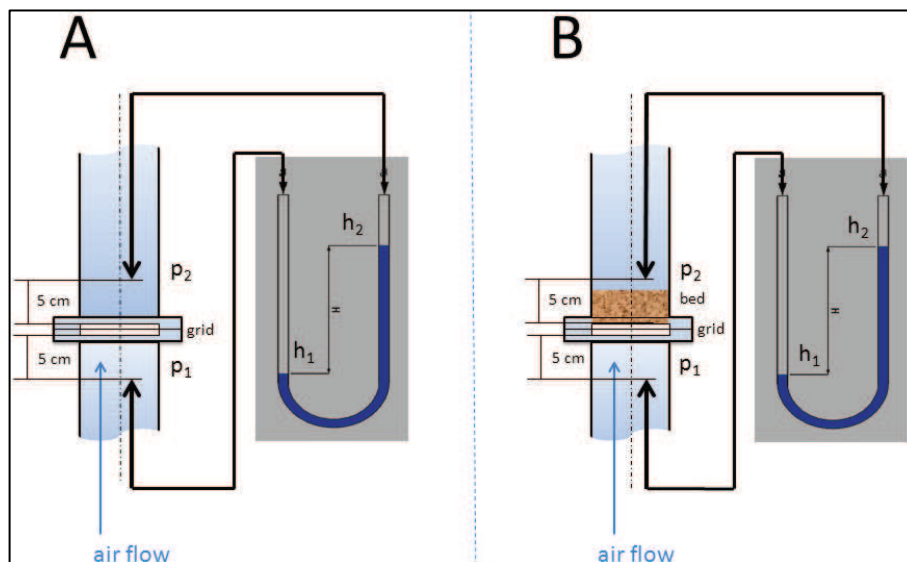


Figure V-5: Measuring the pressure drop with manometer; A, pressure drop on the grid without the bed, B, pressure drop of the bed

Table V-1 lists the values of  $U_{mf}$  (m/s) and  $U/U_{mf}$  (with 10NL/min airflow) calculated with the Wen and Yu correlation (V.4) and compared to the experiments at different temperatures. The details of the measurements can be found in Annexe A14. The difference between the calculated and measured minimum fluidization velocity is significant. The semi-empiric formula was evaluated for pilot and industrial fluidized beds, whereas the design of the laboratory high temperature device is different. Moreover, more precise methods are necessary to measure the pressure drop in the bench-scale device.

Table V-1: The minimum fluidization velocity and  $U/U_{mf}$  at 750, 800 and 900 °C at 10 NL/min gas flow –comparison of the Wen et Yu correlation with experimental results

	semi-empiric Wen et Yu[V-4]	experimental
$U_{mf\ 900\ ^\circ C}$ (m/s)	0.087	0.16
$U_{mf\ 800\ ^\circ C}$ (m/s)	0.091	0.19
$U_{mf\ 750\ ^\circ C}$ (m/s)	0.094	0.18
$U / U_{mf\ 900\ ^\circ C}^*$	4.8	2.6
$U / U_{mf\ 800\ ^\circ C}^*$	4.2	2.0
$U / U_{mf\ 750\ ^\circ C}^*$	3.9	2.1
*At 10 NL/min gas flow (0.42 m/s at 900 °C, d=4.5cm)		

### V.3.4 FLUIDIZATION TESTS IN THE LABORATORY HIGH TEMPERATURE DEVICE

The flow chart of the experimentation setup is shown in Figure V-6.

For each experiment, 80 g of fresh bed material ( $d_p=400-500\mu m$ ) was used. The bed was separated into two halves: one was carefully mixed with the miscanthus ash (0.2 to 3 grams), the other one was placed aside.

The quartz device was heated up to the operating temperature before introducing the bed material and LM1 ash. In order to avoid any material loss, the bed and the miscanthus ash were carefully poured into the quartz device through the gas outlet using a stainless steel pipe (being 70 cm long, 1 cm in diameter). The bed material and ash were loaded in three layers: (1) bed material, (2) mixture of bed material and ash, (3) bed material (Figure V-6/B). This method served to avoid the entrainment of fine ash particles upon opening the air flow. The bed was held unmoved for 8 minutes before opening the gas flow in order to reach the desired temperature and avoid the fly-out of the ash particles.

At the end of the tests the gas flow was maintained till the temperature decreased to 700 °C to avoid agglomeration during the cool-down. After complete cool down, the tubular furnace was opened and the reactor was disassembled with care. We observed approximately 1 g of mass loss due to the fly-out of small particles, the volatilisation of ash compounds and possibly some loss during recovering the bed material.

The bed material was weighed and sieved after each test. The agglomeration ratio (A %) was determined as the ratio of the mass of agglomerates greater than 630  $\mu m$  and the original bed. The 630  $\mu m$  is a standard mesh size which was found to be adequate to determine the agglomeration ratio for the bed (particles between 400-500  $\mu m$ ).

$$A\% = \frac{mass_{>630\mu m}}{mass_{bed}} \quad (V.7)$$

The agglomerates were embedded in resin, polished and analysed by SEM-EDX.

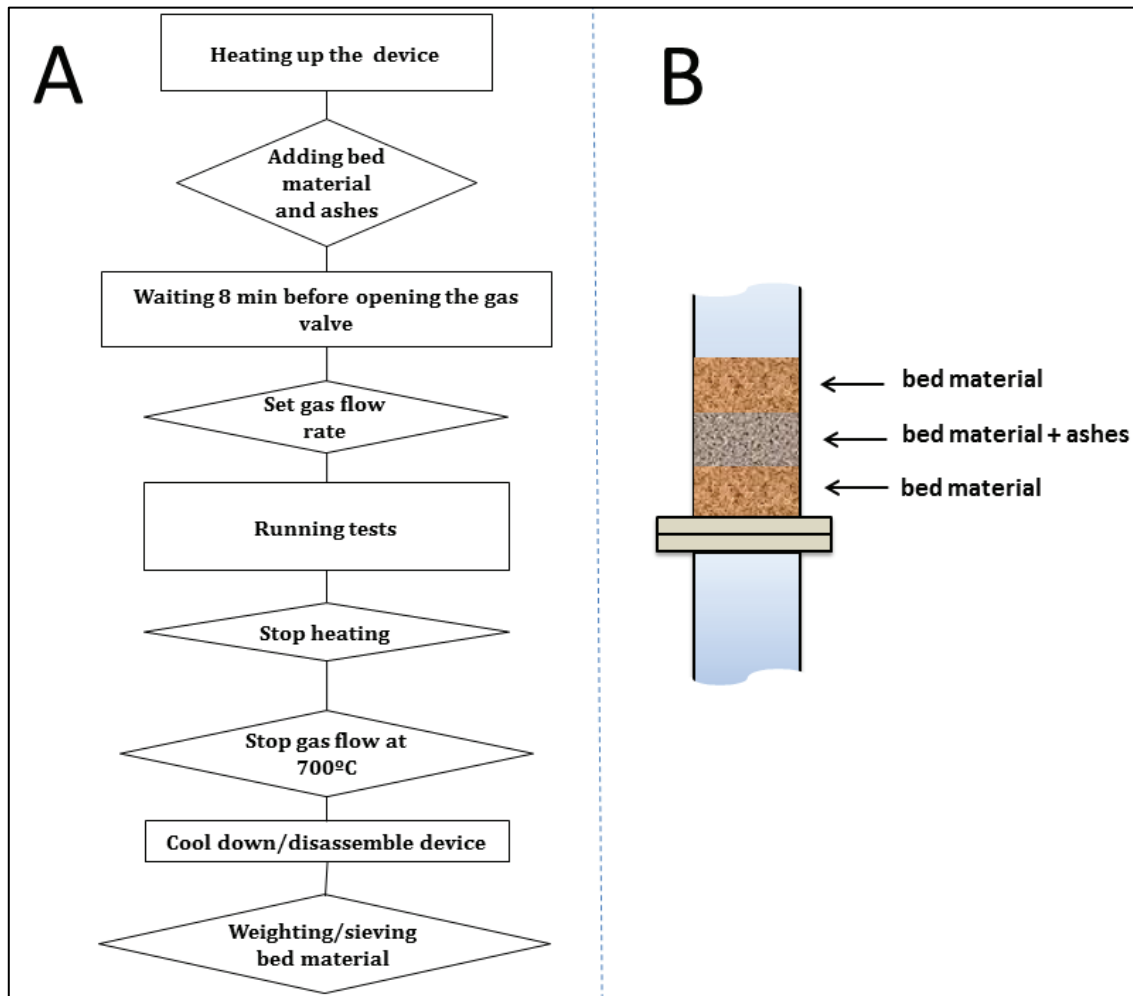


Figure V-6: (A) scheme of the processus of the fluidized bed experiments with the bench scale hot device, (B) bed material placement inside the reactor in three layers: bed, bed+ash, bed

### PARAMETERS

The aim of the experiments was to test the impact of bed material, temperature, fluidization velocity, quantity of ash and additives on the agglomeration ratio. The experiments were carried out for 10 to 300 minutes at different temperatures and gas flow rates. For most of the tests, a moderate gas flow rate, 10 NL/min was chosen. In the case of olivine, a moderate and an elevated gas flow, 4 and 15NL/min were also investigated. Table V-2 summarizes the different process parameters tested during the experimentation.

Table V-2: Experimental set-up

Temperature	750, 800, 900 °C
Air flow rate	4, 10, 15NL/min
Bed material	<ul style="list-style-type: none"> <li>• Silica sand (<math>d_p = 400-500 \mu\text{m}</math>)</li> <li>• Olivine (<math>d_p = 400-500 \mu\text{m}</math>)</li> <li>• Calcined olivine (<math>d_p = 400-500 \mu\text{m}</math>)</li> <li>• Olivine + additives as flour fine powders: <ul style="list-style-type: none"> <li>➤ Dolomite (1.2 wt % and 3 wt %)</li> <li>➤ Kaolin (0.25 wt %)</li> </ul> </li> </ul>
Fuel	<ul style="list-style-type: none"> <li>• LM1 ash (<math>T_{\text{ashing}} = 400 \text{ °C}</math>) 0.2 to 3grams</li> <li>• LM1 washed (<math>T_{\text{ashing}} = 400 \text{ °C}</math>) 1grams</li> </ul>
Duration	10 to 300 min

### V.3.5 EFFECT OF BED MATERIAL ON THE AGGLOMERATION RATIO

Figure V-7 shows the agglomeration ratio (A% (wt %)) versus time with the different bed materials. The experiments were performed at 900 °C with an air flow rate of 10 NL/min using 80 g of bed material and 1 g of ash, corresponding to 0.0125 ash/bed ratio.

As expected from the static interaction tests, the A% increases in the following order: silica sand, olivine and calcined olivine. In each case, a dome in the curves was observed: the A% increases at short contact time, reaches a peak, then declines and becomes steady. In the case of calcined olivine the experiment time is too short to show the stabilization of the A% values. The presence of the dome can be explained by two oppositely acting effects: the formation of interfacial bindings and the abrasion of the agglomerates in the fluidized bed, as discussed below.

Firstly, the increase is due to the time necessary for the formation of sticky particles, namely the melting of the ashes, and the wetting of the bed particles. As it was shown in Chapter IV, the interfacial forces are different among the bed materials. In the case of silica sand only physical adhesion takes place, resulting in a weak increase of the slope and a low agglomeration ratio, around 1%. In the case of natural olivine, a sharp increase was observed, which is due to the diffusion of Fe into the molten ash. The curve of calcined olivine rises more moderately but results in more elevated agglomeration ratios (5 to 8 wt %) than olivine or silica sand. This is due to the reinforced interfacial forces via surface roughness and possible chemical interactions between the iron oxides on the surface of calcined olivine grains and the molten ash.

Secondly, the decrease of the A% after a certain time is associated to the abrasion of agglomerates in the fluidized bed. In the case of silica sand, the agglomeration ratio is too low to show the differences. With natural olivine the decrease is sharp but the A% remains greater than in the case of silica sand, indicating that the diffusion of Fe has a marked contribution to the interfacial forces. With calcined olivine, the decline is much

slower and it does not even finish at the end of the longest experiment time (300 min), indicating that the surface roughness and chemical interaction contribute significantly to the particle adhesion and the kinetic energy of collision is hardly sufficient to break these joints.

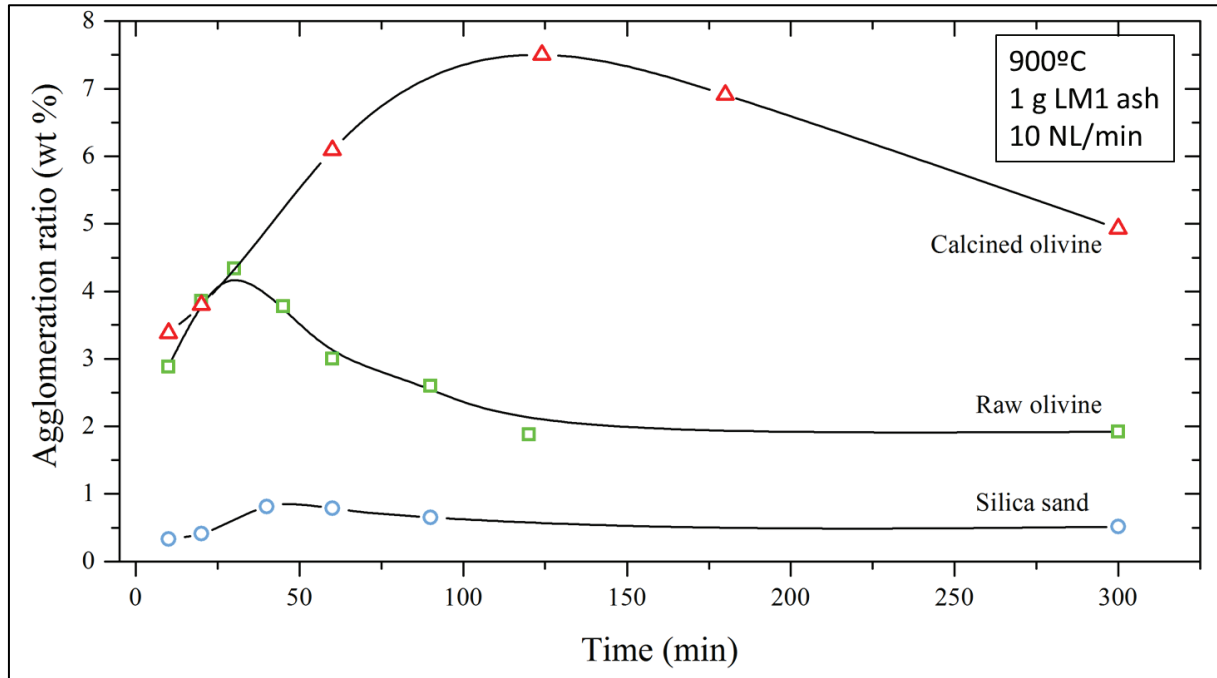


Figure V-7: Agglomeration ratio as a function of time using silica sand, natural olivine and calcined olivine as bed material

### V.3.6 EFFECT OF PROCESS PARAMETERS ON THE AGGLOMERATION RATIO

In this section, the effects of different process parameters (ash quantity, air flow and temperature) on the agglomeration are evaluated.

Figure V-7 plots the agglomeration ratio versus the ash/bed ratio. The upper X-axis displays the calculated miscanthus/bed ratio considering 2.1wt % ash content (see Chapter II.3.1, Table II-3). The quantity of ash was varied between 0.2 and 3 g, the quantity of bed material was always 80 g. All the experiments were performed at 900 °C for 90 min with an air flow rate of 10 NL/min.

Two regions can be differentiated: (1) the fluidisation zone, when the bed remains in fluidized state and (2) the defluidization zone, when the agglomeration inhibits the movement of the bed. The determination of these zones is based on visual observation of the bed movement during the experiments<sup>4</sup>. While the agglomeration ratio increases

<sup>4</sup> The movement of the bed was observed from the top, without opening the tubular furnace. The movement of the bed was checked with a metal rod. In the range of the fluidization zone the quartz

slowly in the fluidization zone due to the counteracting effect of the bed movement, it rises steeper in the defluidization zone as the bed movement weakens. As indicated in Figure V-8, the limit of agglomeration ratio between the fluidization and the defluidization zone is  $A=2-4$  wt %. At this level, the gas flow is not sufficient to maintain the bed movement and the agglomerates stay on the grid. This results in so called “hot-spots” and accelerate the agglomerate growing rate. This can be the reason of the steeper increase of agglomeration ratio in the defluidization zone.

In regard of the ‘riskiness’ of bed material, the same tendency was observed as discussed in Figure V-7, namely the agglomeration ratio reaches the limit of defluidization with 0.01 ash/bed ratio in the case of calcined olivine, while almost twice and three times more ash is necessary for the defluidization of natural olivine and silica sand bed, respectively.

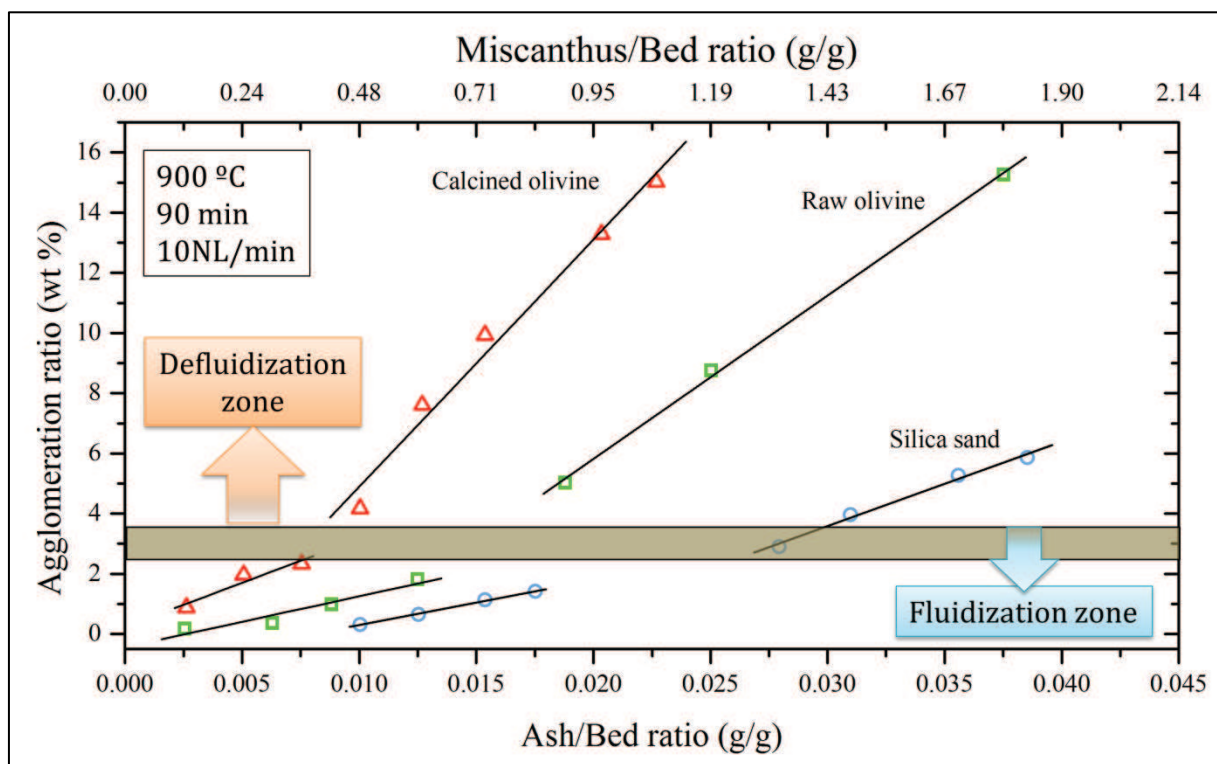


Figure V-7 : Agglomeration ratio versus quantity of ash with silica sand, olivine and calcined olivine as bed material

grid could be easily reached with the metal rod. In the defluidization zone we felt the toughness of the unmoving bed while trying to reach the grid.

Figure V-8 and Figure V-9 present the agglomeration ratio versus ash/bed ratio with different air flow rates (4, 10, 15 NL/min) and different temperatures (750, 800 and 900 °C), respectively. Similarly to the previous tests, the experiments were performed for 90 minutes with 80 g of natural olivine varying the quantity of ash between 0.2 g and 3 g. In the case of different air flow rates the temperature was fixed at 900 °C, and in the case of different temperatures, the air flow rate was 10 NL/min. As anticipated, the agglomeration ratio is inversely proportional to the air flow rate, however the difference is not significant, only  $\pm 1\%$  compared to 10 NL/min in both cases.

Contrary to the air flow rate, more dramatic changes occurred in the case of moderated process temperatures. This variation is due to the amount of molten ash at the different temperatures. As presented previously in Chapter III.3.3 (Figure III-2), according to the thermodynamic calculations the melting of miscanthus ash starts at 755 °C and the estimated quantity of molten ash is  $\sim 5$  wt % at 800 °C and  $\sim 30$  wt % at 900 °C.

Therefore, at 750 °C the ash/bed ratio does not influence the agglomeration ratio, as at this temperature the quantity of molten ash is very low.

At 800 and 900 °C the difference between the A% values is not constant; it increases with increasing ash quantity, in accordance with increasing difference in the amount of molten ash.

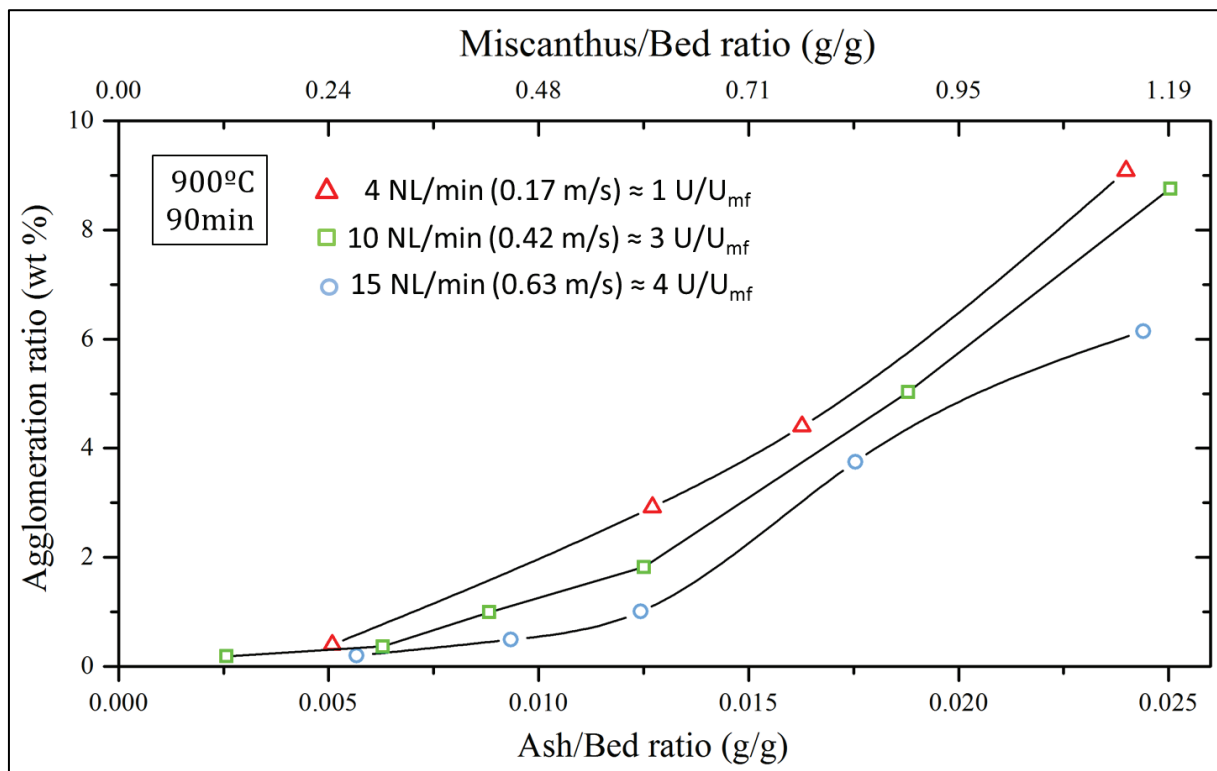


Figure V-8: Agglomeration ratio vs ash/bed ratio in the case of different air flow rates at 900 °C

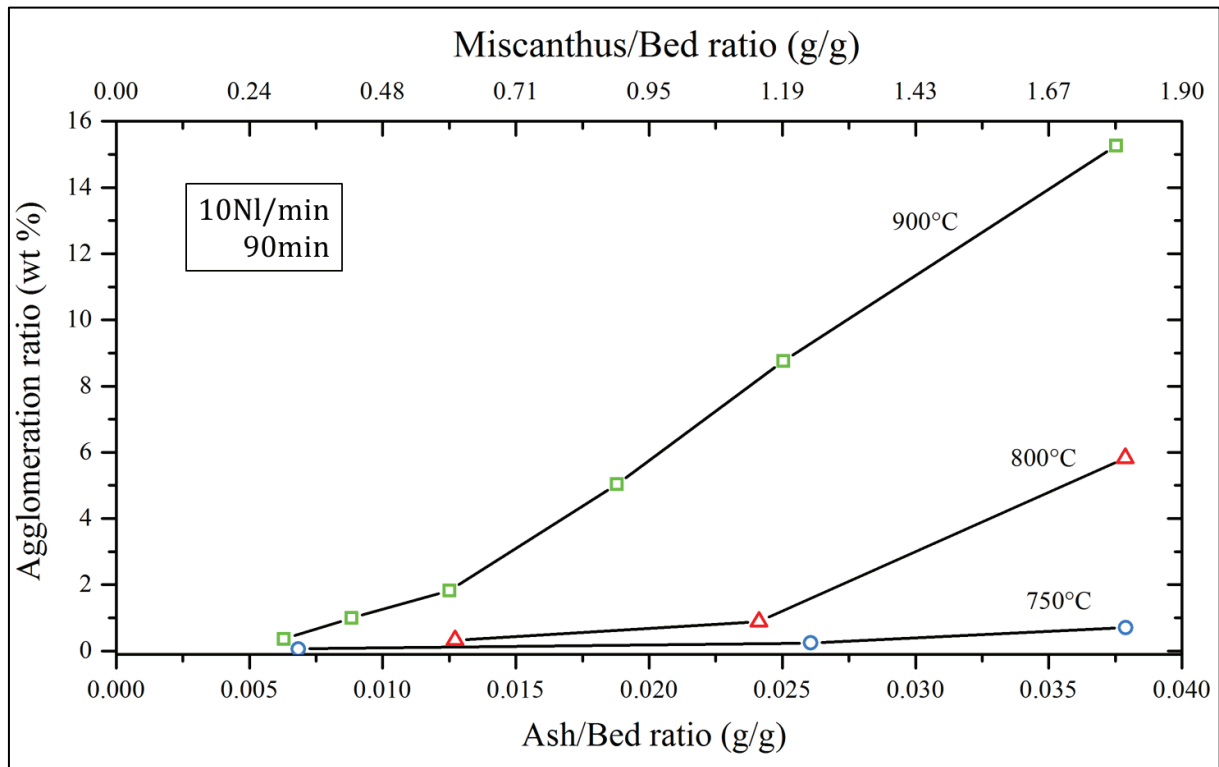


Figure V-9: Agglomeration ratio versus ash/bed ratio at 750 °C, 800 °C and 900 °C

### V.3.7 EFFECT OF ADDITIVES ON THE AGGLOMERATION RATIO

Two different methods were tested to decrease the risks of agglomeration: (1) using additives (dolomite ( $\text{CaMg}(\text{CO}_3)_2$ ) or kaolin ( $\text{AlSiO}_4(\text{OH})_5$ ) and (2) pre-washing the biomass prior to ashing.

The XRD analysis shown that the main phase of dolomite at room temperature is  $\text{CaMg}(\text{CO}_3)_2$  which transforms into  $\text{CaO}(\text{s})$ ,  $\text{MgO}(\text{s})$  and  $\text{CO}_2(\text{g})$  at 900 °C.

In kaolin, the dominating phases are dickite ( $\text{Al}_2\text{Si}_2\text{O}_5(\text{OH})_4$ ), kaolinite ( $\text{Al}_2\text{Si}_2\text{O}_5(\text{OH})_4$ ) and muscovite ( $\text{KAl}_2(\text{Si}, \text{Al})_4\text{O}_{10}(\text{OH})_2$ ) forming metakaolin at high temperature. Both dolomite and kaolin contain a small amount of  $\text{SiO}_2$ . As described earlier in Chapter IV.2.3, kaolin decreases the amount of liquid phase via the formation of K-Al-silicates. These silicates have a higher melting point than the operating temperature.

The use of dolomite as additive or bed material has been studied by many researchers [V-6–10], but only Steenari et al. [V-10] examined the mechanism of the antiagglomeration effect of dolomite. They revealed the formation of different Ca and Mg-silicates ( $\text{CaMg}(\text{SiO}_3)_2$ ,  $\text{MgSiO}_3$  and  $\text{Ca}_2\text{MgSi}_2\text{O}_7$ ) but did not evidence the capture of K and the formation of K-silicates.

In the laboratory tests at CEMHTI, LM1 ash was mixed with dolomite (50-50 wt %) and heat-treated for 6 hours at 900 °C. The X-ray diffractograms of the mixture (presented in Annexe A15) evidenced the evolution of Ca-Mg-silicates and some peaks can be

attributed to K-Mg-silicates ( $K_2MgSiO_4$  or  $K_2MgSi_3O_8$ ). As the diffractogram is “overcharged” in the typical range of silicates, it is difficult to determine the presence of K-Mg-silicates.

The additives had a consistency of fine flour and they were carefully mixed with the olivine particles before loading the bed material into the device in the dynamic tests. The ratios of dolomite to bed material were 1.2 wt % and 3 wt % and in the case of kaolin 0.25 wt %.

To study the effect of biomass pre-washing, dried miscanthus (chopped and blended into small pieces (0.5-1 cm)) was leached in tap water (10 g water for 1 g miscanthus) for 24 hours in a three dimension (rotation, translation and inversion) mixer (TURBULA T2F). Afterwards, the sample was filtered and rinsed with tap water, dried and calcined at 400 °C in an open muffle furnace (Parmilleux, type: FP 1200).

Table V-3 shows the chemical composition of miscanthus ashes before and after the washing. The results are normalised to 100 wt % without taking into account the remaining H, C, N which cannot be quantified via SEM-EDX analysis. As the ash compositions are normalised, with the decrease of the water soluble compounds the value of Si and Ca increase. To quantify the effect of the washing, the concentrations of the elements are referred to the Si concentration as Si is considered to stay completely in the solid residues. According to the analysis, the potassium and phosphorus can be washed out almost completely, while only 30-60% of the Mg, Ca and S are water soluble. The residue is most likely attached to the organic structure of the plant. The chlorine is present in a very small amount in LM1 ash (~0.5-1%), therefore it is not presented in Table V-3 but it is considered to be completely washed out by water.

*Table V-3 : Chemical composition of ashes deriving from non-treated and washed miscanthus (ashing at 400 °C)*

wt %	LM1	washed LM1	Removed
P	1.3	0.0	-100%
K	15.1	2.8	-87%
Mg	3.0	1.8	-59%
S	1.3	1.0	-44%
Ca	16.9	17.0	-30%
O	40.4	45.8	
Si	21.9	31.2	
* (trace elements <1% Cl, Fe, Al not listed)			

The effect of different treatments was compared under dynamic conditions using natural olivine as bed material. The experiments were performed at 900 °C for 90 minutes with an air flow of 10 NL/min with increasing ash/bed material ratio. The agglomeration ratio versus ash/bed ratio is plotted in Figure V-10. As it can be seen, few percent of dolomite can reduce the agglomeration ratio by 30 to 75%. A very small amount of kaolin is sufficient to completely eliminate the agglomeration. Prewashing

the biomass is also a potential method, as it keeps the agglomeration ratio around 1 wt %.

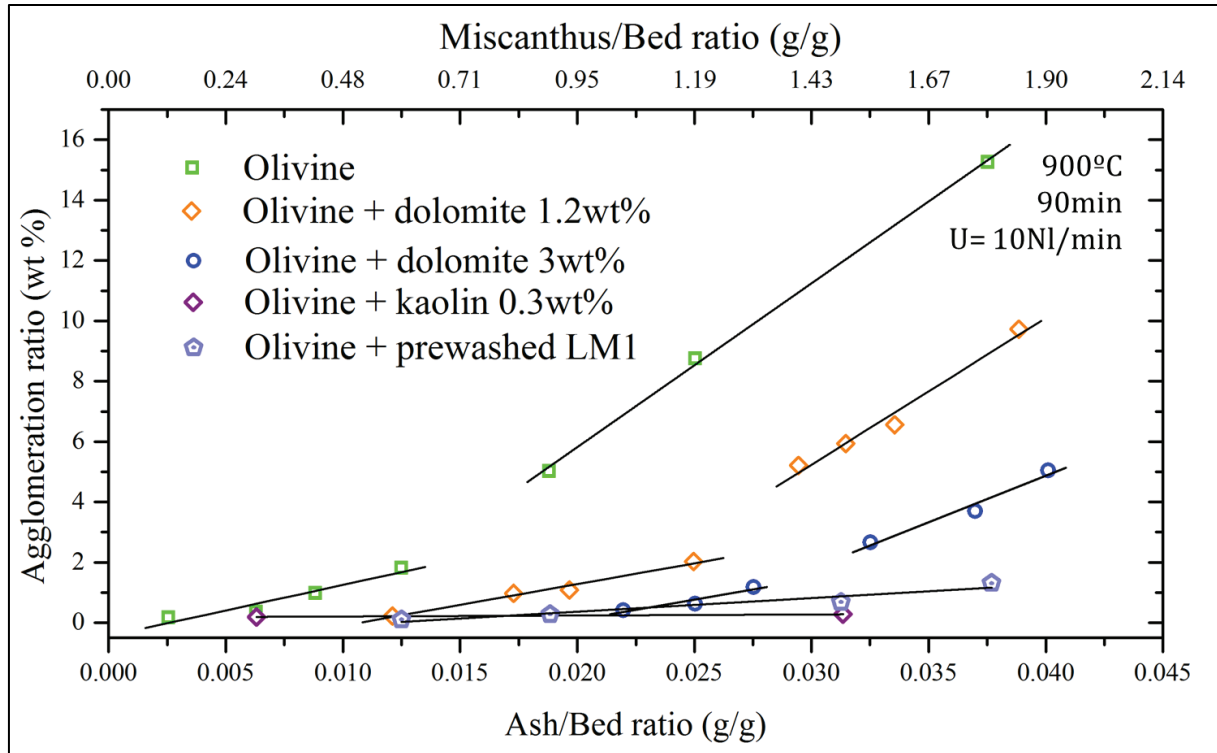


Figure V-10: Agglomeration ratio versus ash/bed ratio with dolomite and kaolin additives and in the case of pre-washing the biomass

Table V-4 summarizes the impact of the different process parameters on the agglomeration ratio. The process temperature, additives and biomass pre-treatment have the most significant effect on the agglomeration ratio. As expected, the ash/bed material ratio increases the agglomeration ratio but it has less drastic effect than the temperature or additives. The choice of the bed material has a medium effect on the agglomeration ratio. The air flow has a moderate impact. The operational time itself does not influence the agglomeration; once the domes of the agglomeration curve decline (approximately after 90 minutes), the A% stays constant. Although, we have to be aware, that in these experiments the 'biomass feed' is not continuous and in reality the quantity of ash increases continuously. To better interpret the effect of the different parameters, the agglomerates have to be analysed.

Table V-4: Effect of the different process parameters on the agglomeration ratio and the impact of the different parameters; + low effect, ++ medium effect, +++ significant effect

Parameters	%A	Effect*
Temperature	↗	+++
Air flow	↘	+
Bed material	↗	++
Ash/bed ratio	↗	++
Operation time	→	+
Additives	↘	+++
Pretreatment of biomass	↘	+++
* + low effect, ++ medium effect, +++ significant effect		

### V.3.8 MORPHOLOGY OF AGGLOMERATES

#### AGGLOMERATES WITH OLIVINE PARTICLES

Figure V-11 shows some agglomerates of the fluidization tests with olivine for 90 minutes at 900 °C. The smaller agglomerates are evenly distributed in the bed, while the big agglomerates are found on the quartz grid. It acts like a ‘hot spot’ in the fluidized bed, resulting in higher quantity of molten ashes attracting more and more olivine particles.



Figure V-11: Agglomerates after the fluidisation tests using olivine as bed material (process parameters; 1g of ash, air flow 10NL/min, time 90 minutes, T=900 °C)

The morphology of the agglomerates were characterised by SEM-EDX analysis. Figure V-12 presents the agglomerates of molten LM1 ash and olivine particles. Figure V-12/A shows a bulk of molten ashes in the middle and the olivine particles attached to the ash. In Figure V-13/B the liquid bridges of molten ash and the good wetting of olivine by the LM1 ashes can be observed. The cross-section analysis by SEM-EDX

shown the diffusion of Fe into the molten ash as it was observed during the static interaction tests (presented in Appendix A16, Figure A16-1).

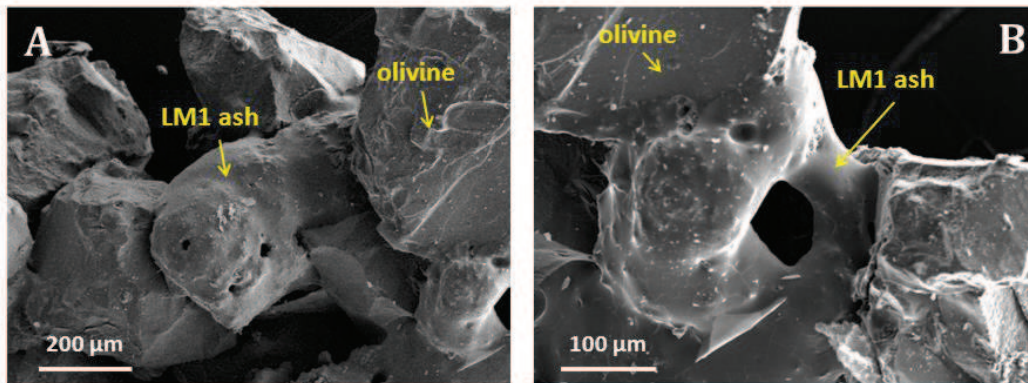


Figure V-12: (A) olivine particles attached by molten LM1 ashes (B) liquid bridge between olivine particles

#### EFFECT OF PROCESS TEMPERATURE

Figure V-13 presents the olivine agglomerates after the experiments at different temperatures. At 750 °C the adhesion between the LM1 ashes and the olivine particles is very weak ( $A < 1$  wt %), the agglomerates can be easily broken by hand and the ash separates from the particles during the sample preparation for SEM analysis. At 800 °C the LM1 ashes are partially molten and small liquid bridges can be observed resulting in somewhat stronger adhesion between the particles ( $A = 1$  wt % at 0.02g ash/bed ratio). At 900 °C the LM1 ashes are completely molten and they form liquid bridges and few  $\mu\text{m}$  thick layers around the particles, resulting in strong adhesion and high agglomeration ratio ( $A = 9$  wt % at 0.02g ash/bed ratio).

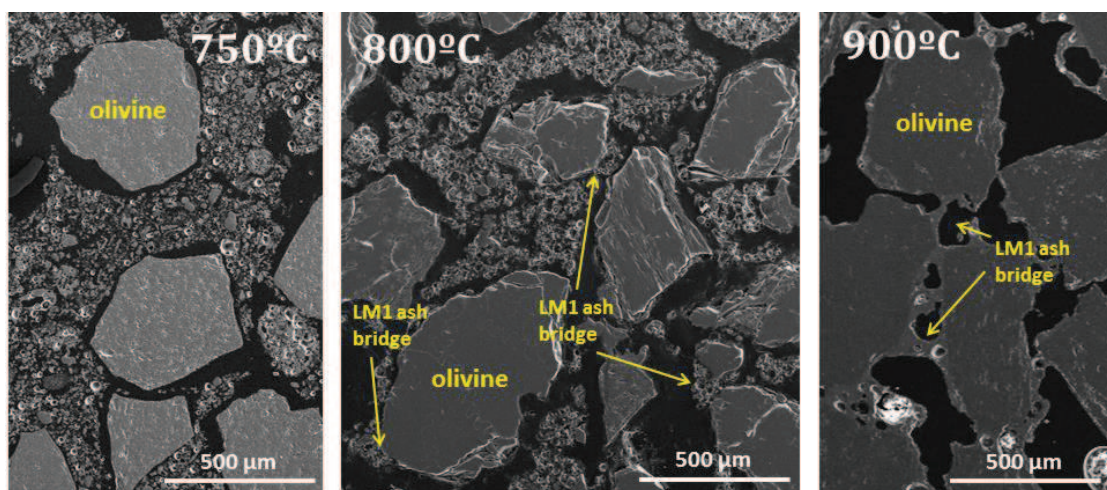
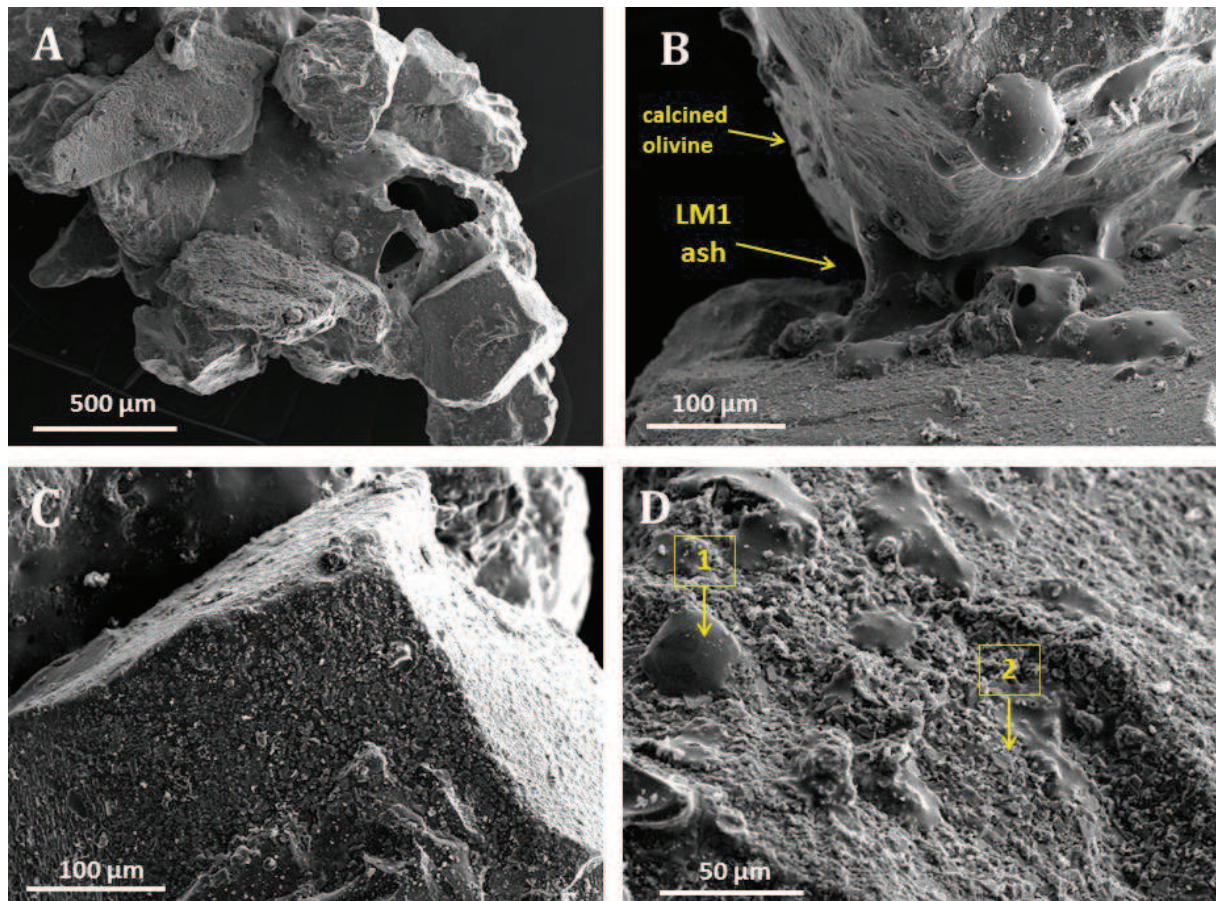


Figure V-13: agglomeration with LM1 ashes and olivine in dynamic condition at different temperatures (1g LM1 ash, 80g bed material, 90 minutes, 10NL/min)

*IMPACT OF SURFACE ROUGHNESS DUE TO THE CALCINATION OF OLIVINE*

Figure V-14 presents the agglomerates of calcined olivine particles with LM1 molten ashes. Figure V-14/A shows a thin shell of molten ashes with the calcined olivine particles and in Figure V-14/B the molten ash bridge between two calcined olivine particles can be observed. Just on the edge of the bed particle there is a small sphere of molten ash which can attract other ash particles and at sufficient volume it can keep them attached. In Figure V-14/C and Figure V-14/D the modification of the olivine surface due to the calcination procedure (1400 °C-4h) can be observed. After the calcination, different iron oxides (Figure V-14/D2  $\text{Fe}_2\text{O}_3$ ,  $\text{Fe}_3\text{O}_4$ ,  $\text{MgFe}_2\text{O}_4$ ) are formed resulting in a rough surface. We assume that the increased surface roughness and the inclusion of the crystals into the molten ash leads to increased agglomerate stiffness and increased agglomeration ratios under dynamic conditions.



*Figure V-14: agglomeration of calcined olivine and LM1 ashes -900 °C, 90 minutes, 10NL/min (A) calcined olivine particles stuck into molten ash (B) liquid bridge between two calcined olivine particles (C) rough surface of calcined olivine due to the formation of iron oxides after heat-treatment at 1400 °C (D- 1) molten ash drop wetting the calcined olivine surface, (D-2) iron oxides*

Figure V-15 shows the cross section of calcined olivine agglomerate. The darker particles in the middle correspond to the calcined olivine. The LM1 ashes assimilate completely the bed particles. In the molten ash different solid phases can be observed; the oxides of Cr, Fe and Mg with 40wt % of Cr (Figure V-15/1), the oxides of Fe, Mg, Cr and Al with 50wt % of Fe (Figure V-15/2) and the silicate of Al, Fe, K with 6% of Al (Figure V-15/3). We assume that the Cr and Fe rich crystals derive from the impurities of the olivine mineral and they accumulate during the calcination procedure on the surface of olivine particles. The small cross-like crystals (Figure V-15/3) are formed during the interaction with molten ashes. The diffusion of Fe is in the same range as in the case of the static tests, about 1-2 wt %. The point by point analysis is presented in Annexe A16 (Figure A16-2).

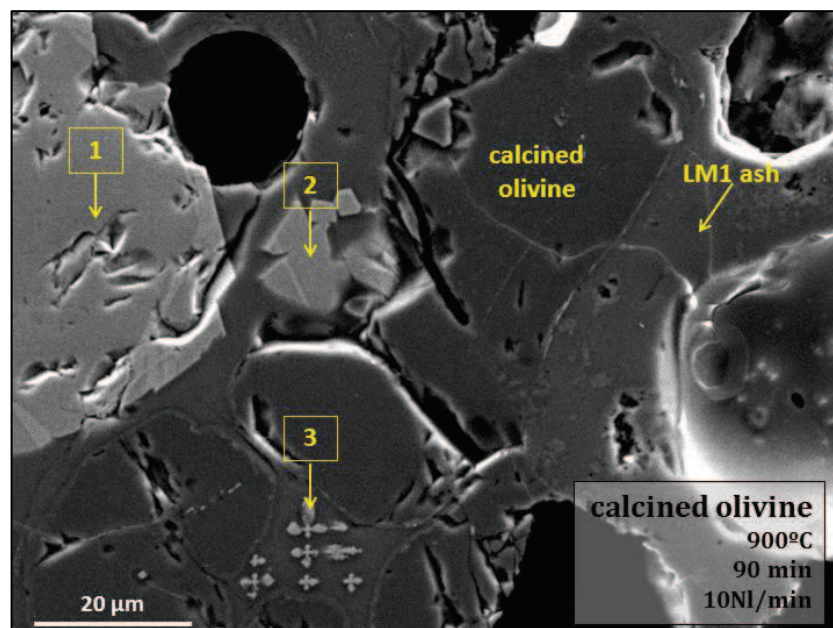


Figure V-15: agglomeration of calcined olivine and LM1 ashes -900 °C, 90 minutes, 10NL/min, (1) Cr-Fe, (2) Mg-Fe silicate, (3) Al-Cr-Fe silicates

### EFFECT OF ADDITIVES

Figure V-16 shows the agglomerates of olivine particles using 3wt % dolomite to bed material. The dolomite consists of fine particles which cover the surface of molten ashes preventing the adhesion of the molten ashes on the olivine particles and decreasing the agglomeration ratio from 15 to 5 wt %. The chemical interaction, namely the formation of solid K-Ca-Mg-silicates and thereby the reduction of liquid phase is possible, but could not be certainly confirmed with XRD analysis.

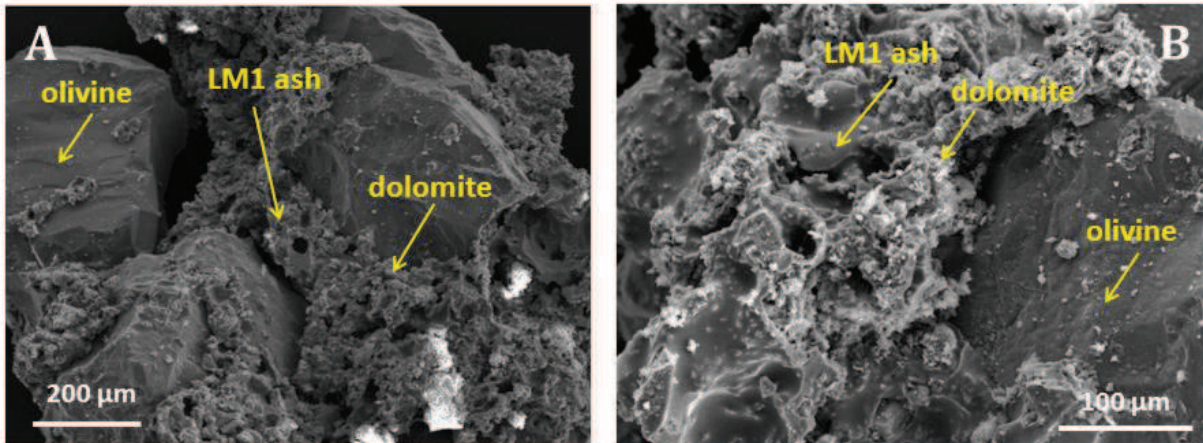


Figure V-16: agglomeration of olivine and LM1 ashes -900 °C, 90 min, 10NL/min with 3% dolomite

Figure V-17 presents the experiment using 0.3wt % kaolin to bed material as additive. Only few liquid bridges can be observed, the amount of the liquid ash is reduced via the formation of K-Al-silicates which have a higher melting point than the process temperature. The structure of the molten ash is porous, therefore the adhesion of bed particles is weak. The agglomeration ratio is very low, less than 1wt %.

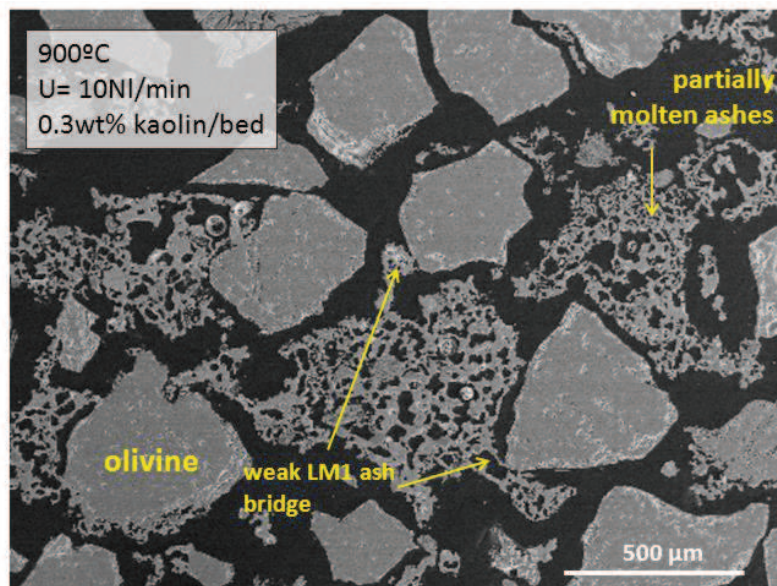
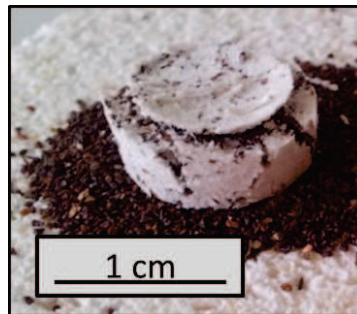


Figure V-17: olivine agglomerates after fluidization test for 90 minutes at 900 °C using 0.3wt % kaolin as additives

#### EFFECT OF PRE-WASHING THE BIOMASS

The effect of prewashing the biomass is presented in Figure V-18 and Figure V-19. It has to be noted that these images were taken of the tests under static conditions but the same morphology is expected after the dynamic tests. Figure V-18 shows the pastilles of

olivine after heat treatment at 900 °C for 72 hours in contact with ashes of prewashed biomass. It can be seen that the ashes stayed in solid form (fine white powder) without sticking to the olivine particles and the pastilles are very fragile. In Figure V-19, the SEM-EDX analysis proves that no agglomeration occurred during the treatment, there is no cohesion between the bed and the ash particles.



*Figure V-18 : olivine with ashes of prewashed biomass after heat treatment at 900 °C for 72 hours*

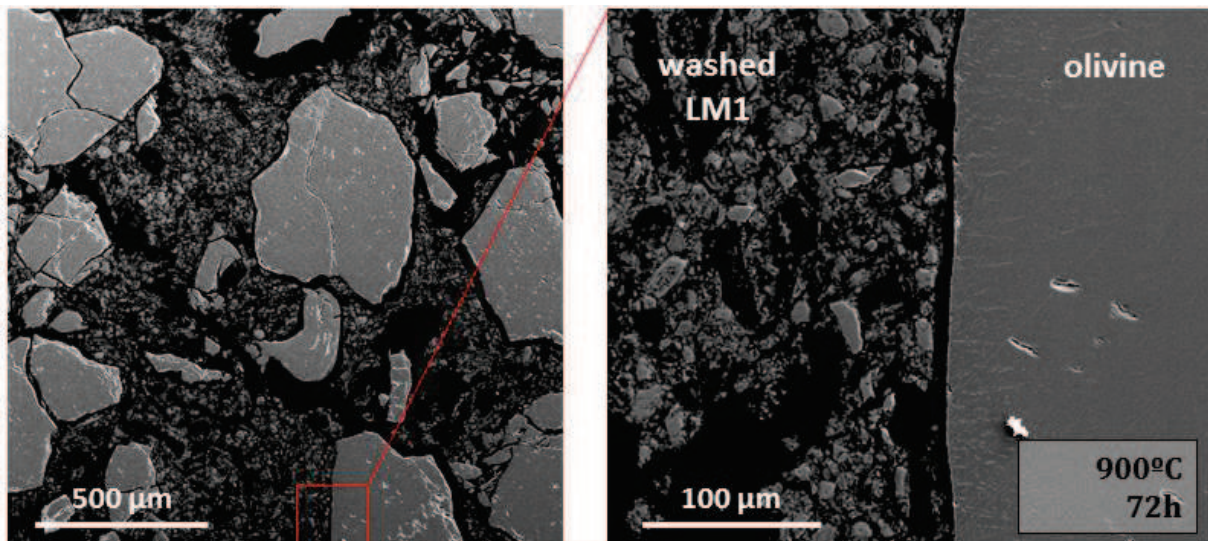


*Figure V-19 : Morphology of olivine grains in contact with molten ash under static conditions for 72 hours at 900 °C*

### V.3.9 DISCUSSION OF LABORATORY HIGH TEMPERATURE EXPERIMENTATION

This subsection discussed the experimentation with the bench scale high temperature fluidized bed. The quartz wall enabled to observe the fluidization and agglomeration of bed particles. The contribution of different parameters to the agglomeration (bed material, ash quantity, temperature, air flow, additives and pre-treatment) was compared and quantified with the agglomeration ratio.

As it was expected from the static interaction tests, the agglomeration ratio increases in the order of sand, olivine and calcined olivine. With increasing ash content, two main regions can be observed. At low agglomeration ratios the bed is in fluidized state. Above a critical value of agglomeration ratio ( $A \approx 4\% \text{wt}$ ), the agglomeration is too significant and the fluidized state cannot be maintained, the bed starts to defluidize. The eligibility of this value should be tested with different granulometries of bed materials and with different biomass ashes.

The agglomeration ratio is inversely proportional to the air flow rate and to the temperature. While the air flow has only a slight influence, lowering the temperature can significantly decrease agglomeration tendencies. 750 °C or 800 °C would be ideal for operating temperature but the heating value of product gases and the tar decomposition also have to be taken into account.

Two additives, dolomite and kaolin were compared. While dolomite sticks into the molten ash preventing the adhesion of olivine particles, kaolin decreases the amount of molten ashes via the formation of K-Al-silicates. The formation of Ca-Mg-silicates and K-Mg-silicates in the case of dolomite is possible but further XRD analyses are required to confirm the presence of these silicates. Kaolin was found to be more efficient, 0.3wt % was sufficient to decrease the agglomeration ratio to 1%, whereas 3wt % of dolomite only lowered but did not prevent the agglomeration. The type of kaolin, its granulometry and its chemical composition should be studied in the future.

Although kaolin is more effective in terms of quantity, other properties, such as the catalytic effect on tar decomposition of dolomite [V-6] and the price of kaolin has to be considered as well.

These results indicate that potassium, which is the responsible compound for the low temperature melting and agglomeration risks can be completely removed by washing the biomass and in consequence interaction between ash and olivine and supposedly other bed materials as well can be avoided.

When considering the anti-agglomerate methods, the costs of the different treatments are the main factor of decision. Therefore, the amount of additives and the conditions of washing have to be optimized.

## V.4 GASIFICATION TRIALS IN FLUIDIZED BED PILOT

The bench scale laboratory experiments were compared with a laboratory fluidized bed gasifier pilot. The aim of this subsection is to validate our predictions of agglomerate formation and to compare the structure of agglomerates from the laboratory tests with samples closer to the industrial conditions.

### V.4.1 EXPERIMENTAL SETUP

In the framework of the GAMECO research project, a fluidized bed pilot was constructed at the laboratory LRGP, CNRS Nancy to perform miscanthus gasification tests. The fuel capacity of the pilot is 7.5 kW and it operates with a cold gas efficiency<sup>5</sup> of 60%.

The gasification experiments were carried out using miscanthus pellets supplied by Novabiom (harvest April 2011 in France,  $l=5$  to 35 mm,  $d=6.3$  mm,  $\rho=560$  kg/m<sup>3</sup>) and olivine (Sibelco, Norvege) as bed material. The gasifying agent is diluted air in nitrogen with an equivalent ratio of 0.25-0.3 to approach the conditions used by EQTEC, the industrial partner of the GAMECO research project.

The pilot is shown in Figure V-21, it consists of a fluidized bed gasifier, a cyclone and four heat exchangers (HX). The gasifier is made of Inox 310 S being 0.8 m high. The reaction zone is 100 mm and the freeboard is 140 mm in diameter. The distributor plate is a 3 mm thick Inox grid with 379 holes ( $d=1$  mm). The gasifier is heated by eight heater shells; the maximum operating temperature is 1000 °C.

The biomass is fed on the top by a sloping screw (maximum feeding rate 5kg/h). The bed is fluidized by air, which is preheated in three steps: (1) HX1 heat exchanger from 20 to 400 °C, (2) in a 10 m long flexible tube placed into an electric furnace (Nabertherm) from 400 to 700 °C and (3) in the plenum.

The produced gas leaves at the top; it is filtered in the cyclone then cooled down in four steps. In the first two heat exchangers (HX1, HX2) the gases are cooled down from 400 to 80 °C with air. The third and fourth heat exchangers (HX3, HX4) are cooled with glycol; they reduce the producer gas temperature from 80 °C to 30 °C. Afterwards, for safety reasons the produced gases are combusted in the flare into CO<sub>2</sub> and H<sub>2</sub>O and collected in a hood.

The gasifier is equipped with 15 sampling points located with a step of 50 mm allowing the measurement of local temperature and/or pressure. The pressure at the top of the freeboard section is continuously registered, above 0.3 bar the process is shut down.

A solid sampler can be introduced at the top of the gasifier and it allows in situ sampling of the bed (around 10 g of bed) during the gasification. Gas is sampled at the exit of the cyclone and goes through two methanol bubbling systems. Tars dissolved in the methanol are analysed by gas chromatography attached to a mass spectrometer and flame ionization detector (GC/MS-FID).

---

<sup>5</sup> Cold gas efficiency can be obtained by multiplying the gas flow with the low calorific heating value of the gas and dividing it by the biomass feed and the low calorific heating value of the biomass

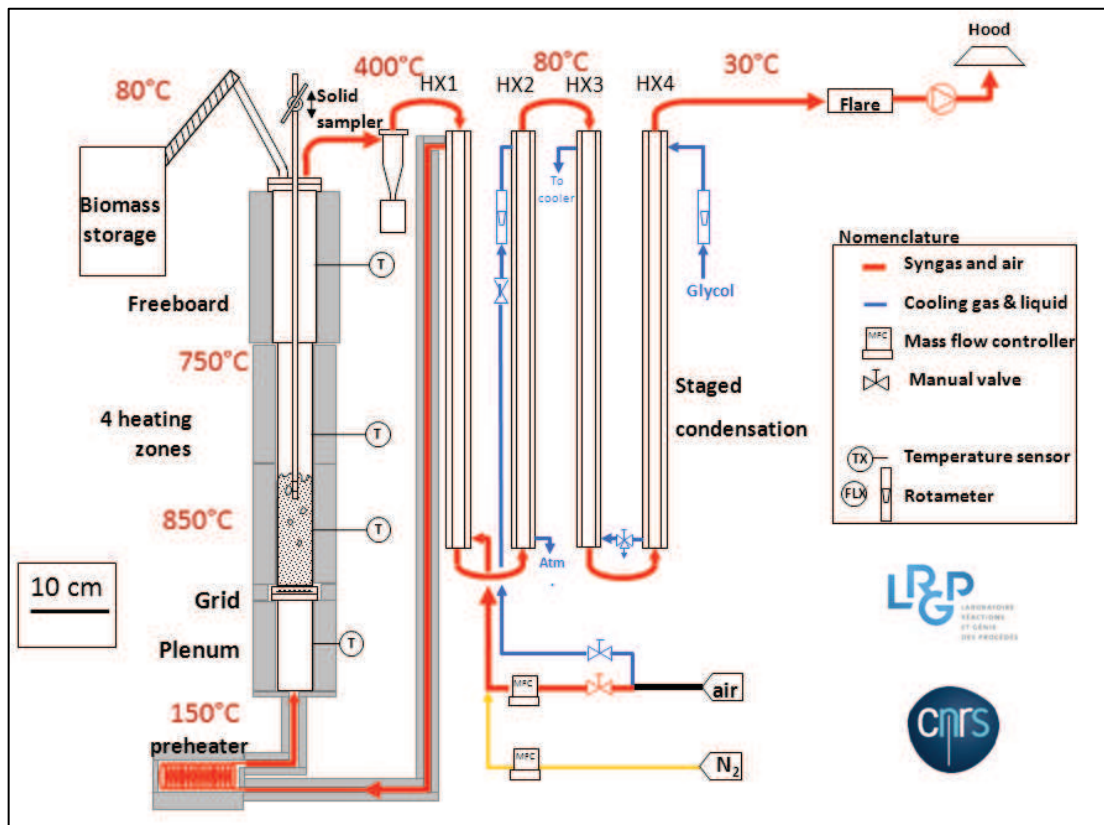


Figure V-20: Scheme of the fluidized bed gasifier pilot at LRGP, Nancy



Figure V-21: Fluidized bed gasifier pilot at the laboratory LRGP, Nancy

## V.4.2 FLUIDIZATION TESTS IN THE GASIFICATION PILOT

In this section, two gasification trials (January 2014 and April 2014) are discussed; the parameters of the experiments are given in Table V-5.

The gasification tests were carried out at 900 °C with a  $U/U_{mf}=5$ . The biomass feed was 1.9 kg/h in the first case and 1.7 kg/h in the second case, the equivalent ratio (ER) varied between 0.25 and 0.3. The bed particles were pre-sieved, for the first test olivine in the range of 500-380 $\mu$ m and in the second case olivine in the range of 380-250  $\mu$ m were used. The tests were stopped when the bed defluidized: after 2h 30 min and 2h 20 min, respectively. The defluidization was indicated by unstable temperature and pressure.

To study the evolution of the agglomeration, bed samples were taken via the solid sampling system during the gasification, about every half an hour.

At the end of the process, the bed was recovered and divided into five parts:

- agglomerates close to the grid
- section IV: 0-10cm from the grid
- section III: 10-20cm from the grid
- section II: 20-30cm from the grid
- section I: 30-40cm from the grid

The solid samples collected during the gasification and at the end of the tests were sieved to determine the size distribution of agglomerates the same way as in the bench scale trials (V.7):

$$A\% = \frac{mass_{>630\mu m}}{mass_{bed}}$$

*Table V-5: Experimental setup used in fluidized bed pilot at LRGP, Nancy*

	January 2014	April 2014
Temperature	900 °C	900 °C
Biomass feed	1.9kg/h; In total 4.72kg/2h30min	1.7kg/h; In total 3.68kg/2h20
Bed material mass	4 kg	4 kg
Particle size	500-380 $\mu$ m	380-250 $\mu$ m
$U/U_{mf}$	5	5
Duration	2h 30min	2h 20min
Equivalent ratio (ER)	0.3	0.25

## V.4.3 AGGLOMERATION RATIO IN THE GASIFICATION PILOT

Table V-6 summarises the agglomeration ratio in the different bed sections and in the entire bed in the case of the trials in January and April 2014. In the case of the test in January, the segregation of the bed is evident. The bed section taken close to the grid contains most of the agglomerates and the amount of agglomerates decreases with the distance from the grid.

In the case of the test in April, the high agglomeration ratio in sections I and II are due to the unburnt char which could not be separated from the agglomerates (Figure V-22). In the January test, the amount of char was less significant and it could be separated from the bed.

Table V-6: Agglomeration ratio during the two gasification trials in the different sections of the bed and in total

	Agglomeration ratio (wt %)		
	January 2014 (ER=0.3)	April 2014 (ER=0.25)	
I	5.5	27.0	40 cm
II	7.8	8.8	30 cm
III	6.7	2.2	20 cm
IV	8.3	3.8	10 cm
Grid	14.3	99.2	0 cm
<b>Total</b>	<b>7.3</b>	<b>9.3</b>	

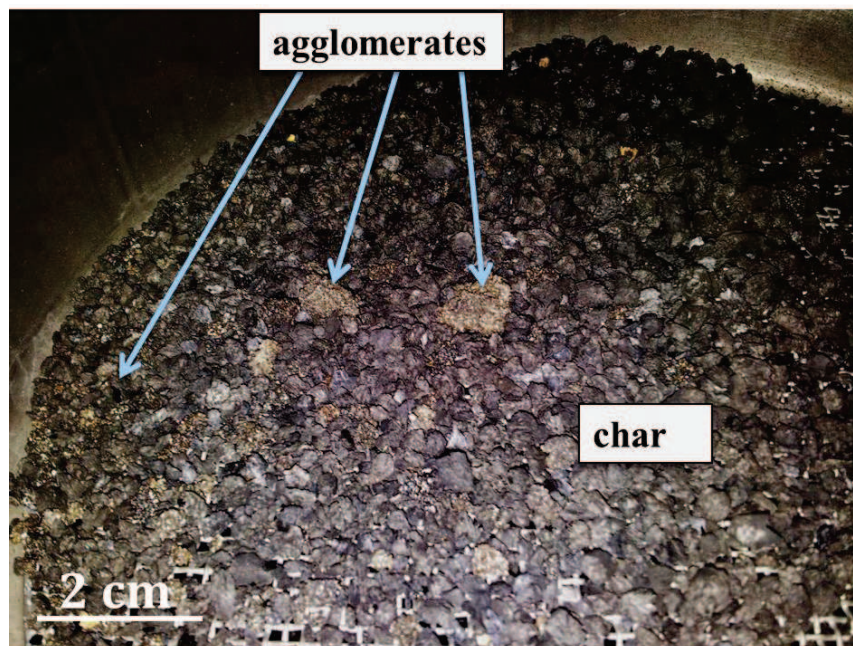


Figure V-22: Agglomerates and char from the upper section of the bed (April 2014)

#### V.4.4 EVOLUTION OF AGGLOMERATION RATIO DURING GASIFICATION

The solid sampling device allowed in situ sampling of the bed material during the gasification tests. Approximately 10 g of bed can be taken at each sampling and the evolution of the agglomeration ratio can be determined by sieving.

The test in January was carried out for 150 min, the test in April for 120 min. In both cases the experiment was stopped due to the defluidization of the bed.

It was shown with the hot device at CEMHTI, CNRS that the ash/bed material ratio has a significant effect but the operational time above 90 min does not influence the agglomeration ratio significantly (see Figure V-). Therefore the agglomeration ratios obtained from the gasification pilot tests were compared with the bench scale experiments based on the ash/bed material ratio in Figure V-23 (all the bench scale experiments in this series were carried out for 90 min).

The pilot tests were carried out with 4 kg of bed material and approximately 1.7 and 1.9 kg/h biomass feed (see Table V-5). Considering 2.1 wt % ash content on dry basis, the ash/bed material ratio can be calculated for the sampling times and the values can be compared with the laboratory experiments using different amount of ashes.

The pilot test in January shows very good agreement with the bench scale laboratory test. The test in April had to be cut at smaller ash/bed material ratio due to the defluidization of the bed but the quadratic polynomial curve predicts the same tendency for the evolution of agglomeration ratio.

The difference in the agglomeration ratios during the pilot tests can be due to two facts; firstly to the different bed particle size, secondly to the difference in the equivalent ratios (ER)<sup>6</sup>. In the second case the average bed particle size is smaller; however the agglomeration ratio was calculated in the same way (fraction above 630 $\mu$ m is considered as agglomerates). Moreover, the lower equivalent ratio results in more unburnt carbon influencing the calculated values.

In the second case the defluidization occurs above  $A=4$  wt % which is in good agreement with the laboratory hot device experiments regarding the threshold between the fluidization and defluidization zone (Figure V-7). As many parameters differ in the two cases, further experimentation are required to validate these findings.

---

<sup>6</sup> ER=supplied air/stoichiometric amount of air for the complete combustion

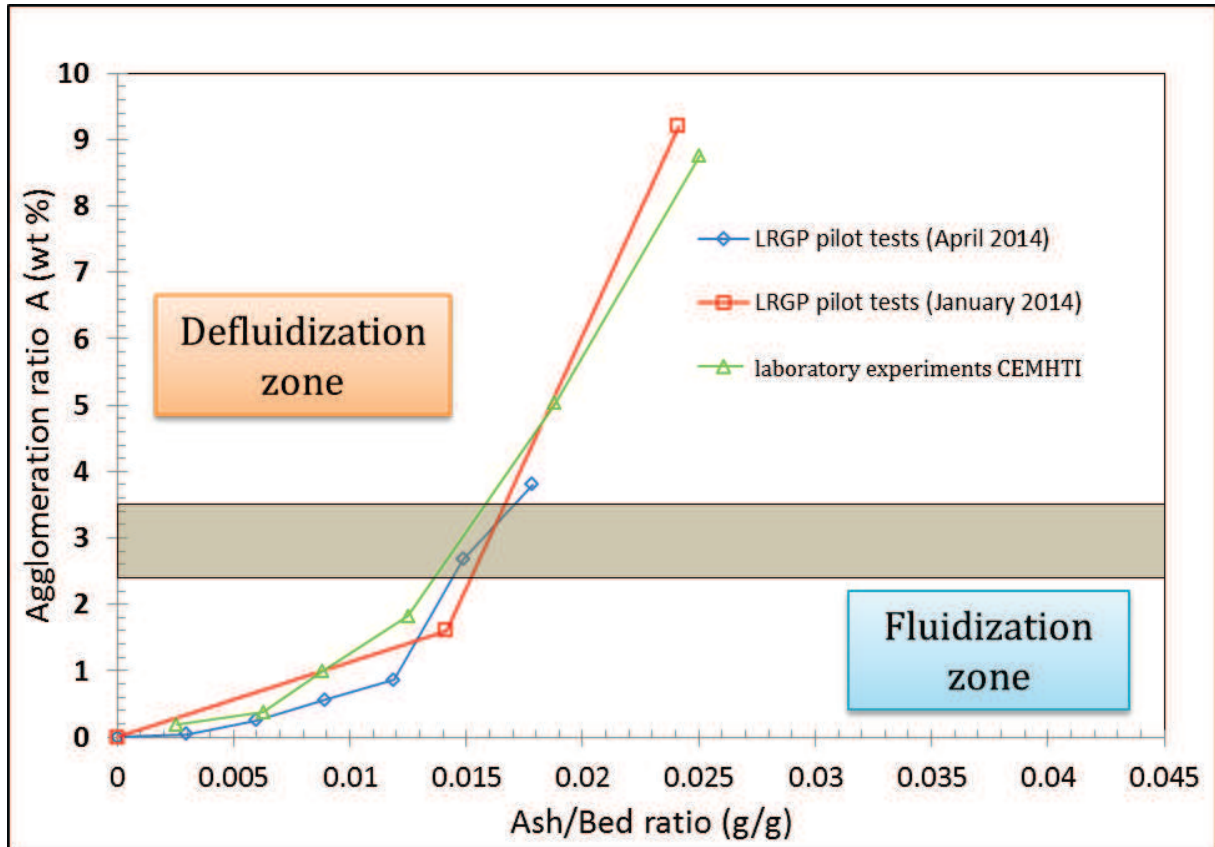


Figure V-23: Comparison of agglomeration ratio in the pilot and bench scale fluidized beds

## V.4.5 MORPHOLOGY OF AGGLOMERATES

Figure V-24 presents the agglomerates collected from the gasification test in April 2014. In Figure V-24/A- C, different kinds of agglomerates are shown. The small agglomerates (<0.5 cm) in Figure V-24/A are shining black due to the vitrified char. They were collected from the second section of the bed (upper part of the bed, 20-30 cm from the grid). Figure V-25/B shows an agglomerate collected from the grid; the channels of gas flow can be observed along its left side. In Figure V-24/C, different types of smaller agglomerates can be observed. It is interesting to note how the gas flow formed them into a drop-like shape while the ashes were still molten. Figure V-24/D is actually an odd-one-out image: it shows the small pieces of Ca-carbonates incorporating some silicates which were formed during the gasification. (The formation of solid silicates and their accumulation in the molten ashes were already witnessed during the laboratory tests as presented in Appendix A17).

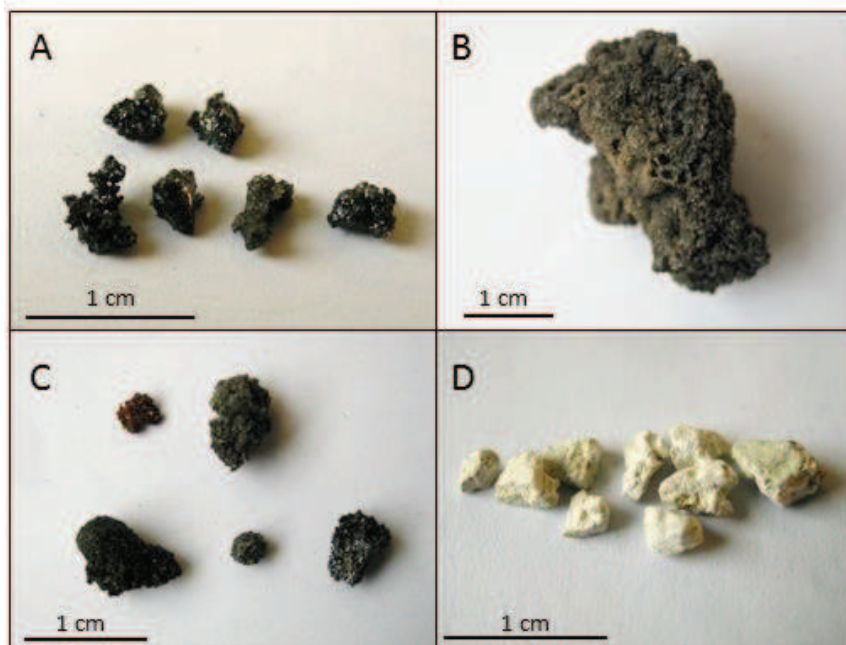


Figure V-24: (A, B, C) agglomerates; (D) solid crystals formed during trial (test April 2014)

The SEM-EDX analysis reveals the main components of the molten ash in the different agglomerates. In Figure V-25/A, the molten ash completely covers the bed particles, the main components are  $\text{SiO}_2$  and  $\text{K}_2\text{O}$  but P, Mg and Fe are also present, this latter causing the silvery colour of the sample. Figure V-25/B shows how the liquid bridges are stretched due to the movement of the bed. The molten ash contains the same compounds and Al and Mn as trace elements. The formation of solid alkali earth silicates can be also observed.

Figure V-27 shows two types of agglomerates. In Figure V-27/A the particles are partially covered, the composition of the molten phase is similar to the olivine; the major compounds are  $\text{MgO}$  and  $\text{SiO}_2$  with traces of Fe and Al. In Figure V-27/B, the particles are hold together by liquid bridges.

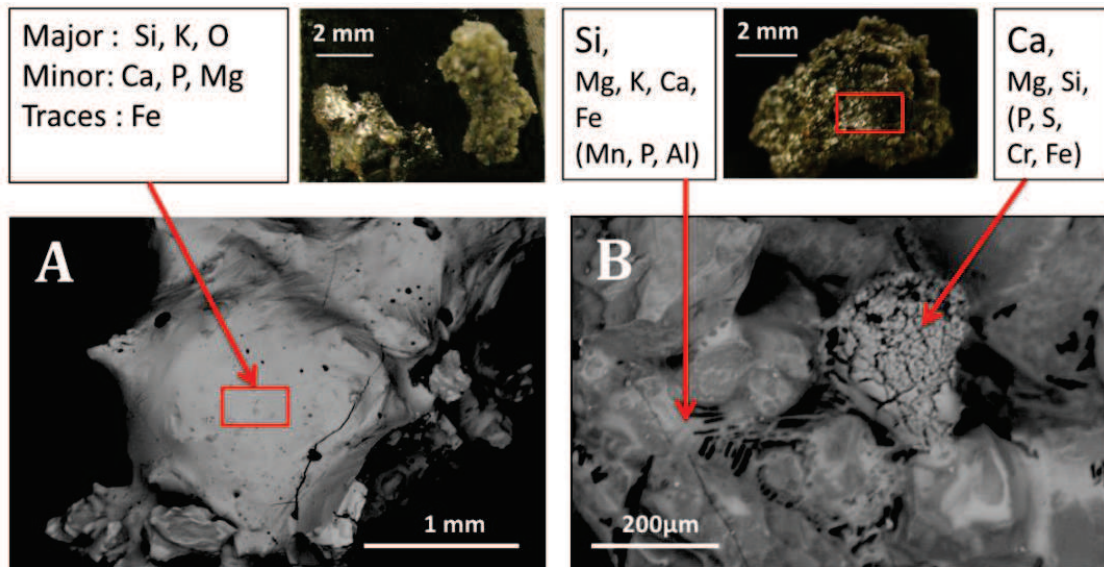


Figure V-25: SEM images of agglomerates from test April 2014; (A) the bed particles are completely covered with molten ash, (B) the molten ash stretches between the particles and solid phases containing Ca and Mg silicates

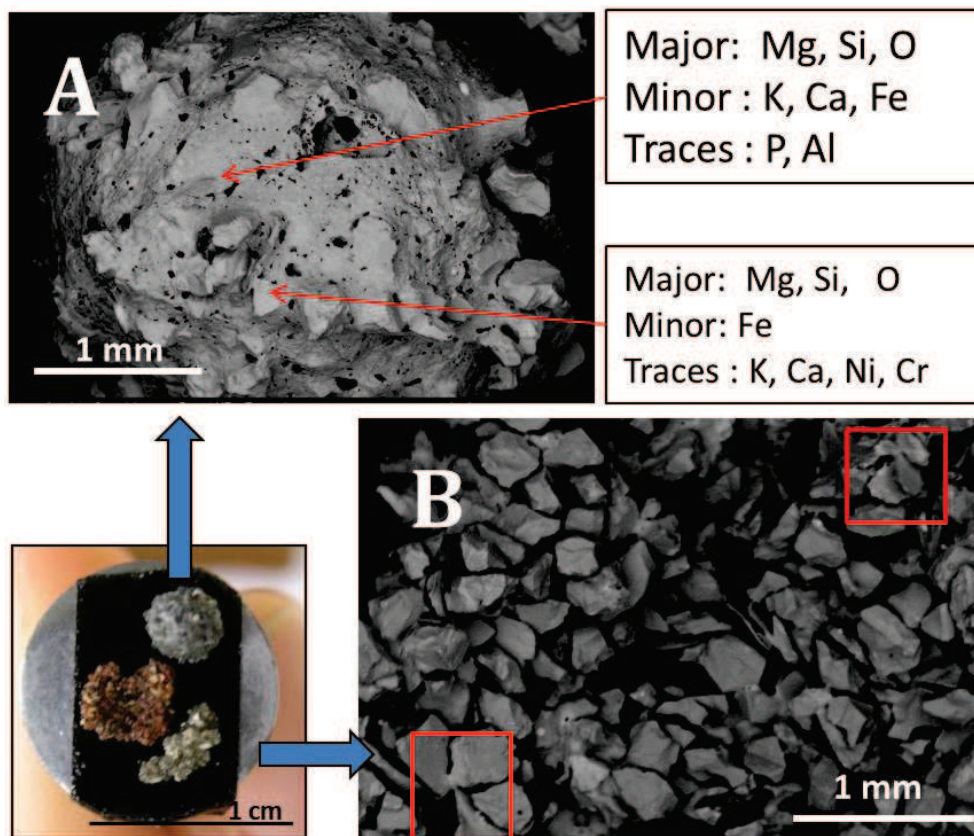


Figure V-26: SEM images of agglomerates from test April 2014 (A) bed particles covered with molten ashes (the major components are K, Ca, Mg and Si, (B) small liquid bridges holding together olivine particles

In Figure V-27, the agglomerates collected at the grid are presented. In all cases, the two sides of the agglomerate differed. While one side was molten with the bed particles completely embedded in the molten ash, the other side contained less liquid phase and had a rough surface.

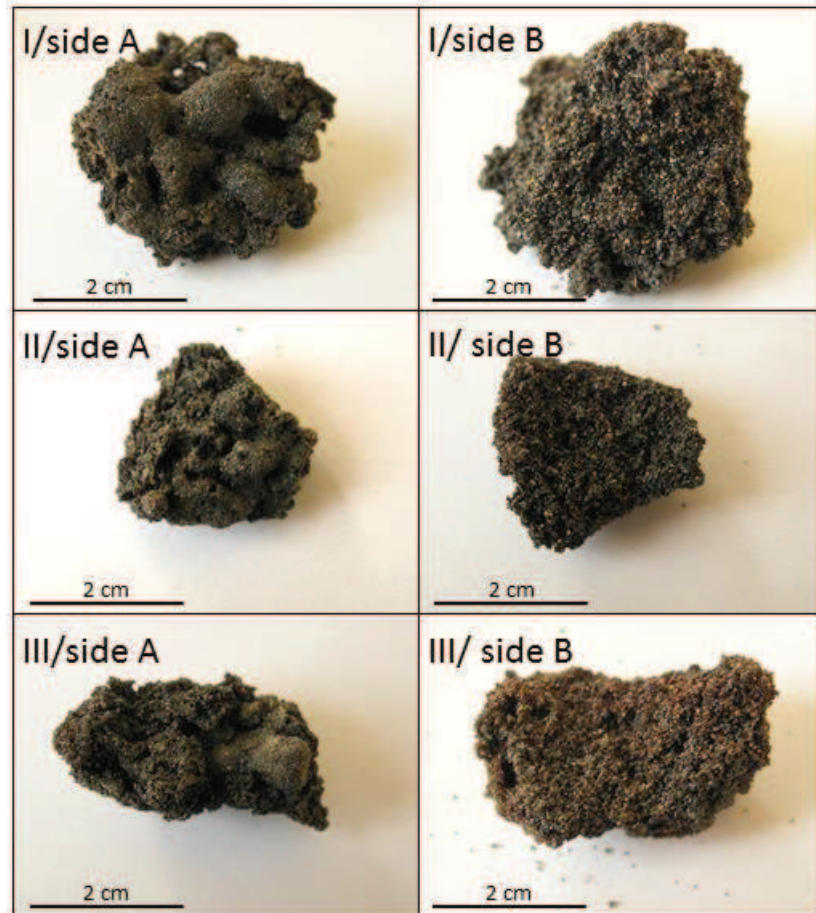


Figure V-27: Agglomerates collected from the grid (test April 2014)

The SEM-EDX analysis revealed the difference in the composition of the two sides. Figure V-28/A and Figure V-28/B show the upper, rough side of the agglomerates. The molten ash is mainly composed of  $K_2O$ ,  $CaO$  and  $SiO_2$  but also contains Fe, Al and Cr. In the bottom side (Figure V-28/C-D) and inclusion of Fe-Cr particles can be observed and the molten ash is extremely rich in Fe. The olivine particles have an outer layer containing Al, Ca and Cr. The point by point SEM-EDX analysis (Annexe A18) shown that the concentration of Fe is higher in the molten ash than in the olivine particles. Therefore we assume that the Fe derives from an outer source, in particular from the erosion of the grid and of the reactor wall. The reactor is made of Inox 310 S containing 0.12 wt % C, 23-26 wt % Cr, 18-21 wt % Ni, 1 wt % Si, 1 wt % Mg and 50-53 wt % Fe. The quantity of the Fe and Cr are in the same order of magnitude as the inclusion in Figure V-28/C, which strengthens our hypothesis. On the other hand, both the static and dynamic tests at CEMHTI shown the presence of Cr and Al as impurities in the olivine. As the amount of the bed used in the gasification pilot is more significant than in the

laboratory tests (4 kg versus 1 to 80g), it is also possible that the detected Cr and Al are coming from the impurities.

Therefore, more gasification tests with bed material not containing Cr and Fe such as sand are necessary to validate our findings.

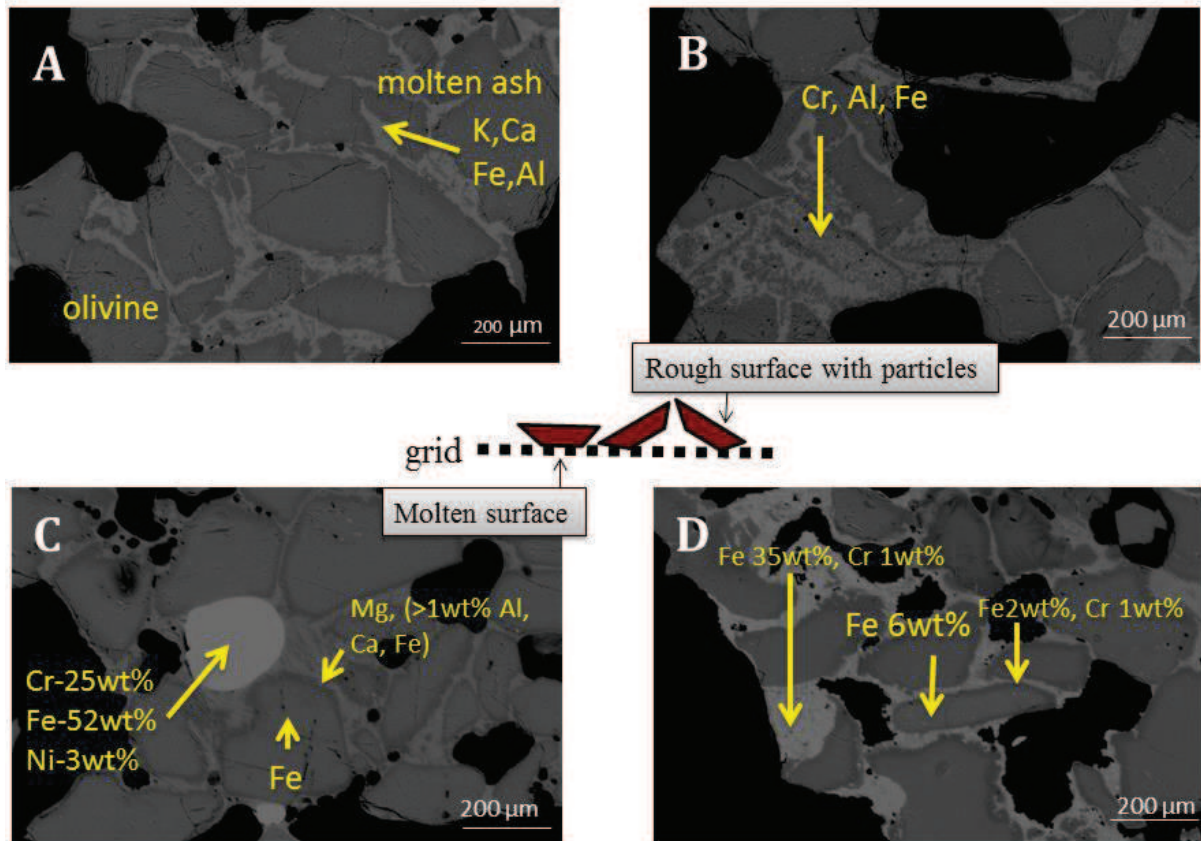
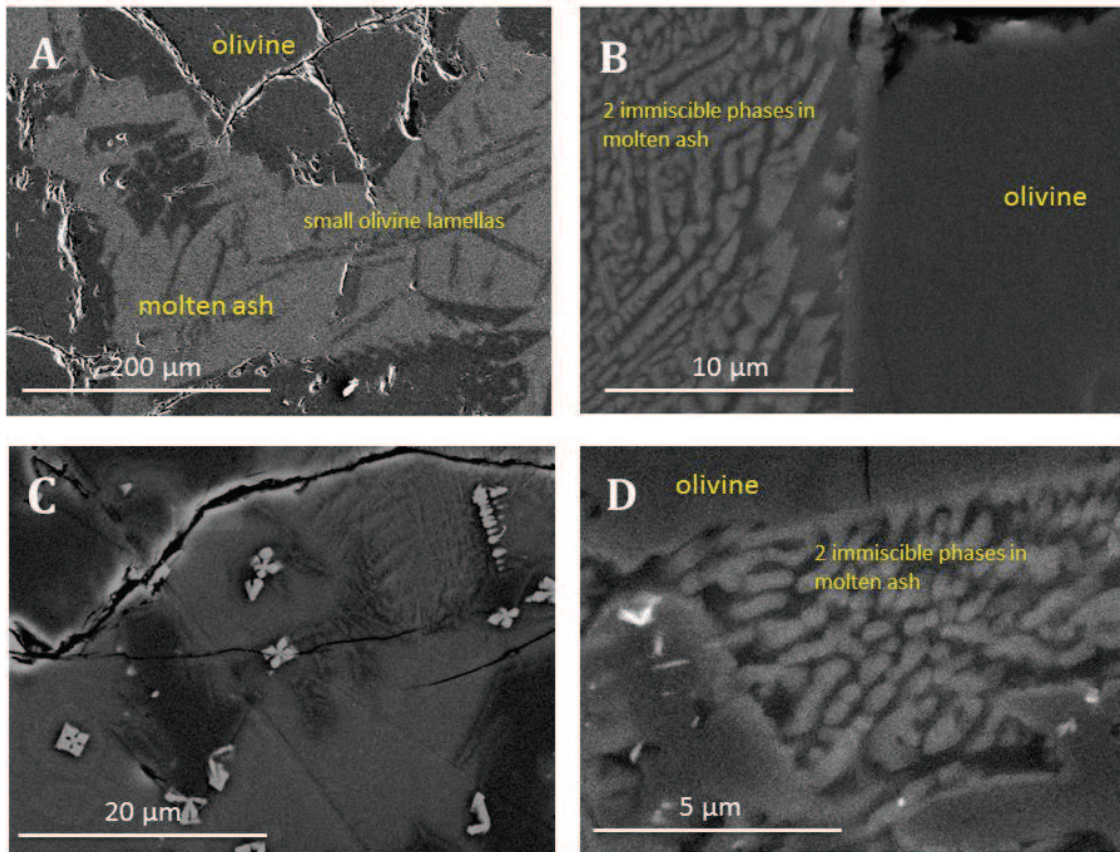


Figure V-28: SEM-EDX analysis of the agglomerates collected from the grid: upper side (A,B) and bottom side (C,D)

Figure V-29 shows the SEM-EDX analysis of agglomerates from the pilot test in January 2014. In Figure V-29/A, the damaged surface of the olivine particles and small olivine lamellas can be observed in the molten ash. Figure V-29/B and D show that in some areas the molten ash consists of two immiscible phases. Both phases contain Mg, Ca, K, Fe and Si, but the darker one is richer in K and Fe, while the lighter one in Ca and Mg. In Figure V-29/C, small cross like crystals appear which were already remarked both during the static reducing tests with calcined olivine carried out at LTB-LITEN (CEA, Grenoble) and the dynamic laboratory test in oxidizing atmosphere at CEMHTI. These cross-like crystals consists of 50 % wt of Fe, 10 wt % of Mg, wt % Si, and 5 wt % of Al. In the samples of the pilot tests Cr was also present in the crystals at the expense of Al.



*Figure V-29: Agglomerates from the pilot test January 2014: (A) olivine lamellas in the molten ash, (B) two immiscible phases in the ash, (C) small cross like crystals in the molten ash, (D) two immiscible phases in the ash*

Table V-7 summarises the findings about the agglomerate morphology of miscanthus gasification pilot (LRGP, Nancy) tests and compares them with the findings of laboratory experiments both in oxidizing and reducing atmospheres under dynamic and static conditions. In the gasification pilot the liquid phase is rich in Fe, in some cases two immiscible phases were observed. Due to the movement of the bed the surface of the olivine is eroded and small lamellas can stiffen the agglomerates. Cr and Al can be observed as impurities. In the bench scale hot device at CEMHTI, only one liquid phase was observed with moderate Fe concentration (around 2 wt %). The static tests in reducing atmosphere shown two immiscible phases in some cases but the quantity of Fe remained moderate in the molten phase. Impurities of Cr, Al were rather observed in the case of calcined olivine, when the naturally occurring impurities accumulate during the calcination process (1400 °C for 4 h).

Table V-7: Comparison of agglomerate morphology of the samples from miscanthus gasification pilote with static and dynamic tests

	<b>Liquid phase</b>	<b>Solid phase</b>
<b>Gasification pilot at LRGP, Nancy</b>	two immiscible liquid phases, or liquid phase rich in Fe (>5 wt %)	Abrasion of olivine, possible erosion of reactor wall Inclusion of Cr rich crystals, presence of Al
<b>Dynamic tests in oxidizing atmosphere CEMHTI (CNRS, Orleans)</b>	one liquid phase Fe(<2 wt %)	Olivine has plain surface Calcined olivine has rough surface
<b>Static tests in oxidizing/reducing atmosphere at CEMHTI (CNRS, Orleans)</b>	2 liquid phase in the case of red. atm, 1 liquid phase in air Fe concentration is about 2wt % in both cases	Fe, Al or Cr containing crystals only in the case of calcined olivine due to the migration of impurities during the calcination, the surface of olivine is smooth, but the surface of calcined olivine is rough due the formation of ferrous crystals and their migration

## V.5 CONCLUSION

In this chapter the ash-bed material interaction was investigated under dynamic conditions. Two different experimental setups were studied: a bench scale laboratory quartz fluidized bed and a fluidized bed pilot.

The bench scale laboratory quartz fluidized bed which enables to observe the agglomeration tendencies using biomass ashes and different bed materials in oxidizing conditions. A parametric study was carried out examining the impact of bed material, ash/bed ratio, temperature, fluidization velocity and temperature on the agglomeration ratio. Two additives and the pre-treatment of biomass were also tested. It was found that temperature has the most significant effect on the agglomeration ratio and biomass washing or the addition of kaolin are the most effective tools to reduce agglomeration risks. Among the different bed materials, calcined olivine presents most of the risks. Its rough surface due to the formation of iron oxides increases the adhesion between the particles and the molten ashes.

The results with olivine bed were compared to gasification experiments in a pilot fluidized bed (LRGP, Nancy) using miscanthus pellets and olivine as bed material. Although the agglomeration ratios showed good agreement with the pilot tests, the morphology of the agglomerates are quite different in the two cases.

In the pilot gasifier different phenomena were observed as it is shown in Figure V-31: the segregation of unburnt char on the top of the bed and the segregation of large agglomerates on the grid. The SEM-EDX analysis revealed that the main compounds of the liquid phases are  $K_2O$ ,  $CaO$ ,  $SiO_2$ ,  $MgO$  and  $Fe$ . The amount of  $Fe$  is greater than in the laboratory static and dynamic tests, also more  $Cr$  and  $Al$  were found in the agglomerates. It is possible that the elevated level of  $Fe$ ,  $Cr$  and  $Al$  is due to the big amount of olivine (4 kilograms compared to few grams) which is intensively mixed with the biomass but the high metal content can also derive from the erosion of the reactor wall. More fluidization tests both with olivine and other type of bed materials (silica sand) have to be carried out to validate our findings.

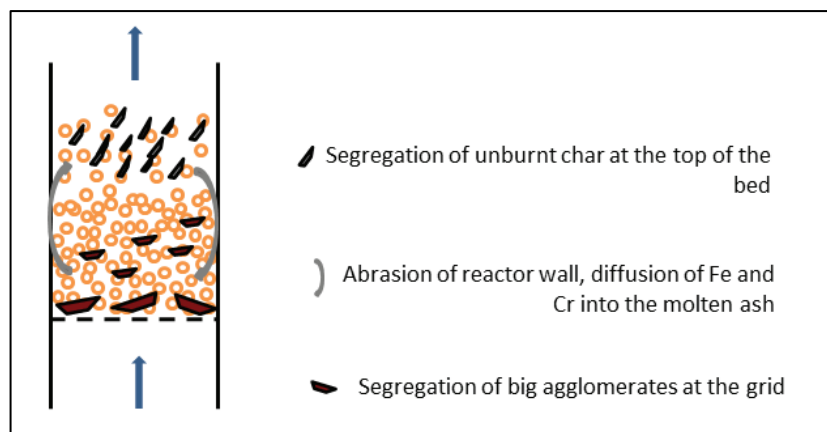


Figure V-30: Illustration of fluidized bed gasification

## V.6 REFERENCES OF CHAPTER V

- [V-1] Drelich J, Miller JD. A critical review of wetting and adhesion phenomena in the preparation of polymer-mineral composites. *Miner Metall Process* 1995;12:197–204.
- [V-2] Balland M. Etude de l'influence des cendres de biomasse sur le phénomène d'agglomération en réacteur à lit fluidisé. thesis INP Lorraine at CEA Grenoble/Liten, supervisors Jacques Poirier and Karine Froment, to be defended in 2016.
- [V-3] Basu P. *Combustion and Gasification in Fluidized Beds*. Taylor&Francis Group, LLC; 2006.
- [V-4] Antonini G. Transferts thermiques-Lits fluidisés: Caractéristiques générales et applications. vol. 42214210. Editions T, 2007, p. 1–22.
- [V-5] Thonglimp V, Hiquily N, Laguerie C. Vitesse Minimale de Fluidisation et Expansion des Couches Fluidisées par un Gaz. *Powder Technol* 1984;38:233–53.
- [V-6] Corella J, Toledo JM, Padilla R. Olivine or Dolomite as In-Bed Additive in Biomass Gasification with Air in a Fluidized Bed : Which Is Better ? *Energy* 2004;2000:713–20.
- [V-7] Sutton D, Kelleher B, Ross JRH. Review of literature on catalysts for biomass gasification. *Fuel Process Technol* 2001;73:155–73.
- [V-8] Devi L, Ptasinski KJ, Janssen FJJG, van Paasen SVB, Bergman PCA, Kiel JHA. Catalytic decomposition of biomass tars: use of dolomite and untreated olivine. *Renew Energy* 2005;30:565–87.
- [V-9] Weerachanchai P, Horio M, Tangsathitkulchai C. Effects of gasifying conditions and bed materials on fluidized bed steam gasification of wood biomass. *Bioresour Technol* 2009;100:1419–27.
- [V-10] Steenari B-M, Lindqvist O. High temperature reactions of straw ash and the anti-sintering additives kaloin and dolomite. *Biomass and Bioenergy* 1998;14:67–76.
- [V-11] Wadell H. Volume, Shape and Roundness of Quartz Particles. *J Geol* 1935;43:250–80.



---

## CONCLUSION AND PERSPECTIVES

---

## CONCLUSION AND PERSPECTIVES

In this work the role of inorganics in ash-bed material interaction was studied.

In the frame of the ANR research project GAMECO, a promising alternative biomass, miscanthus (species *Miscanthus X Giganteus*) was selected. Miscanthus is a lignocellulosic energy crop with good yield and heating value which makes it an annealing candidate as renewable feedstock. However, as it is the case for all herbaceous plants, it contains relatively high amount of potassium and silica rich ash compared to traditional woody biomass. These compounds can form liquid silicates at the process temperature promoting the agglomeration of the fluidized bed. Agglomerates create so called "hot spots" in the bed declining the good mixing of the fluidized bed and disturbing the isothermal operating conditions. As a result, the process efficiency of biomass conversion decreases and in worse scenario the agglomeration leads to the defluidization of the bed and process shut down.

This work had three main objectives:

1. to describe the transformation of inorganics at high temperature
2. to reveal their role in the agglomeration phenomenon
3. to provide recommendations for miscanthus gasification in fluidized bed

Firstly, the composition and the phase transformations of miscanthus ash as a function of temperature had to be revealed. The main ash forming elements in miscanthus are K, Si, Ca, Mg, P, S and Cl. Depending on their role in the plant, they can be found in different forms: salts, organically bond elements, silica gel or minerals.

To study their transformation, the organic matrix of miscanthus had to be degraded. A relatively low temperature, 400°C was selected to prepare miscanthus ashes for further analysis. This ashing temperature allows the characterisation of the inorganic compounds without major modification of the chemical phases.

As the biomass ashes are complex systems containing both crystalline and amorphous phases, complementary analytical techniques were used; inductive coupled plasma-mass spectrometer (ICP-MS) to determine the chemical composition of the samples, X-ray diffractogram to study the crystalline phases and scanning electron microscopy to describe the morphology of the ash.

The SEM-EDX analysis revealed that the outer rigid part of the miscanthus stem is rich in Si while the main component of the inner spongy part is potassium.

The detailed XRD analysis revealed that the ashes are composed of silica, carbonates and salts at low temperature. The carbonates and salts decompose and volatilise around 700°C and at elevated temperature the dominant solid phases are silica and alkali earth silicates.

It is important to note that the molten phase is composed of the quaternary oxide system  $\text{SiO}_2\text{-K}_2\text{O-CaO-MgO}$  regardless of the nature of atmosphere and the harvest time.

The two main components are SiO<sub>2</sub> (70-75 wt%) and K<sub>2</sub>O (20-25 wt%). The amount of CaO and MgO varies between 3-8 wt% and their ratio depends on the harvest rate.

It was found that the harvest time significantly influences the ash composition. The miscanthus harvested in September contains a high amount of potassium in the form of salts (sulphates, chlorides and carbonates), which results in greater quantity of liquid phase and volatilised inorganics at high temperature.

The main difference of inorganic behaviour in oxidizing and reducing atmosphere is the form of the sulfur. In oxidizing atmosphere, sulfur forms potassium sulphates, in reducing atmosphere it is released into the gas phase and traces of potassium sulphides retained in the unburnt char can be found.

The experimental results were compared with thermodynamic calculations to evaluate the accuracy of thermodynamic prediction tool.

The calculations were carried out with the software package FactSage 6.3<sup>®</sup>. The calculations complemented the experiments; they helped to determine the evolution of phases at equilibrium and to estimate to proportion of liquid and solid phases as a function of temperature. Two different oxide databases were compared; FToxid which is available in the Factsage software package and GToxid database which was recently developed by GTT technologies to improve the available oxide system databases. The equilibrium solid phases were compared to the XRD analysis and the equilibrium liquid phases to the SEM-EDX analysis. The crystalline phases are better described with the FToxid database while GToxid gives better approximation for the liquid phases.

Comparing the thermodynamic calculation with laboratory experiments showed differences in the temperature range of the formation and decomposition of certain compounds.

When performing the calculations, one has to be aware that the thermodynamic calculations consider infinite reaction time and equilibrium composition. In reality, the kinetics also has to be considered, the solid-solid or solid-liquid reactions are in general slower than solid-gas or gas-gas reactions. The presence of organic matrix and the diffusion of inorganics are not taken into account either in the calculations.

In general, we observed that the formation of silicates and the volatilisation of salts occurred at higher temperature in the laboratory experiments. For silica formation the alkali earth metals first have to be released from the organic matrix and get in contact with silica. The salts can be trapped by the organic structure or the molten ash phase.

In conclusion, FToxid database with FToxid-SlagA liquid solution phase and FTsalt database with FTsalt-SaltF can be used to follow the trends of the main phase transformations at high temperature but the calculations have to be completed and validated with laboratory experiments.

The interaction between the molten ash and different bed materials was studied under static and dynamic conditions both in oxidizing and reducing atmospheres. Regarding the agglomeration phenomenon, two main mechanisms are described in the literature;

the adhesive layer formation around the particles and the melt induced agglomeration. In both cases, the good wetting of the particles by the molten ash is observed. As it is revealed in the PhD work of Michael Balland<sup>1</sup>, the capillary forces of molten ash between two bed particles have prior importance and they are sufficient to keep the particles attached in the bubbling fluidized bed. The adhesive forces can be reinforced by other interactions; diffusion of phase components or chemical reactions at the ash-bed material interface.

Three different bed materials were evaluated: silica sand, olivine and calcined olivine. Silica sand is the most common bed material in fluidized processes; most of the agglomeration related studies were carried out with this bed material.

Olivine is an annealing bed material, as it has catalytic effect in tar decomposition due to its Fe content. The catalytic effect can be enhanced via the calcination of the particles above 900°C, which increases the Fe concentration at the particle surface. In the literature, olivine is mostly studied for its catalytic effect and its role in agglomeration is less understood.

The aim of the static interaction tests was to evaluate the wetting of olivine particles by molten ashes and to characterise the agglomerates of miscanthus ashes and the bed materials under different conditions.

The static interaction tests were carried out in a laboratory furnace with ash-bed material pastilles, when the contact of the ash and bed particles is assured.

The heat-treated pastilles were characterised by SEM-EDX analysis. No chemical interaction was observed between the molten ashes and silica sand. We found that the agglomeration is due the good wetting and adhesion of the silica sand particles. In case of olivine, the diffusion of Fe into the molten phase was observed. It was also evidenced that the calcination of the olivine particles significantly influences the interaction. During the calcination, iron oxides develop at the olivine surface, and enhance the contact due to surface roughness and partial inclusion into the molten ash.

From the static interaction tests the following conclusions can be drawn:

- The wetting of bed material by molten ashes is a key parameter of the agglomeration
- The adhesion between the miscanthus ashes and bed materials increases in the following order: silica sand → olivine → calcined olivine
- there is no significant difference in the agglomeration mechanism in oxidizing or reducing atmosphere regarding the adhesion and the interaction of the molten ash and bed particles
- However, in reducing atmosphere, two immiscible liquid phases can occur and the presence of unburnt char and traces of sulphides was also observed.

---

<sup>1</sup> "Etude de l'influence des cendres de biomasse sur le phénomène d'agglomération en réacteur à lit fluidisé", 2013-2016, LTB-LITEN, CEA, Grenoble, supervisors: Karine Froment and Jacques Porier

To study the impact of the hydrodynamics in the fluidized bed, the ash-be material interaction was studied under dynamic conditions at two different scales. Firstly, in a bench-scale quartz fluidized bed installed at *CEMHTI, CNRS, Orleans* and secondly, in a fluidized bed gasifier pilot (7.5 kW) installed at laboratory *LRGP, CNRS, Nancy*.

The bench scale device allows observing the agglomeration tendencies using miscanthus ashes and bed materials in oxidizing atmosphere. The agglomeration ratio of the bed was determined by sieving the bed before and after the tests. After the parametric investigation of the agglomeration ratio, it was found that the operating temperature has the most significant effect on the agglomeration ratio and the pre-washing of biomass and the addition of kaolin are the most effective tools to reduce agglomeration risks.

The gasification pilot tests carried out at LRGP Nancy allowed comparing the findings of the bench-scale experimentations with the miscanthus pellet gasification in olivine bed close to industrial application.

Although the agglomeration ratios determined with the bench scale device showed good agreement with the pilot tests, the morphology of the agglomerates were quite different. The movement of the bed in the pilot caused the abrasion of the olivine particles and small lamellas were found in the molten ash. Moreover, the liquid phase contained elevated amount of Fe and Cr. Another difference is the presence of unburnt char during gasification which can lead to the miscalculation of the agglomeration ratio and it can also participate in the agglomerate formation.

The main findings concerning the pilot reactor can be summarized as:

- Segregation of the bed occurred during gasification: unburnt char was found on the top of the bed and large agglomerates on the grid.
- The liquid phase is composed of  $K_2O$ ,  $CaO$ ,  $SiO_2$ ,  $MgO$  and iron oxide. The concentration of Fe in the molten phase is greater than in case of the laboratory static and dynamic tests
- Erosion of the bed material and possible erosion of the reactor wall was evidenced due to the fluidized bed movements

The investigation of the miscanthus ash behaviour, the interaction tests under laboratory conditions and the gasification trials in the fluidized bed pilot permit to offer some recommendations to minimize the risk of agglomeration in case of miscanthus thermal conversion in bubbling fluidized bed.

As summarized in the following table, the most important parameters are the alkali content of the bed, the operating temperature and the type of bed material. The usage of low alkali content (<10 wt %) biomass would be favourable but the mixing of different types of biomass or the washing of miscanthus can also help to reduce the alkali concentration.

The operating temperature should be around 800-850 °C, in this range silica sand and olivine were evaluated as safe bed materials.

At higher temperature and in case of risky biomass, the usage of additives can significantly decrease the agglomeration ratio; 3 wt % of dolomite to bed material reduces the agglomeration rate by 60 wt % and 0.3 wt % kaolin to bed material can basically eliminate the agglomeration risks.

---

### Recommendation

#### for miscanthus thermal conversion in bubbling fluidized bed

<b>Biomass feed</b>	<ul style="list-style-type: none"><li>➤ Ash composition: K less than 10%</li><li>➤ Mix with other feedstocks</li><li>➤ Wash biomass in water</li></ul>
<b>Operating conditions</b>	<ul style="list-style-type: none"><li>➤ 800 °C, maximum 850 °C</li><li>➤ Otherwise use additives</li></ul>
<b>Bed material</b>	<ul style="list-style-type: none"><li>➤ &lt;850 °C any kind of bed material</li><li>➤ &gt;850 °C silica sand</li></ul>
<b>Additives</b>	<ul style="list-style-type: none"><li>➤ 0.2-0.3 wt % kaolin to bed</li><li>➤ 3 wt % dolomite to bed</li></ul>

---

Although the miscanthus ash behaviour and the agglomeration with bed material was studied in details in this thesis, the investigation of ash-bed material interaction is far from being complete, this work only opens the door to further perspectives.

Concerning the ash behaviour, the phase transformation was revealed in details in oxidizing atmosphere. However, the main phases were only qualitatively described. Chemical fractionation analysis would allow quantifying the inorganic compounds in the ash. A systematic analysis in the range of 250 to 1400°C would complete the current findings of miscanthus ash behaviour. Qualify and quantify the volatilisation of the inorganics would be necessary to fully describe the transformation of the ashes.

In reducing atmosphere, only few experiments have been carried out. We evidenced the different behaviour of sulfur and the presence of unburnt carbon but further experiments are necessary to be able to describe the main phase transformations and to quantify the solid and liquid phases.

The characterisation of the ash samples and the ash-bed material pastilles could be completed with other techniques. The ash pellet compression tests (also known as test under load) are used to determine the melting temperature of the biomass ash. The ash samples are heat-treated at different temperatures. After cooling down, the

compression strength of the samples is measured in a standard device. The sintering temperature of the ash is indicated by a sharp increase in the measured strength values versus temperature.

Firstly, this technique could validate the calculated ash melting temperatures as the ash fusibility test and the thermogravimetric analysis proved to be not reliable methods.

Moreover, with the compression strength measurement the agglomerate samples both prepared under static conditions and obtained from the dynamic interaction tests could be qualified and the impact of the different parameters (temperature, bed material, additives) on the strength of agglomerates could be compared.

Thermodynamic tools (FactSage®) and databases were evaluated for the miscanthus transformation. As a next step, the calculations have to be expanded to study the ash-bed material interaction. In this work, the interaction was only studied by SEM-EDX analysis. XRD analysis was not considered, as the samples are so complex that it is not possible to interpret the diffractograms. Using the thermodynamic tools, based on the SEM-EDX point by point analysis, the equilibrium phases at the interface could be determined. The calculations could be used as complementary tool to interpret the diffractograms and the formation of liquid phases in contact with bed material or additives could be evaluated.

Using the FactSage 6.3® software package, a calculation series was performed to investigate the effect of main ash forming elements on the amount of liquid phase in miscanthus ashes. In this series, the concentration of the elements was varied one by one and plotted versus the ratio of liquid to liquid plus solid phases ( $L/(L+S)$ ). This study has to be completed with factor analysis to take into account the interactions between the different elements. The factor analysis would allow describing the coupling effects between the elements. The relation between the elemental concentration of miscanthus ashes and the amount of liquid phase could be used to define a novel index number to evaluate the agglomeration risks.

Regarding the ash-bed material interaction tests, the wetting of silica sand by molten ashes has not been evaluated, additional wettability tests would permit to compare the wetting of silica to the wetting of olivine and calcined olivine.

Concerning the laboratory hot temperature device (operating with biomass ashes and bed material), the parametric experimentation has to be completed. The most important is to evaluate the effect of temperature with other bed materials. The usage of dolomite and kaolin could be further investigated regarding the optimal concentration or testing of different kaolin types. Besides, further additives and other types of biomass (alone or mixed with miscanthus) can be investigated.

Regarding the pilot gasifier (operating with biomass pellets and bed material), the experimentation will be continued to carry out a systematic evaluation of the process parameters. First of all, the source of Fe, Cr and Al in the agglomerates has to be found

out. For this, dynamic tests with Fe free bed materials (silica sand) have to be performed.

All these findings concerning the study of miscanthus ash behaviour, the structure of agglomerates and the agglomeration ratio as a function of process parameters should serve to create a predictive model of agglomeration in bubbling fluidized bed. This model is out of the perspectives of this work and would be the subject of a new thesis.

This model would be based on a force balance approach taking into account both the physicochemical aspects of agglomeration (adhesion via physical binding of particles, capillary forces, diffusion and chemical interactions) and the hydrodynamics in a fluidized bed on a laboratory scale. For the model, some assumptions have to be taken;

- (1) the bed particles are uniform spheres
- (2) the collision of particles is elastic
- (3) the agglomeration is due to the liquid bridges between the bed particles
- (4) the molten ash consists of  $\text{SiO}_2$ ,  $\text{K}_2\text{O}$ ,  $\text{CaO}$  and  $\text{MgO}$  regardless the biomass and the operating conditions
- (5) the molten ash is highly viscous (its viscosity can be calculated by FactSage or use literature data of molten glasses)

The adhesion work between the sticky particles could be calculated from the literature data or estimated using the compression strength measurement.

The factors of the model should include the elemental composition of the biomass ashes, the type and granulometry of the bed material, the operating temperature, fluidization velocity and the biomass feed.

The model parameters should be evaluated via parametric experimentation with the hot device at CEMHTI and the gasifier pilot at LRGP, Nancy.

Finally, the findings of this work should be evaluated with experiments at industrial scale. These experiments would serve to determine the limits of laboratory experimentation and to validate our recommendation for miscanthus gasification in bubbling fluidized bed.

---

# APPENDICES

---

## LIST OF APPENDICES

---

### TABLE OF CONTENTS

List of appendices .....	192
Appendix-A 1 : Staining method.....	194
Appendix-A 2: Observation of stem degradation with optical microscope.....	195
Appendix-A 3: LM1 ashes after 10 min heat treatment at 1000 °C in Air.....	196
Appendix-A 4: XR diffractog of LM2 ashes .....	197
Appendix-A 5: Calculating the input data of miscanthus ashes for FactSage .....	198
Appendix-A 6: FToxid, FTsalt and FTpulp database- solution phases with components for the miscanthus ash system.....	199
Appendix-A 7: Selecting the solution phases for thermodynamic calculations.....	202
A7.1 Possible solution phases for the miscanthus system .....	202
A7.2 The effect of solid solution phases .....	204
A7.3 Comparison of liquid solution phases.....	206
Appendix-A 8: Comparison of liquid and solid phases at 850 °C .....	209
Appendix-A 9: Influence of main ash forming elements.....	210
Appendix-A 10: FToxid and GToxid databases.....	220
Appendix-A 11: Comparing liquid phase composition at 1000 °C.....	222
Appendix-A 12: Wetting of bed materials by molten LM1 and LM2 ashes.....	223
Appendix-A 13: Magnesium Ferrite in calcined olivine .....	224
Appendix-A 14: Determining the minimum fluidization rate at 750 °C .....	225
Appendix-A 15: Dolomite plus ashes heat treated at 900 °C .....	228
Appendix-A 16: SEM-EDX analysis of agglomerates from laboratory fluidized bed (CEMHTI).....	229
Appendix-A 17: Minerals from laboratory fluidized bed (CEMHTI) .....	230
Appendix-A 18: SEM-EDX analysis of agglomerate from the gasification pilot.....	231



## APPENDIX-A 1 : STAINING METHOD

---

Staining is a widely used technique in biology to study the different organs of the plant. This method is based on the fact, that the cellulose and lignin can be stained with different colorant resulting in a better contrast of the microstructure. Usually two staining agents are used together which have different affinities to the different tissues. In this work we used the carmine-iodine staining agent pair. The phloem cells which have cellulose rich cell walls can be stained pink by carmine (carminic acid,  $C_{22}H_{20}O_{13}$ ). The cells of xylem which are impregnated by lignin can be stained green with iodine solution.

To obtain good contrast, the stem has to be freshly cut and directly placed into a fixing agent (formaldehyde solution) to preserve its original structure.

The method is the following:

- Fixing: the freshly cut stem is kept in formaldehyde-acetic acid-ethanol (FAA) solution to avoid air bubbles in the cells
- (Dehydration: the stem is put in different water-alcohol baths with increasing alcohol concentration –this step is necessary only in case of embedding to promote the impregnation of wax into the cells)
- (Embedding the 1-2cm piece of stem in wax, this step is not necessary)
- Sectioning: the stem is cut into very thin slices with the help of a blade, washed in water
- Staining:
  1. Rinsing in water
  2. 15 min in bleach
  3. 3x1min in water bath
  4. 2 min in acetic water
  5. 6 min in carmine-iodine solution
  6. 1 min in water
- Inclusion:
  1. A gelatine ball is heated on a piece of microscope glass on a laboratory hot plat
  2. The stained samples are placed into the molten gelatine ball
  3. The samples are hermetically included with a second microscope glass (air bubbles are gently pressed towards the edge of the glasses)

Once the gelatine solidified, the samples can be observed by optical microscope.

APPENDIX-A 2: OBSERVATION OF STEM DEGRADATION WITH OPTICAL MICROSCOPE

The degradation of miscanthus stem was observed by optical microscope (Olympus BX51). For each image, 30-64 photos with the same adjustment but different focal length were taken. The photos were then superposed with the help of a focus stacking free licenced software (Combine ZP). Figure A2-1 shows the cross section, Figure A2-2 the longitudinal cut of a miscanthus stem.

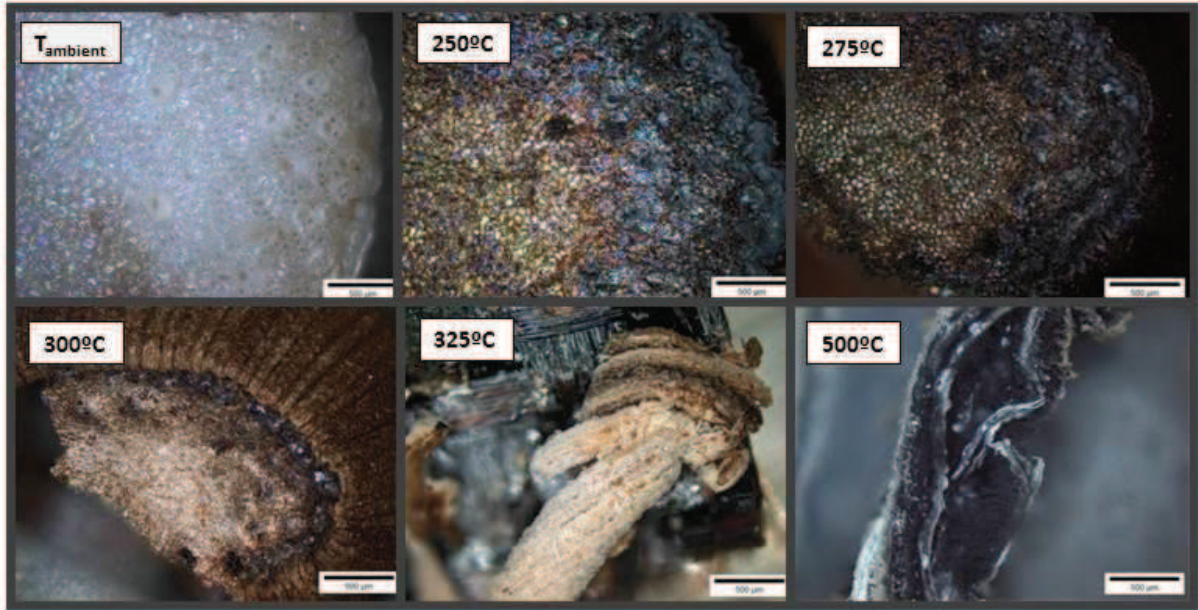


*Figure A2-1: degradation of miscanthus as a function of temperature-cross section*

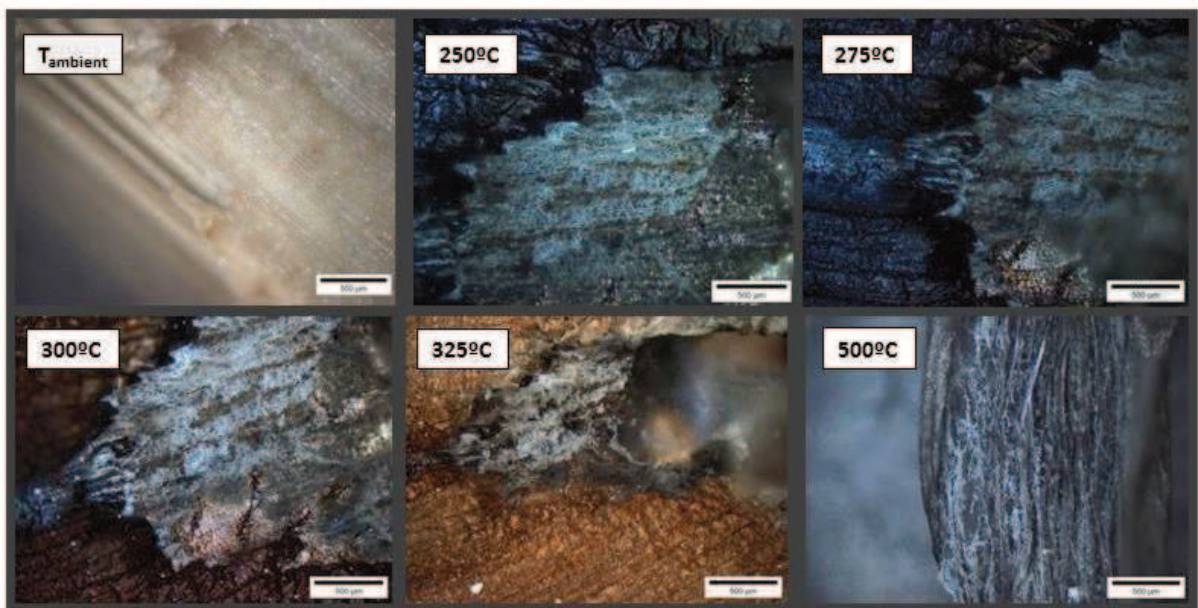


*Figure A2-2: degradation of miscanthus as a function of temperature-cross section*

APPENDIX-A 3: LM1 ASHES AFTER 10 MIN HEAT TREATMENT AT 1000 °C IN AIR

---

After 10 min of heat treatment at 1000 °C in air, small pieces of the miscanthus stem can be still observed. These pieces will become molten silica “islands” after longer residence time.

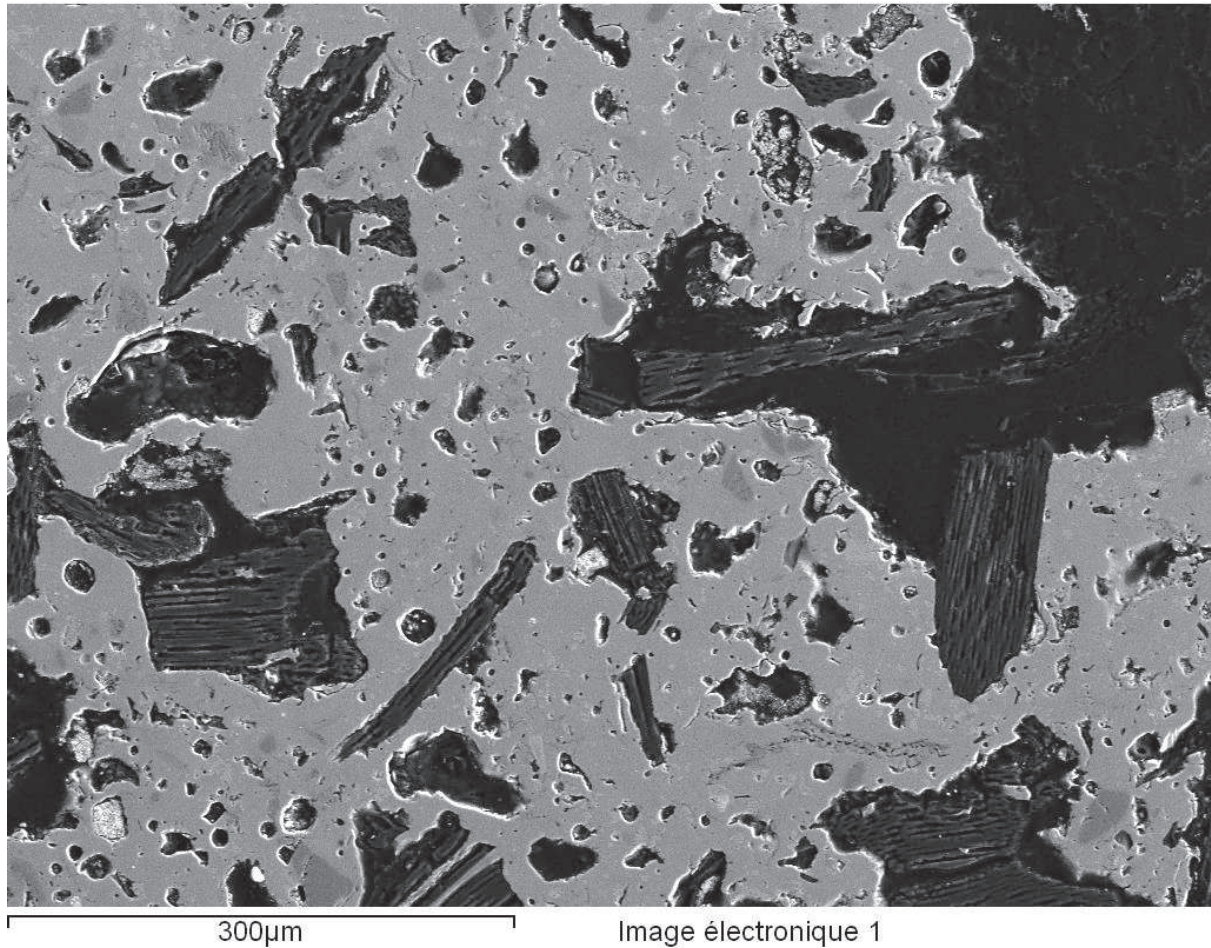


*Figure A3-1: LM1 ashes after 10 min of heat-treatment at 1000 °C in air*

APPENDIX-A 4: XR DIFFRACTOG OF LM2 ASHES

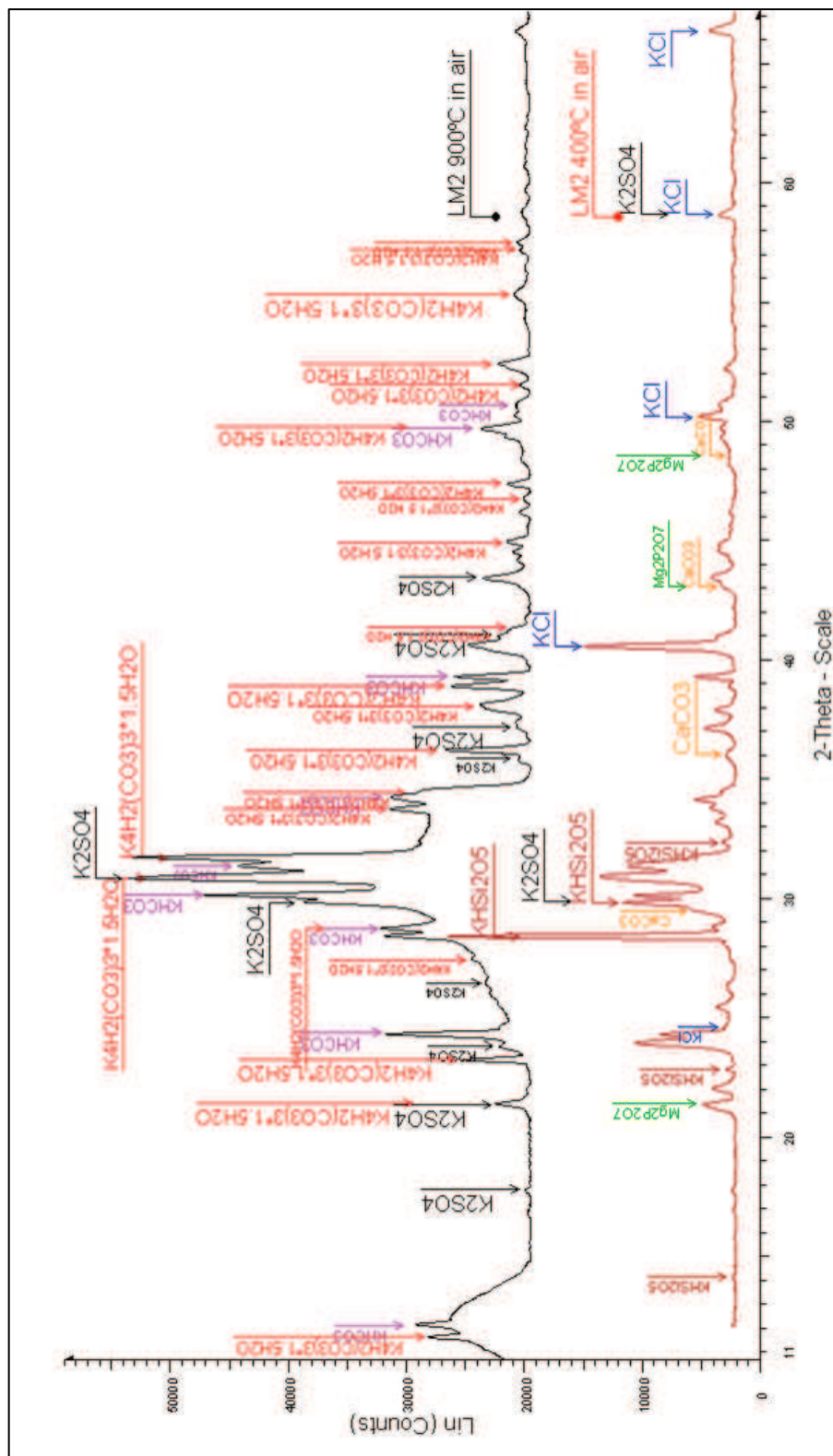


Figure A4-1: XR diffractog of LM2 ashes at 400 and 900 °C in air for 6h

APPENDIX-A 5: CALCULATING THE INPUT DATA OF MISCANTHUS ASHES FOR FACTSAGE

The first column shows the composition of ash. The second column shows the percentage of oxides in the plant considering 2.1% ash on dry base. The last column is the mass percentage of elements in the plant. The calculation is shown via the example of SiO<sub>2</sub>.

The ash consists of 66% SiO<sub>2</sub>. As the ash content of the plant on dry base is 2.1wt %, the SiO<sub>2</sub> content of the plant is  $66 \times 2.1 / 100 = 1.39 \text{ wt \%}$ . One mol of SiO<sub>2</sub> is  $28.1 + 2 \times 16 = 60.1 \text{g}$ . The weight percentage of Si in SiO<sub>2</sub> is  $28.1 / 60.1 \times 100 = 46.75 \approx 47\%$ .

From this, we obtain the weight percentage of Si in the plant by multiplying the SiO<sub>2</sub> content of the plant with the rate of Si in SiO<sub>2</sub>, namely  $1.39 \times 0.47 = 0.65$ .

Table A5-1: calculating the percentage of the main ash forming elements

ash	wt % in ash	wt % in plant	elements	rate of element in its oxide	wt % of elements in plant
SiO <sub>2</sub>	66	$66 \times 2.1 / 100 = 1.386$	Si	0.47	0.648
CaO	10.4	0.218	Ca	0.71	0.156
MgO	2.5	0.053	Mg	0.60	0.032
Na <sub>2</sub> O	1.1	0.023	Na	0.74	0.017
K <sub>2</sub> O	14.1	0.296	K	0.83	0.246
SO <sub>3</sub>	1.5	0.032	S	0.40	0.013
P <sub>2</sub> O <sub>5</sub>	1.6	0.034	P	0.44	0.015
<i>total</i>	<i>97.2</i>	<i>2.042</i>		<i>4.19</i>	<i>1.13</i>

APPENDIX-A 6: FTOXID, FTSALT AND FTPULP DATABASE- SOLUTION PHASES WITH COMPONENTS FOR THE MISCANTHUS ASH SYSTEM

Table A6-1: Components of the liquid and solid solution phases in FToxid database in case of 1 kg miscanthus

FT oxid -Solution Phases	
Liquid solution phases	FToxid-SLAGA : Na <sub>2</sub> O, K <sub>2</sub> O, SiO <sub>2</sub> , CaO, MgO, Na <sub>2</sub> S, K <sub>2</sub> S, SiS <sub>2</sub> , CaS, MgS
	FToxid-SLAGB : MgO, Na <sub>2</sub> O, SiO <sub>2</sub> , CaO, K <sub>2</sub> O, Na <sub>2</sub> SO <sub>4</sub> , K <sub>2</sub> SO <sub>4</sub> , CaSO <sub>4</sub> , MgSO <sub>4</sub>
	FToxid-SLAGC : MgO, Na <sub>2</sub> O, SiO <sub>2</sub> , CaO, Na <sub>3</sub> (PO <sub>4</sub> ), Ca <sub>3</sub> (PO <sub>4</sub> ) <sub>2</sub> , Mg <sub>3</sub> (PO <sub>4</sub> ) <sub>2</sub>
	FToxid-SLAGD : MgO, Na <sub>2</sub> O, SiO <sub>2</sub> , CaO, K <sub>2</sub> O, MgCO <sub>3</sub> , Na <sub>2</sub> CO <sub>3</sub> , K <sub>2</sub> CO <sub>3</sub> , CaCO <sub>3</sub>
	FToxid-SLAGE : MgO, Na <sub>2</sub> O, SiO <sub>2</sub> , CaO, K <sub>2</sub> O, H <sub>2</sub> O, NaOH, Ca(OH) <sub>2</sub> , Mg(OH) <sub>2</sub> , KOH
	FToxid-SLAGH :MgO, Na <sub>2</sub> O, SiO <sub>2</sub> , CaO, K <sub>2</sub> O, NaCl, KCl, CaCl <sub>2</sub> , MgCl <sub>2</sub>
	<b>Restrictions: None of them can be used simoultaneously</b>
Solid solution phases	FToxid-MeO_: Monoxide Rocksalt-str. Fe(2),Ca,Mg,Ni,Co,Mn(2);dilute Zn,Al,Cr,Fe(3),Mn(3), Cu,Zr
	FToxid-cPyr*: Clinopyroxene CaMgSi <sub>2</sub> O <sub>6</sub> , MgMgSi <sub>2</sub> O <sub>6</sub>
	FToxid-oPyr*: Orthopyroxene CaMgSi <sub>2</sub> O <sub>6</sub> , MgMgSi <sub>2</sub> O <sub>6</sub>
	FToxid-pPyr*: Protopyroxene CaMgSi <sub>2</sub> O <sub>6</sub> , MgMgSi <sub>2</sub> O <sub>6</sub>
	FToxid-LcPy*: LowClinopyroxene CaMgSi <sub>2</sub> O <sub>6</sub> , MgMgSi <sub>2</sub> O <sub>6</sub>
	FToxid-WOLL: Wollastonite MgSiO <sub>3</sub> , CaSiO <sub>3</sub>
	FToxid-bC2S: Mg <sub>2</sub> SiO <sub>4</sub> , Ca <sub>2</sub> SiO <sub>4</sub>
	FToxid-aC2S: Mg <sub>2</sub> SiO <sub>4</sub> , Ca <sub>2</sub> SiO <sub>4</sub>
	FToxid-OlivA*:Olivine MgMgSiO <sub>4</sub> , CaCaSiO <sub>4</sub> , CaMgSiO <sub>4</sub> , MgCaSiO <sub>4</sub>
	FToxid-NCSO: Na <sub>2</sub> Ca <sub>2</sub> Si <sub>3</sub> O <sub>9</sub> , Na <sub>4</sub> CaSi <sub>3</sub> O <sub>9</sub>
	* Possible miscibility gap when Ca is present

Table A6-2: Components of the liquid and solid solution phases in FTsalt database in case of 1 kg miscanthus

FT salt -Solution Phases	
Liquid solution phases	FTsalt-SALTA :NaCl, KCl, NaOH, KOH, MgCl <sub>2</sub> , CaCl <sub>2</sub> , CaO, Na <sub>2</sub> O, K <sub>2</sub> O, MgO,Ca(OH) <sub>2</sub> , Mg(OH) <sub>2</sub>
	FTsalt-SALTF :NaCl, KCl, NaOH, KOH, Na <sub>2</sub> SO <sub>4</sub> , K <sub>2</sub> SO <sub>4</sub> , Na <sub>2</sub> CO <sub>3</sub> , K <sub>2</sub> CO <sub>3</sub> , NaNO <sub>3</sub> , KNO <sub>3</sub>
	FTsalt-SALT?: NaCl, KCl, NaOH, KOH, Na <sub>2</sub> SO <sub>4</sub> , K <sub>2</sub> SO <sub>4</sub> , Na <sub>2</sub> CO <sub>3</sub> , K <sub>2</sub> CO <sub>3</sub> , NaNO <sub>3</sub> , KNO <sub>3</sub> , MgCl <sub>2</sub> , CaCl <sub>2</sub> , CaO, Na <sub>2</sub> O, K <sub>2</sub> O, MgO, Ca(OH) <sub>2</sub> , Mg(OH) <sub>2</sub>
	FTsalt-SAL2B: MgCl <sub>2</sub> , CaCl <sub>2</sub>
	FTsalt-LCSO : K <sub>2</sub> SO <sub>4</sub> , CaSO <sub>4</sub> , K <sub>2</sub> CO <sub>3</sub> , CaCO <sub>3</sub>
	FTsalt-LSUL : CaSO <sub>4</sub> , MgSO <sub>4</sub> , Na <sub>2</sub> SO <sub>4</sub>
<b>Restrictions:</b> <i>FTsalt_ACL_A cannot be used simoultaneously with FTsalt_ACL_C and FTsalt_ACL_?</i> <i>FTsalt_SALT A cannot be used simoultaneously with FTsalt_SALT F and FTsalt_SALT ?</i> <i>FTsalt_LCSO cannot be used simoultaneously with FTsalt_SALT, FTsalt_SAL2B and FTsalt_LSUL</i>	
Solid solution phases	FTsalt-ACL_A : NaCl, KCl, CaCl <sub>2</sub> , MgCl <sub>2</sub>
	FTsalt-ACL_C :NaCl, KCl, NH <sub>4</sub> Cl
	FTsalt-ACL_? : NaCl, KCl, CaCl <sub>2</sub> , MgCl <sub>2</sub> , NH <sub>4</sub> Cl
	FTsalt-ALKN : KNO <sub>3</sub> , NaNO <sub>3</sub>
	FTsalt-ALOH : NaOH, KOH
	FTsalt-AMX4A : Na <sub>2</sub> MgCl <sub>4</sub> , K <sub>2</sub> MgCl <sub>4</sub> , Na <sub>2</sub> CaCl <sub>4</sub> , K <sub>2</sub> CaCl <sub>4</sub>
	FTsalt-AOH_ : KOH, NaOH
	<b>FTsalt-CSOB : Na<sub>2</sub>CO<sub>3</sub>, K<sub>2</sub>CO<sub>3</sub>, Na<sub>2</sub>SO<sub>4</sub>, K<sub>2</sub>SO<sub>4</sub></b>
	FTsalt-KCO_ : Na <sub>2</sub> CO <sub>3</sub> , K <sub>2</sub> CO <sub>3</sub> , Na <sub>2</sub> SO <sub>4</sub> , K <sub>2</sub> SO <sub>4</sub>
	FTsalt-KCOH: KOH, KCl
	FTsalt-KNSO: K <sub>3</sub> Na(SO <sub>4</sub> ) <sub>2</sub> , Na <sub>4</sub> (SO <sub>4</sub> ) <sub>2</sub>
	<b>FTsalt-KSO_ : Na<sub>2</sub>SO<sub>4</sub>, K<sub>2</sub>SO<sub>4</sub>, Na<sub>2</sub>CO<sub>3</sub>, K<sub>2</sub>CO<sub>3</sub></b>
	FTsalt-MCIL: CaCl <sub>2</sub> , MgCl <sub>2</sub>
	FTsalt-MCOH: MgCl <sub>2</sub> , Mg(OH) <sub>2</sub>
	FTsalt-NCOA: NaCl, NaOH
	FTsalt-NCOB: NaCl, NaOH
	FTsalt-NHCl: NH <sub>4</sub> Cl, KCl
	FTsalt-NKCA: Na <sub>2</sub> CO <sub>3</sub> , K <sub>2</sub> CO <sub>3</sub> low temperature
	FTsalt-NKCB: Na <sub>2</sub> CO <sub>3</sub> , K <sub>2</sub> CO <sub>3</sub> high temperature
	FTsalt-PRVKA: perovskite NaMgCl <sub>3</sub> , KMgCl <sub>3</sub> , NaCaCl <sub>3</sub> , KCaCl <sub>3</sub>
	FTsalt-NKSO : Na <sub>2</sub> SO <sub>4</sub> , K <sub>2</sub> SO <sub>4</sub>
	FTsalt-SCMO: CaSO <sub>4</sub> , MgSO <sub>4</sub>
	FTsalt-SCSO : K <sub>2</sub> SO <sub>4</sub> , CaSO <sub>4</sub> , K <sub>2</sub> CO <sub>3</sub> , CaCO <sub>3</sub>
FTsalt-SSUL : CaSO <sub>4</sub> , MgSO <sub>4</sub> , Na <sub>2</sub> SO <sub>4</sub>	
FTsalt-SCSO : K <sub>2</sub> SO <sub>4</sub> , CaSO <sub>4</sub> , K <sub>2</sub> CO <sub>3</sub> , CaCO <sub>3</sub>	

Table A6-3: Components of the liquid and solid solution phases in FTpulp database in case of 1 kg miscanthus

FT pulp -Solution Phases	
Liquid solution phases	FTpulp-MELTA : NaCl, KCl, NaOH, KOH, Na <sub>2</sub> SO <sub>4</sub> , K <sub>2</sub> SO <sub>4</sub> , Na <sub>2</sub> CO <sub>3</sub> , K <sub>2</sub> CO <sub>3</sub> , Na <sub>2</sub> S, K <sub>2</sub> S
	FTpulp-MELTB : NaCl, KCl, NaOH, KOH, Na <sub>2</sub> SO <sub>4</sub> , K <sub>2</sub> SO <sub>4</sub> , Na <sub>2</sub> CO <sub>3</sub> , K <sub>2</sub> CO <sub>3</sub> , Na <sub>2</sub> O, K <sub>2</sub> O, Na <sub>2</sub> S <sub>2</sub> O <sub>7</sub> , K <sub>2</sub> S <sub>2</sub> O <sub>7</sub> , Na <sub>2</sub> O <sub>2</sub> , K <sub>2</sub> O <sub>2</sub> , Na <sub>2</sub> S <sub>3</sub> O <sub>10</sub> , K <sub>2</sub> S <sub>3</sub> O <sub>10</sub>
	FTpulp-MELTC : Na <sub>2</sub> S, K <sub>2</sub> S, Na <sub>2</sub> S <sub>2</sub> , K <sub>2</sub> S <sub>2</sub> , Na <sub>2</sub> S <sub>3</sub> , K <sub>2</sub> S <sub>3</sub> , Na <sub>2</sub> S <sub>4</sub> , K <sub>2</sub> S <sub>4</sub> , Na <sub>2</sub> S <sub>5</sub> , K <sub>2</sub> S <sub>5</sub> , Na <sub>2</sub> S <sub>6</sub> , K <sub>2</sub> S <sub>6</sub> , Na <sub>2</sub> S <sub>7</sub> , K <sub>2</sub> S <sub>7</sub> , Na <sub>2</sub> S <sub>8</sub> , K <sub>2</sub> S <sub>8</sub> , Na, K
	<b>Restrictions: None of them can be used simultaneously</b>
Solid solution phases	FTpulp-Hexa:Na <sub>2</sub> CO <sub>3</sub> , K <sub>2</sub> CO <sub>3</sub> , Na <sub>2</sub> SO <sub>4</sub> , K <sub>2</sub> SO <sub>4</sub> , Na <sub>2</sub> S, K <sub>2</sub> S
	FTpulp-OrtA:Na <sub>2</sub> SO <sub>4</sub> , K <sub>2</sub> SO <sub>4</sub> , Na <sub>2</sub> CO <sub>3</sub> , K <sub>2</sub> CO <sub>3</sub>
	FTpulp-OrtB: Na <sub>2</sub> SO <sub>4</sub> , K <sub>2</sub> SO <sub>4</sub> , Na <sub>2</sub> CO <sub>3</sub> , K <sub>2</sub> CO <sub>3</sub>
	FTpulp-KCO: Na <sub>2</sub> CO <sub>3</sub> , K <sub>2</sub> CO <sub>3</sub> , Na <sub>2</sub> SO <sub>4</sub> , K <sub>2</sub> SO <sub>4</sub>
	FTpulp-NKCB: Na <sub>2</sub> CO <sub>3</sub> , K <sub>2</sub> CO <sub>3</sub> , Na <sub>2</sub> SO <sub>4</sub> , K <sub>2</sub> SO <sub>4</sub>
	FTpulp-NKCA: Na <sub>2</sub> CO <sub>3</sub> , K <sub>2</sub> CO <sub>3</sub> , Na <sub>2</sub> SO <sub>4</sub> , K <sub>2</sub> SO <sub>4</sub>
	FTpulp-Gsrt: K <sub>3</sub> Na(SO <sub>4</sub> ) <sub>2</sub> , Na <sub>4</sub> (SO <sub>4</sub> ) <sub>2</sub>
	FTpulp-KPYR:K <sub>2</sub> S <sub>2</sub> O <sub>7</sub> , Na <sub>2</sub> S <sub>2</sub> O <sub>7</sub>
	FTpulp-NPYR: K <sub>2</sub> S <sub>2</sub> O <sub>7</sub> , Na <sub>2</sub> S <sub>2</sub> O <sub>7</sub>
	FTpulp-ALKA: Na, K
	FTpulp-NAKS: Na <sub>2</sub> S, K <sub>2</sub> S
	FTpulp-KNS2: Na <sub>2</sub> S <sub>2</sub> , K <sub>2</sub> S <sub>2</sub>
	FTpulp-AOH: KOH, NaOH
	FTpulp-ACL: NaCl, KCl, NaOH, KOH

## APPENDIX-A 7: SELECTING THE SOLUTION PHASES FOR THERMODYNAMIC CALCULATIONS

---

The main restriction of FactPS database is that it does not contain any solution phases. As the use of solutions can significantly affect the liquid phase formation, it is necessary to evaluate the possible solution phases for the current system and the most adequate ones.

### A7.1 POSSIBLE SOLUTION PHASES FOR THE MISCANTHUS SYSTEM

All the solid and liquid solution phases in FTsalt, FToxid and FTpulp databases were systematically tested for the miscanthus system in oxidizing and reducing atmosphere between 400 and 1000 °C at 1atm.

In most of the cases more solution phases can be selected at the same time and the software calculates the possible equilibrium compositions. Although in few cases the solution phases have to be tested one by one:

- The liquid solution phase of FToxid database (FToxid-SlagA, SlagB, slagC...), when the major oxide species dissolve different kind of salts
- The liquid salt solution phases FTsalt-SaltA (chlorides and oxides) and FTsalt-SaltF (chlorides, sulphates and carbonates)
- The liquid salt solution phases in FTpulp database: FTpulp-MeltA , FTpulp-MeltB (chlorid, sulphates, carbonates, oxides, sulphides) and FTpulp-MeltC (sulphides) in FTpulp database
- The solid salt solution in Ftsalt database; FTsalt-ACl\_A (alkali and alkaline earth metal chlorides) and FTsalt-ACl\_C(alkali metal and ammonium chlorides)

In some cases, incompatibility of the solution phases occurs, because the different solution phases were not optimized together. For example, FTsalt\_LCSO(K<sub>2</sub>SO<sub>4</sub>(l), CaSO<sub>4</sub>(l), K<sub>2</sub>CO<sub>3</sub>(l), CaCO<sub>3</sub>(l)) cannot be used simultaneously with FTsalt-SaltA/F (alkali and alkaline earth chloride, sulphate, carbonate and hydrdoxide), FTsalt\_SAL2B (MgCl<sub>2</sub>(l) and CaCl<sub>2</sub>(l)) and FTsalt\_LSUL (CaSO<sub>4</sub>(l), MgSO<sub>4</sub>(l), Na<sub>2</sub>SO<sub>4</sub>(l)).

When choosing a solution phase, the possibility of two or three immiscible phases can be also selected. While two immiscible phases can occur sometimes, three immiscible phases are usually never present<sup>1</sup>. Testing several solution phases in the same time has also a limit; the software can handle maximum 40 solution phases at once including the immiscible phases. Therefore, it is better to choose only single solution phases at first.

---

<sup>1</sup> ([Http://www.crct.polymtl.ca/fact/documentation](http://www.crct.polymtl.ca/fact/documentation))

Once the appropriate solution phases are chosen, the possibility of immiscible phases can be also tested.

After carrying out systematic calculations for combustion ( $ER > 1$ ) and gasification ( $ER = 0.33$ ) of 1 kg miscanthus, it was found that:

- Solid solution phases are calculated in each database (FToxid, FTpulp and FTsalt)
- The solid solution phases in FTpulp and FTsalt are identical. As no FTpulp liquid solution was calculated, this database can be neglected
- Four solid FTsalt solutions are possible in the range of 400 and 1000 °C:
  1. FTsalt-KSO\_ (Na and K sulphates and carbonates)
  2. FTsalt-SCMO (Ca and Mg sulphate)
  3. FTsalt-ACIA/ACIC (Na and K chloride)
  4. FTsalt-CSOB (Na and K sulphates and carbonates)
- Two solid oxide solution phases are present starting from 500 °C :
  1. FToxid-cPyrA clinopyrexene ( $CaMgSi_2O_6$ - $Mg_2SiO_6$ )
  2. FToxid -Wolla woolastonite ( $CaSiO_3$ - $MgSiO_3$ )
- No liquid salt solution was calculated for the current system
- Liquid solution phase is only present in case of FToxid

Three out of the four solid salt solutions (KSO\_, ACIA/C, SCMO) can be neglected from the further calculations for two reasons. Firstly, in these solution phases the weight percentage of the major compound is 99.99%. Secondly, these solution phases are present only at lower temperatures (between 400 and 600 °C), therefore their selection for high temperature applications is not indispensable.

As liquid oxide phase is present in the temperature range of fluidized bed gasification (800-900 °C), it has to be further investigated and the different liquid oxide solutions (FToxid-slagA, B...) have to be compared.

Table A7-1 summarizes the solid and liquid compounds in case of selecting or not selecting the solution phases.

*Table A7-1: summary of solid and liquid compounds using or not using solution phases*

Compounds	Selecting solution phases
$CaMgSi_2O_6$ (s)	$CaMgSi_2O_6$ - $MgMgSi_2O_6$ (FToxid cPyr)
$CaSiO_3$ (s)	$CaSiO_3$ - $MgSiO_3$ (FToxid Wolla)
$K_2SO_4$ (s)	$K_2SO_4$ - $Na_2SO_4$ (FTsalt KSO_ or FTsalt CSOB)
KCl (s)	KCl- $NaCl$ (FTsalt ACIA/C)
$CaSO_4$ (s)	$CaSO_4$ (FTsalt_SCMO), basically remains single species
$SiO_2$ (s)	Remains single species
$Na_2Ca_3Si_6O_{16}$ (s)	Remains single species
$Ca_2Mg_5Si_8O_{22}(OH)_2$ (s)	Remains single species
$Ca_5HO_{13}P_3$ (s)	Remains single species
$K_2Si_4O_9$ (s)	Remains single species
$Ca_3(PO_4)_2$ (s)	Remains single species
$K_2Si_4O_9$ (l)	$K_2O$ - $SiO_2$ - $Na_2O$ (FToxid slag) diluting salts

A7.2 THE EFFECT OF SOLID SOLUTION PHASES

As a next step, the effect of selecting solid solution phases on the phase transformation was studied both in combustion (ER>1) and gasification (ER=0.33). In all cases, FToxid-SlagA as liquid oxide solution was selected beside the solid solutions.

As seen in Figure A7-2, in case of combustion, 5-10% difference was found in the liquid to liquid plus solid ratio (L/(L+S)). Up to 875 °C there is more liquid phase using solid solution species, but this trend turns at 900 °C, and then the quantity of liquid phase becomes equal starting from 925 °C. The details of the calculation and the amount of solid and liquid compounds as a function of temperature are presented in Table A7-2.

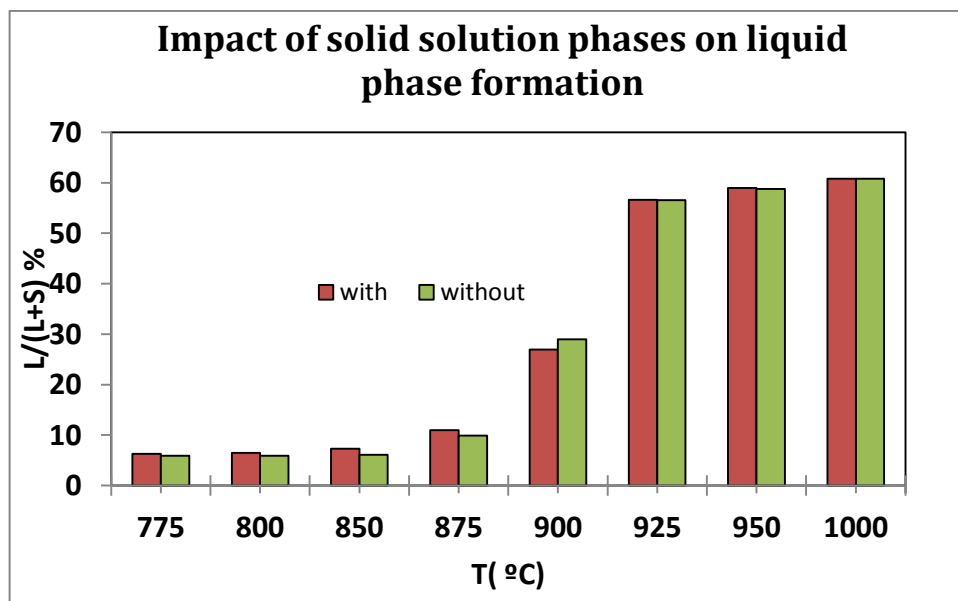


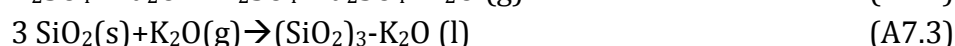
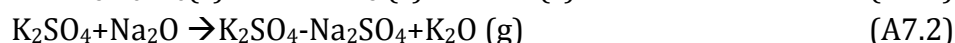
Figure A7-1: comparing the quantity of liquid and solid phases in case of selecting or not selecting solid solution phases

Table A7-2: comparing the quantity of liquid and solid phases in case of selecting or not selecting solid solution phases

Temperature (Cels)		775	800	850	875	900	925	950	1000
Liquid (L) (g)	with	1.37	1.42	1.59	2.38	5.63	11.17	11.61	11.93
	without	1.30	1.30	1.32	2.14	6.02	11.15	11.57	11.93
Solid (S) (g)	with	20.59	20.50	20.23	19.24	15.26	8.55	8.08	7.68
	without	<b>20.66</b>	<b>20.61</b>	<b>20.48</b>	<b>19.45</b>	<b>14.73</b>	<b>8.57</b>	<b>8.12</b>	<b>7.68</b>
L/(S+L) %	with	6.26	6.46	7.27	11.00	26.96	56.65	58.96	60.83
	without	5.92	5.93	6.07	9.90	29.01	56.56	58.78	60.83
<b>L/(S + L) without</b>		0.95	0.92	0.84	0.90	1.08	1.00	1.00	1.00
<b>L/(S + L) with</b>									

Table A7-3 and Table A7-4 show the difference in the amount of the main compounds in case of selecting or not selecting solid solution phases in combustion (ER>1) and gasification (ER=0.33). Altering trends in the composition indicates that there are competing reactions present.

Without solution phases, the formation of Na<sub>2</sub>Ca<sub>3</sub>Si<sub>6</sub>O<sub>16</sub> is favoured, while using solution phases promote the formation of K<sub>2</sub>SO<sub>4</sub>-Na<sub>2</sub>SO<sub>4</sub> via the decomposition of Na<sub>2</sub>Ca<sub>3</sub>Si<sub>6</sub>O<sub>16</sub> into NaO, CaSiO<sub>3</sub> and SiO<sub>2</sub>. This results in more SiO<sub>2</sub> and K<sub>2</sub>O and in consequence more liquid potassium silicate solution.



Above 900 °C the solid sulphates and silicates start to decompose and form liquid oxides.

As K<sub>2</sub>SO<sub>4</sub>-Na<sub>2</sub>SO<sub>4</sub> thermodynamically is more stable than K<sub>2</sub>SO<sub>4</sub>, its decomposition is slower. This results in more solid phase between 900 and 1000 °C. With the complete decomposition of sulphates and silicates above 1000 °C, the difference in liquid to solid ratio using or not using solid solutions disappears.

Table A7-3: difference in the amount of main compounds (s-solid, l-liquid, g-gas) in case of combustion (ER>1)

Δ with -without								
Temperature (Cels)	775	800	850	875	900	925	950	1000
Na <sub>2</sub> Ca <sub>3</sub> Si <sub>6</sub> O <sub>16</sub> (s)	-0.13	-0.20	-0.45	-0.61	-0.52	-0.04	-0.07	0.00
Na <sub>2</sub> SO <sub>4</sub> (s)	0.03	0.05	0.11	0.14	0.13	0.00	0.00	0.00
K <sub>2</sub> SO <sub>4</sub> (s)	-0.04	-0.06	-0.12	-0.11	0.17	0.00	0.00	0.00
CaSiO <sub>3</sub> (s)	0.09	0.13	0.29	0.39	0.34	0.06	0.10	0.08
SiO <sub>2</sub> (s)	-0.01	-0.02	-0.06	0.01	0.45	0.00	-0.01	0.00
SiO <sub>2</sub> (l)	0.05	0.09	0.19	0.18	-0.29	0.01	0.03	0.00
K <sub>2</sub> O (l)	0.02	0.03	0.07	0.06	-0.09	0.00	0.00	0.00
Na <sub>2</sub> O (l)	0.00	0.00	0.00	0.00	0.00	0.00	0.01	0.00
SO <sub>2</sub> (g)	0.00	0.00	0.00	-0.02	-0.12	0.00	0.00	0.00

In reductive atmosphere the S does not form solid sulphates; therefore the Na remains bounded in the Na<sub>2</sub>Ca<sub>3</sub>Si<sub>6</sub>O<sub>16</sub> and no difference can be observed in liquid to solid ratios. There is only slightly difference starting from 800 °C. When no solid solution is selected, there is more CaMgSi<sub>2</sub>O<sub>6</sub> present, while selecting solid solution phases results in more Mg<sub>2</sub>Si<sub>2</sub>O<sub>6</sub>, MgSiO<sub>3</sub>, CaSiO<sub>3</sub>.

Table A7-4: difference in the amount of main compounds (s-solid, l-liquid) in case of gasification (ER=0.33)

$\Delta$ with -without							
Temperature (Cels)	400	500	600	700	800	900	1000
Na <sub>2</sub> O(l)	0.00	0.00	0.00	0.00	0.00	0.00	0.00
K <sub>2</sub> O(l)	0.00	0.00	0.00	0.00	0.00	0.00	0.00
SiO <sub>2</sub> (l)	0.00	0.00	0.00	0.00	0.00	0.01	0.00
CaO(l)	0.00	0.00	0.00	0.00	0.00	0.00	0.00
MgO(l)	0.00	0.00	0.00	0.00	0.00	0.00	0.00
CaMgSi <sub>2</sub> O <sub>6</sub> (s)	0.00	0.00	0.00	-0.01	-0.03	-0.06	-0.15
MgMgSi <sub>2</sub> O <sub>6</sub> (s)	0.00	0.00	0.00	0.00	0.00	0.01	0.02
MgSiO <sub>3</sub> (s)	0.00	0.00	0.00	0.00	0.01	0.02	0.05
CaSiO <sub>3</sub> (s)	0.00	0.00	0.00	0.01	0.01	0.04	0.08
NaCl(s)	0.00	0.00	0.00	0.00	0.00	0.00	0.00
KCl(s)	0.00	0.00	0.00	0.00	0.00	0.00	0.00
SiO <sub>2</sub> (s)	0.00	0.00	0.00	0.00	0.00	0.00	0.00
K <sub>2</sub> Si <sub>2</sub> O <sub>5</sub> (s)	0.00	0.00	0.00	0.00	0.00	0.00	0.00
K <sub>2</sub> Si <sub>4</sub> O <sub>9</sub> (s)	0.00	0.00	0.00	0.00	0.00	0.00	0.00
Na <sub>2</sub> Ca <sub>3</sub> Si <sub>6</sub> O <sub>16</sub> (s)	0.00	0.00	0.00	0.00	0.00	-0.02	0.00
C(s)	0.00	0.00	0.00	0.00	0.00	0.00	0.00
Ca <sub>3</sub> (PO <sub>4</sub> ) <sub>2</sub> (s)	0.00	0.00	0.00	0.00	0.00	0.00	0.00
Ca <sub>5</sub> HO <sub>13</sub> P <sub>3</sub> (s)	0.00	0.00	0.00	0.00	0.00	0.00	0.00

### A7.3 COMPARISON OF LIQUID SOLUTION PHASES

For 1 kg miscanthus, the presence of liquid oxide solution phase (FToxid-Slag) was calculated. The Ftoxid-Slag database consist of CaO, K<sub>2</sub>O, SiO<sub>2</sub> and MgO dissolving different inorganic compounds such as sulphides (*SlagA*), sulphates (*SlagB*), phosphates (*SlagC*), carbonates (*SlagD*), hydroxides (*SlagE*), nitride, carbide and cyanide (*SlagG*) and chlorides (*slagH*). The solution phase FToxid-Slag? contains all the above mentioned forms of inorganics but cannot be used reliably as it was not validated.

All the liquid solution phases were systematically tested for ER=0.33 and ER>1 between 400 and 1000 °C at 1 atm.

The calculation could not been performed in case of the *slagG* and *slag?*. The other six solution phases gave similar results regarding the solidus temperature, except the case of *SlagC*. Although the solution phases were selected with possibility of two immiscible phases, only one solution phase were predicted up to 1000 °C.

Figure A7-2 and Figure A7-3 compare the quantity of solid and liquid phases and the liquid to solid ratio in combustion (ER>1) and in gasification (ER=0.33) atmosphere at 1000 °C in case of selecting different FToxid-Slag solution phases. As it can be seen, all

but one (SlagC) solution phases give similar results. The solidus temperature is between 760 and 770 °C in all cases.

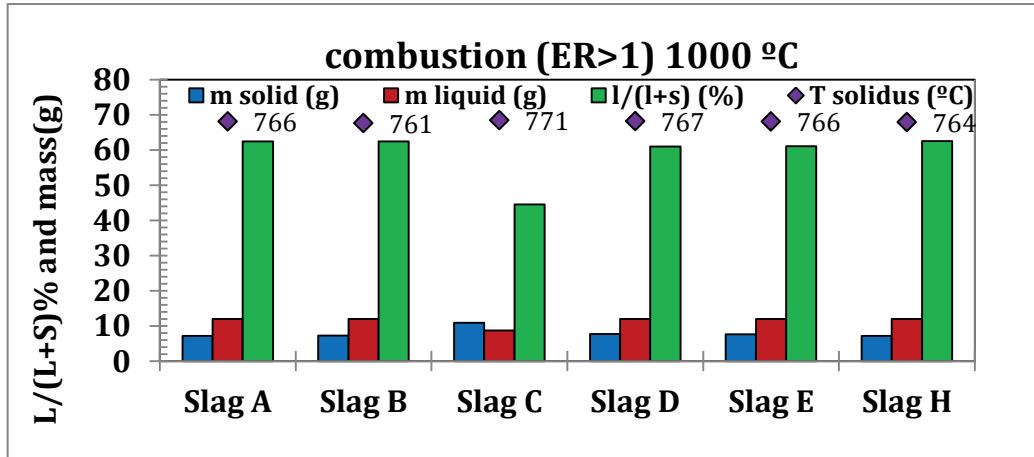


Figure A7-2: Quantity of solid and liquid phases and the liquid to solid ratio in oxidizing atmosphere(ER>1) at 1000 °C in case of selecting different FT<sub>oxid</sub>-Slag solution phases. Above the bars, the liquidus temperature is noted

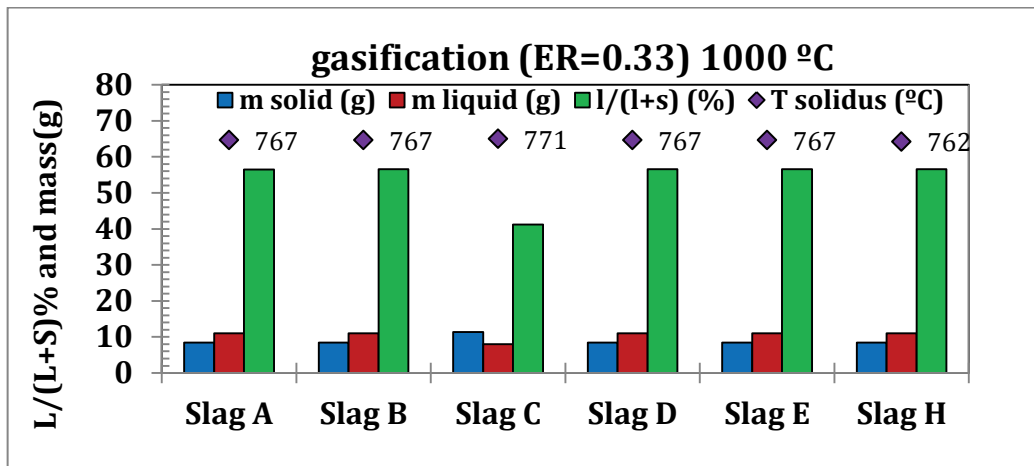


Figure A7-3: Quantity of solid and liquid phases and the liquid to solid ratio in reducing atmosphere (ER=0.33) at 1000 °C in case of selecting different FT<sub>oxid</sub>-Slag solution phases. Above the bars, the liquidus temperature is noted

Figure A7-4 and Figure A7-5 compare the composition of liquid phase in case of selecting different slag solutions at 1000 °C in oxidizing (ER>1) and in reducing (ER=0.33) atmosphere. The composition of liquid phase is similar in each case. According to the calculation, the liquid phase is composed of K<sub>2</sub>O and SiO<sub>2</sub> and a very small amount of Na<sub>2</sub>O. One exception is *SlagC* solution phase, where liquid phase is present as a pure compound (K<sub>2</sub>Si<sub>4</sub>O<sub>9</sub>) at 771 °C and liquid solution only forms at 1021 °C. It has to be noted that in oxidising atmosphere, at lower temperature (around 850 °C) K<sub>2</sub>SO<sub>4</sub> can be dissolved in the liquid oxide phase in case of FT<sub>oxid</sub>-SlagB, but it was not calculated at higher temperatures. In the case of the other solution phases, the

amounts of dissolved salts in the liquid oxide solution such as carbonates and hydroxides are not significant (wt % < 0.001). At 1000 °C the amount of Na<sub>2</sub>O increases and the K<sub>2</sub>SO<sub>4</sub> in *slagB* decomposes.

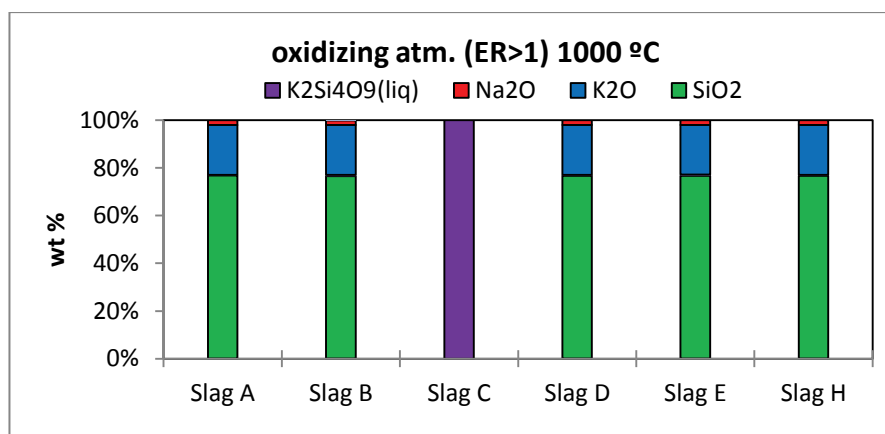


Figure A7-4: Composition of liquid phase at 1000 °C in oxidizing atmosphere (ER > 1) in case of selecting different FT<sub>oxid</sub>-Slag solution phases

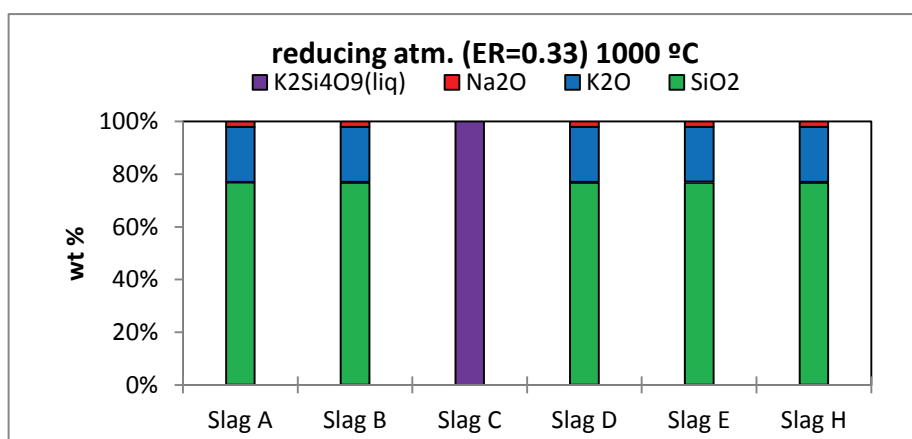


Figure A7-5: Composition of liquid phase at 850 °C and 1000 °C using different slags in gasification (ER = 0.33)

FT<sub>oxid</sub>-SlagC is rejected from our choice as it does not agree with the experimental observation about slag formation. All the different liquid solution phases give almost identical values for the composition of liquid phase. The main components of liquid phase are K<sub>2</sub>O and SiO<sub>2</sub>. The concentration of minor components available in the different solution phases (carbonates, sulphides, halides) is not relevant in combustion. In case of SlagB, 2% of sulphate was calculated at 850 °C. As the CaO-K<sub>2</sub>O-SiO<sub>2</sub> ternary system has not yet been validated in FactSage, the error deriving from using/not using slagB for the calculation in combustion is not significant.

APPENDIX-A 8: COMPARISON OF LIQUID AND SOLID PHASES AT 850 °C

The composition of ash for combustion and gasification is compared at 850 °C in Table A8-1. Although the composition of slag is the same in gasification and combustion, there is a big difference in the rate of the liquid phase, it is much higher in gasification than in combustion (Table A8-2). As the composition of slag is identical in combustion and gasification, the viscosity of slag is also the same. As expected, the viscosity of slag decreases as a function of temperature as shown in Table A8-1. The value of viscosity is in the range of that of corn syrup or honey.

Table A8-1: Composition of solid and liquid phases at 850 °C in gasification and combustion

T=850 °C, slagA		Er>1 combustion		ER=0.33 gasification	
		m(g)	wt %	m(g)	wt %
solid	SiO <sub>2</sub>	9.3	42.6	3.3	17
	CaMgSi <sub>2</sub> O <sub>6</sub> -Mg <sub>2</sub> Si <sub>2</sub> O <sub>6</sub>	2.6	12.1	2.6	13
	Ca <sub>5</sub> H <sub>13</sub> P <sub>3</sub>	0.5	2.5	0.5	3
	Na <sub>2</sub> Ca <sub>3</sub> Si <sub>6</sub> O <sub>16</sub>	2.0	9.3	2.1	10.8
	CaSiO <sub>3</sub>	1.4	6.5	1.4	7
	K <sub>2</sub> SO <sub>4</sub> -Na <sub>2</sub> SO <sub>4</sub>	4.3	19.8	0	0
	slag	SiO <sub>2</sub>	1.2	5.4	7.1
	K <sub>2</sub> O	0.4	1.8	2.4	12
L/(L+S) %		7.3		48.9	

Table A8-2 Composition of slag at 850 °C in gasification and combustion

	T=850 °C, slagA	
	Er>1 combustion	ER=0.33 gasification
L/(L+S)	6%	48%
wt % K <sub>2</sub> O	25.4	25.4
wt % SiO <sub>2</sub>	74.2	74.2
wt % Na <sub>2</sub> O	0.4	0.4
wt % CaO	0.02	0.02

Table A8-3: Viscosity of slag at 850 and 1000 °C in gasification and combustion

	viscosity ln[Pa s]	
T ( °C)	gasification	combustion
850	10.4	10.5
1000	8.0	8.0

APPENDIX-A 9: INFLUENCE OF MAIN ASH FORMING ELEMENTS

The input data for the calculation is:

- 1 kg of miscanthus (LM1):

S, Ca, Mg, K, P, Na, Cl and Al were chosen as variables and Si as fix component. As 1kg miscanthus contains 6.5g Si (analysed by SOCOR), the quantity of the variables was chosen between 0 and 6.5g. The original amount and ratio to Si of the elements are presented in Table A9- 1.

Table A9-1: amount of chosen elements in 1 kg of miscanthus and their ratio to Si

	Mass (g)	X*/Si
S	1.7	0.26
Ca	1.6	0.25
Mg	0.3	0.05
K	2.5	0.38
P	0.1	0.02
Cl	1	0.15
Na	0.2	0.03
Al	-	-
X*= S, Ca, Mg, K, P, Cl, Na and Al		

- Reagent:

Combustion (ER=1.01): 1341g O<sub>2</sub>

Gasification with limited air supply (ER=0.33): 444g O<sub>2</sub>

- Temperature: 900 °C

- Pressure: 1 atm

- Databases: FactPS, FToxid, FTsalt

- Solid solution phases

FToxid AWollastonite (components for the current calculation: MgSiO<sub>3</sub>, CaSiO<sub>3</sub>)

FToxid AClinopyroxene (components for the current calculation: CaMgSi<sub>2</sub>O<sub>6</sub>, MgMgSi<sub>2</sub>O<sub>6</sub>)

FTsalt-AAlkCl-ss\_rocksalt (components for the current calculation: KCl, NaCl)

FTsalt-CSOB (components for the current calculation: Na<sub>2</sub>CO<sub>3</sub>, K<sub>2</sub>CO<sub>3</sub>, Na<sub>2</sub>SO<sub>4</sub>, K<sub>2</sub>SO<sub>4</sub>)

FTsalt-SCMO (components for the current calculation: CaSO<sub>4</sub>, MgSO<sub>4</sub>)

- Liquid solution phases:

FToxid-slagA (components for the current calculation: Na<sub>2</sub>O, K<sub>2</sub>O, SiO<sub>2</sub>, CaO, MgO, Na<sub>2</sub>S, K<sub>2</sub>S, SiS<sub>2</sub>, CaS, MgS)

Figure A9-1 and Figure A9-2 illustrate the liquid to solid plus liquid ratio versus quantity of variables. The dots represent the original concentration of the elements in miscanthus ashes.

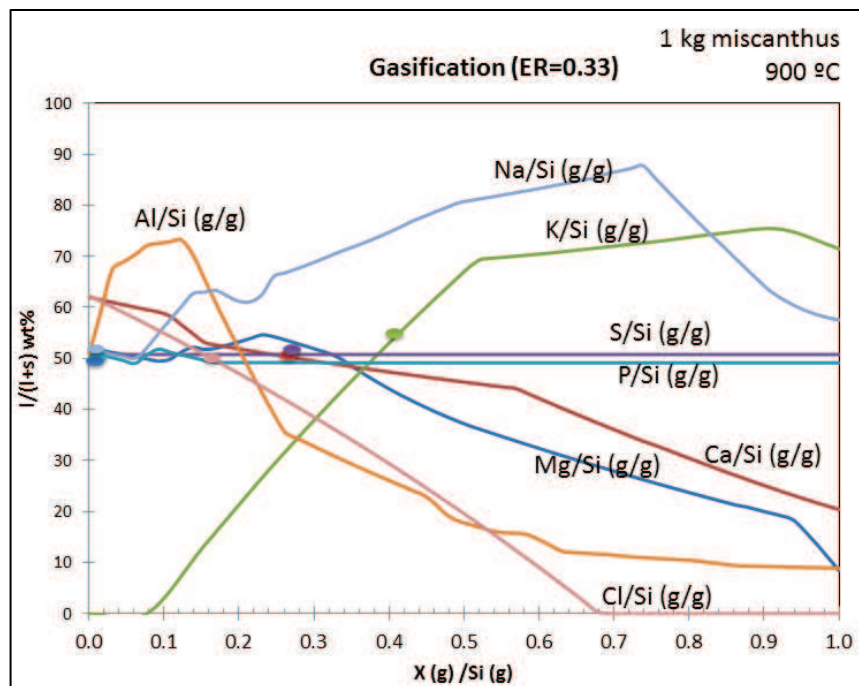


Figure A9-1: Liquid to solid ratio as a function of ash composition at 900 °C in case of gasification (ER=0.33)

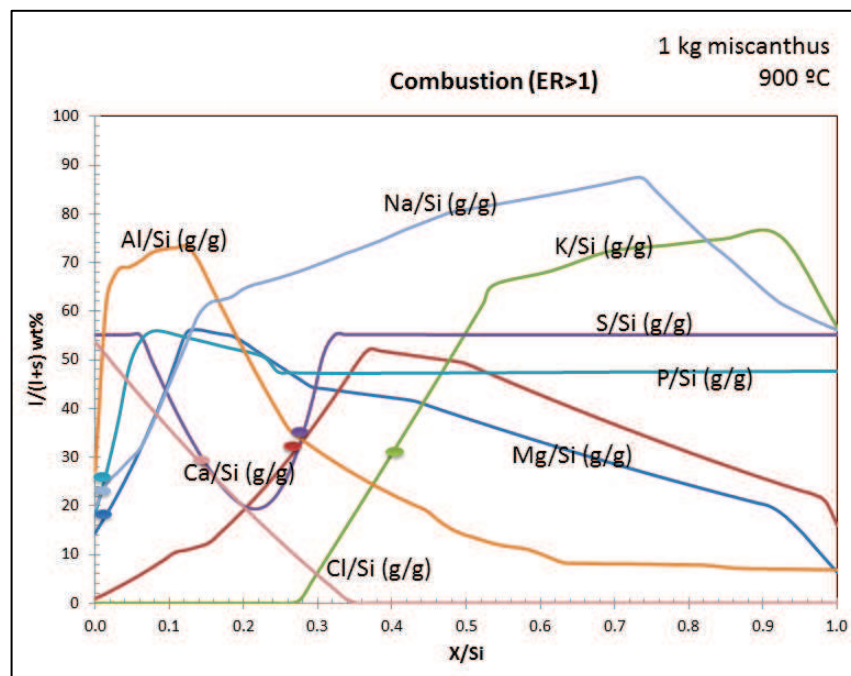


Figure A9-2: Liquid to solid ratio as a function of ash composition at 900 °C in case of combustion (ER=1.01)

Figure A9-3 shows the effect of increasing sulphur (S) in case of combustion. At certain range of S concentration, solid  $K_2SO_4$  forms. While K is retained in the solid phase,  $SiO_2$  is in solid form as well. However, above a certain concentration of S, the  $K_2SO_4$  is not stable any more, and the amount of liquid  $SiO_2$ - $K_2O$  rises again. Increasing the amount of S has no more effect on liquid and solid phase ratio, as S does not stay in the condensed phase but forms directly  $SO_2(g)$  in case of combustion. In case of gasification, sulphur is released into the gaseous phase as  $H_2S(g)$ . Figure A9-4 and Figure A9-5 show the distribution of solid and liquid phases in gasification and combustion versus K concentration. Increasing K promotes the formation of liquid phase ( $SiO_2$ - $K_2O$ ). At very high quantity of K a new solid phase  $K_2SiO_5$  develops which slightly decreases the liquid to solid ratio. In combustion, K can be retained as  $K_2SO_4$ ; therefore the amount of liquid phase starts to increase somewhat higher K concentration. To avoid high amount of liquid, K has to be minimised as much as possible.

The same tendency was observed in case of increasing Na concentration (Figure A9-6 and Figure A9-7).

The increase of Ca and Mg concentration promotes the formation of  $CaSiO_3$  and  $Mg_2SiO_4$  both in combustion and gasification (Figure A9-10 to A9-13), therefore they can be considered as an additives to avoid agglomeration. However, attention has to be paid in case of combustion. At lower concentration both Ca and Mg increase the amount of liquid phase by promoting the decomposition of  $K_2SO_4$ . In combustion, the increase of Mg and Ca is only suggested if their original concentration is already elevated.

The increasing concentration of Cl decreases the quantity of liquid phase but increases the amount of gaseous HCl and KCl which will cause corrosion and deposition on the heat exchangers (Figure A9-8 and Figure A9-9). High Cl concentration should be avoided.

The addition of Al in small concentration increases the amount of liquid phase as it contributes to the slag formation via  $Al_2O_3$  (l) (Figure A9-14 and Figure A9-15). However, at higher concentration, new solid phases are formed;  $KAlSi_2O_6$ ,  $CaAl_2Si_2O_8$ ,  $Al_6Si_2O_{13}$  and  $Al_2O_3$ , therefore amount of liquid phase significantly decreases.

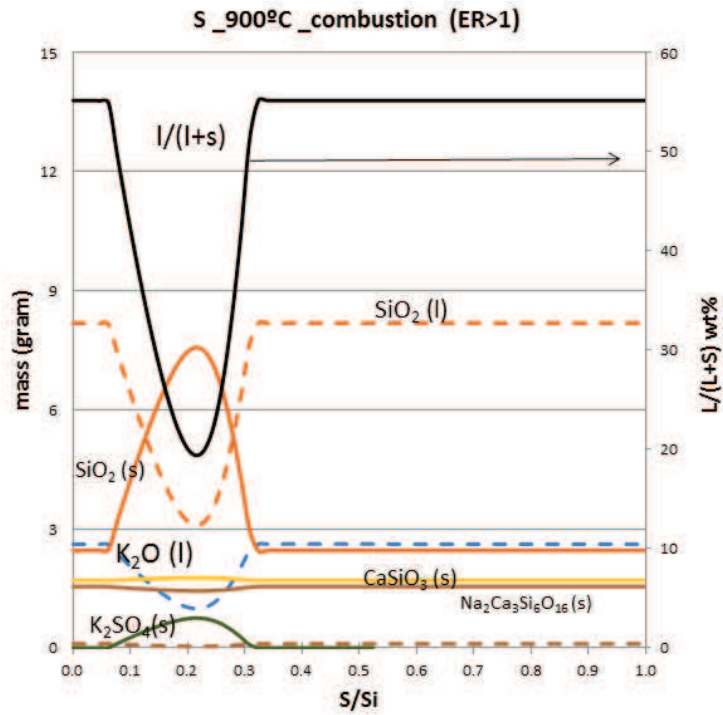


Figure A9-3: distribution of solid and liquid phases in ash as a function of S concentration (900 °C, ER=1.01)

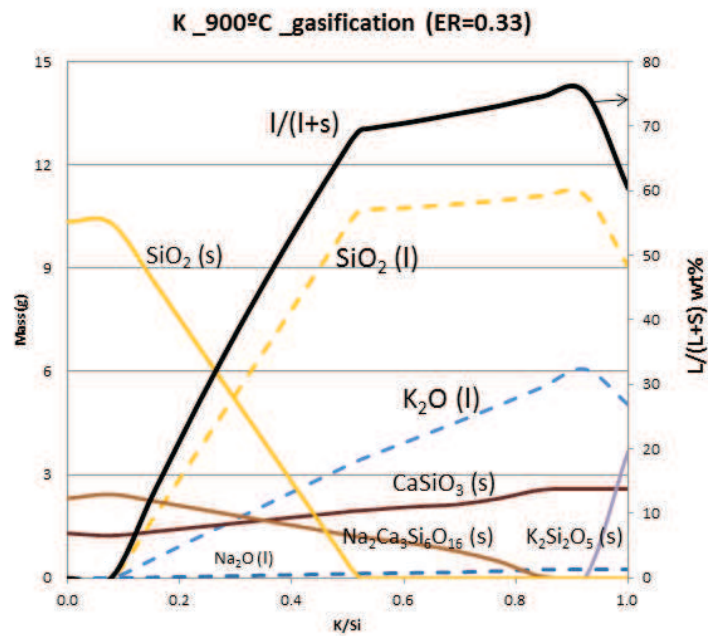


Figure A9-4: evolution of liquid to liquid plus solid ratio and main compounds versus K concentration at 900° in case of gasification ER=0.33

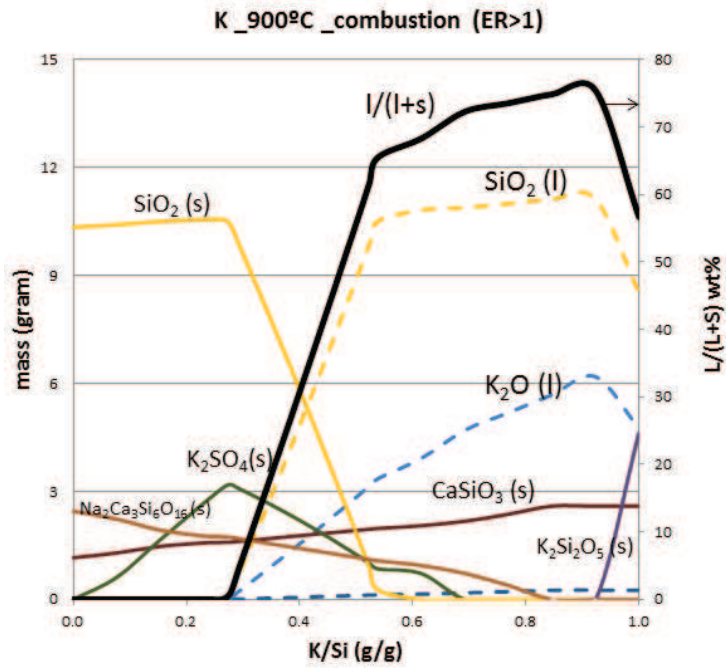


Figure A9-5: evolution of liquid to liquid plus solid ratio and main compounds versus K concentration at 900° in case of combustion ER>1

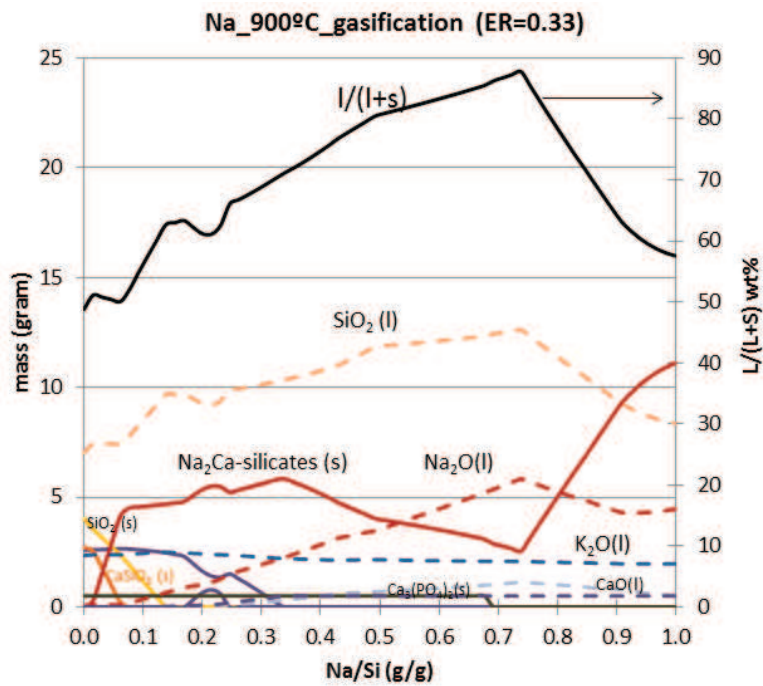


Figure A9-6: evolution of liquid to liquid plus solid ratio and main compounds versus Na concentration at 900° in case of gasification ER=0.33

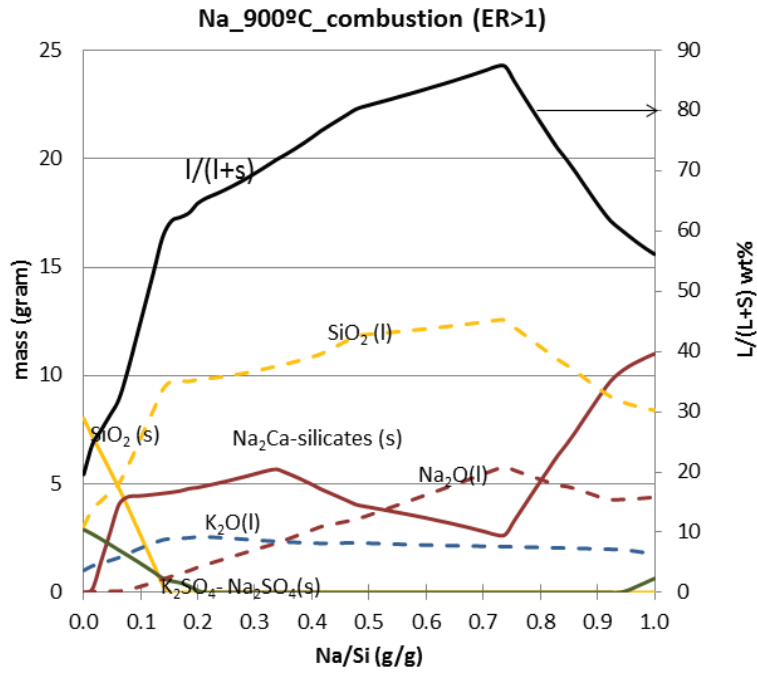


Figure A9-7: evolution of liquid to liquid plus solid ratio and main compounds versus Na concentration at 900° in case of combustion ER>1

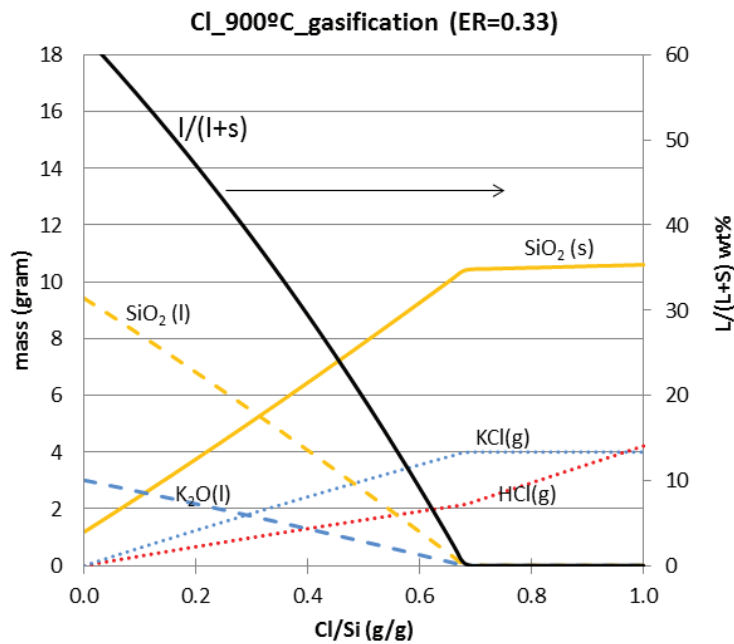


Figure A9-8: evolution of liquid to liquid plus solid ratio and main compounds versus Cl concentration at 900° in case of gasification ER=0.33

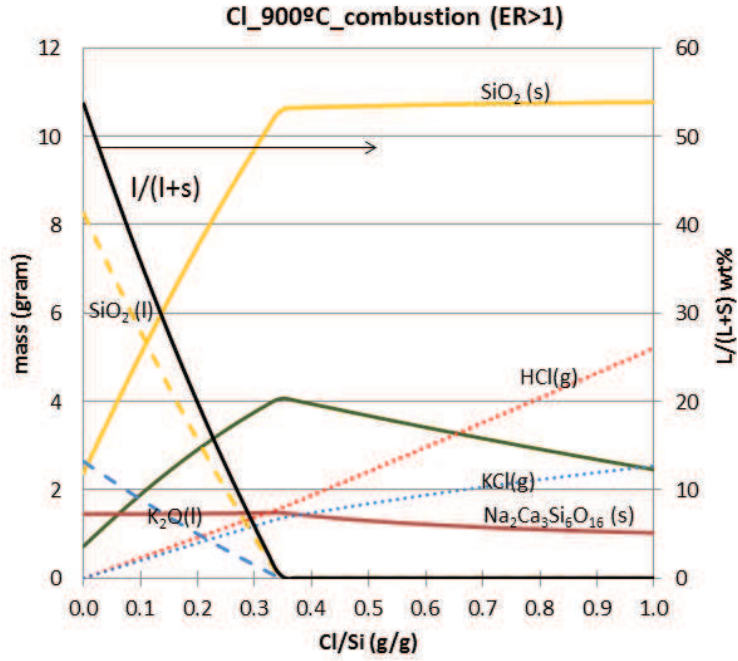


Figure A9-9: evolution of liquid to liquid plus solid ratio and main compounds versus Cl concentration at 900° in case of combustion ER>1

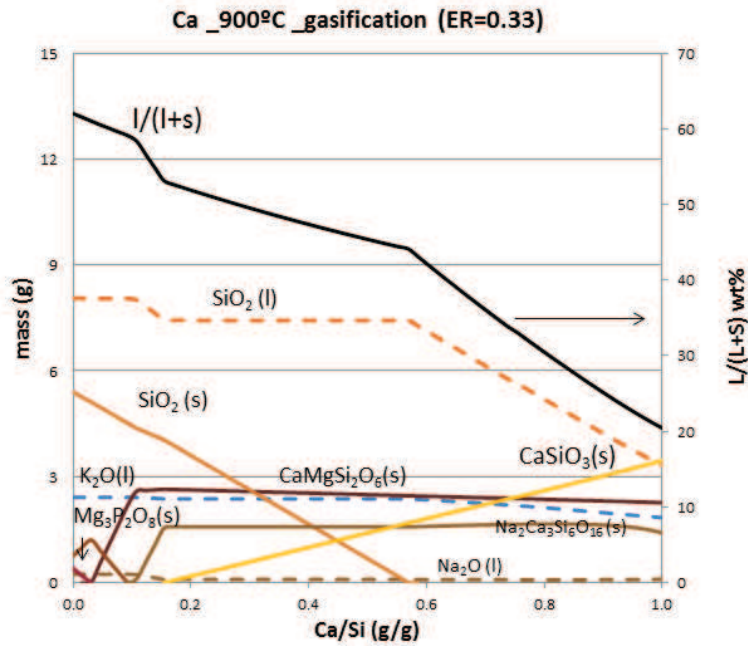


Figure A9-10: evolution of liquid to liquid plus solid ratio and main compounds versus Ca concentration at 900° in case of gasification ER=0.33

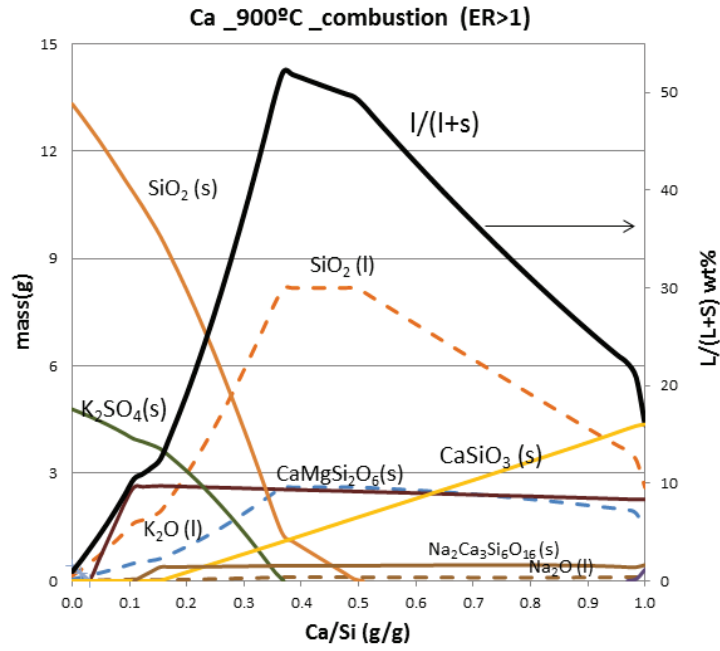


Figure A9-11: evolution of liquid to liquid plus solid ratio and main compounds versus Ca concentration at 900° in case of combustion ER>1

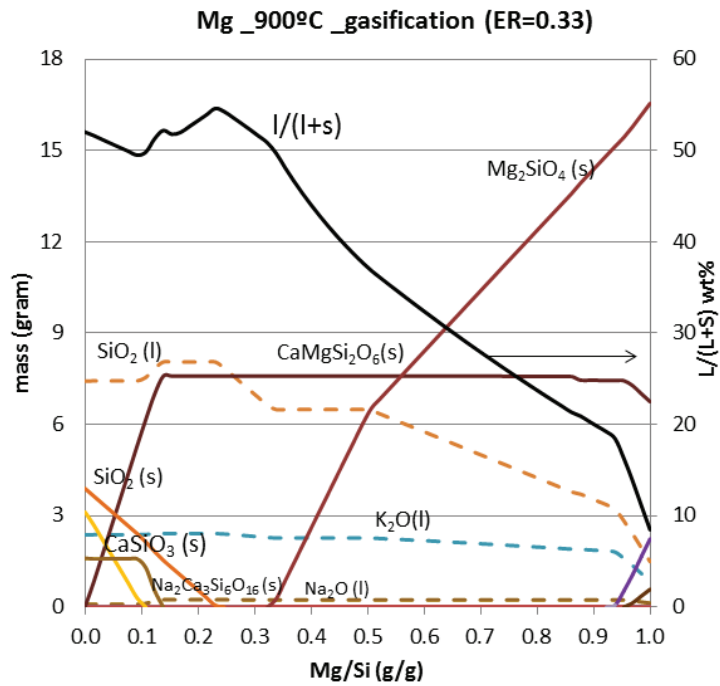


Figure A9-12: evolution of liquid to liquid plus solid ratio and main compounds versus Mg concentration at 900° in case of gasification ER=0.33

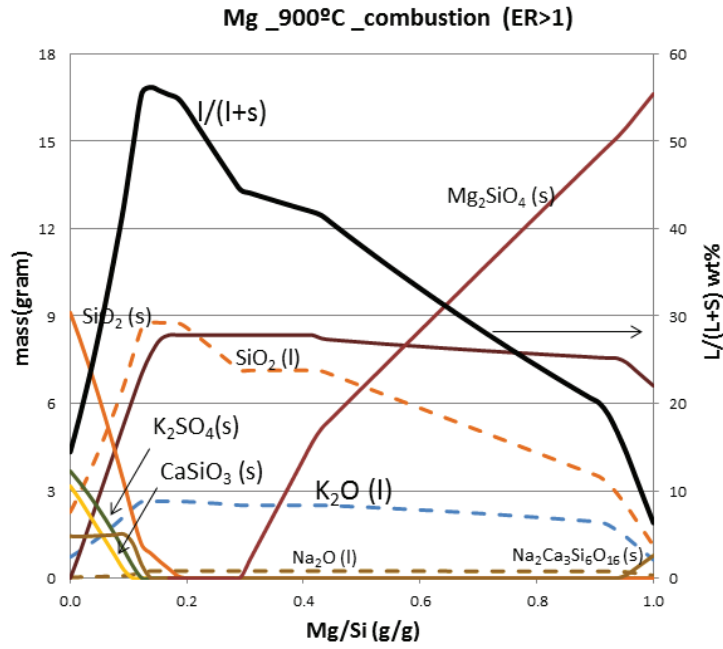


Figure A9-13: evolution of liquid to liquid plus solid ratio and main compounds versus Mg concentration at 900° in case of combustion ER>1

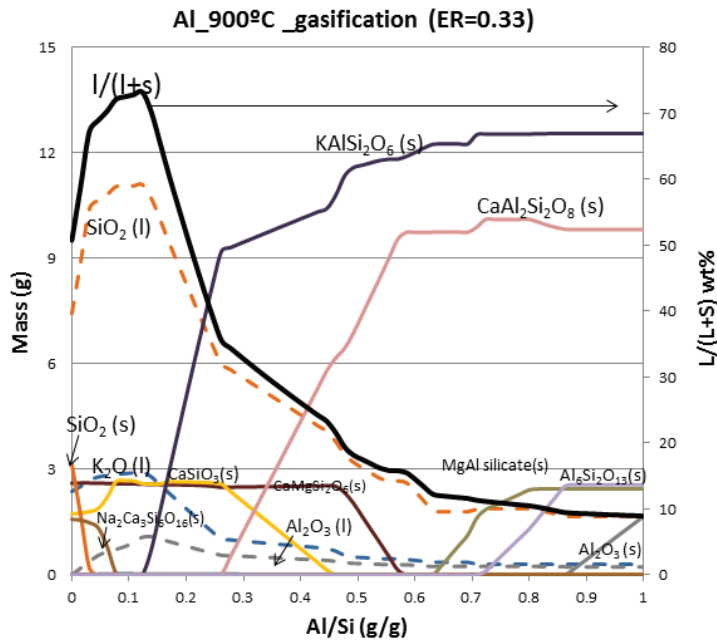


Figure A9-14: evolution of liquid to liquid plus solid ratio and main compounds versus Al concentration at 900° in case of gasification ER=0.33

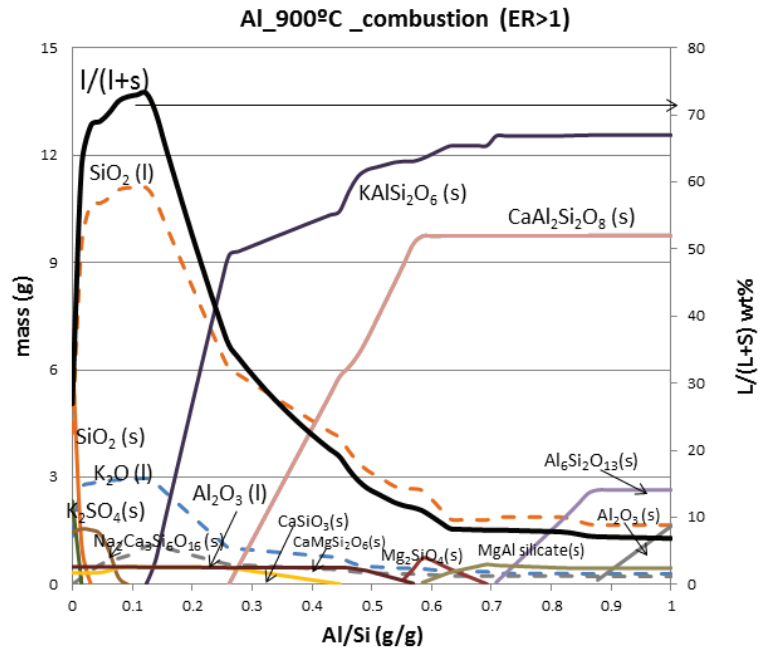


Figure A9-15: evolution of liquid to liquid plus solid ratio and main compounds versus Al concentration at 900° in case of combustion ER>1

APPENDIX-A 10: FTOXID AND GTOXID DATABASES

Table A10-1: Comparison of solid and liquid compounds in combustion calculated using FToxid or GToxid database

combustion				Ftoxid	Gtoxid
solid phase	salts	chloride	KCl	✓	✓
		sulphates	K <sub>2</sub> SO <sub>4</sub>	✓	✓
			CaSO <sub>4</sub>	✓	✓
		phosphates	Ca <sub>3</sub> (PO <sub>3</sub> ) <sub>4</sub>	✓	✓
			Ca <sub>5</sub> HO <sub>13</sub> P <sub>3</sub>	✓	✓
	silicates	silica	SiO <sub>2</sub>	✓	✓
		silicates with alkali metals	Na <sub>2</sub> Ca <sub>3</sub> Si <sub>6</sub> O <sub>16</sub>	✓	✓
			<b>K<sub>2</sub>Si<sub>4</sub>O<sub>9</sub></b>	✓	✗
			<b>K<sub>2</sub>Si<sub>5</sub>MgO<sub>12</sub></b>	✗	✓
			<b>K<sub>2</sub>Si<sub>12</sub>Mg<sub>5</sub>O<sub>30</sub></b>	✗	✓
			<b>Ca<sub>2</sub>K<sub>2</sub>Si<sub>9</sub>O<sub>21</sub></b>	✗	✓
			<b>Ca<sub>3</sub>K<sub>2</sub>Si<sub>6</sub>O<sub>16</sub></b>	✗	✓
		silicates with alkaline earth metal	<b>Ca<sub>2</sub>Mg<sub>5</sub>Si<sub>8</sub>O<sub>22</sub>(OH)<sub>2</sub></b>	✓	✗
			<b>CaSiO<sub>3</sub>-MgSiO<sub>3</sub> (WOLLA)</b>	✓	✗
	CaMgSi <sub>2</sub> O <sub>6</sub> - MgMgSi <sub>2</sub> O <sub>6</sub>		✓(cPyrA#1)	✓(CLIN)	
liquid phase	slag	Na <sub>2</sub> O(SLAGA)	✓	✗	
		SiO <sub>2</sub> (SLAGA)	✓	✗	
		K <sub>2</sub> O(SLAGA)	✓	✗	
	molten salt	<b>Na<sub>2</sub>SO<sub>4</sub>(SALTF)</b>	✗	✓	
		<b>K<sub>2</sub>SO<sub>4</sub>(SALTF)</b>	✗	✓	
	molten silicates	K <sub>2</sub> Si <sub>2</sub> O <sub>5</sub> (LIOX)	✗	✓	
		K <sub>2</sub> Si <sub>4</sub> O <sub>9</sub> (LIOX)	✗	✓	
		Si <sub>2</sub> O <sub>4</sub> (LIOX)	✗	✓	
		Si <sub>2</sub> Na <sub>2</sub> O <sub>5</sub> (LIOX)	✗	✓	
		CaSiO <sub>3</sub> (LIOX)	✗	✓	
		SiMgO <sub>3</sub> (LIOX)	✗	✓	
		Na <sub>2</sub> Ca <sub>3</sub> Si <sub>6</sub> O <sub>16</sub> (LIOX)	✗	✓	
	K <sub>2</sub> Si <sub>5</sub> MgO <sub>12</sub> (LIOX)	✗	✓		

Table A10-2: Comparison of solid and liquid compounds in combustion calculated using FToxid or GToxid database

gasification			FToxid	GToxid	
solid phase	salts		C	✓	✓
		chloride	KCl	✓	✓
		phosphates	Ca <sub>3</sub> (PO <sub>3</sub> ) <sub>4</sub>	✓	✓
	Ca <sub>5</sub> HO <sub>13</sub> P <sub>3</sub>		✓	✓	
	silicates	silica	SiO <sub>2</sub>	✓	✓
		silicates with alkali metals	Na <sub>2</sub> Ca <sub>3</sub> Si <sub>6</sub> O <sub>16</sub>	✓	✗
			Na <sub>2</sub> CaSi <sub>5</sub> O <sub>12</sub>	✗	✓
			K <sub>2</sub> Si <sub>2</sub> O <sub>5</sub>	✓	✗
			K <sub>2</sub> Si <sub>4</sub> O <sub>9</sub>	✓	✗
			K <sub>2</sub> Si <sub>5</sub> MgO <sub>12</sub>	✗	✓
			Ca <sub>2</sub> K <sub>2</sub> Si <sub>9</sub> O <sub>21</sub>	✗	✓
			Ca <sub>3</sub> K <sub>2</sub> Si <sub>6</sub> O <sub>16</sub>	✗	✓
			Ca <sub>23</sub> K <sub>2</sub> Si <sub>12</sub> O <sub>48</sub>	✗	✓
		silicates with alkaline earth metal	Ca <sub>2</sub> Mg <sub>5</sub> Si <sub>8</sub> O <sub>22</sub> (OH) <sub>2</sub>	✓	✗
			CaSiO <sub>3</sub> -MgSiO <sub>3</sub> (WOLLA)	✓	✗
CaMgSi <sub>2</sub> O <sub>6</sub> - MgMgSi <sub>2</sub> O <sub>6</sub> (cPyrA#1)			✓	✗	
liquid phase	slag	Na <sub>2</sub> O(SLAGA)	✓	✗	
		SiO <sub>2</sub> (SLAGA)	✓	✗	
		K <sub>2</sub> O(SLAGA)	✓	✗	
	molten salt	NaCl(SALTF#1)	✗	✓	
		KCl(SALTF#1)	✗	✓	
	molten silicates	K <sub>2</sub> Si <sub>2</sub> O <sub>5</sub> (LIOX)	✗	✓	
		Si <sub>2</sub> O <sub>4</sub> (LIOX)	✗	✓	
		CaSiO <sub>3</sub> (LIOX)	✗	✓	
		Si <sub>2</sub> Na <sub>2</sub> O <sub>5</sub> (LIOX)	✗	✓	
		CaSiO <sub>3</sub> (LIOX)	✗	✓	
SiMgO <sub>3</sub> (LIOX)	✗	✓			

APPENDIX-A 11: COMPARING LIQUID PHASE COMPOSITION AT 1000 °C

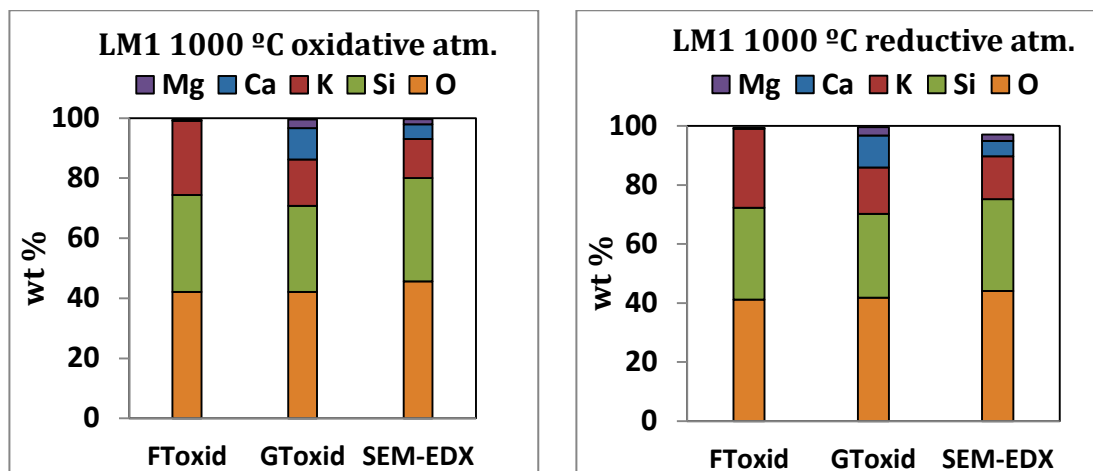


Figure A11-2: Comparison (FToxid, GToxid, SEM analysis) of liquid phase composition of LM1 ashes at 1000 °C in oxidizing and in reducing atmosphere

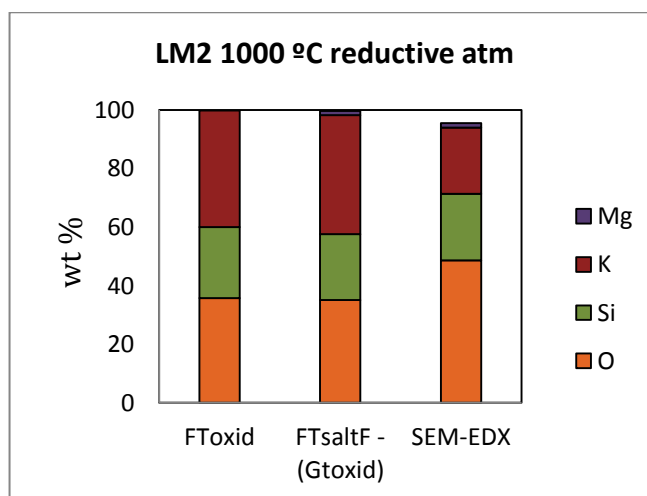
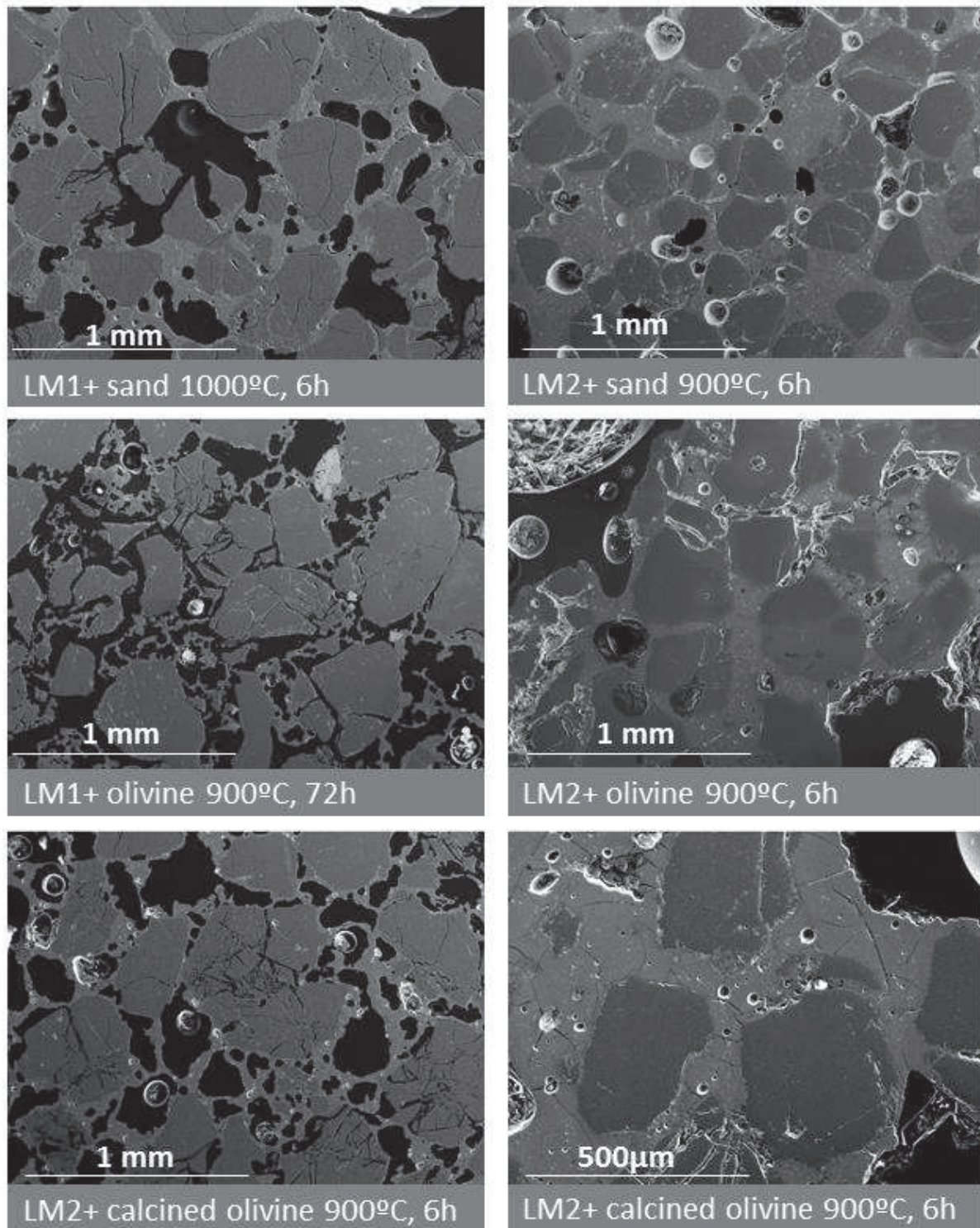


Figure A11-1: Comparison (FToxid, GToxid, SEM analysis) of liquid phase composition of LM2 ashes at 1000 °C in reducing atmosphere

APPENDIX-A 12: WETTING OF BED MATERIALS BY MOLTEN LM1 AND LM2 ASHES



*Figure A12-1: Wetting of sand, olivine and calcined olivine by LM1 and LM2 miscanthus ashes at high temperature(900 and 1000 °C)*

APPENDIX-A 13: MAGNESIUM FERRITE IN CALCINED OLIVINE

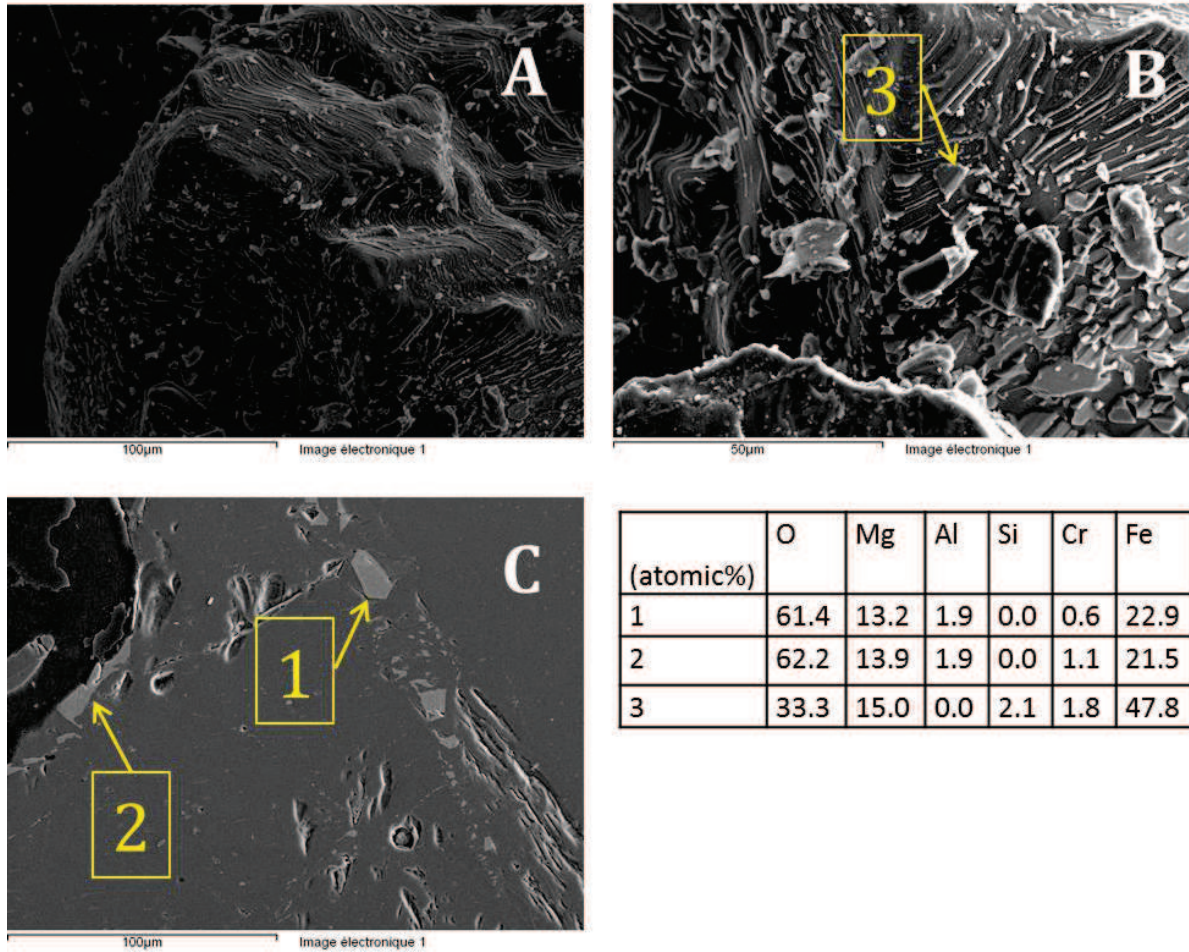


Figure A13-1 : Magnesium ferrite ( $MgFe_2O_4$ ) in calcined olivine

APPENDIX-A 14: DETERMINING THE MINIMUM FLUIDIZATION RATE AT 750 °C

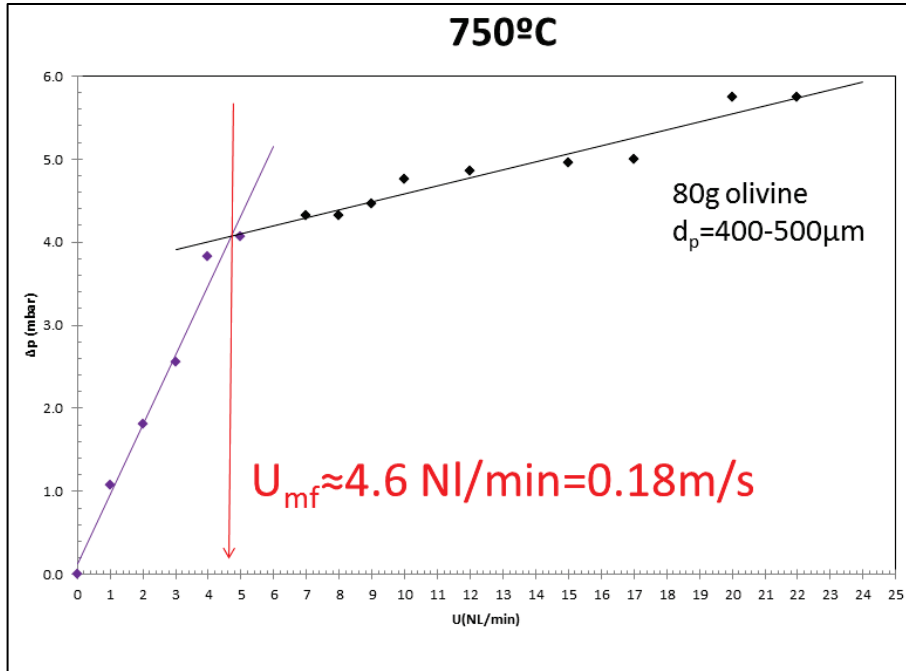


Figure A14-1 : Determining the minimum fluidization rate from the pressure drop over the bed at 750 °C

Table A14-1 : the pressure drop in the fluidized hot device (CEMHTI, CNRS) at 750 °C

MESURE A CHAUD (750°C)											
Conditions	Q (l/min)	H1 (mm)	H2 (mm)	Htotal (m)	ΔP (Pa)	ΔP (mbar)	ΔP fritté (mbar)	ΔP bed (mbar)	ΔPexp/ΔPtheo (lit)	X	σ
Montage à vide Tfour=750°C	0	0	0	0.0000	0.0	0.0	Non mesuré				
	1	3	3	0.0060	58.9	0.6					
	2	7.5	8	0.0155	152.1	1.5					
	3	11	11	0.0220	215.8	2.2					
	4	16	16	0.0320	313.9	3.1					
	5	21	21	0.0420	412.0	4.1					
	6	26	26	0.0520	510.1	5.1					
	7	30.5	30.5	0.0610	598.4	6.0					
	8	35	35	0.0700	686.7	6.9					
	9	39.5	40	0.0795	779.9	7.8					
	10	43.5	44	0.0875	858.4	8.6					
	12	50.5	51	0.1015	995.7	10.0					
15	60	61	0.1210	1187.0	11.9						
17	65	66	0.1310	1285.1	12.9						
20	72	73	0.1450	1422.5	14.2						
22	76	77.5	0.1535	1505.8	15.1						
Fluidisation 80g olivine 400-500μm T°C = 750°C	0	0	0	0.0000	0.0	0.0	Non mesuré		0.0	0.000	
	1	8.5	8.5	0.0170	166.8	1.7		0.0	1.1	0.229	
	2	17	17	0.0340	333.5	3.3		1.8	0.384		
	3	24	24	0.0480	470.9	4.7		2.6	0.540		
	4	35.5	35.5	0.0710	696.5	7.0		3.8	0.810		
	5	41.5	42	0.0835	819.1	8.2		4.1	0.862		
	6	47.5	48	0.0955	936.9	9.4		4.3	0.904		
	7	52	53	0.1050	1030.1	10.3		4.3	0.914		
	8	57	57	0.1140	1118.3	11.2		4.3	0.914		
	9	62	63	0.1250	1226.3	12.3		4.5	0.945		
	10	67.5	68.5	0.1360	1334.2	13.3		4.8	1.008		0.994
	12	75	76	0.1510	1481.3	14.8		4.9	1.028		
15	85	86.5	0.1715	1682.4	16.8		5.0	1.049			
17	90	92	0.1820	1785.4	17.9		5.0	1.059			
20	101	102.5	0.2035	1996.3	20.0		5.7	1.215			
22	105	107	0.2120	2079.7	20.8		5.7	1.215			

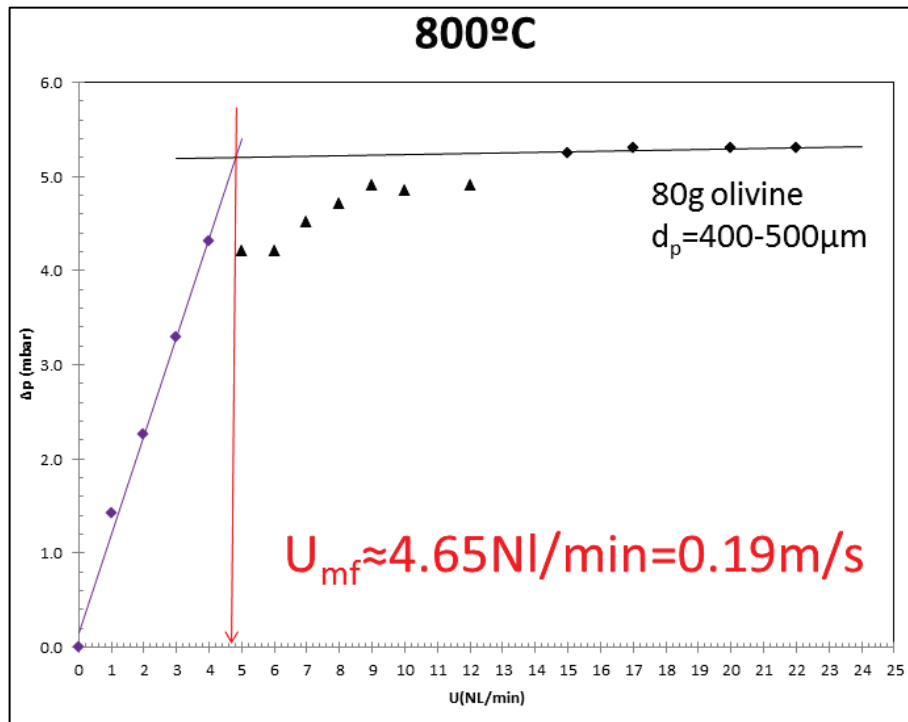


Figure A14-2 : Determining the minimum fluidization rate from the pressure drop over the bed at 800 °C

Table A14-2 : the pressure drop in the fluidized hot device (CEMHTI, CNRS) at 800 °C

MESURE A CHAUD (800°C)												
Conditions	Q (l/min)	H1 (mm)	H2 (mm)	Htotal (m)	ΔP (Pa)	ΔP (mbar)	ΔP fritté (mbar)	ΔP lit (mbar)	ΔPexp/ΔPtheo (lit)	X	σ	
Montage à vide Tfour=800°C	0	0	0	0.0000	0.0	0.0	Non mesuré					
	1	3	3	0.0060	58.9	0.6						
	2	7	7	0.0140	137.3	1.4						
	3	11	11	0.0220	215.8	2.2						
	4	17	17	0.0340	333.5	3.3						
	5	23	23	0.0460	451.3	4.5						
	6	28	28	0.0560	549.4	5.5						
	7	33	34	0.0670	657.3	6.6						
	8	37.5	37.5	0.0750	735.8	7.4						
	9	42	42.5	0.0845	828.9	8.3						
	10	47	48	0.0950	932.0	9.3						
	12	54	56	0.1100	1079.1	10.8						
15	64	65	0.1290	1265.5	12.7							
17	70	72	0.1420	1393.0	13.9							
20	79	81	0.1600	1569.6	15.7							
22	84	86	0.1700	1667.7	16.7							
Fluidisation 80g olivine 400-500μm T°C = 800°C	0	0	0	0.0000	0.0	0.0	Non mesuré		0.0	0.000		
	1	10.5	10	0.0205	201.1	2.0			1.4	0.301		
	2	18.5	18.5	0.0370	363.0	3.6			2.3	0.478		
	3	27.5	28	0.0555	544.5	5.4			3.3	0.696		
	4	39	39	0.0780	765.2	7.7			4.3	0.914		
	5	44	45	0.0890	873.1	8.7			4.2	0.893		
	6	49	50	0.0990	971.2	9.7			4.2	0.893		
	7	56	57	0.1130	1108.5	11.1			4.5	0.956		
	8	61	62	0.1230	1206.6	12.1			4.7	0.997		
	9	66.5	68	0.1345	1319.4	13.2			4.9	1.039		
	10	71.5	73	0.1445	1417.5	14.2			4.9	1.028		
	12	79	81	0.1600	1569.6	15.7			4.9	1.039		
15	90	92.5	0.1825	1790.3	17.9			5.2	1.111			
17	97	99	0.1960	1922.8	19.2			5.3	1.122			
20	106	108	0.2140	2099.3	21.0			5.3	1.122	0.995		
22	111	113	0.2240	2197.4	22.0			5.3	1.122			

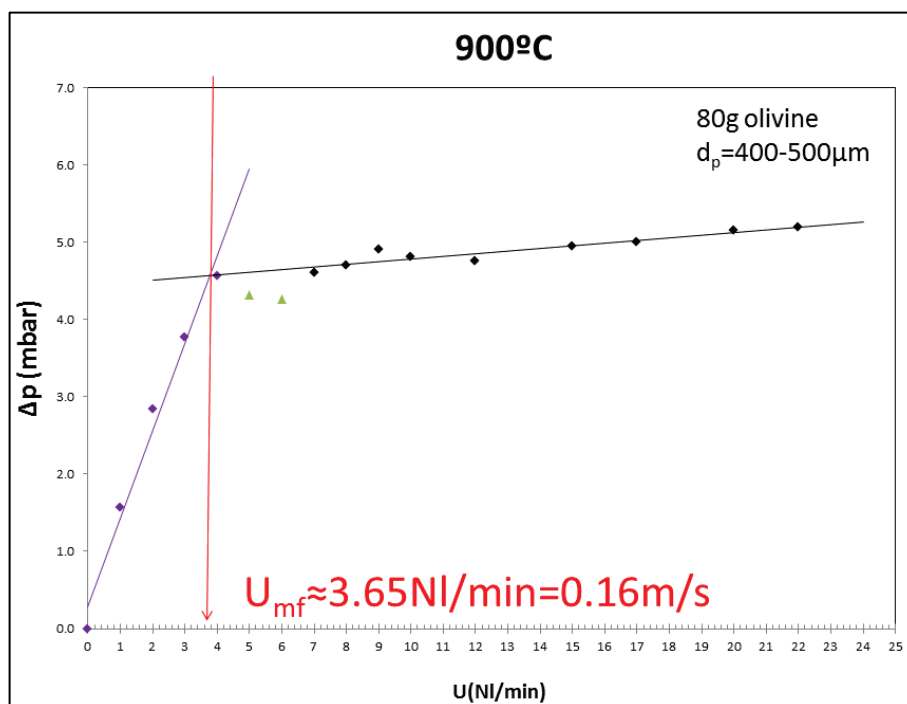


Figure A14-3 : Determining the minimum fluidization rate from the pressure drop over the bed at 900 °C

Table A14-3 :the pressure drop in the fluidized hot device (CEMHTI, CNRS) at 800 °C

MESURE A CHAUD (900°C)												
Conditions	Q (l/min)	H1 (mm)	H2 (mm)	Htotal (m)	ΔP (Pa)	ΔP (mbar)	ΔP fritté (mbar)	ΔP lit (mbar)	ΔPexp/ΔPtheo (lit)	X	σ	
Montage à vide Tfour=900°C	0	0	0	0.0000	0.0	0.0	Non mesuré					
	1	3	3	0.0060	58.9	0.6						
	2	7.5	7.5	0.0150	147.2	1.5						
	3	11	11	0.0220	215.8	2.2						
	4	16	16	0.0320	313.9	3.1						
	5	22	22	0.0440	431.6	4.3						
	6	27	27	0.0540	529.7	5.3						
	7	32.5	33	0.0655	642.6	6.4						
	8	37	37.5	0.0745	730.8	7.3						
	9	41.5	42	0.0835	819.1	8.2						
	10	47	48	0.0950	932.0	9.3						
	12	55	57	0.1120	1098.7	11.0						
15	65	67	0.1320	1294.9	12.9							
17	72	73.5	0.1455	1427.4	14.3							
20	80.5	83	0.1635	1603.9	16.0							
22	86	88	0.1740	1706.9	17.1							
Fluidisation 80g olivine 400-500μm T°C = 900°C	0	0	0	0.0000	0.0	0.0	Non mesuré		0.0	0.000		
	1	11	11	0.0220	215.8	2.2			1.6	0.332		
	2	22	22	0.0440	431.6	4.3			2.8	0.602		
	3	30	30.5	0.0605	593.5	5.9			3.8	0.800		
	4	39	39.5	0.0785	770.1	7.7			4.6	0.966		
	5	43	45	0.0880	863.3	8.6			4.3	0.914		
	6	48	49.5	0.0975	956.5	9.6			4.3	0.904		
	7	55.5	57	0.1125	1103.6	11.0			4.6	0.976		
	8	60.5	62	0.1225	1201.7	12.0			4.7	0.997		
	9	66	67.5	0.1335	1309.6	13.1			4.9	1.039	0.942	
	10	71	73	0.1440	1412.6	14.1			4.8	1.018		
	12	79	81.5	0.1605	1574.5	15.7			4.8	1.008		
15	90	92.5	0.1825	1790.3	17.9			5.0	1.049			
17	97	99.5	0.1965	1927.7	19.3			5.0	1.059			
20	107	109	0.2160	2119.0	21.2			5.2	1.091			
22	112	115	0.2270	2226.9	22.3			5.2	1.101			

APPENDIX-A 15: DOLOMITE PLUS ASHES HEAT TREATED AT 900 °C

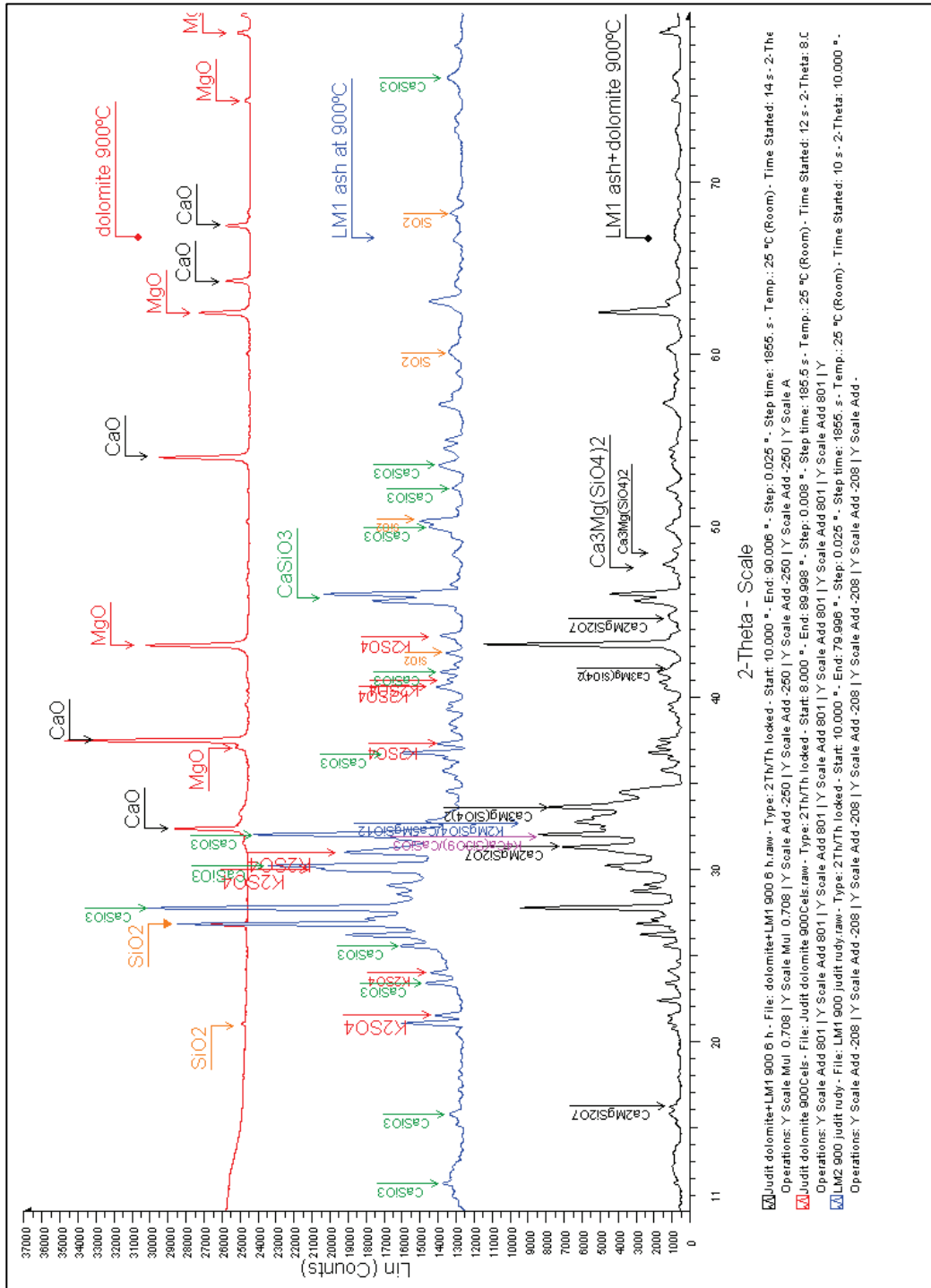


Figure A15-1 : XR-fiffractog of dolomite, LM1 ashes and their mixture at 900 °C

APPENDIX-A 16: SEM-EDX ANALYSIS OF AGGLOMERATES FROM LABORATORY FLUIDIZED BED (CEMHTI)

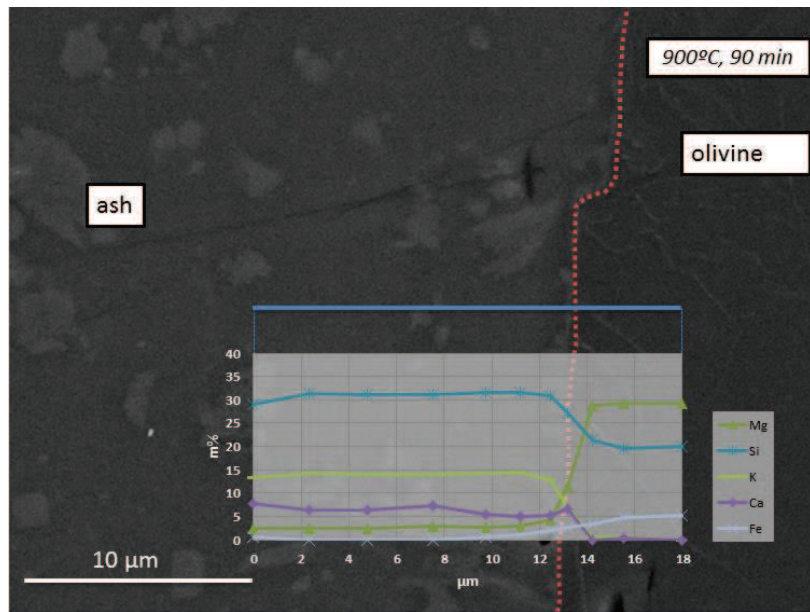


Figure A16-1 : LM1 ash-olivine interface after dynamic fluidized test at 900 °C for 90 min in air

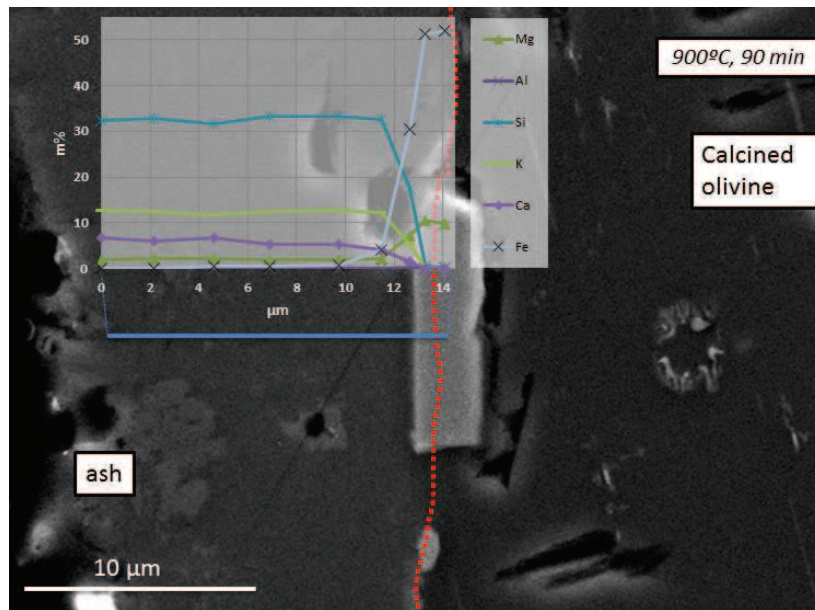


Figure A16-2 : LM1 ash-calcined olivine interface after dynamic fluidized test at 900 °C for 90 min in air

APPENDIX-A 17: MINERALS FROM LABORATORY FLUIDIZED BED (CEMHTI)

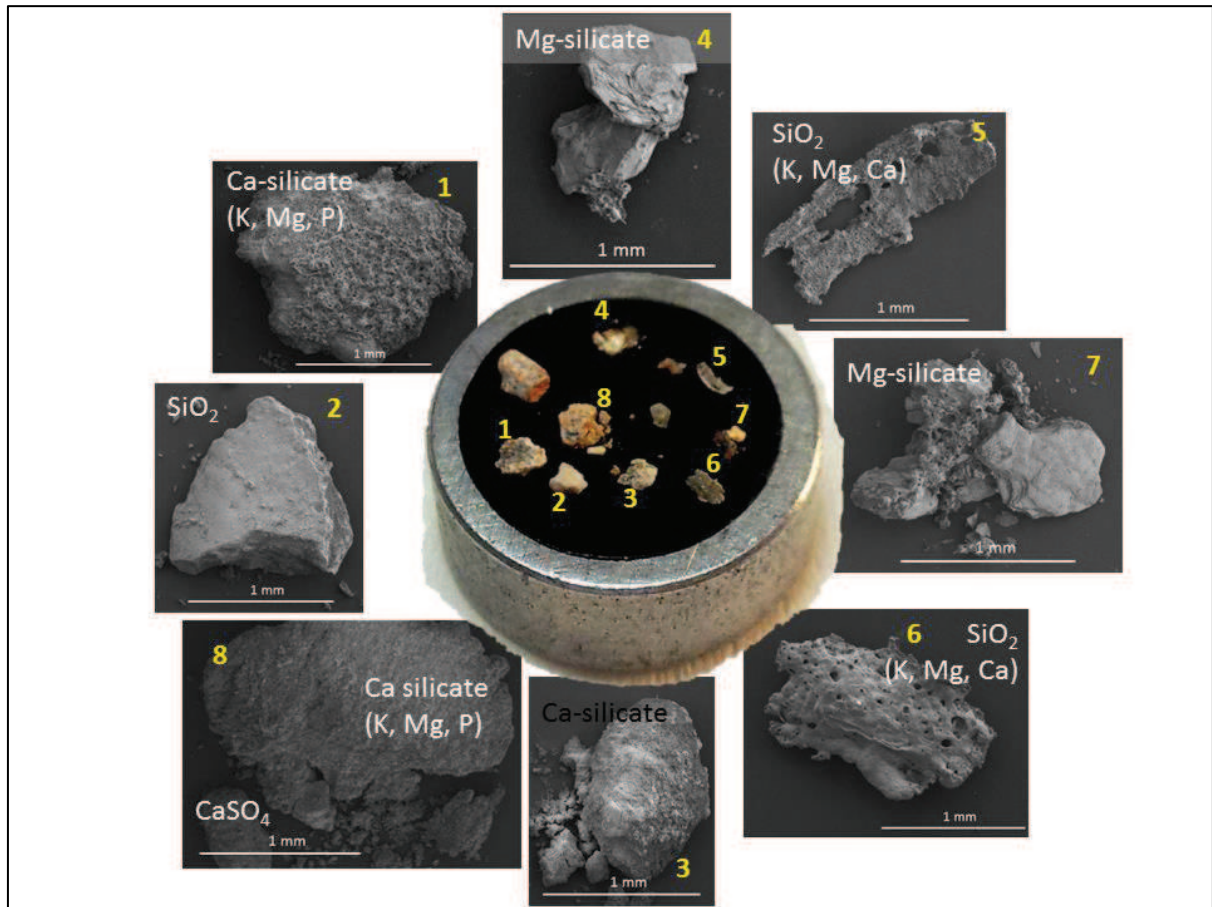


Figure A17-1: minerals formed during the experimentation with the hot device at CEMHTI, CNRS

APPENDIX-A 18: SEM-EDX ANALYSIS OF AGGLOMERATE FROM THE GASIFICATION PILOT

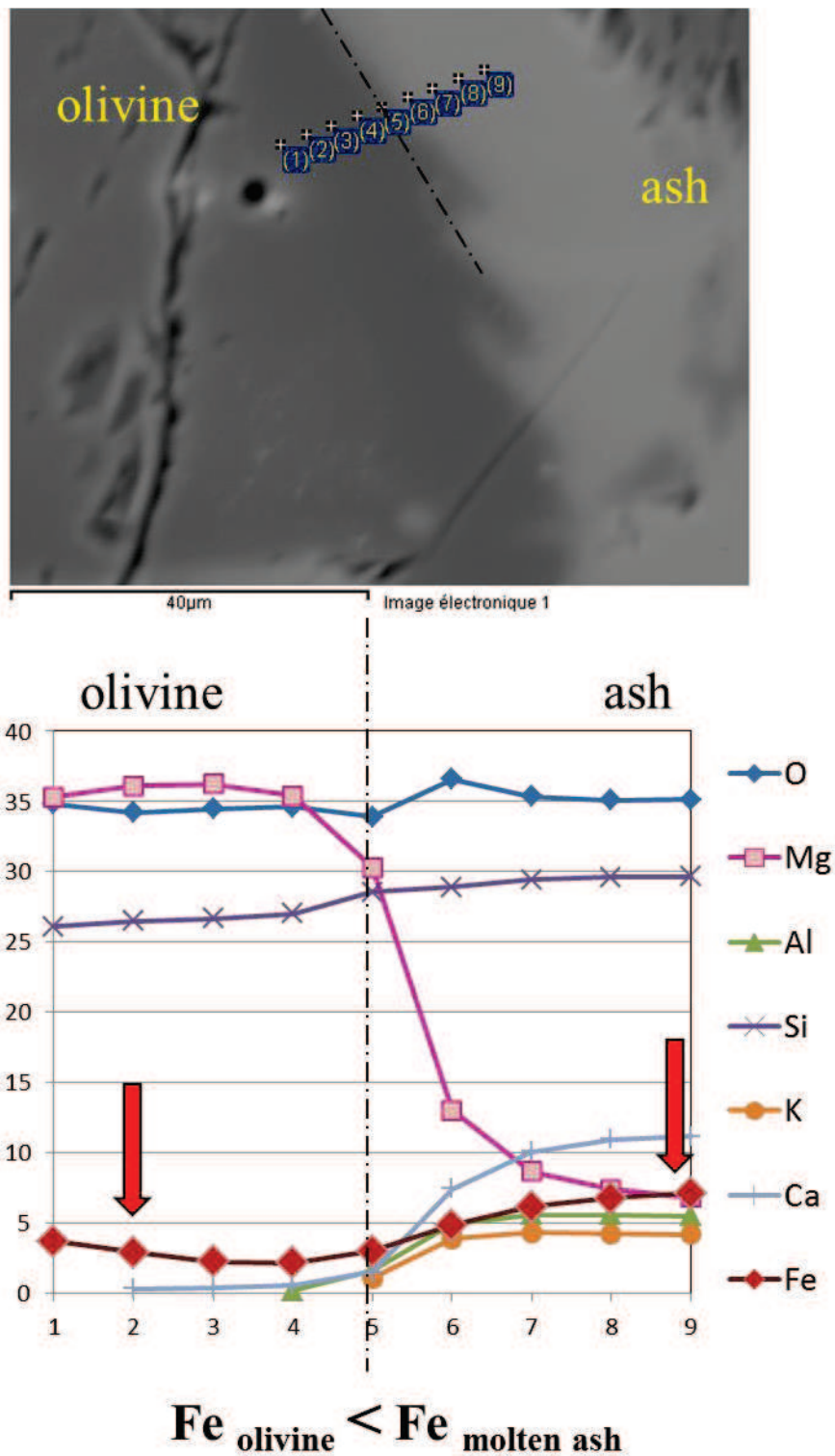


Figure A18-1: SEM-EDX analysis of agglomerate from the gasification pilot, test carried out in April 2014 at Nancy, CNRS



---

# SYNTHESE DE LA THESE EN FRANÇAIS

---

## INTRODUCTION

La diminution des réserves en combustibles fossiles et l'augmentation des émissions de gaz à effet de serre sont à l'origine d'une prise de conscience des gouvernements et des organisations internationales sur la nécessité de développer des énergies alternatives.

La biomasse est une alternative intéressante. Cette ressource est largement disponible. Elle , peut être directement convertie en bio carburant, en l'électricité ou en produits chimiques [1]. Le terme biomasse fait référence à toutes les matières organiques renouvelables à une échelle de temps humaine, telles que le bois, le fumier ou les sous-produits agricoles... La biomasse lignocellulosique (résidus agricoles et forestiers, cultures énergétiques) est un excellent candidat pour la production d'énergie car elle ne concurrence pas l'agriculture.

La gazéification est une technologie appropriée pour la conversion de la biomasse en gaz de synthèse (mélange de CO et H<sub>2</sub>). Ce gaz peut être transformé en chaleur, en électricité ou encore en produits chimiques (hydrocarbures légers par exemple).

Les lits fluidisés sont bien adaptés à la gazéification car ils permettent

- 1) une bonne homogénéisation de la biomasse
- 2) un processus à températures relativement basses
- 3) et enfin des installations d'échelles moyennes.

La gazéification à lit fluidisé n'est cependant pas encore une technologie mature.

Cette thèse, financée par la Région Centre, fait partie du programme ANR GAMECO (Gazéification AMéliorée des applications COgénération), qui vise à améliorer la technologie de la gazéification en lit fluidisé bouillonnant. Le projet GAMECO se concentre plus particulièrement sur la modélisation de l'hydrodynamique, sur la décomposition du goudron et enfin sur l'agglomération des matériaux du lit. Le laboratoire CEMHTI contribue à ce projet par son expertise sur le comportement des inorganiques à haute température.

Cette thèse étudie le rôle des cendres de miscanthus dans l'agglomération en lit fluidisé avec une approche physico-chimique. Nous nous sommes particulièrement intéressés à la transformation des phases inorganiques à haute température et aux interactions cendres-particules du lit.

Dans le cadre de cette thèse, nous avons également travaillé en collaboration avec le Laboratoire des Technologies de la Biomasse (LTB Liten, CEA, Grenoble) sur les aspects thermodynamiques des transformations de phases de cendres ainsi que sur une étude expérimentales en atmosphère réductrice.

Les expériences ont été réalisées à partir de Miscanthus Giganteus. Le Miscanthus est une plante herbacée originaire de l'est de l'Asie. Cette plante à croissance rapide est considérée comme une excellente source d'énergie. Elle a été largement étudiée au cours des 20 dernières années à la fois en Europe et aux États-Unis. Cependant, sa haute teneur en alcalins pose

problème durant la gazéification en lit fluidisé car elle provoque un fort taux d'agglomération des particules du lit.

Ce travail a un double objectif, scientifique et technologique :

- comprendre le rôle des composés inorganiques dans l'agglomération ;
- fournir des recommandations industrielles sur le choix du matériau de lit et sur l'optimisation des paramètres du procédé.

La thèse est divisée en 5 chapitres.

Le premier chapitre présente le contexte général, sur les énergies renouvelables et sur l'utilisation de la biomasse dans le secteur de l'énergie (dans le monde et en France).

Le deuxième chapitre concerne la transformation des cendres de miscanthus à haute température. La structure de la tige de miscanthus et le rôle des composés inorganiques dans la physiologie et le métabolisme de la plante sont présentés. La transformation des composés inorganiques en température ainsi que les effets de différents paramètres tels que l'époque des récoltes ou l'atmosphère de réaction sont ensuite étudiés en détails.

Le troisième chapitre porte sur les calculs thermodynamiques. Ces derniers sont souvent utilisés comme outils prédictifs pour le comportement des cendres à haute température. Ils sont cependant limités car l'état d'équilibre n'est pas toujours atteint dans les procédés industriels.

Le quatrième chapitre se concentre sur l'interaction, à haute température, entre les cendres de biomasse et les différents matériaux du lit dans des conditions statiques. Nous avons étudié l'importance des forces d'interface et les différentes interactions existantes entre les cendres et particules du lit.

Le cinquième chapitre présente les résultats des expériences d'interaction dynamiques qui ont été réalisées à deux échelles; à l'échelle du laboratoire et à l'échelle d'un réacteur pilote de gazéification.

Le dispositif à l'échelle du laboratoire a servi pour l'étude de l'agglomération en utilisant directement des cendres en atmosphère oxydante. Différents matériaux constituant le lit ont été testés.

Le réacteur pilote a été mis en place au laboratoire LRGP à Nancy. Il permet d'étudier l'agglomération en atmosphère réductrice dans des conditions proches de celles de la gazéification industrielle. Le réacteur est alimenté de granulés de miscanthus et le lit est constitué d'olivine.

## CHAPITRE I

L'objectif de ce chapitre est de présenter le contexte et les enjeux des énergies renouvelables.

Le terme biomasse comprend toute la matière organique non fossile et biodégradable provenant de plantes, d'animaux et de micro-organismes [2,3]. Il comprend aussi les résidus agricoles ou forestiers et les fractions organiques des déchets industriels et municipaux [2,3]. Les biocarburants de première génération posent problème. En effet leur production nécessite l'utilisation de surface importante généralement utilisées pour l'agriculture. Ces biocarburants concurrencent donc directement les ressources alimentaires et peuvent en faire augmenter les prix [4]. De nouvelles ressources de biomasse doivent donc être utilisées. L'expression «biomasse de deuxième génération" se réfère aux matériaux lignocellulosique (bois, résidus...), qui ne sont pas compétitifs avec des produits alimentaires.

Le Miscanthus est une plante herbacée largement étudié pour la production d'énergie. Il existe environ dix génotypes différents et la forme la plus généralement utilisé est un clone stérile : Giant Miscanthus ou Miscanthus giganteus X (MXG), qui est une hybridation de Miscanthus sinensis et Miscanthus sacchariflorus [5]. Il se multiplie par rhizomes ou par culture in vitro [6].

Le Miscanthus géant s'est avéré être un choix approprié à la fois d'un point de vue économique et écologique grâce aux propriétés suivantes:

- une voie photosynthétique de type C4
- un rendement important [6]: jusqu'à deux fois supérieur à d'autres biomasses utilisées pour la gazéification, comme le Panicum virgatum (switchgrass en anglais) [1,7]
- une bonne adaptabilité à différents climats [6]: il peut survivre aux hivers froids (jusqu'à -20 ° C) [7]et pousser sur des sols très différents (pH 5,5 à 8)
- une bonne assimilation de CO<sub>2</sub> à haute et à basse température (15 ° C) [8]
- une faible exigence en engrais et en pesticides

### LA GAZEIFICATION

La gazéification est une oxydation partielle de la biomasse ; la matière organique est transformée en gaz combustibles [9]. Le gaz de synthèse (CO et H<sub>2</sub>) permet une large gamme d'application : la production de chaleur ou la synthèse produits chimiques et de biocarburants par la synthèse Fischer-Tropsch[10] . La température du procédé de gazéification varie entre 750 à 1400°C, en fonction de la conception du gazéificateur [11].

Fondamentalement, la gazéification est un ensemble de réactions endothermiques entre le carbone, le dioxyde de carbone et/ou la phase vapeur d'eau [9]. Dans une installation industrielle, la gazéification est réalisée en différentes étapes [9,11]:

- un chauffage et le **séchage** de la biomasse ;
- une décomposition thermique (**pyrolyse**): entre 150-400 ° C, qui produit du charbon, des hydrocarbures, H<sub>2</sub>O, CO<sub>2</sub> et H<sub>2</sub> ;
- **une combustion** partielle des gaz en CO, CO<sub>2</sub> et H<sub>2</sub>O qui fournir la chaleur nécessaire au séchage de la biomasse, à la pyrolyse et aux réactions endothermiques ;
- une réduction (**gazéification**) du charbon en CO, CH<sub>4</sub> et H<sub>2</sub>.

## LE LIT FLUIDISE

Dans les réacteurs à lit fluidisé, les matériaux du lit sont des particules minérales inertes résistantes à la chaleur qui sont maintenues à l'état fluidisé par le flux de gaz [12].

Les lits fluidisés sont adaptés à la gazéification de la biomasse car :

- 1) les températures de processus sont faibles (800 à 900°C)
- 2) ils permettent un bon mélange du matériau
- 3) les conditions de fonctionnement sont isothermes
- 4) et enfin, les gaz produits possèdent une forte valeur énergétique [12-14].

La température de fonctionnement du lit fluidisé peut être adaptée en fonction des flux entrants de gaz et de biomasses [39].

Les inconvénients des réacteurs à lit fluidisé sont :

- 1) leur sensibilité à la taille des particules de biomasse injectées
- 2) une forte teneur en goudron
- 3) une importante concentration en poussière dans les gaz produits [13].

## LES CHALLENGES

Malgré les nombreux avantages du lit fluidisé pour la gazéification de biomasse, de nombreux défis techniques doivent être surmontés. Les principaux obstacles sont liés à la production de goudron, à l'hydrodynamique du lit et à l'agglomération [15].

L'agglomération est favorisée par les espèces inorganiques initialement présentes dans la biomasse. La biomasse lignocellulosique contient notamment de fortes concentrations en alcalins et en silice. Ces derniers forment des alcali-silicates durant le procédé et ces derniers ont tendance à fondre au-dessous de la température de réaction de gazéification. Les particules du lit deviennent alors collantes et forment des agglomérats qui ne peuvent pas être maintenus en suspension par le débit de gaz. Dans ces conditions, le lit se dé fluidise [10].

La dé fluidisation a pour conséquences une forte diminution de la pression et une distribution inégale de la chaleur dans le réacteur [16,17].

L'agglomération dépend fortement de la température du procédé [18]. Elle est favorisée par des températures élevées [16,17].

Le gradient de température entre les particules de combustible et les particules du lit est également un paramètre important car il peut favoriser le transfert d'éléments alcalins vaporisés vers le lit de particules [18]. La dé fluidisation pourrait être évitée en utilisant des températures de fonctionnement inférieures à 700°C, mais la formation de goudrons serait alors favorisée [18]. L'augmentation de la vitesse du gaz pourrait disloquer les agglomérats mais elle conduirait à une mise en suspension des charbons et à une perte d'énergie. D'autres paramètres doivent également être pris en compte, comme la composition des inorganiques de la biomasse ou des matériaux constituant de lit [19].

## CHAPITRE II

La composition de cendres est souvent exprimée sous forme d'oxydes. Cela ne reflète que partiellement la réalité car les composés inorganiques peuvent être présents sous différentes formes comme des sels, des carbonates et des oxydes. La forme chimique des inorganiques est un paramètre très important car il influence leur réactivité et leur répartition dans les phases gazeuses, solides et liquides pendant la gazéification.

Ce chapitre a deux objectifs:

- 1 décrire la décomposition thermique de la tige de miscanthus en prêtant une attention particulière à la formation des phases cristallines et amorphes
- 2 étudier la transformation des inorganiques entre 400°C et 1400°C pour comprendre leur rôle dans l'agglomération.

Les principaux éléments inorganiques présents dans la biomasse lignocellulosique sont K, Na, Ca, Mg, Si, P, S et Cl et en moindre quantité Al, Fe et Mn. Ces inorganiques ont des fonctions physiologiques et structurales différentes dans la plante et peuvent exister sous différentes formes. Selon les travaux de Bryers [4], le soufre peut se trouver dans des composés organiques, dans des sulfates ou encore dans des sels. Le chlore se trouve principalement dans des sels inorganiques et le phosphore sous forme de phosphate, de sels minéraux solubles, d'esters et de pyrophosphates. Les métaux alcalins, les métaux alcalino-terreux, l'aluminium, le fer et le manganèse forment des sels minéraux solubles. Ils peuvent également exister sous forme d'ions libres dans des solutions [20,21] ou encore être associés à des fibres [20,21].

Le silicium a des effets bénéfiques sur la croissance, le développement, le rendement et la résistance aux maladies [22]. Il se retrouve sous forme polymérisé et sous forme de gel de silice ( $\text{SiO}_2 \cdot n\text{H}_2\text{O}$ ) dans la tige des végétaux, l'épiderme et les tissus vasculaires [22]. Le silicium n'est pas mobile : il s'accumule pendant le vieillissement de la plante [22].

D'autres minéraux peuvent également exister dans la biomasse. Leurs concentrations sont généralement dépendantes de paramètres extérieurs comme la pollution [23]. Ces minéraux (sous la forme d'oxydes) sont moins réactifs que les inorganiques possédants une fonction biologique. Ils peuvent cependant jouer un rôle important lors de la gazéification et modifier le comportement de cendres [23,24].

Tableau II-1 présente l'analyse élémentaire du miscanthus utilisé pendant cette étude ainsi que la composition et la fusibilité des cendres à 815°C. Ces analyses et ces caractérisations ont été effectuées par un laboratoire indépendant (Socor Laboratoire) sur la demande de la société NovaBiom.

Table II-1: analyse élémentaire de *Miscanthus Giganteus X* (récolte avril 2011, La Ferté Chevresis, France)

<b>Miscanthus (La Ferté Chevresis)</b>	<b>Analyse par Socor</b>
Moisture content	15.1
Ash content at 815°C (%dry)	2.1
Carbon (wt%dry)	48.6
Oxygen (wt%dry)	43.0
Hydrogen (wt%dry)	5.8
Nitrogen (wt%dry)	< 0.3
Sulphur (mg/kg dry)	1669
Chlorine (mg/kg dry)	1002
Cellulose (wt%dry)	48.4
Hemicellulose (wt%)	23.9
Lignine (wt%brut)	10.9
Ash composition (wt%)	
SiO <sub>2</sub>	66
K <sub>2</sub> O	14.1
CaO	10.4
MgO	2.5
Na <sub>2</sub> O	1.1
P <sub>2</sub> O <sub>5</sub>	1.6
SO <sub>3</sub>	1.5
Al <sub>2</sub> O <sub>3</sub>	1.0
Fe <sub>2</sub> O <sub>3</sub>	1.1
TiO <sub>2</sub>	<0.1
MnO <sub>2</sub>	0.3

Le paragraphe suivant présente la structure de la tige de miscanthus et sa dégradation en température. Nous nous sommes intéressés à la distribution des composés inorganiques entre la partie extérieure rigide (le cortex) et la structure spongieuse interne (la moelle). La moelle se dégrade en une fine structure (de type toile d'araignée) à partir de 325°C et le cortex commence à se décomposer autour de 390-400°C. La formation de petits cristaux a été observée sur le cortex autour de 380-385°C et la structure en « toile d'araignée » disparaît vers 350°C.

Le cortex est principalement composé de silicium pour renforcer sa structure mais d'autres éléments comme le calcium, le magnésium et le potassium sont également présents. La partie intérieure de la tige est constituée de cellules spongieuses et de faisceaux vasculaires. La partie interne de la tige est riche en K et Cl, mais les faisceaux vasculaires contiennent aussi du Si, Mg, Ca, P et S. Le silicium et le potassium sont détectés à partir de 250 à 300°C et les métaux alcalino-terreux (Ca, Mg) apparaissent à partir de 350 à 400°C. En raison de leur faible concentration, les éléments Cl, P et S ne sont qu'occasionnellement détectables en dessous de 600 °C, mais leur présence est attestée à partir de 700°C. Na et Al sont présents en très faible quantité, alors que Fe et Mn n'ont jamais été observés.

En conclusion, soumise à un traitement thermique, la matrice organique commence à se décomposer entre 350°C et 400°C et les matières inorganiques commencent à cristalliser à environ 400 et 500°C. Ces réactions ont lieu simultanément et il est difficile de distinguer précisément la température de début de formation des cristaux de la température de fin de dégradation de la structure organique. En général, des matières inorganiques sont encore détectables autour de 375 à 400°C et la partie organique se décompose totalement entre 700 et 800°C. Cette étude a montré que 400°C est une température adéquate pour produire des cendres de miscanthus en atmosphère oxydante.

La méthode d'analyse de fractionnement chimique a été utilisée pour déterminer les différentes formes chimiques des inorganiques. Cette analyse a montré que ces inorganiques sont généralement à température ambiante sous forme ionique réactive dans le miscanthus. Après traitement thermique (1000°C), les cendres sont essentiellement composées de silicates.

L'analyse par diffraction des rayons X (DRX) révèle des transformations de phases complexes en température dans les cendres de miscanthus. Les principales transformations de phases en atmosphère oxydante sont résumées dans la Figure II-1. A température modérée (<775°C), la plupart des composés inorganiques sont sous forme de sels, de carbonates et de silice. A plus haute température, les carbonates se décomposent, les chlorures se volatilisent et de nouvelles phases de silicates apparaissent. Au-dessus de 1000°C, les phases cristallines commencent à fondre et le dernier solide disparaît entre 1300 et 1350°C.

La période de récolte du miscanthus peut modifier sensiblement la composition des cendres. Le miscanthus récolté en septembre (LM2) contient presque deux fois plus de potassium que la récolte de printemps (LM1). Pour la récolte de septembre, il en résulte une présence de sels de potassium, de carbonates et de silicates à haute température (900°C).

Les principales différences au cours des transformations en atmosphère oxydante et réductrice sont la présence de carbone non brûlé en atmosphère réductrice et la partition du soufre. En atmosphère réductrice le  $K_2SO_4$  n'est pas présent; mais une petite quantité de  $K_2S$  peut être détectée par microscopie électronique à balayage (MEB).

Quel que soit le type d'atmosphère, l'analyse MEB a montré que les principaux composés de cendres fondues à haute température sont  $SiO_2$  et  $K_2O$ .  $CaO$  et  $MgO$  sont présents en plus faible quantité.

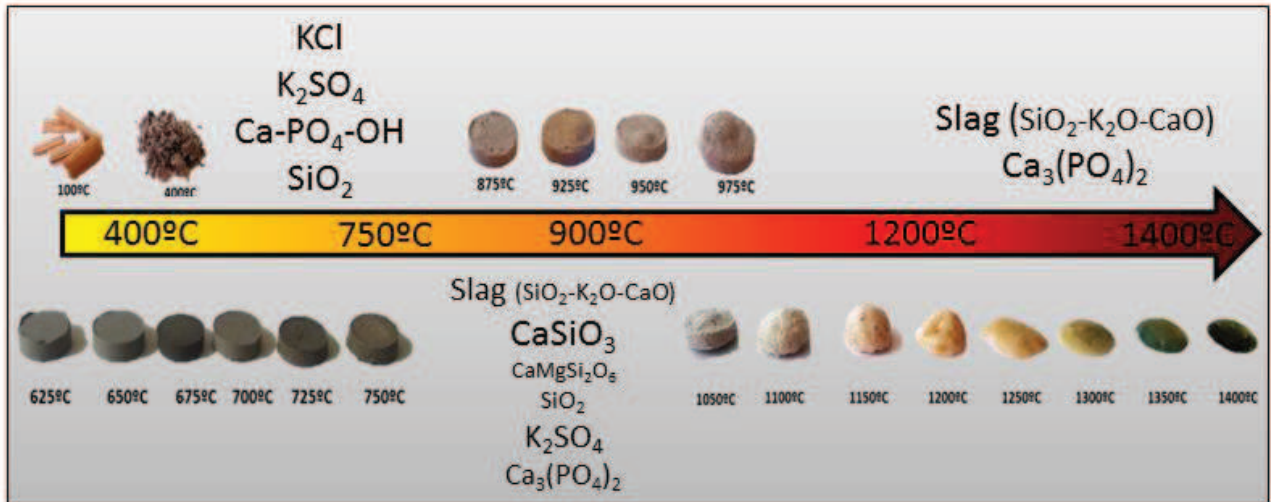


Figure II-1: Transformation des phases solides dans les cendres de l'échantillon LM1 en fonction de la température

## CHAPITRE III

Le but de ce chapitre est de décrire et prévoir les transformations des phases de cendres de miscanthus par des calculs thermodynamiques sous différentes conditions. Les résultats des calculs ont été comparés avec des expériences en laboratoire.

Les calculs ont été effectués avec le logiciel FactSage 6.3<sup>®</sup>. Les expériences de laboratoire ont été effectuées en condition statiques, en atmosphère oxydante (laboratoire CEMHTI-CNRS, Orléans) et en atmosphère réductrice (laboratoire LTB-Liten -Laboratoire des Technologies de la Biomasse-Laboratoire d'Innovation verser les Technologies, CEA, Grenoble).

Les calculs ont été effectués avec les bases de données FactPS, FToxid et FTsalt. La composition initiale du miscanthus (ultimate analysis) a été introduite dans le logiciel pour calculer la quantité stœchiométrique d'air nécessaire à la combustion de 1 kg de miscanthus. Les calculs ont été effectués à pression atmosphérique pour des températures allant de 400 à 1400°C. Deux atmosphères ont été testées correspondant à une quantité stœchiométrique d'air et une quantité limitée d'air (définie par notre partenaire industriel).

La Figure III-1 et Figure III-2 illustrent la répartition des composés volatilisés et des composés condensés des cendres dans des atmosphères oxydantes et réductrices. A basse température (<700°C) la cendre est constituée de sels (KCl, K<sub>2</sub>SO<sub>4</sub>, CaSO<sub>4</sub>, Ca-phosphates) et de silicates (SiO<sub>2</sub>, CaSiO<sub>3</sub>, CaMgSiO<sub>3</sub>, Na-Ca-silicate et une petite quantité de K<sub>2</sub>Si<sub>4</sub>O<sub>9</sub>). Avec l'augmentation de la température, KCl se volatilise tandis que CaSO<sub>4</sub> et K<sub>2</sub>SO<sub>4</sub> se décomposent. Le soufre est libéré dans la phase gazeuse ; Ca forme des silicates solides et K se retrouve principalement dans la phase liquide.

La phase liquide apparaît à 755-760°C. Elle est composée de K<sub>2</sub>O, SiO<sub>2</sub>, CaO et d'une petite quantité de NaO. La quantité de phase liquide augmente progressivement avec la température. La proportion des trois principaux composants (K<sub>2</sub>O, SiO<sub>2</sub>, CaO) change à haute température car les silicates solides fondent au-dessus de 1300°C. La quantité de CaO augmente de manière significative avec la fusion de CaSiO<sub>3</sub>. Avec la fusion de CaMgSi<sub>2</sub>O<sub>6</sub>, MgO apparaît également dans le laitier. La quantité de K<sub>2</sub>O diminue légèrement, ce qui s'explique par la volatilisation de K. La seule phase solide au-dessus de 1300 ° C est le Ca<sub>3</sub>(PO<sub>4</sub>)<sub>2</sub>.

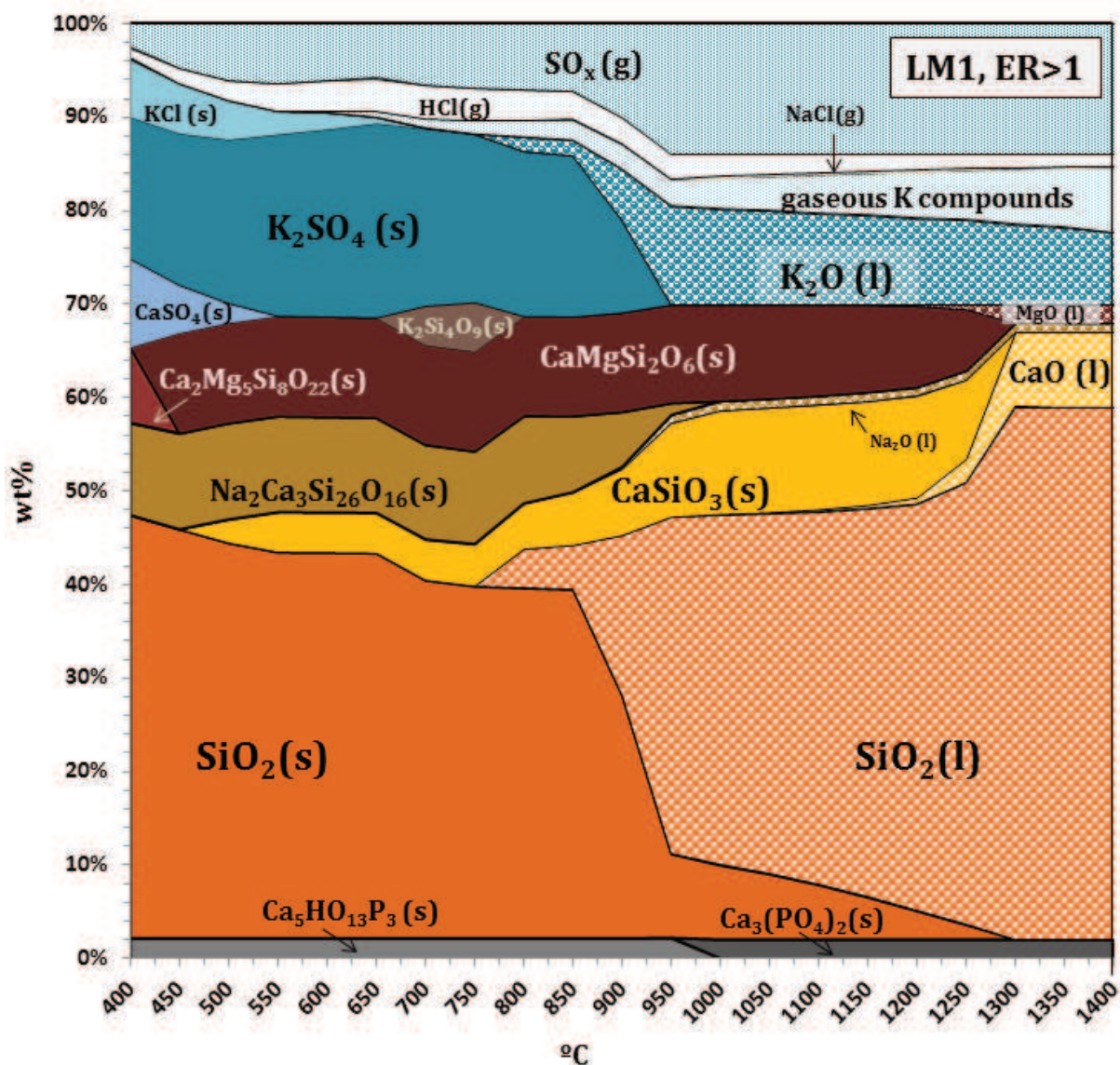


Figure III-1: Distribution des composés solides gazeux et liquides dans les cendres de miscanthus en fonction de la température en combustion

En atmosphère réductrice, deux différences peuvent être observées. Le S ne forme pas de sels alcalins, mais se trouve principalement associé à différents composés gazeux (principalement  $H_2S$ ,  $COS$  et une petite quantité de  $HS$  et  $SO_x$ ). Une plus grande quantité de silicates de potassium se forme. Le composé K-silicate ayant un faible point de fusion ( $755^\circ C$ ), la quantité de phase liquide entre  $755$  à  $900^\circ C$  est significativement plus importante que lors de la combustion.

En résumé, la forme chimique du soufre au cours de la gazéification ou de la combustion a une influence sur le rapport  $L/(S+L)$ . La formation de  $K_2SO_4$  est favorisée et une partie du potassium reste présent en phase solide.

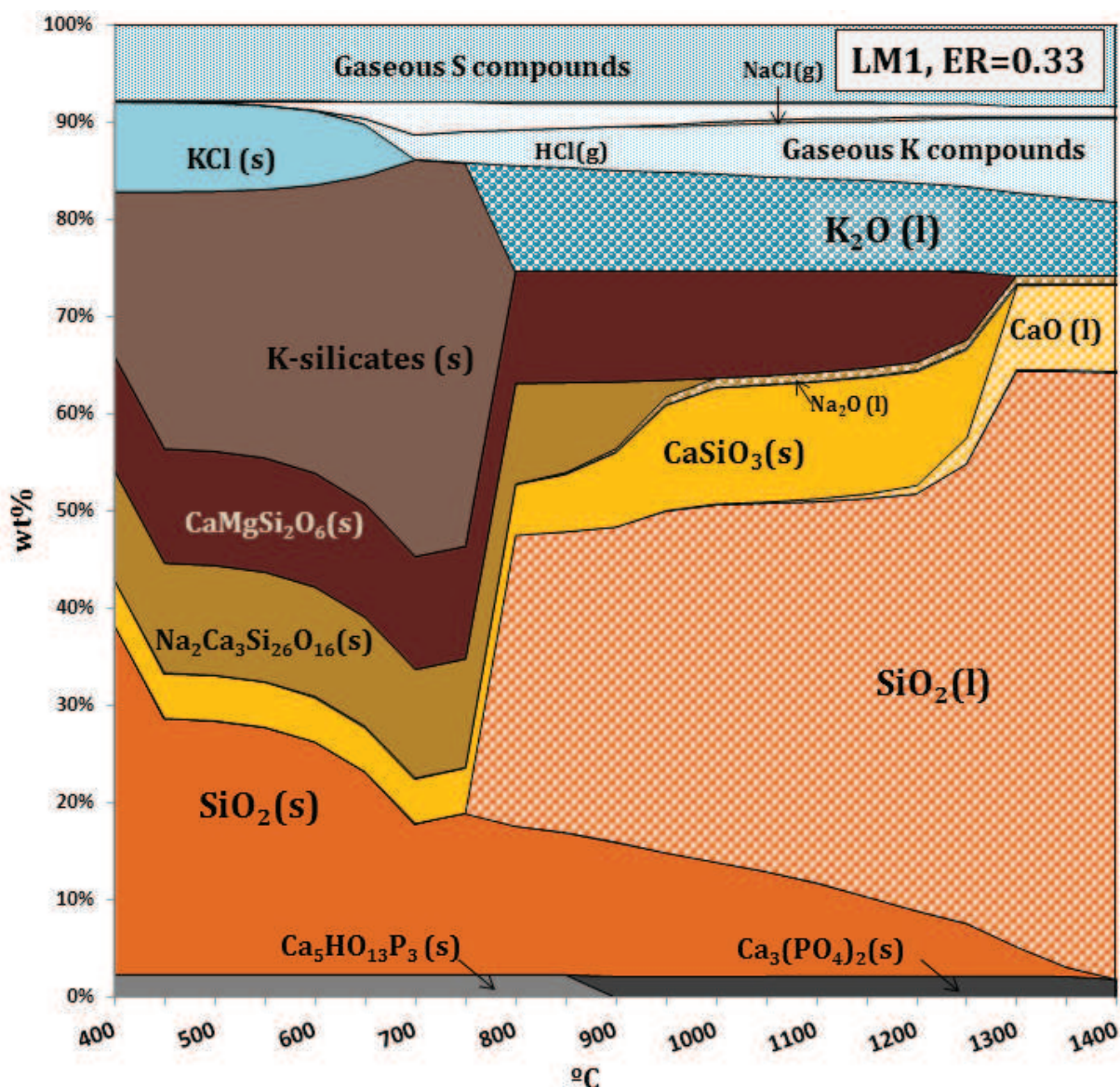


Figure III-2: Distribution des composés solides gazeux et liquides dans les cendres de miscanthus en fonction de la température dans le cas de la gazéification

#### COMPARAISON DES BASE DE DONNEES THERMODYNAMIQUES

Les calculs avec la base de données FToxid doivent être effectués avec précaution. En effet, cette base n'a pas été optimisée pour les cendres de biomasse, notamment pour le système SiO<sub>2</sub>-K<sub>2</sub>O-CaO. Récemment, une autre base de données a été développée par GTT Technologie pour les systèmes d'oxydes.

Le comportement de la cendre de miscanthus a donc été étudié avec deux bases de données différentes (FToxid et GToxid).

Dans le cas de FToxid, la solution liquide SlagA a été choisie. Dans le cas de GToxid, la base de données ne contient qu'une seule solution liquide, GToxid-LIOX. La principale différence entre

ces deux bases de données concerne la forme des silicates solides et liquides. La base de données FToxid contient les K-silicates et les Ca-Mg silicates ; la base de données GToxid contient K-Mg-silicates et K-Ca-silicates. Les Na-Ca-silicates existent dans les deux bases de données, mais sous des formes différentes. Les quantités de phases liquides et solides en fonction de la température sont comparées sur la Figure III-3. Malgré une différence dans les températures de solidus, la formation de la phase liquide montre la même tendance dans le cas de la combustion. Dans le cas de la gazéification, la quantité de phase liquide est beaucoup plus importante avec la base FToxid entre 766 à 950°C. La phase liquide apparaît à plus basse température en utilisant GToxid mais sa quantité reste limitée en dessous de 10m% jusqu'à 850°C. Elle augmente de manière significative à plus haute température jusqu'à dépasser la quantité de liquide calculée à partir de FToxid au-delà de 1000°C.

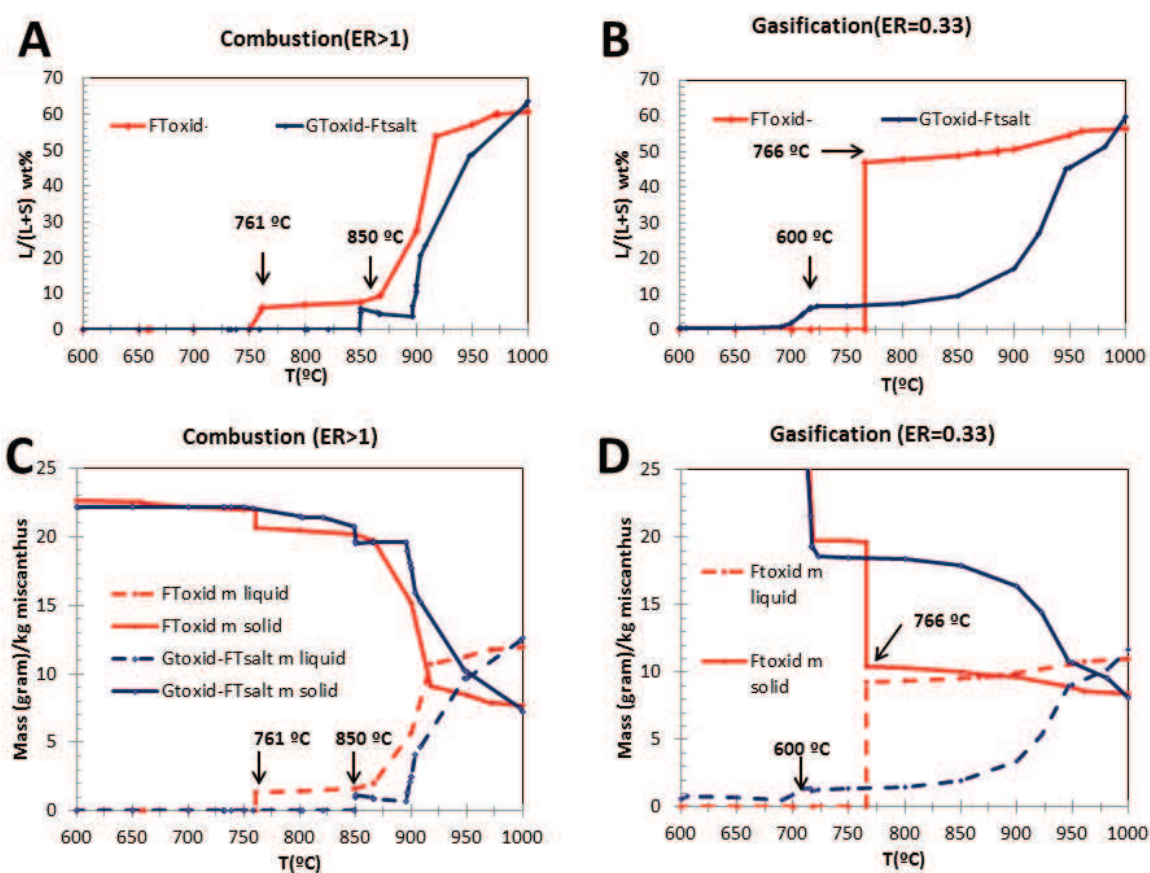


Figure III-3: Ratio liquide / solide ( $L/(L+S)$ ) en combustion (A) et en gazéification (B); quantités de phases liquides et solides dans les cendres de miscanthus en fonction de la température en combustion (C) et en gazéification (D). Calcul effectué avec les bases FToxid et GToxid

En résumé, les deux bases de données FToxid et GToxid génèrent des résultats très différents concernant la température de solidus et les proportions des phases liquides. La base de données GToxid prédit une température de solidus supérieure à la fois en combustion et en gazéification, ce qui s'explique par la formation de composés K-Mg-silicate solides plus stables que les composés K-silicate.

Les calculs thermodynamiques avec la base de données GToxid font apparaître une solution de sel fondu. Ceci peut s'expliquer par l'absence de  $\text{SiO}_2$  nécessaire à la formation des solutions de silicates liquides.  $\text{SiO}_2$  reste en phase solide sous la forme de K-Mg-silicate. Dans ces conditions, les solutions solides de  $\text{K}_2\text{SO}_4\text{-Na}_2\text{SO}_4$  (cas de la combustion) et  $\text{KCl-NaCl}$  (cas de la gazéification) peuvent fondre et former une solution de sel fondu jusqu'à ce que le  $\text{SiO}_2$  soit libéré lors de la décomposition de  $\text{K}_2\text{Si}_5\text{MgO}_{12}$ . Il en résulte des compositions de la phase liquide complètement différentes à  $900^\circ\text{C}$  entre les bases de données FToxid et GToxid.

#### VALIDATION DU MODELE THERMODYNAMIQUE A L'AIDE D'EXPERIENCES DE LABORATOIRE

Pour valider le modèle thermodynamique, les calculs ont été comparés avec des données expérimentales. Les expériences ont été réalisées avec des cendres de miscanthus (préparées à  $400^\circ\text{C}$  sous air) en condition statique. Pour la validation des calculs en atmosphère oxydante, les cendres ont été traitées dans un four de laboratoire standard. Pour la validation des calculs en atmosphère réductrice, les échantillons de cendres ont été traités dans un four à atmosphère contrôlée avec un flux de  $\text{CO}_2$  et  $\text{H}_2$ . Une analyse microGC a montré que les gaz injectés dans le four atteignent l'équilibre thermodynamique. La pression partielle de l'oxygène au cours des expériences en atmosphère réductrice est de  $10^{-17}\text{bar}$ .

Les ratios quantité de liquide / liquide plus solide ( $\text{L}/(\text{L}+\text{S})\%$ ) calculés avec les bases de données FToxid et GToxid ont été comparées aux mesures de températures caractéristiques de la fusibilité des cendres (Figure III-4). L'évolution de la phase liquide en utilisant la base de données FToxid peut être divisée en quatre zones. Lorsque le rapport  $\text{L}/(\text{L}+\text{S})\%$  est d'environ 25m% (calcul FToxid), nous observons expérimentalement une température caractéristique de contraction à  $902^\circ\text{C}$ . Entre  $950\text{-}1100^\circ\text{C}$ , la quantité de phase liquide est de 60mt%. Cette valeur correspond à la température caractéristique de déformation observée à  $968^\circ\text{C}$ . Entre  $1100$  et  $1250^\circ\text{C}$ , la quantité de liquide atteint 75m%, ce qui correspond à la température caractéristique d'une hémisphère ( $1118^\circ\text{C}$ ). À  $1250\text{-}1300^\circ\text{C}$ , la quantité de liquide est supérieure à 95wt%. Cette quantité peut être associée à une température caractéristique d'écoulement ( $1326^\circ\text{C}$ ).

Le ratio ( $\text{L}/(\text{L}+\text{S})\%$ ) calculé en utilisant des calculs GToxid est présenté pour des températures allant de  $800^\circ\text{C}$  à  $1000^\circ\text{C}$ . L'évolution de la phase liquide est lente. La phase liquide apparaît à  $850^\circ\text{C}$  (3m%) et atteint 20m% à  $905^\circ\text{C}$ , ce qui est une bonne corrélation avec la température caractéristique de contraction observée expérimentalement à  $902^\circ\text{C}$ . À  $950^\circ\text{C}$ , le rapport  $\text{L}/(\text{L}+\text{S})\%$  atteint 50% et dépasse 60m% à  $1000^\circ\text{C}$ . Cette augmentation correspond bien à la température de déformation observée à  $968^\circ\text{C}$ .

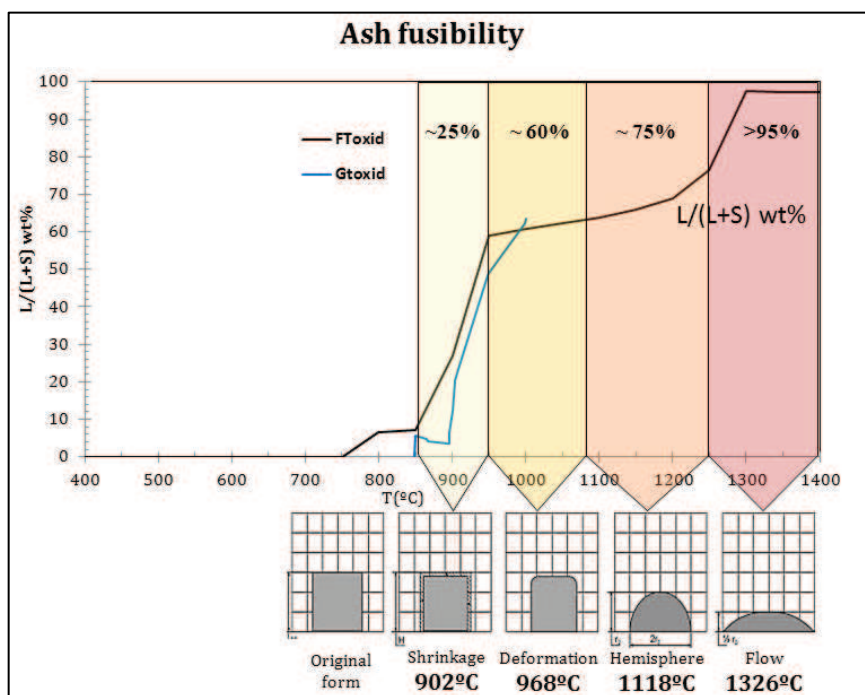


Figure III-4: Comparaison des tests de fusibilité des cendres avec les calculs thermodynamiques

Le Tableau III-1 compare les résultats expérimentaux de diffraction des rayons X avec les calculs thermodynamiques (FToxid et GToxid).

A basse température (400-700°C), les principales phases cristallines sont KCl, K<sub>2</sub>SO<sub>4</sub>, SiO<sub>2</sub> et Ca<sub>9</sub>HPO<sub>4</sub>(PO<sub>4</sub>)<sub>5</sub>OH. Les silicates de potassium n'ont pas été identifiés par DRX mais l'ont été par analyse MEB. Aux températures plus élevées (800 à 1200°C), les principaux composés sont K<sub>2</sub>SO<sub>4</sub>, Ca<sub>3</sub>(PO<sub>4</sub>)<sub>2</sub> et des silicates de métaux alcalino terreux. Les diffractogrammes des cendres à haute température (800-1000°C) révèlent la présence de CaSiO<sub>3</sub> et de CaMgSi<sub>2</sub>O<sub>6</sub>. Les silicates Ca<sub>2</sub>K<sub>2</sub>Si<sub>9</sub>O<sub>21</sub> et K<sub>2</sub>Si<sub>5</sub>MgO<sub>12</sub> présents dans la base de données GToxid n'ont pas été identifiés par DRX.

Deux principales différences peuvent être observées entre les expériences de laboratoire et les calculs thermodynamiques. Tout d'abord, les sels de métaux alcalins existent à des températures plus élevées que celles calculées. KCl et K<sub>2</sub>SO<sub>4</sub> sont toujours présents à 800 °C et 1000 °C respectivement alors que le calcul prévoit leurs volatilisations à 600 °C et 1000°C. Ceci pourrait s'expliquer par une condensation des composés volatiles sur la surface des échantillons de cendres, ou par l'influence du mode de préparation de l'échantillon (en pastille pressée) sur la volatilisation des sels.

La deuxième différence réside dans la formation de minéraux alcalins et alcalino-terreux. Les résultats DRX révèlent leur existence à partir de 800/ 850 °C, tandis que dans les calculs prévoient leur formation dès 400°C. La formation de nouvelles phases minérales dépend de la disponibilité des éléments. La formation de silicates alcalins et alcalino-terreux ne peut s'effectuer qu'à partir de 700 / 800 °C après la décomposition de la matrice organique contenant la silice et les éléments alcalins et alcalino-terreux.

Table III-1: Comparaison entre les différents composants solides observés dans les cendres de l'échantillon LM1 par DRX avec les calculs thermodynamique en atmosphère oxydante.

LM1 (avril 2011) atmosphère oxydante			
Compounds	XRD	FToxid-Ftsalt	GToxid-FTsalt
KCl (s)	400-800°C	400-600°C	400-600°C
K <sub>2</sub> SO <sub>4</sub> (s)	400-1200	400-1000°C	400-1000°C
CaCO <sub>3</sub> (s)	450°C	✗	✗
Ca <sub>3</sub> (PO <sub>4</sub> ) <sub>2</sub> (s)	500-1300°C	400-1400°C	400-1400°C
SiO <sub>2</sub> (s)	400-1150°C	400°C	✗
K-silicate (s)	SEM	600-700°C	✗
CaSiO <sub>3</sub> (s)	850-1150°C	400-1200°C	950-1050°C
MgSiO <sub>3</sub> (s)	?	700-1200°C	950-1050°C
CaMgSi <sub>2</sub> O <sub>6</sub> (s)	?	400-1200°C	750-950°C
Mg <sub>2</sub> SiO <sub>4</sub> (s)	?	✗	600-700°C
Na-Ca-silicate (s)	?	400-900°C	400-550°C
Ca-K-silicate (s)	?	✗	400-950°C
Mg-K-silicate (s)	?	✗	400-950°C
? presence incertaine ; ✗ non présent			

La Figure III-5 compare les compositions des phases liquides calculées avec celles mesurées par analyses MEB (EDX) pour des échantillons traités à 900°C en atmosphère oxydante et réductrice. Dans l'ensemble, la base de données GToxid donne des résultats plus proches des résultats expérimentaux que ceux obtenus avec la base FToxid, que ce soit en atmosphère réductrice et oxydante. La base de données FToxid prévoit deux composants principaux; K<sub>2</sub>O, SiO<sub>2</sub> et une très petite quantité de Na<sub>2</sub>O (<1wt%). La base de données GToxid prédit aussi l'existence de MgO et CaO, confirmée par analyse MEB. La présence de 2-4 m% de Na prévue par GToxid n'a pas été confortée par l'expérimentation.

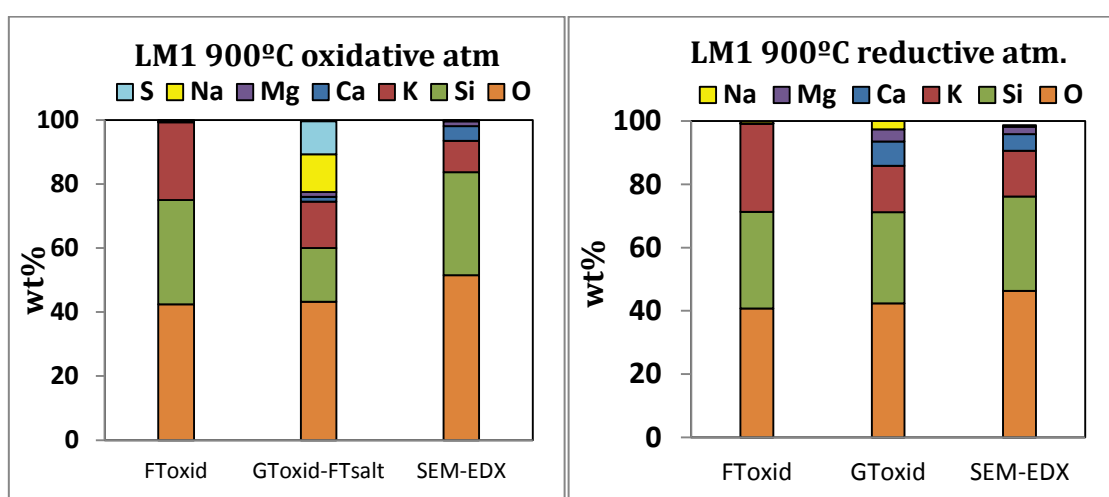


Figure III-5: Composition de la phase liquide (MEB et calculs thermodynamiques), cendres de l'échantillon LM1 à 900°C

En résumé, les calculs correspondent assez bien aux données expérimentales. La base de données FToxid apparaît mieux adaptée pour les calculs d'équilibres des phases solides. La base GToxid est appropriée pour la prédiction des phases liquides.

Les calculs d'équilibre peuvent être utilisés pour estimer le comportement à haute température de cendres de biomasse. Ces calculs sont un outil complémentaire pour interpréter les expériences. Cependant, les résultats doivent être interprétés avec précaution, car les calculs thermodynamiques ont certaines limites; les bases de données disponibles ne sont pas complètes et toutes les données n'ont pas été validées par des expériences. En outre, l'état d'équilibre thermodynamique n'est pas toujours atteint dans les procédés industriels.

## CHAPITRE IV

L'agglomération lors de la gazéification et lors de la combustion à lit fluidisé est due à la fusion de cendres de la biomasse à une température relativement basse (<850°C). Les cendres fondues agissent comme une « colle » et elles peuvent lier les particules du lit lors de collisions. Les agglomérats formés peuvent perturber l'état fluidisé, diminuer le rendement et augmenter les coûts de maintenance. Pour apporter une solution à ce phénomène, les mécanismes de formation des agglomérats doivent être étudiés.

Beaucoup de chercheurs ont déjà étudié les interactions existantes entre la silice et des biomasses de type bois ou paille de blé [10,25–28]. Bien que l'effet catalytique de l'olivine dans la décomposition du goudron soit connu, il n'existe que très peu d'études portant sur l'interaction de l'olivine (comme matériaux du lit fluidisé) avec une biomasse [10].

Dans ce chapitre, les interactions entre les cendres de miscanthus et les matériaux du lit fluidisé ont été étudiées en conditions statiques en atmosphère oxydante et réductrice. Le but de ce travail était de comprendre le rôle des paramètres clés dans la formation d'agglomérats:

- la composition des cendres de miscanthus
- la transformation de phases de la matière du lit
- L'atmosphère
- Le temps de contact
- la température

Trois matériaux de lit ont été utilisés dans cette étude : la silice, l'olivine et l'olivine calcinée. L'olivine provient d'Aheim (Norvege - Sibelco). L'olivine calcinée a été obtenue par traitement thermique (1400°C pendant 4 heures) dans un four de laboratoire.

Différents additifs (kaolin - Tapez Kerbrient ; dolomie - Neau, France) ont été testés comme additifs pour diminuer les risques de l'agglomération.

Les transformations de phase de l'olivine à haute température ont été étudiées par Michel et al [28]. Deux techniques complémentaires, la DRX in-situ et la spectrométrie Raman ont montré que la Fayalite ( $\text{Fe}_2\text{SiO}_4$ , l'une des deux principales composantes de l'olivine) se décompose en  $\text{Fe}_2\text{O}_3$  et  $\text{SiO}_2$ -dessus de 725°C.  $\text{Fe}_2\text{O}_3$  s'oxyde et forme des veines sombres sur la surface des particules d'olivine à des températures supérieures à 1100°C.

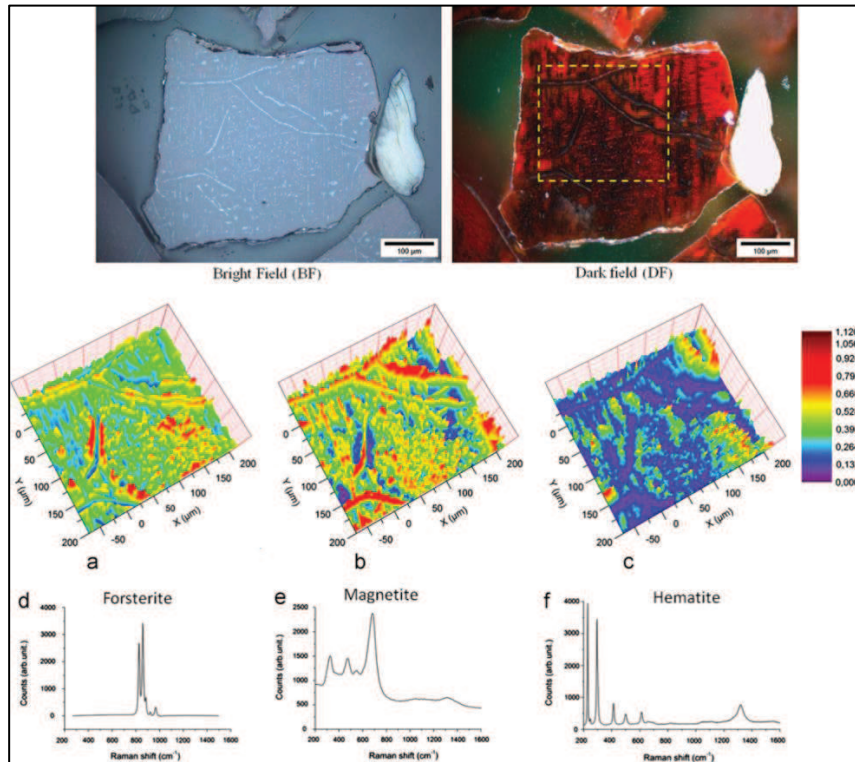


Figure IV-1: Cartographie Raman d'échantillons d'olivine calcinée; distributions de la forstérite, magnétite et hématite [29]

Le paramètre clé de la formation d'agglomérats est le mouillage des particules du lit par les cendres fondues et l'énergie d'adhésion entre les particules. Si l'énergie d'adhésion est plus grande que l'énergie cinétique de la collision des particules, les particules forment des agglomérats. La Figure IV-2 montre le mouillage de l'olivine par les cendres liquides visqueuses de miscanthus.

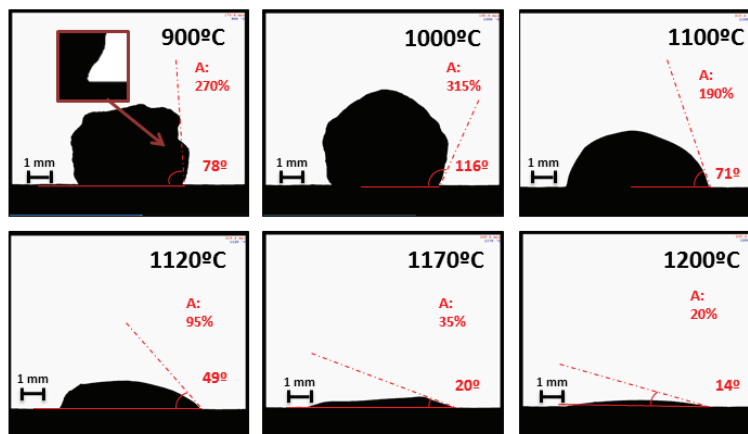


Figure IV-2: Mouillage de l'olivine calcinée par des cendres de miscanthus en température

Les forces interfaciales entre les particules peuvent être modifiées par la diffusion des éléments, par l'interaction chimique ou par la rugosité des surfaces.

La Figure IV-3 présente l'analyse MEB et EDX de cendres de miscanthus (LM1) en contact avec les matériaux constituant le lit (silice; olivine; olivine calcinée) après un traitement thermique à 900°C pendant 6 heures

Dans le cas de la silice, l'agglomération est principalement due à une adhérence directe. Dans le cas de l'olivine et de l'olivine calcinée, une couche interne et mince riche en Ca-silicates ainsi que la diffusion de Fe dans les cendres fondue ont été observées. La concentration en fer dans les cendres fondues est relativement faible (2-3m%) et la diffusion peut atteindre 10-15 µm dans les cendres pour des temps de contact élevés.

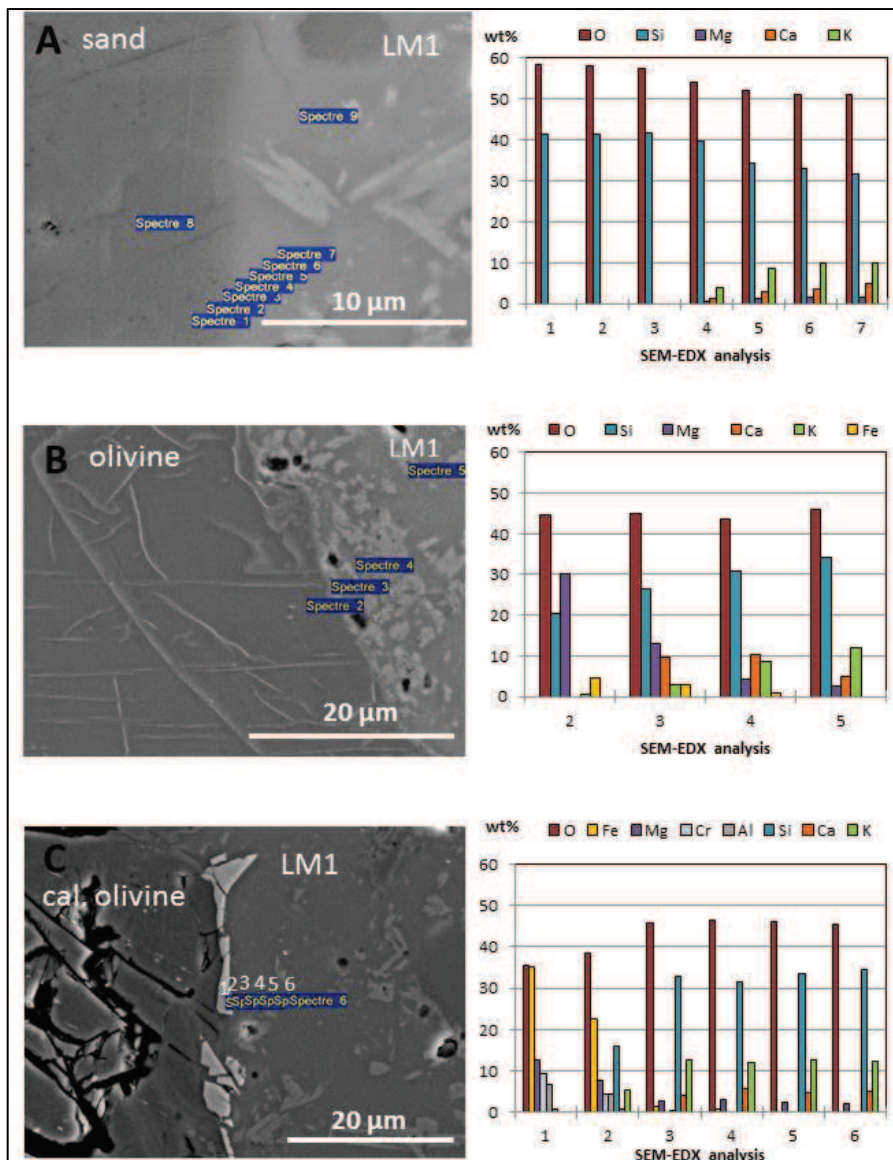


Figure IV-3: Analyse MEB et EDX de cendres de miscanthus (LM1) en contact avec les matériaux constituant le lit (A, silice; B, olivine; C, olivine calcinée) après un traitement thermique à 900°C pendant 6 heures

Dans le cas de l'olivine calcinée, un composé de ferrite de magnésium ( $MgFe_2O_4$ ) a été observée à l'interface cendres / particules du lit. Lors de l'augmentation du temps de contact et de la température, la taille des cristaux peut atteindre 10 à 20  $\mu m$ . Ces cristaux augmentent la rugosité de surface et renforcent l'adhérence entre les particules (Figure IV-4), D'autres études seront nécessaires pour déterminer si une réaction chimique a lieu entre les oxydes de fer et la cendre fondue.

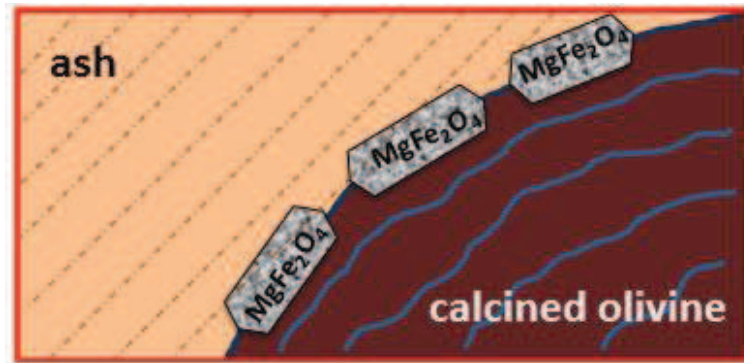


Figure IV-4: formation d'un composé de ferrite de magnésium ( $MgFe_2O_4$ ) à l'interface cendres / olivine calcinée

L'atmosphère réductrice n'a pas d'influence sur la mouillabilité des matériaux du lit. La principale différence observée par rapport à une atmosphère oxydante est la présence de cristaux FeS ainsi que la formation de deux phases liquides non miscibles.

**Compte tenu de ces constats, les conclusions suivantes peuvent être tirées :**

- 1. La capacité de mouillage des cendres est le paramètre clé de l'agglomération*
- 2. L'adhérence entre les cendres miscanthus et les matériaux du lit augmentent dans l'ordre suivant: sable  $\rightarrow$  olivine  $\rightarrow$  olivine calcinée*
- 3. Il n'y a pas de différence significative dans les mécanismes d'agglomération en atmosphère oxydante ou réductrice*

## CHAPITRE V

Le but de ce chapitre est d'étudier les interactions entre les cendres et les matériaux du lit sous conditions dynamiques (mouvement continu du mélange des particules du lit et des cendres). Dans un lit fluidisé, les particules solides sont mises en état de fluidification par un flux de gaz ou de liquide [30]. Les particules du lit sont placées sur une plaque poreuse (perforée) et l'agent de gazéification est injecté par la partie inférieure du lit. Pour une vitesse lente de gaz, le lit reste fixe. Avec une augmentation de la vitesse du gaz, le lit se dilate jusqu'à la vitesse minimale de fluidisation : le lit est alors « en sustentation » dans le flux de gaz. Une augmentation supplémentaire de la vitesse du gaz peut modifier le régime de fluidisation : bouillonnement, turbulent et enfin fluidisation rapide [30]. À très haute vitesse de gaz, les particules du lit peuvent être entraînées hors du réacteur [30,31].

Un dispositif haute température à l'échelle du laboratoire a été conçu pour étudier et visualiser l'agglomération entre les cendres et les matériaux du lit (Figure V-1). Il se compose d'un support en aluminium (Figure V-1/1), d'un four tubulaire (Figure V-1/2) et d'un réacteur en quartz (Figure V-1/3).

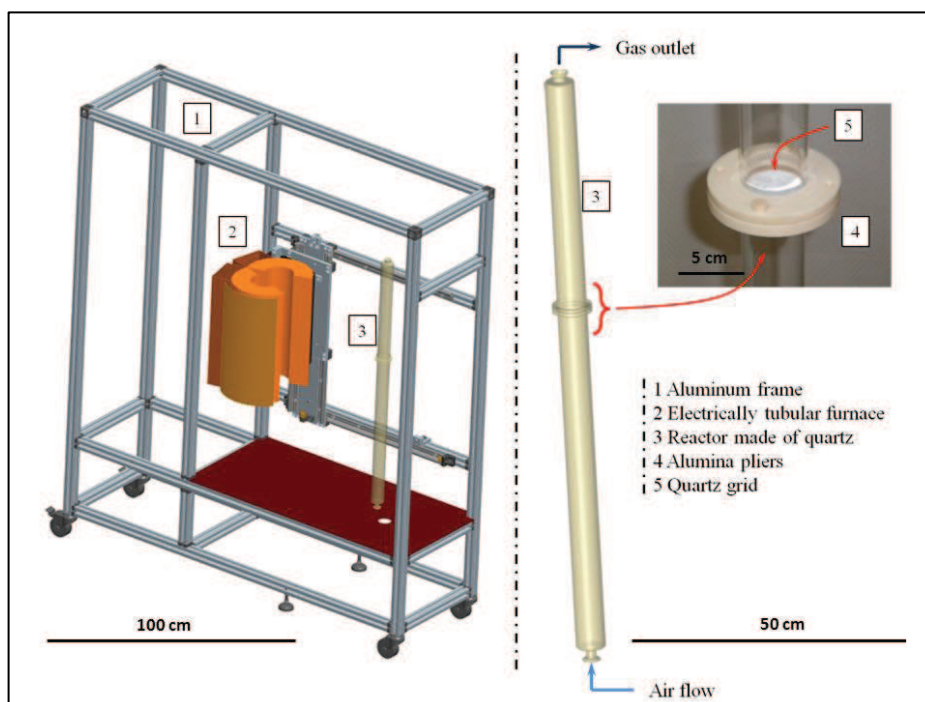


Figure V-1: Schéma du réacteur à lit fluidisé (CEMHTI)

Le but de nos expériences était de tester l'impact de différents paramètres (matériaux de lit, température, vitesse de fluidisation, quantité de cendre et d'additifs) sur les taux d'agglomération des particules du lit. Les taux d'agglomération augmentent selon la nature des matériaux du lit dans l'ordre suivant : la silice, l'olivine et l'olivine calcinée. Un taux d'agglomération maximum est systématiquement observé entre 30 et 125 min selon le matériau constituant le lit. On observe ensuite une diminution suivie d'une stabilisation du

taux d'agglomération. Dans le cas de l'olivine calcinée, le temps d'expérience s'est révélé trop court pour observer la stabilisation du taux d'agglomération. Les maximums peuvent être expliqués par deux effets antagonistes: la formation de liaisons entre les particules et l'abrasion des agglomérats dans le lit fluidisé. Le Tableau V-1 présente les effets des différents paramètres sur les taux d'agglomération

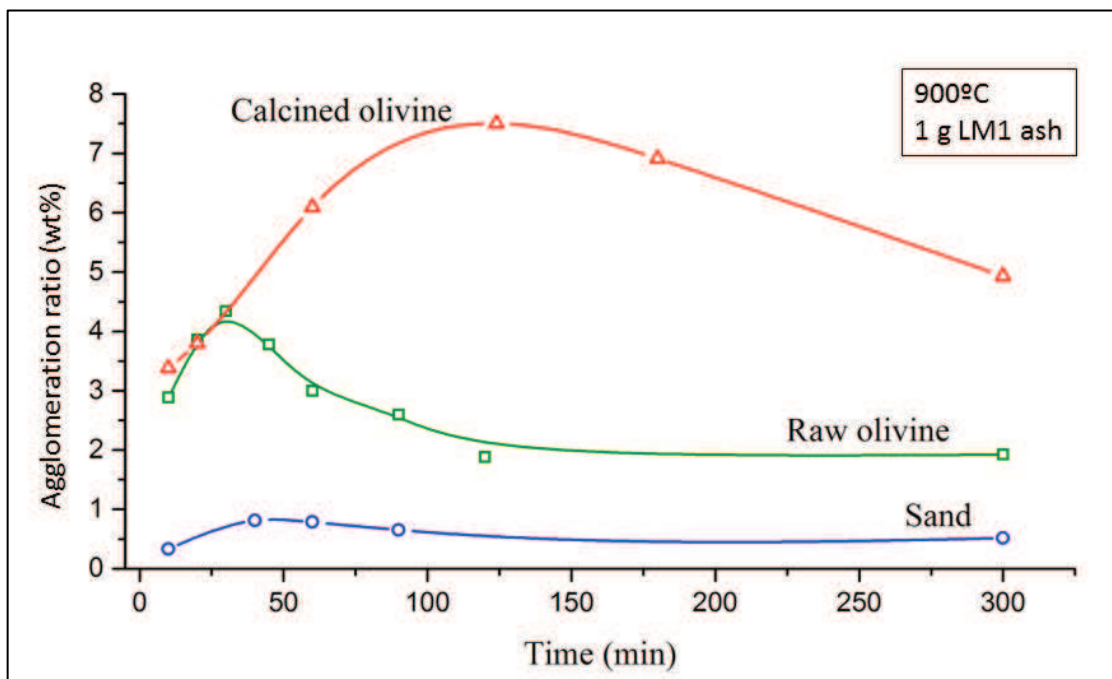


Figure V-2: Taux d'agglomérations en fonction du temps

Tableau V-1: Effets de différents paramètres sur les taux d'agglomération: + effet léger, ++ effet moyen, +++ effet important

Parameters	%A	Effect*
Temperature	↗	+++
Air flow	↘	+
Bed material	↗	++
Ash/bed ratio	↗	++
Operation time	→	+
Additives	↘	+++
Pretreatment of biomass	↘	+++
* + low effect, ++ medium effect, +++ significant effect		

La quantité de cendres a un impact important sur la fluidisation du lit. Deux domaines principaux peuvent être observés (Figure V-3). Pour des quantités faibles de cendre, le lit est à l'état fluidisé. A plus forte quantité de cendres (au-dessus d'une valeur critique), le taux d'agglomération devient important (>4 %), et l'état fluidisé ne peut être maintenu. Le lit commence à défluidiser.

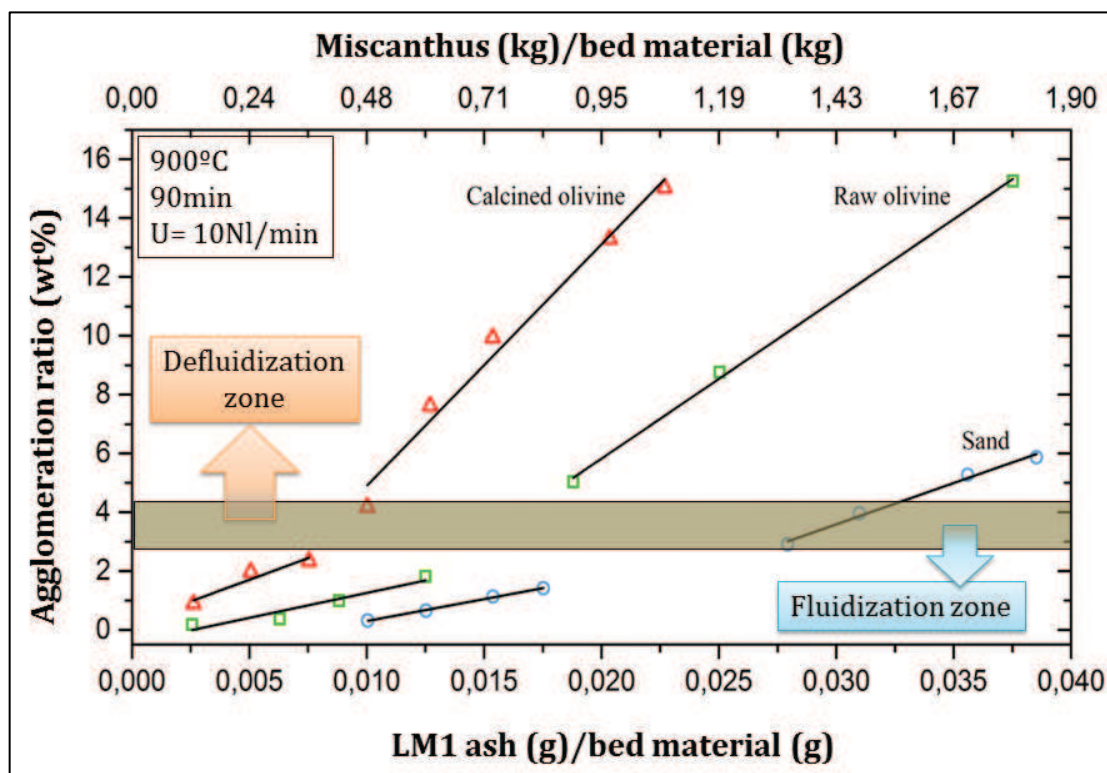


Figure V-3: Taux d'agglomération en fonction de la quantité de cendres avec de la silice, de l'olivine ou de l'olivine calcinées comme constituants du lit

Le taux d'agglomération est inversement proportionnel à la vitesse de fluidisation et à la température. La vitesse de fluidisation n'a qu'une légère influence sur l'agglomération. Une diminution de la température peut limiter significativement les tendances d'agglomération. 750°C ou 800°C seraient des températures optimales de fonctionnement des gazéificateurs. Cependant, dans ces conditions le pouvoir calorifique du gaz produit est limité et les goudrons ne sont pas suffisamment décomposés.

Deux additifs : le kaolin et la dolomite ont été testés. Un lavage de la biomasse a aussi été testé afin d'éliminer le potassium présent sous forme de sel dans la biomasse. La dolomite limite l'adhérence entre les cendres et les particules d'olivine. Le kaolin diminue la quantité de cendres fondues. En effet, il favorise la formation de composés de type K-Al-silicates ayant une température de fusion élevée. La formation de Ca-Mg-silicates et K-Mg-silicates est aussi possible avec l'ajout de dolomite, mais des analyses complémentaires (XRD) sont nécessaires pour confirmer la présence de ces phases. Le kaolin apparaît plus efficace pour limiter l'agglomération : 0,3wt. % semble suffisant pour diminuer significativement le taux d'agglomération (à de très faibles valeurs : 1%). 3 m% de dolomite permet une diminution

appréciable de l'agglomération. Le lavage de la biomasse est aussi efficace. Il limite le taux d'agglomération à 1 %. Ce résultat indique que le potassium, qui est le composé responsable de la fusion des cendres à basse température peut être complètement éliminé par lavage de la biomasse.

Ces résultats ont été comparés à ceux obtenus par des expériences de gazéification de granulés de miscanthus en lit fluidisé réalisées dans le pilote du LRGP, situé à Nancy. De l'olivine a été utilisée comme matériau du lit. Les taux d'agglomération présentent un bon accord. Cependant la morphologie des agglomérats est très différente.

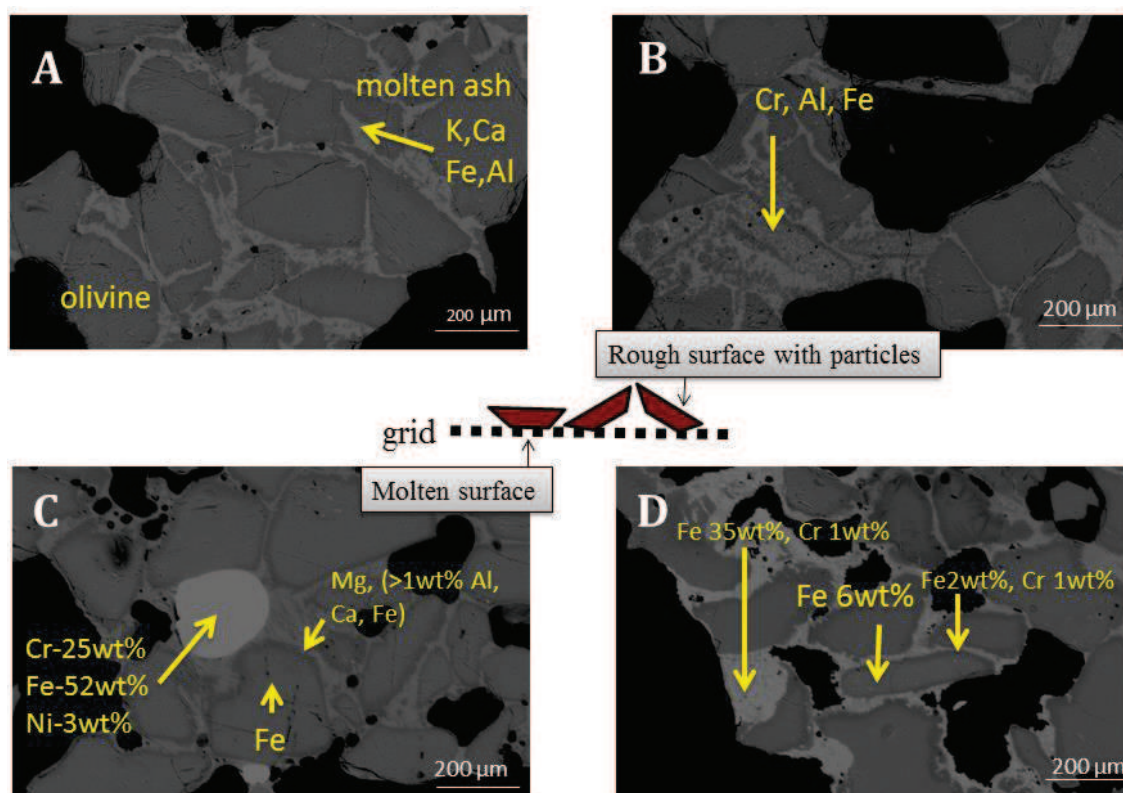
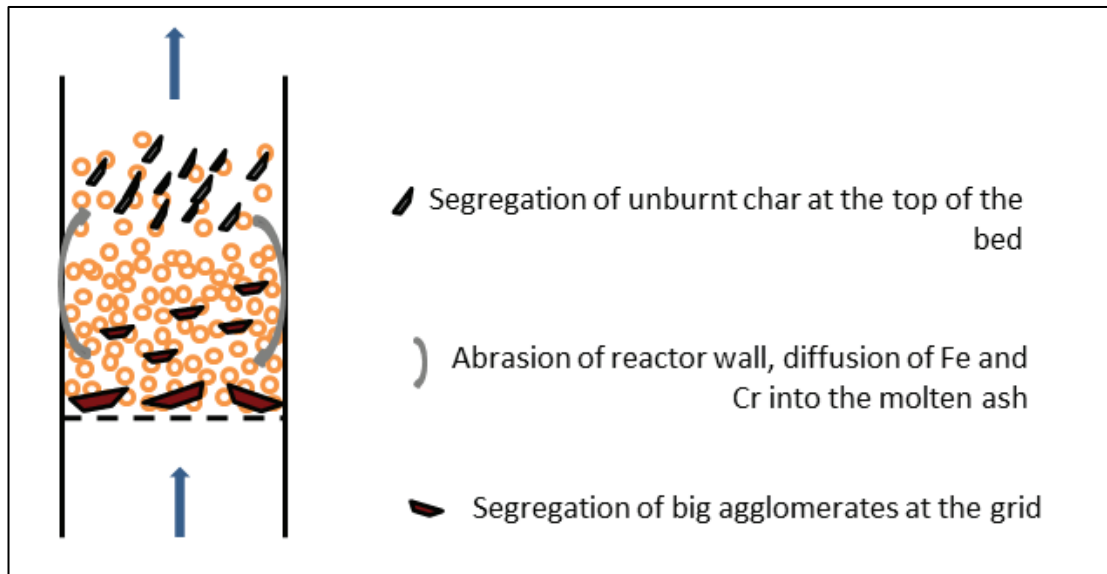


Figure V-4: Analyses MEB EDX d'agglomérats prélevés sur la grille du réacteur pilote situé au LRGP Nancy, coté haut (A,B) et coté bas (C,D)

Différents phénomènes ont été observés dans le pilote de gazéification (Figure V-31): une ségrégation de carbone imbrûlé dans la partie supérieure du lit et des gros agglomérats sur la grille.

L'analyse MEB-EDX a montré que les principaux constituants de la phase liquide sont  $K_2O$ ,  $CaO$ ,  $SiO_2$ ,  $MgO$  et  $Fe$ . La quantité de  $Fe$  est plus importante dans les cendres fondues que lors des expériences menées à l'échelle des essais de laboratoire (tests statiques et dynamiques). Les teneurs en  $Cr$  et  $Al$  des agglomérats sont également plus importantes. Il est possible que le niveau élevé de  $Fe$ ,  $Cr$  et  $Al$  soit dû à la grande quantité d'olivine utilisée dans le pilote (4kg comparé à quelques grammes). Ces teneurs élevées en métaux peuvent également provenir de l'altération par abrasion des parois du réacteur. D'autres essais de fluidisation avec différents matériaux constituant le lit à (olivine, silice...) doivent être réalisés pour valider ces résultats.



*Figure V-5: Illustration de la gazéification en lit fluidisé.*

## CONCLUSIONS ET PERSPECTIVES

Ce travail s'inscrit dans le projet ANR GAMECO qui s'intéresse à la gazéification de *Miscanthus* (notamment le *Miscanthus Giganteus X*) en lit fluidisé. Il s'agit d'étudier les interactions entre les cendres de *Miscanthus* et les matériaux constituant le lit (silice, olivine, olivine calcinée).

Ce travail avait trois principaux objectifs :

- Comprendre et décrire les transformations des inorganiques à haute température ;
- Comprendre leur rôles dans les processus d'agglomération ;
- Proposer des recommandations pour une gazéification optimale du *Miscanthus* en lit fluidisé.

Les principaux éléments présents dans le *Miscanthus* susceptibles de favoriser une agglomération sont K, Si, Ca, Mg, P, S et Cl. Les analyses MEB – EDX ont montré que Si est l'élément majoritaire dans le cortex du *Miscanthus*. K est majoritaire dans les tissus formant la moelle de la plante. A basse température, les analyses XRD ont révélé que les cendres de *Miscanthus* sont principalement constituées de silice, de carbonates et de sels. Les carbonates et les sels se décomposent et se volatilisent à partir de 700 °C. Les phases cristallines dominantes à haute températures sont la silice et les silicates alcalino-terreux. La phase liquide peut être décrite par le système quaternaire  $\text{SiO}_2 - \text{K}_2\text{O} - \text{CaO} - \text{MgO}$ , quel que soit la nature de l'atmosphère (oxydante ou réductrice).

La partition du soufre est la principale différence observée dans le comportement des inorganiques en fonction de l'atmosphère, oxydante ou réductrice. En atmosphère oxydante, le soufre se trouve sous forme de sulfates de potassium. En atmosphère réductrice, le soufre est surtout présent dans la phase gazeuse. Quelques sulfures de potassium peuvent aussi être trouvés dans des résidus carbonés non brûlés.

Les résultats expérimentaux ont été comparés avec des calculs thermodynamiques. Des différences dans les températures de formation et de décomposition de certains composés existent. Ces différences peuvent être expliquées par différents mécanismes observés expérimentalement, non pris en compte par le calcul :

- Les métaux alcalino terreux sont libérés de la matrice organique à haute température et entrent en contact avec la silice, favorisant ainsi la formation de silicates.
- Les sels se vaporisent à haute température

Ces résultats montrent que les bases de données FToxid (avec la solution liquide FToxid-SlagA) et FTsalt (avec FTsalt-SaltF) peuvent être utilisées pour prévoir les grandes tendances des transformations de phases en température. Les résultats doivent cependant être complétés, et validés, par des résultats expérimentaux.

Les interactions entre les cendres fondues et différents matériaux constituant le lit fluidisé (silice, olivine et olivine calcinée) ont été étudiées en conditions statiques et dynamiques, sous atmosphères oxydantes et réductrices.

Les principales conclusions tirées des expériences menées en condition statique sont les suivantes :

- La mouillabilité des cendres sur les matériaux du lit est un paramètre clé dans les mécanismes d'agglomération.
- L'adhésion entre les cendres et les matériaux du lit augmente selon l'ordre suivant : silice → olivine → olivine calcinée.
- Le temps de réaction impacte fortement la composition des cendres, et par conséquent, la nature des interactions.
- Il y a peu de différences dans les mécanismes d'agglomération (adhésion, interactions cendres fondues / matériaux du lit) sous atmosphère oxydante ou réductrice.
- La présence de deux liquides immiscibles a été observée en atmosphère réductrice. Des traces de sulfures et de carbone non brûlé ont aussi été mises en évidence dans ces conditions.

Les expériences menées en conditions dynamiques ont permis d'étudier l'impact de l'hydrodynamique sur les interactions entre les cendres fondues et les matériaux du lit. Ces tests ont été effectués à deux échelles : à l'échelle d'un dispositif expérimental haute température (CEMHTI, CNRS Orléans) et à l'échelle d'un réacteur pilote à lit fluidisé pilote de 7.5 KW (LRGP, CNRS Nancy). Les résultats ont montré que :

- La température n'a que peu d'influence sur les taux d'agglomération.
- Le lavage de la biomasse et l'adjonction de kaolin permettent de fortement limiter l'agglomération.

Les principaux résultats concernant le réacteur pilote du LRGP à Nancy sont les suivants :

- 1) Il y a une ségrégation des matériaux du lit : les résidus carbonés se déposent à la tête du lit et les gros agglomérats se retrouvent au niveau de la grille.
- 2) La phase liquide est principalement formée de  $K_2O$ ,  $CaO$ ,  $SiO_2$ ,  $MgO$  et  $Fe$ . Les teneurs en fer sont plus importantes que celles observées en laboratoire.
- 3) La fluidisation peut provoquer une érosion des matériaux du lit et de la paroi du réacteur.

L'ensemble de ce travail permet de proposer plusieurs recommandations (résumé ci-dessous) pour limiter les risques d'agglomération lors de la gazéification de miscanthus en lit fluidisé. Les résultats obtenus devront être comparés avec des expérimentations menées à l'échelle industrielle afin de déterminer la validité des résultats obtenus en laboratoire et de conforter nos recommandation pour la gazéification du miscanthus.

---

### **Recommandation**

#### **Pour la gazéification du miscanthus en lit fluidisé bouillonnant**

<b>Biomasse</b>	<ul style="list-style-type: none"><li>➤ Composition de cendres: au-dessous de 10wt%</li><li>➤ Mélanger avec autre biomasse</li><li>➤ Prélavage du miscanthus a l'eau</li></ul>
<b>Conditions</b>	<ul style="list-style-type: none"><li>➤ 800°C, maximum 850°C</li><li>➤ &gt;850°C utilisation des additives</li></ul>
<b>Matériau du lit</b>	<ul style="list-style-type: none"><li>➤ &lt;850°C - n'importe quel type de matériau du lit</li><li>➤ &gt;850°C -silice</li></ul>
<b>Additifs</b>	<ul style="list-style-type: none"><li>➤ 0.2-0.3 m% kaolin dans le lit</li><li>➤ 3 m% dolomite dans le lit</li></ul>

---

Les résultats de cette thèse offrent de nouvelles perspectives comme le développement d'un modèle prédictif d'agglomération.

## BIBLIOGRAPHIE

- [1] Heaton EA, Dohleman FG, Miguez AF, Juvik JA, Lozovaya V, Widholm J, et al. Miscanthus : A Promising Biomass Crop Biology. *Adv Bot Res* 2010;56:75–137.
- [2] Basu P. Introduction (Chapter 1). *Biomass Gasif. Pyrolysis*, 2010.
- [3] McKendry P. Energy production from biomass (part 1): overview of biomass. *Bioresour Technol* 2002;83:37–46.
- [4] Naik SN, Goud V V., Rout PK, Dalai AK. Production of first and second generation biofuels: A comprehensive review. *Renew Sustain Energy Rev* 2010;14:578–97.
- [5] Hodgson EM, Nowakowski DJ, Shield I, Riche a, Bridgwater a V, Clifton-Brown JC, et al. Variation in Miscanthus chemical composition and implications for conversion by pyrolysis and thermo-chemical bio-refining for fuels and chemicals. *Bioresour Technol* 2011;102:3411–8.
- [6] Lewandowski I, Clifton-brown JC, Scurlock JMO, Huisman W. Miscanthus : European experience with a novel energy crop 2008;19:209–27.
- [7] Pyter R, Voigt T, Heaton E, Dohleman F, Long S. Giant Miscanthus : Biomass Crop for Illinois 2007:39–42.
- [8] Jørgensen U. Benefits versus risks of growing biofuel crops: the case of Miscanthus. *Curr Opin Environ Sustain* 2011;3:24–30.
- [9] Basu P. Gasification Theory and Modeling of Gasifiers (Chapter 5). *Biomass Gasif. Pyrolysis*. First Edit, © 2010 Elsevier Inc.; 2010, p. 117–65.
- [10] Bartels M, Lin W, Nijenhuis J, Kapteijn F, van Ommen JR. Agglomeration in fluidized beds at high temperatures: Mechanisms, detection and prevention. *Prog Energy Combust Sci* 2008;34:633–66.
- [11] Ruiz J a., Juárez MC, Morales MP, Muñoz P, Mendivil M a. Biomass gasification for electricity generation: Review of current technology barriers. *Renew Sustain Energy Rev* 2013;18:174–83.
- [12] Basu P. Design of Biomass Gasifiers (Chapter 6). *Biomass Gasif. Pyrolysis*. First Edit, © 2010 Elsevier Inc.; 2010, p. 167–228.
- [13] Obernberger I, Thek G. Combustion and gasification of solid biomass for heat and power production in Europe-State of the art and relevant future development. In: Cenertec P, editor. 8th Eur. Conf. Ind. Furn. Boil., Vilamoura, Portugal: 2008, p. 1–24.
- [14] Öhman M, Pommer L, Nordin A. Bed Agglomeration Characteristics and Mechanisms during Gasification and Combustion of Biomass Fuels. *Energy & Fuels* 2005;19:1742–8.
- [15] GAMECO ANR Project: Gazéification AMéliorée pour des applications. *Biomass* 2010.
- [16] Olofsson G, Ye Z, Bjerle I, Andersson A. Bed Agglomeration Problems in Fluidized-Bed Biomass Combustion. *Ind Eng Chem Res* 2002;41:2888–94.
- [17] Lin W, Dam-Johansen K, Frandsen FJ. Agglomeration in bio-fuel fired fluidized bed combustors. *Chem Eng J* 2003;96:171–85.
- [18] Liliedahl T, Sjöström K, Engvall K, Rosén C. Defluidisation of fluidised beds during gasification of biomass. *Biomass and Bioenergy* 2011;35:S63–S70.

- [19] Li S, Shang L, Teng H, Lu Q. A model for agglomeration in bio-fuel fired fluidized bed. *J Therm Sci* 2010;19:451–8.
- [20] Bryers RW. Fireside slagging, fouling, and high-temperature corrosion of heat-transfer surface due to impurities in steam-raising fuels. *Prog Energy Combust Sci* 1996;22:29–120.
- [21] Werkelin J, Skrifvars B-J, Zevenhoven M, Holmbom B, Hupa M. Chemical forms of ash-forming elements in woody biomass fuels. *Fuel* 2010;89:481–93.
- [22] Ma JF, Yamaji N. Silicon uptake and accumulation in higher plants. *Trends Plant Sci* 2006;11:392–7.
- [23] Vassilev S V., Baxter D, Andersen LK, Vassileva CG. An overview of the composition and application of biomass ash. Part 1. Phase–mineral and chemical composition and classification. *Fuel* 2013;105:40–76.
- [24] Boström D, Skoglund N, Grimm A, Boman C, Ohman M, Brostrom M, et al. Ash transformation Chemistry during Combustion of Biomass. *Energy & Fuels* 2012;26:85–93.
- [25] Visser HJM. The influence of fuel composition on agglomeration behaviour in fluidised-bed combustion. 2004.
- [26] Brus E, Öhman M, Nordin A. Bed Agglomeration during Combustion of Biomass Fuels - Mechanism and Measures for Prevention n.d.;46:9195.
- [27] Ergudenler A, Ghaly AE. Agglomeration of alumina sand in a fluidized bed straw gasifier at elevated temperatures. *Bioresour Technol* n.d.;43:259–68.
- [28] Steenari B-M, Lundberg A, Pettersson H, Wilewska-Bien M, Andersson D. Investigation of Ash Sintering during Combustion of Agricultural Residues and the Effect of Additives. *Energy & Fuels* 2009;23:5655–62.
- [29] Michel R, Ammar MR, Poirier J, Simon P. Phase transformation characterization of olivine subjected to high temperature in air. *Ceram Int* 2013;39:5287–94.
- [30] Basu P. *Combustion and Gasification in Fluidized Beds*. Taylor&Francis Group, LLC; 2006.
- [31] Antonini G. *Transferts thermiques-Lits fluidisés: Caractéristiques générales et applications*. vol. 42214210. Editions T, 2007, p. 1–22.

**Judit KAKNICS**

**Gazéification de la biomasse en lit fluidisé bouillonnant:  
Interactions à haute température entre les composés inorganiques et  
les matériaux granulaires**

**Résumé**

Ce travail traite du rôle des interactions entre les composés inorganiques (cendres) et les matériaux du lit pendant la gazéification de miscanthus en lit fluidisé. Les objectifs étaient :-1) de décrire la transformation des inorganiques à haute température ; -2) de comprendre leur rôle dans l'agglomération ; et -3) de proposer des recommandations. Les principaux éléments inorganiques présents dans le miscanthus sont K, Si, Ca, Mg, P, S et Cl. Les cendres sont constituées de silice, de carbonates et de sels. Les carbonates et les sels se décomposent et se volatilisent à 700 °C. Les Ca et Mg silicates sont les phases solides majoritaires à haute température. La phase liquide est constituée de SiO<sub>2</sub>, K<sub>2</sub>O, CaO et MgO quel que soit la nature de l'atmosphère. Les résultats expérimentaux ont été comparés aux calculs thermodynamiques. Il apparaît que les bases de données FToxid et FTsalt peuvent être utilisées pour prévoir les tendances des transformations de phases en température. Les interactions entre les cendres et les matériaux du lit ont été étudiées en conditions statiques et dynamiques. Les conclusions sont les suivantes : -1) la mouillabilité des cendres sur les matériaux du lit est un paramètre clé dans l'agglomération ; -2) l'adhésion augmente dans l'ordre suivant : silice → olivine → olivine calcinée ; -3) il y a peu de différences en atmosphère oxydante ou réductrice -4) la présence de deux liquides immiscibles est observée en atmosphère réductrice. Des traces de sulfures et de résidus carbonés ont aussi été observées. Des expériences ont été effectuées à haute température, en conditions dynamiques, avec un dispositif expérimental de laboratoire et avec un pilote de gazéification à lit fluidisé. En condition dynamique, la température est un paramètre très important. Le lavage de la biomasse et l'ajout de kaolin permettent de limiter l'agglomération. Dans le gazéifieur pilote, les gros agglomérats se retrouvent préférentiellement au niveau de la grille et limite la fluidisation. Les teneurs en Fe, Cr et Al de la phase liquide sont plus importantes que celles observées en laboratoire.

**Mots clés : miscanthus, gazéification, lit fluidisé, agglomération, calculs thermodynamiques**

**Biomass gasification in bubbling fluidized bed: high temperature  
interaction between inorganic compounds and granular materials**

**Summary**

This work studies the role of inorganics in ash-bed material interaction during thermal conversion of miscanthus in fluidized bed. The objectives were (1) to describe the transformation of inorganics at high temperature, (2) to reveal their role in the agglomeration and (3) to provide recommendations for miscanthus gasification in fluidized bed. The main ash forming elements in miscanthus are K, Si, Ca, Mg, P, S and Cl. The ashes are composed of silica, carbonates and salts. The carbonates and salts decompose and volatilise at 700°C, at elevated temperature the dominant solid phases are Ca and Mg silicates. The liquid phase is composed of SiO<sub>2</sub>, K<sub>2</sub>O, CaO, MgO regardless of the atmosphere. The accuracy of thermodynamic prediction tool was evaluated with the experimental results. In conclusion, FToxid and FTsalt databases can be used to follow the trends of the main phase transformations at high temperature. The ash-bed interaction was studied under static and dynamic conditions. We found that the wetting of bed material by molten ashes is the key parameter of the agglomeration. The adhesion of particles increases in the order of sand, olivine, calcined olivine. There is no significant difference in the agglomeration mechanism in oxidizing or reductive atmosphere. However, in reductive atmosphere, two immiscible liquid phases can occur and the presence of unburnt char and traces of sulphides was also observed. The ash-bed material interaction was studied under dynamic conditions in a bench scale device and in a fluidized bed gasifier pilot. The parametric investigation showed that the operating temperature has the most significant effect on the agglomeration ratio and the biomass pre washing or the addition of kaolin are the most effective tools to reduce agglomeration risks. During the trials in the gasification pilot the large agglomerates segregated on the grid accelerating the defluidization. Compared to the laboratory tests, the liquid phase is enriched in Fe, Cr and Al.

**Keywords: miscanthus, gasification, fluidized bed, agglomeration, thermodynamic calculation**



**CEMHTI**  
1d Avenue de la Recherche Scientifique  
45071 Orléans CEDEX 2

